Technical Report Documentation Page

1. Report No. FHWA/TX-08/1401-1	2. Government Accession No.	3. Recipient's Catalog No.
4. Title and Subtitle **Bending Fatigue Response of Grouted Stay Cables**		5. Report Date July 2008 6. Performing Organization Code
7. Author(s) Sharon L. Wood, Marcel Poser, Karl H. Frank, Matthew J. Bean, Joseph A. Dowd, John C. Eggers, Dylan Freytag, Loukas F. Kallivokas, Jun Ki Lee, Aaron J. Pebley, Jennifer E. Ridd, Margaret Warpinski, Eric B. Williamson, and Adrienne Willox		8. Performing Organization Report No. 0-1401-1
9. Performing Organization Name and Address Center for Transportation Research The University of Texas at Austin 3208 Red River, Suite 200 Austin, TX 78705-2650		10. Work Unit No. (TRAIS) 11. Contract or Grant No. Research Project 0-1401
12. Sponsoring Agency Name and Address Texas Department of Transportation Research and Technology Implementation Office P.O. Box 5080 Austin, TX 78763-5080		13. Type of Report and Period Covered Technical Report (3/2000 - 8/2006) 14. Sponsoring Agency Code

15. Supplementary Notes

Project performed in cooperation with the Texas Department of Transportation and the Federal Highway Administration.

16. Abstract

Both the Fred Hartman Bridge and the Veterans Memorial Bridge have experienced large-amplitude vibrations of the stay cables. A major concern resulting from these vibrations is the possibility of fatigue damage to the parallel, seven-wire, prestressing strand in the grouted stay cables – and the overall safety of the bridges.

An experimental investigation was conducted to determine the susceptibility of grouted stay cables to fatigue damage. Two series of experiments were conducted: twelve stay-cable specimens were subjected to bending fatigue loads in the first series and three small-diameter specimens were subjected to bending fatigue loads in the second series.

The test results indicate that fatigue damage is expected to be concentrated in the regions of highest bending stress: the ends of the stays and locations where a damper or restrainer induces local bending in the stay. The risk of fatigue damage was considered to be low at the tension ring, along the free length of the stay, and in the vicinity of unintentionally crossed strands. The acoustic monitoring systems installed on the Fred Hartman Bridge and the Veterans Memorial Bridge provided a reliable means of detecting wire breaks in the laboratory specimens. However, the actual location of a wire break may be 2 to 3 ft from the location identified by the acoustic sensors. Transverse stiffness and natural frequencies of the test specimens were not sufficiently sensitive to detect the accumulation of fatigue damage.

Accumulation of fatigue damage is a slow process, and many wire fractures can be tolerated before the strength or stiffness of the grouted stay cable is compromised. However, if the number of wire breaks detected at a single location exceeds a threshold level of 10% of the total number of wires in the stay, corrective action is recommended for an existing grouted stay cable.

17. Key Words Cable stays, fatigue, acoustic monitoring, grout, strand, fretting, damage accumulation,	18. Distribution Statement No restrictions. This document is available to the public through the National Technical Information Service, Springfield, Virginia 22161; www.ntis.gov.

19. Security Classif. (of report) Unclassified	20. Security Classif. (of this page) Unclassified	21. No. of pages 270	22. Price

Form DOT F 1700.7 (8-72) Reproduction of completed page authorized

Bending Fatigue Response of Grouted Stay Cables

Sharon L. Wood
Marcel Poser
Karl H. Frank
Matthew J. Bean
Joseph A. Dowd
John C. Eggers
Dylan Freytag
Loukas F. Kallivokas
Jun Ki Lee
Aaron J. Pebley
Jennifer E. Ridd
Margaret Warpinski
Eric B. Williamson
Adrienne Willox

CTR Research Report:	0-1401-1
Report Date:	July 2008
Research Project:	0-1401
Research Project Title:	Determination of Fatigue Damage in Stay Cables
Sponsoring Agency:	Texas Department of Transportation
Performing Agency:	Center for Transportation Research at The University of Texas at Austin

Project performed in cooperation with the Texas Department of Transportation and the Federal Highway Administration.

Center for Transportation Research
The University of Texas at Austin
3208 Red River
Austin, TX 78705

www.utexas.edu/research/ctr

Disclaimers

Author's Disclaimer: The contents of this report reflect the views of the authors, who are responsible for the facts and the accuracy of the data presented herein. The contents do not necessarily reflect the official view or policies of the Federal Highway Administration or the Texas Department of Transportation (TxDOT). This report does not constitute a standard, specification, or regulation.

Patent Disclaimer: There was no invention or discovery conceived or first actually reduced to practice in the course of or under this contract, including any art, method, process, machine manufacture, design or composition of matter, or any new useful improvement thereof, or any variety of plant, which is or may be patentable under the patent laws of the United States of America or any foreign country.

Notice: The United States Government and the State of Texas do not endorse products or manufacturers. If trade or manufacturers' names appear herein, it is solely because they are considered essential to the object of this report.

Engineering Disclaimer

THIS REPORT IS NOT INTENDED FOR CONSTRUCTION, BIDDING,
OR PERMIT PURPOSES.

Sharon L. Wood, Texas P.E. #83804
Research Supervisor

Acknowledgments

This research project was funded by the Texas Department of Transportation (TxDOT) under Project No. 0-1401. The support of the project director, Keith Ramsey (BRG) is greatly appreciated.

Products

Research Product P1, procedures for estimating the likelihood of fatigue damage at critical sections along the length of stays, and Research Produce P2, procedures for estimating the relationship between stress range, curvature, or rotation and the fatigue life of stay cables, are included in Chapter 5 of this research report. Research Product P3, recommendations on the effectiveness of NDT techniques for identifying fatigue damage in stay cables, is included in Chapter 6 of this research report.

TABLE OF CONTENTS

LIST OF FIGURES

LIST OF TABLES

SUMMARY

Both the Fred Hartman Bridge and the Veterans Memorial Bridge have experienced large-amplitude vibrations of the stay cables. A major concern resulting from these vibrations is the possibility of fatigue damage to the parallel, seven-wire, prestressing strand in the grouted stay cables – and the overall safety of the bridges.

An experimental investigation was conducted to determine the susceptibility of grouted stay cables to fatigue damage. Two series of experiments were conducted. In the first series, twelve stay-cable specimens were subjected to bending fatigue loads. The cross section of the stay-cable specimens was nominally identical to that of the smallest diameter stays on the Fred Hartman Bridge. The length of the stay-cable specimens, however, was less than one-sixth the length of the shortest of the prototype stays. The results from the first series of bending fatigue tests were used to determine the expected locations of fatigue damage, the parameters that have the largest impact on the fatigue life of a grouted stay cable, how much fatigue damage can occur before the structural integrity of the stay cable is compromised, and if nondestructive methods provide a reliable assessment of the extent of fatigue damage.

In the second series of tests, three, small-diameter specimens were also subjected to bending fatigue loads. The number of strands in these specimens was much smaller than the prototype stays and the cross-sectional properties did not vary along the length of the specimen. However, the ratio of axial stiffness to flexural stiffness was representative of the prototype stays. The results from the second series of tests were used to determine if nondestructive methods provide a reliable assessment of the extent of fatigue damage and how stress in the strand varies within the cross section and along the length of the stay cable.

The test results indicate that fatigue damage is expected to be concentrated in the regions of highest bending stress: the ends of the stays and locations where a damper or restrainer induces local bending in the stay. The risk of fatigue damage was considered to be low at the tension ring, along the free length of the stay, and in the vicinity of unintentionally crossed strands. The acoustic monitoring systems installed on the Fred Hartman Bridge and the Veterans Memorial Bridge provided a reliable means of detecting wire breaks in the laboratory specimens. However, the actual location of a wire break may be 2 to 3 ft from the location identified by the acoustic sensors. Transverse stiffness and natural frequencies of the test specimens were not sufficiently sensitive to detect the accumulation of fatigue damage.

Accumulation of fatigue damage is a slow process, and many wire fractures can be tolerated before the strength or stiffness of the grouted stay cable is compromised. However, if the number of wire breaks detected at a single location exceeds a threshold level of 10% of the total number of wires in the stay, corrective action is recommended for an existing grouted stay cable.

CHAPTER 1: INTRODUCTION

Cable-stayed bridges have been built in rapidly increasing numbers since 1950. They are especially economical for medium to long-span bridges and are now used where previously a truss or suspension bridge might have been the first choice. Although cable-stayed bridges have many advantages, their popularity and wide usage is often based on prestige rather than structural efficiency or economy Menn (2000).

Despite the wide usage of cable-stayed bridges, there are still numerous areas of concern, especially with the corrosion protection system for the stay cables. Early stays used locked coil cables without an additional barrier for corrosion protection. Many of these unprotected stays sustained extensive corrosion damage. The U.S. practice in the 1990s was to design stay cables using standard approaches for post-tensioned tendons: the stays were constructed using uncoated, high-strength, seven-wire prestressing strand inside a high-density polyethylene (PE) duct filled with portland cement grout. This stay configuration was used in both cable-stay bridges in Texas: the Veterans Memorial Bridge and the Fred Hartman Bridge. More recently, cable-stay bridges have been constructed with individually sheathed or coated strands inside the PE duct with wax filler.

All stays used in the U.S. must be tested to ensure that their anchorage details provide adequate axial fatigue strength and that the fabricated stay has sufficient tensile strength. In addition, the strand itself is also tested to ensure that its fatigue properties are adequate. However, the influence of bending, due to vibrations of the stays, is not considered directly in the design process of the stay cables.

Large-amplitude vibrations have been observed on numerous bridges around the world, including both cable-stayed bridges in Texas (Zuo and Jones 2005). Structural solutions to minimize the cable vibrations have been studied carefully on both the Fred Hartman and Veterans Memorial Bridges. A major concern resulting from these vibrations is possible fatigue damage on the parallel seven-wire strand in the cables. Information about the fatigue behavior of grouted stay cables with prestressing strands subjected to transverse vibrations is quite limited. In contrast, the fatigue behavior of stay cables under axial load is established and numerous axial fatigue tests, especially on anchorages, have been performed.

1.1 HISTORY OF CABLE-STAYED BRIDGES

German engineers pioneered the design of cable-stayed bridges after World War II, when they were challenged to find new, innovative, and inexpensive bridge designs to replace most of the Rhine river crossings that had been destroyed in the war. Dischinger proposed systems where the central span was supported by a suspension system and stay cables carried the outer parts. Dischinger's combined solutions were never adopted for an actual bridge, but his studies influenced the development of the true cable-stayed bridge system. It was not until the 1950s that Dischinger designed the first true cable-stayed bridge. The Strömsund Bridge (1955) had a main span of 599 ft and two side spans of 245 ft. Gimsing (1999) attributes the increase in cable-stayed bridge designs to the availability of improved structural analysis tools. The Germans further developed the design of cable-stayed bridges in the following

decades. The series of bridges near Dusiburg across the Rhine River are examples of these pioneering German bridges.

The first cable-stayed bridge in the United States was the Sitka Harbor Bridge in Alaska, which was opened to traffic in 1971. The two cable-stayed bridges in the inventory of the Texas Department of Transportation (TxDOT) are the Veterans Memorial Bridge near Port Arthur (Figure 1.1) and the Fred Hartman Bridge across the Houston Ship Channel (Figure 1.2).

The longest cable-stayed bridge in the 20th century was built as part of the Honshu-Shikoki Bridge Project in Japan. The Tatara Bridge has a main span of 920 ft and was completed in 1999 (Figure 1.3). Table 1.1 lists the ten longest cable-stayed bridges in the world.

Figure 1.1 Veterans Memorial Bridge

Figure 1.2 Fred Hartman Bridge

Figure 1.3 Tatara Bridge, Japan

1.2 CONCERNS ON THE FRED HARTMAN BRIDGE

Large-amplitude stay cable vibrations were observed on the Fred Hartman Bridge numerous times since its opening in 1995. One of the first estimates (Poston 1998) of the amplitude of these vibrations is from visual observations during a four-day period between 1 April and 4 April 1997 (Table 1.2). Video taken on 4 April 1997 (Figure 1.4) show the large-amplitude deformations of cable 24 during this event. At 650 ft, cable 24 is the longest cable on the bridge.

Table 1.1 Longest Cable-Stayed Bridges

Number	Name	Country	Span (ft)	Year
1	Tatara Bridge	Japan	2,920	1999
2	Pont de Normandie	France	2,808	1995
3	Third Nanjing Yangtze Bridge	China	2,126	2005
4	Second Nanjing Yangtze Bridge	China	2,060	2001
5	Baishazhou Bridge	China	1,018	2000
6	Mingjiang Bridge	China	1,985	1999
7	Yangpu Bridge	China	1,975	1993
8	Xupu Bridge	China	1,936	1997
9	Meiko Chuo Bridge	Japan	1,936	1997
10	Rio-Antirio Bridge	Greece	1,837	2004
…				
…	Fred Hartman Bridge	USA	1,250	1995

Table 1.2 Observed Cable Vibrations

Cable ID	Mode	Frequency (Hz)	Approximate Amplitude (in.)
9	2	2.1	15
1, 2, 3	1	0.8	25
10, 11	2	> 1.5	4
15, 16	1	1.0	12
23, 24	2	1.2	26
24	3	1.8	42

These large-amplitude vibrations caused visual damage to the Fred Hartman Bridge. Broken guide pipes (Figure 1.5) were found on more than 100 of the 192 cables. The broken guide pipes are a visual indication of the forces and displacements generated by these events and the damage that might occur. Of great concern is the possible hidden fatigue damage of the stay cables and the anchorage. The stays would have to be dismantled to detect damage reliably. Nondestructive inspection techniques are not applicable due to the limited access at the anchorages and the grout surrounding the strand.

Figure 1.4 Stay Cable Vibrations – Fred Hartman Bridge

Figure 1.5 Broken Guide Pipe – Fred Hartman Bridge

1.3 REPAIR AND EVALUATION OF THE FRED HARTMAN BRIDGE

Whitlock, Dalrymple, Poston, and Associates (WDP), Johns Hopkins University, Texas Tech University, and the University of Texas at Austin (UT) were retained by TxDOT to investigate the large-amplitude vibrations observed on the Fred Hartman Bridge and the Veterans Memorial Bridge.

WDP (Witthoft et al. 2001) developed the designs to repair the existing damage and to minimize future cable vibrations. The broken guide pipes were strengthened with stiffeners. A temporary solution to control the cable vibrations was the installation of restrainers (Figure 1.6). The restrainers connect the stay cables and allow vibration energy to be transferred between adjacent stays. These restrainers proved to be a very effective means of reducing the cable displacements and were left in place on the bridge.

Figure 1.6 Cable Restrainers

Two types of dampers were designed and tested by WDP as possible methods to prevent the large-amplitude vibrations. A linear damper, which is attached perpendicular to the cable (Figure 1.7) and a pressurized bladder system, developed by Freyssinet, which surrounds the cable (Figure 1.8), were installed on selected cables on the Fred Hartman Bridge. The dampers were designed to match the stiffness and frequency characteristics of each stay cable. After these initial trials, the linear damper was selected and installed on all stay cables on the bridge. The linear dampers, along with the cable restrainer system, significantly reduced the amplitude of the cable displacements (Zuo and Jones 2005).

Figure 1.7 Linear Damper

Figure 1.8 Freyssinet Damper

Researchers at Johns Hopkins University monitored the performance of the stay cables on the Fred Hartman Bridge and the Veterans Memorial Bridge for several years. These data were used to identify the causes of the large-amplitude vibrations and to evaluate the effectiveness of the damper and cable restrainer systems.

Researchers at Texas Tech University evaluated aerodynamic damping solutions. They proposed a solution which consisted of a number of rings wrapped around the cable to prevent the formation of the rainwater rivulets. This system was not installed due to the cost to retrofit the cables in the field.

The studies at the University of Texas at Austin focused on the fatigue behavior of the stay cables of the Fred Hartman Bridge. The research program included full-size bending fatigue tests of stay cables and evaluation of the acoustic monitoring system used to detect wire fractures in the stay cables. The results of that investigation are documented in this report

1.4 STAY CABLE VIBRATIONS

Numerous cable vibration mechanisms have been identified and characterized with the four most common phenomena being vortex shedding, galloping, deck – cable interaction, and wind and rain induced vibrations (Gimsing 1997, Gimsing 1999, Ito 1999, Miyazaki 1999, Virlogeux 1998, Zuo and Jones 2005). A combination of these mechanisms to played a role in the vibrations of the stays on the Fred Hartman Bridge.

1.4.1 Vortex Shedding

Vortex shedding is essentially the phenomenon that makes a flag flutter in the wind. Airflow that is forced around an object produces vortices shedding off the object as indicated in Figure 1.9. Consecutive vortices that shed off opposite sides of the object produce alternating perpendicular forces. If the frequency of the alternating forces matches any of the natural frequencies of the cable, large amplitude vibrations of the order of the cable diameter will occur.

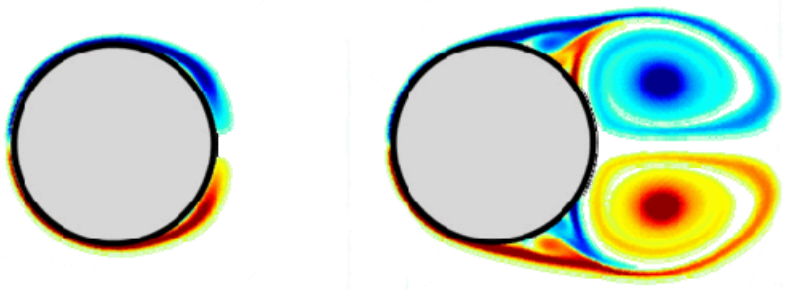

Figure 1.9 Development of Vortices

1.4.2 Galloping

Galloping is a phenomenon that occurs because of aerodynamic instability where the airflow creates uplift forces around an unsymmetrical cross section. Galloping may occur on stay cables if the airflow hits at an angle such that the effective aerodynamic shape of the cable is an elliptical cross section. In addition, formation of ice on the cable can also change the cross section of a stay cable to induce galloping perpendicular to the airflow.

1.4.3 Deck and Cable Interaction

Cable vibrations occur when the structural vibrations of the bridge deck or the pylon are transferred through the anchorage into the stay cable. Deck and pylon vibration can occur because of aerodynamic effects or because of periodic traffic loads.

1.4.4 Wind and Rain-Induced Vibrations

The phenomenon that produces by far the largest displacement amplitudes is wind and rain-induced vibrations. The first time that this kind of vibration was described and investigated was in 1984 during the construction of the Meikonishi Bridge in Japan.

Interestingly, it was noticed that the vibrations only occur on stay cables that are covered with a smooth polyethylene pipe at relatively low wind speeds with a light rain falling, hence the term wind and rain-induced vibrations. The rainwater forms one or two rivulets generated by the airflow around the cable. The rivulets of water change the aerodynamic cross section of the stay cable, which make it susceptible to vibrations (Figure 1.10). Once the cable starts vibrating, the rivulets start to oscillate at the same frequency as the cable. Wind and rain-induced vibrations have not been reported during heavy winds. Apparently, the rivulets are blown off the cable surface when the wind speed increases.

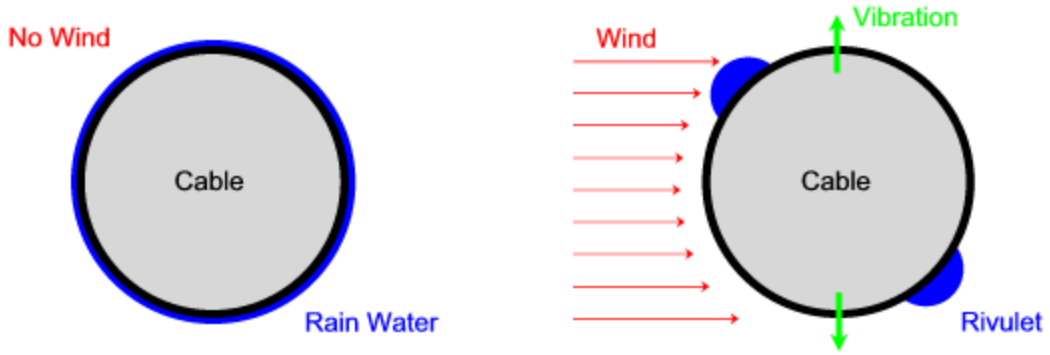

Figure 1.10 Wind-Rain Vibration Mechanism

1.4.5 Vibration Mechanisms on the Fred Hartman Bridge

Zuo and Jones (2005) summarized the vibration characteristics of the cables on the Fred Hartman Bridge. The analysis of these vibrations led to identification of the following types of vibrations: vortex-induced vibrations, wind and rain-induced vibrations, large-amplitude dry cable vibrations, deck-induced vibrations, and an uncategorized type of vibrations. Their analyses indicated that the wind and rain-induced vibrations share many characteristics with vortex-induced vibrations and the large-amplitude dry cable vibrations, which suggests that the wind and rain-induced vibrations may be caused by aeroelastic instability that is inherent in yawed and inclined stay cables.

The dynamic response of the stay cables was monitored before and after the restrainers and linear dampers were installed on the Fred Hartman Bridge. The measurements indicate that the dampers and restrainers have been effective in mitigating large-amplitude cable-vibrations.

1.5 Fatigue of Stay Cables

Over the years, numerous stay cable systems have been developed and successfully used on cable-stayed bridges. However, the most widely used system in the 20th century was the parallel-strand cable system. The system consists of a bundle of parallel, seven-wire, 0.6-in diameter strands surrounded by a polyethylene (PE) pipe, which is then grouted to protect the strand from corrosion. This type of system is used on the Fred Hartman Bridge and the Veterans Memorial Bridge. The anchorage system for the Fred Hartman Bridge is shown in Figure 1.11.

The axial fatigue performance of the stays on the Fred Hartman Bridge is summarized in Section 1.5.1. These tests were conducted at the Ferguson Structural Engineering Laboratory (Frank 1990, Frank and Burkett 1989, Frank, et al. 1989) to verify the performance of the anchorage system. Tests of this type are required for all cable-stayed bridges constructed in the United States.

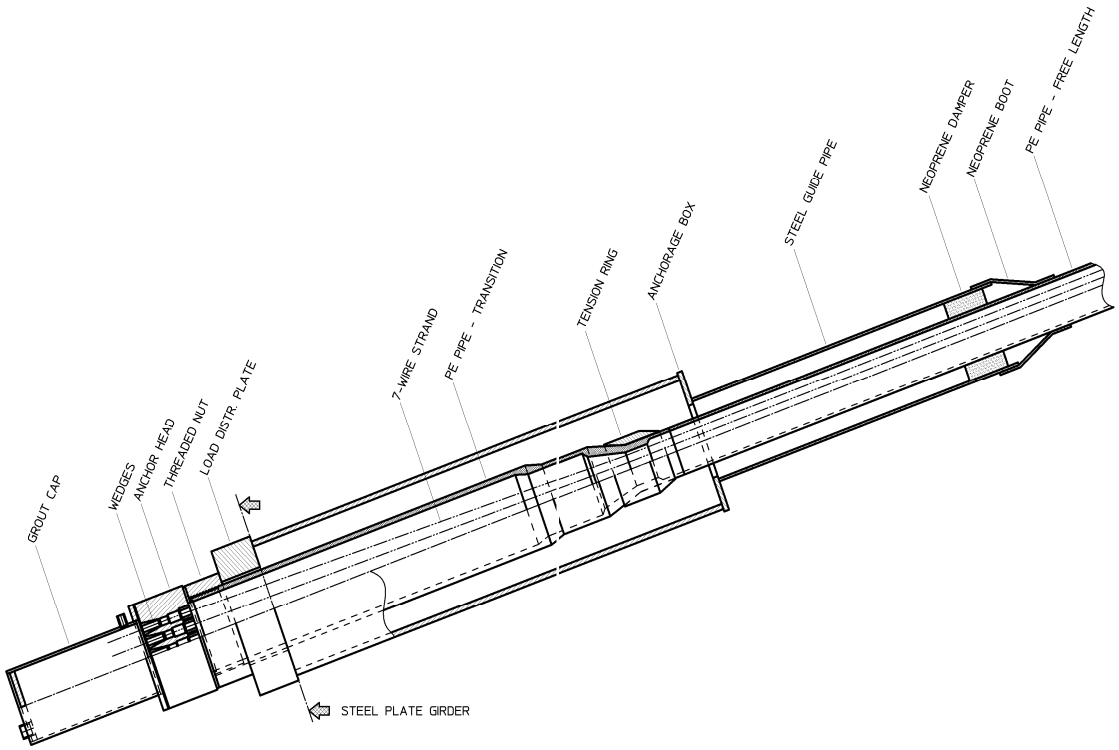

Figure 1.11 Configuration of the Anchorage Zone on the Fred Hartman Bridge

In an axial fatigue test, the entire length of the specimen is subjected to the same applied stress range. Initial flaws in the strand can lead to fatigue cracks and wire fractures away from the anchorage. A specimen subjected to bending has only a few regions along the length where the strands are highly stressed. These occur near the anchorage and at other restraints along the length. Therefore, the probability that an initial flaw is present in a region of higher stress is much smaller in a specimen subjected to bending fatigue than to axial fatigue. However, the data from axial fatigue tests should provide an understanding of the fatigue behavior of strand.

Very few bending fatigue tests of stay cables have been performed worldwide. A summary of a well-documented bending fatigue test, conducted in Japan, is presented in Section 1.5.2. However, the tested specimens were not constructed using parallel strands.

1.5.1 Axial Fatigue Tests of Stay Cables

Axial fatigue tests were performed at the Ferguson Structural Engineering Laboratory on four types of cable specimens for the Fred Hartman Bridge. All four test specimens were 17′-4″ long and were tested vertically. The specimens were stressed to an initial load of 40% GUTS before grouting. After grouting, they were tensioned to the lower fatigue load level and then cycled at a constant load range for 2 million cycles at frequencies between 0.6 and 1.5 Hz. The load range for each specimen resulted in

roughly the same stress range of 23 ksi. Table 1.3 summaries the load and the strand stress ranges, assuming an even distribution of load among the strands.

Wedge seating and stiffness checks were also performed before and during the fatigue test. After the fatigue test, the specimen was tested statically to failure. Because of the static tests, it was not possible to determine whether a wire break occurred during the fatigue test or fractured during the static test from a fatigue crack. However, by examining the fracture surfaces, it was possible to determine if the wire break was initiated by fatigue.

Table 1.3 Load and Stress Ranges used in Axial Fatigue Tests at FSEL

Specimen	#1	#2	#3	#4
Number of Strands	19	43	55	55
Lower Load Level (kip)	406.3	916.6	1176.2	1176.2
Upper Load Level (kip)	500.9	1133.7	1450.1	1450.1
Load Range in Stay (kip)	94.6	217.1	273.9	273.9
Load Range in Strand (kip)	5.0	5.0	5.0	5.0
Stress Range (ksi)	**22.9**	**23.3**	**22.9**	**22.9**

Table 1.4 Location of Fatigue Wire Breaks of FSEL Test

Specimen	#1	#2	#3	#4	Total	%
Number of Strands	19	43	55	55		
Number of Wires	**133**	**301**	**385**	**385**		
Failures at Top Wedges	3		2		**5**	**9%**
Failures in Top Transition Region	2	1	11	13	**27**	**50%**
Failures in Free Length			6		**6**	**11%**
Failures at Contact Points with Helix			8		**8**	**15%**
Failures at Bottom Transition Region		7			**7**	**13%**
Failure at Bottom Wedges			1		**1**	**2%**
Total Failures	**5**	**8**	**28**	**13**	**54**	
%	**3.8%**	**2.7%**	**7.3%**	**3.4%**		

All four specimens experienced fatigue cracks and wire breaks during the 2 million cycles of fatigue loading. The location and the number of fatigue cracks are summarized in Table 1.4. Note that all four specimens experienced wire breaks in the top transition region and only test #2 showed wire fractures in the bottom transition region. Fifty-nine percent of the breaks occurred in the top anchorage region (wedges and transition region), 26% in the free length or at contact points with the helical spacer wire in the free length, and 15% in the bottom anchorage (wedges and transition region).

In the autopsy of the specimens, circumferential cracks spaced approximately 1 in. on center were observed in the grout. Longitudinal cracks over the entire specimen length were found above strands where wire breaks occurred. Dark corrosion spots on strands were reported at various locations along the specimens. Some specimens, particularly specimen #3, showed heavy corrosion at the top and bottom anchor heads.

As shown in Table 1.4, none of the four specimens fulfilled the fatigue test requirement of fewer than 2% wire breaks after 2 million cycles – the recommendation of the Post-Tensioning Institute Committee on Stay Cable Bridges (2001). It should also be mentioned that specimen #3 (55 strands) specimen did not reach 95% of guaranteed ultimate tensile strength (GUTS) as shown in Table 1.5. The ultimate tensile test is a requirement in some bridge specifications.

As a result of the four tests performed at FSEL, one extra strand was added to all stay cables in the Fred Hartman Bridge to reduce the service stress ranges in the stays and increase their strength.

Table 1.5 Tensile Strength of Specimens

Specimen	#1	#2	#3	#4
Number of Strands	19	43	55	55
Ultimate Tensile Test (kip)	1140	2577	3165	—
95% of GUTS (kip)	1114	2576	3271	3271
Difference (kip)	**+26**	**+1**	**-106**	**—**

1.5.2 Bending Fatigue Tests of Stay Cables

Probably the most comprehensive series of full-size axial and bending fatigue tests on bridge cables was undertaken as part of the Honshu-Shikoki Bridge Project in Japan. The tests were conducted at the Japan Construction Method and Machinery Research Institute (Miki et al. 1992).

Axial fatigue was an important issue for the cable-stayed bridges on the Kojima-Sakaida route because of the large variation of the live load, combined highway and rail traffic route. Bending fatigue was of general concern because of bending at the anchorage due to the deflection of the girders under live load. Oscillation of the cables due to the various vibration mechanisms was an additional fatigue concern.

The two types of stay cables were tested, (HiAm SPWS-163 and NEW PWS-163), both are non-grouted parallel wire cables with button heads and a socket at both ends. Each cable had 163 individually galvanized wires with a diameter of 0.28 in. and a tensile strength of 240 ksi. The free space within the

socket was filled with a compound (steel balls, zinc powder, and epoxy resin) for the HiAm SPWS-163 cable and with a zinc-copper alloy for the NEW PWS-163 cable. Both cable configurations were covered with a polyethylene pipe. The cables were prestressed to a tension force of 330 to 440 kip. The bending fatigue tests were performed using a displacement-controlled ram, which cycled the cable at mid-span (Figure 1.12).

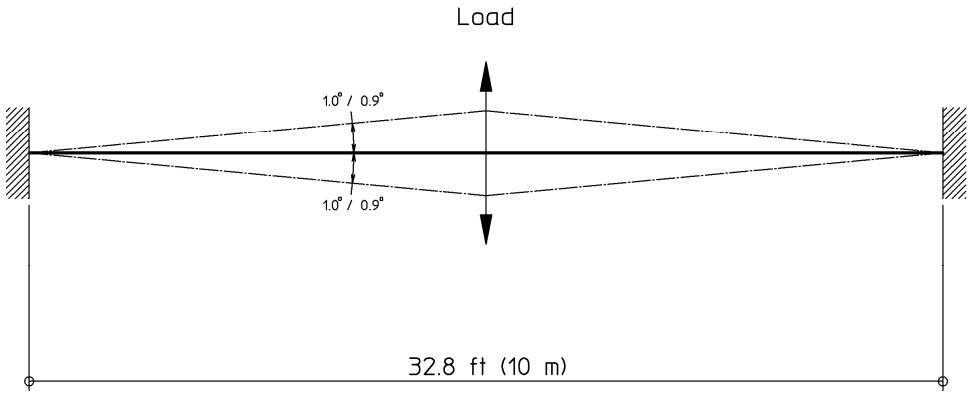

Figure 1.12 Setup for Bending Fatigue Tests – Honshu-Shikoki Bridge Project

The estimated bending stresses at the end of the socket were ±29.0 ksi for the NEW PWS-163 and ±30.4 ksi for the HiAm SPWS-163 (Table 1.6).

Table 1.6 Summary of Bending Fatigue Tests – Honshu-Shikoki Bridge Project

Stay Cable Type	Bending stress at socket	α
HiAm SPWS-163	±30.4 ksi	±1.0°
NEW PWS-163	±29.0 ksi	±0.9°

No fatigue failures were detected on either cable after 10 million cycles with applied bending angles of ±1.0° and ±0.9° respectively. The authors stated that the measured stresses within the socket varied widely. Therefore, it was assumed that the cable did not behave as a single elastic body. The overall conclusion was that the stay cables behaved very well when subjected to bending fatigue. Follow-up tests using an angle range of ±1.35° for each cable produced fatigue failures at 0.262 million cycles for the HiAm stay and 0.326 million cycles for the NEW stay.

1.6 SCOPE OF REPORT

The experimental research conducted at the Ferguson Structural Engineering Laboratory at the University of Texas on the bending fatigue response of grouted stay cables is documented in this report. Chapter 2 provides an overview of the experimental program and identifies the six primary questions that were addressed in this research. Two series of specimens were tested. The bending fatigue response of twelve, large-scale, stay-cable specimens is summarized in Chapter 3 and the bending fatigue response of

three, small-scale specimens is summarized in Chapter 4. The large-scale, stay-cable specimens had the same anchorage details as the smallest stays on the Fred Hartman Bridge. Anchorage details representative of the Veterans Memorial Bridge – including the saddle detail at the pylon – were not included in the experimental phases of this investigation.

Chapter 5 provides a brief discussion of the expected locations of fatigue damage in grouted stay cables and Chapter 6 summarizes the effectiveness of two nondestructive methods that were used to identify the extent of fatigue damage in the test specimens. The acoustic monitoring system described in this section was installed on both the Fred Hartman and Veterans Memorial Bridges. Specific recommendations for evaluating the fatigue life of the two cable-stayed bridges in Texas are provided in Chapter 7.

Due to the large number of fatigue tests conducted during this project, more detailed information about the performance of individual specimens is provided in the five appendices. The material characteristics of the strand used to construct the test specimens is documented in Appendix A. The procedures used to construct the stay-cable specimens are summarized in Appendix B and to construct the small-scale specimens are summarized in Appendix C. The measured response of the twelve cable-stay specimens is documented in Appendix D and the measured response of the three small-scale specimens is documented in Appendix E.

CHAPTER 2: OVERVIEW OF EXPERIMENTAL PROGRAM

The primary objective of this research project was to investigate the bending fatigue response of grouted stay cables. The experimental program was designed to answer basic questions about the behavior of stay cables subjected to transverse bending, including:

(1) Where is fatigue damage likely to occur?
(2) What parameters have the largest impact on the fatigue life of a grouted stay cable?
(3) What mechanisms contribute to fatigue failure of the strand?
(4) How much damage can occur before the structural integrity of the grouted stay cable is compromised?
(5) Do nondestructive methods provide a reliable assessment of the extent of fatigue damage?
(6) How does the stress in the strand vary within the cross section and along the length of a grouted stay cable?

The experimental program was divided into two series of tests. In the first series, twelve, large-diameter, stay-cable specimens were subjected to bending fatigue loads. The cross section of the stay-cable specimens was nominally identical to that of the smallest diameter stays on the Fred Hartman Bridge. The length of the stay-cable specimens, however, was less than one-sixth the length of the shortest of the prototype stays. The results from the first series of tests were used primarily to answer questions one through five.

In the second series of tests, three, small-diameter specimens were also subjected to bending fatigue loads. The number of strands in these specimens was much smaller than the prototype stays and the cross-sectional properties did not vary along the length of the specimen. However, the ratio of axial stiffness to flexural stiffness was representative of the prototype stays, whereas the flexural stiffness dominated the response of the stay-cable specimens. The results from the second series of tests were used primarily to answer questions four through six.

The configuration of the test specimens and the experimental program are summarized in this chapter. The stay-cable specimens are discussed in Section 2.1 and the small-diameter specimens are discussed in Section 2.2. Additional information, including a discussion of the construction procedures, is provided in Appendix B for the stay-cable specimens and Appendix C for the small-diameter specimens.

2.1 BENDING FATIGUE TESTS OF STAY-CABLE SPECIMENS

The stay-cable specimens were modeled after the smallest diameter stays on the Fred Hartman Bridge (Figure 2.1). The anchor heads could accommodate a maximum of nineteen, 0.6-in. strands. Although much shorter than the prototype stays, the test specimens were constructed in a similar fashion using anchorage components that were nominally identical to those in the prototype stays. The strands were assembled within polyethylene (PE) pipe and stressed to 40% of the minimum breaking strength of the strand. After stressing, the PE pipe was filled with a portland cement-based grout.

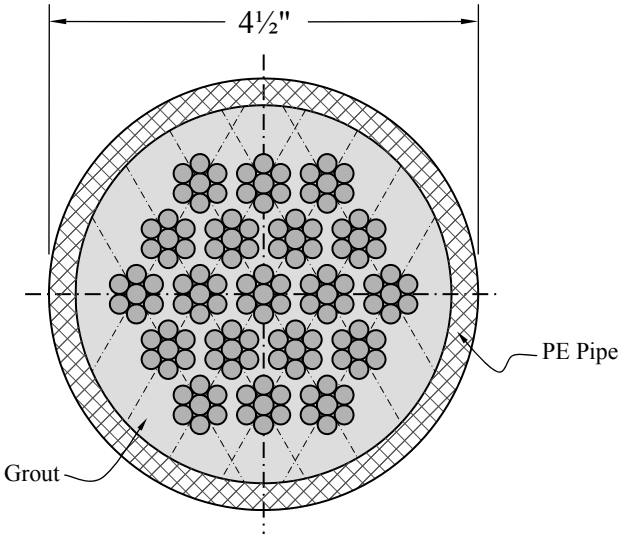

(a) Cross Section along Free Length of Specimen

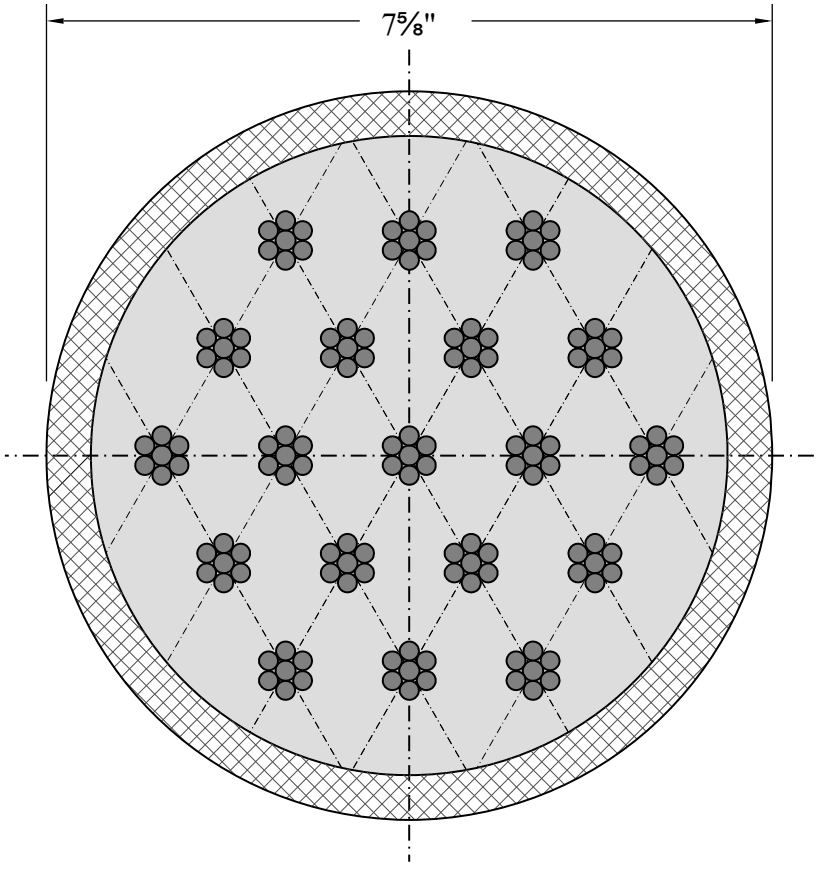

(b) Cross Section at Anchor Head

Figure 2.1 Cross-Sectional Geometry of Cable-Stay Specimens

The twelve specimens were constructed and tested in two phases. The first four specimens comprised the first phase. All anchorage hardware for these tests was purchased from VSL International and the components were fabricated based on the design drawings for the Fred Hartman Bridge (Figure 2.2). The remaining eight specimens comprised the second phase. Only the strand wedges were purchased from VSL International for these specimens. All other anchorage hardware was fabricated at a local machine shop, and the connection between the PE transition pipe and the anchor head was simplified to facilitate construction (Figure 2.3).

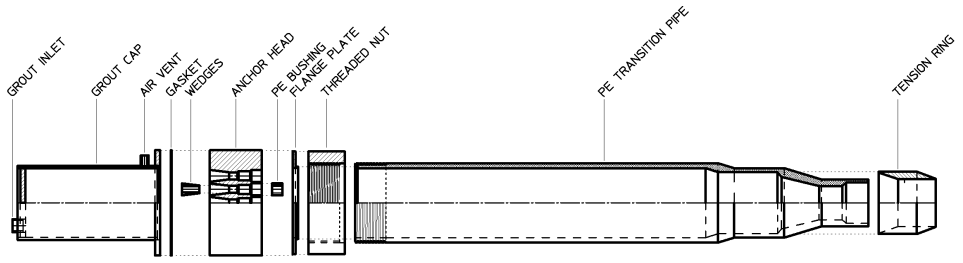

Figure 2.2 Exploded View of Deck Anchorage Elements for Cable-Stay Specimens (Phase 1)

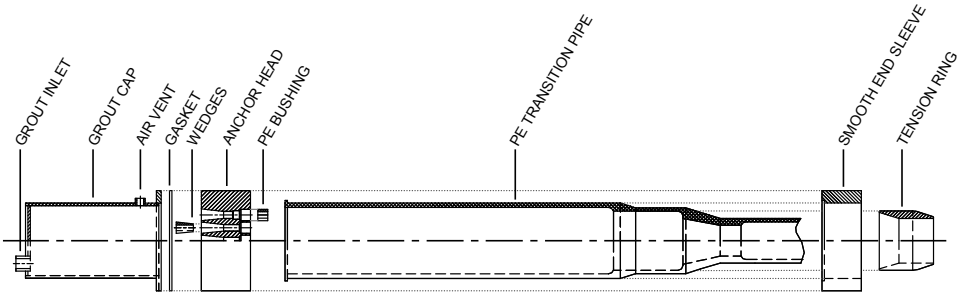

Figure 2.3 Exploded View of Deck Anchorage Elements for Cable-Stay Specimens (Phase 2)

Although the stay-cable specimens were tested horizontally, the terms "deck anchorage" and "tower anchorage" are used throughout this report. The tower end of the specimen was elevated during the grouting procedure (Figure 2.4). In all cases, the grout was pumped into the specimen through the grout cap at the deck (lower) end and the pumping operation was stopped when the grout emerged at the tower (upper) end. In most cases, the tower end of the specimen was also the live end during the stressing operation.

Figure 2.4 Position of Cable-Stay Specimen during Grouting

2.1.1 Geometry

The test specimens were constructed in an external, self-reacting frame, which was designed to resist the initial prestress force in the stay-cable specimen and the loads induced during the fatigue test. The distance between the outside faces of the load distribution plates, which were attached to the self-reacting frame, was 32′-7⅜″. The anchor head and either a threaded nut (phase 1) or a smooth end sleeve (phase 2) were positioned outside the load distribution plates at each end of the test specimens. In phase 1, two shims were also positioned between the load distribution plate and the threaded nut at the tower end. Therefore, the total length of the test specimens – measured between the outside faces of the anchor heads – was 34′-4⅞″ for the first four specimens (Figure 2.5) and 34′-0⅞″ for the remaining eight specimens (Figure 2.6). The two shims at the tower end represent the difference in the length of the specimens.

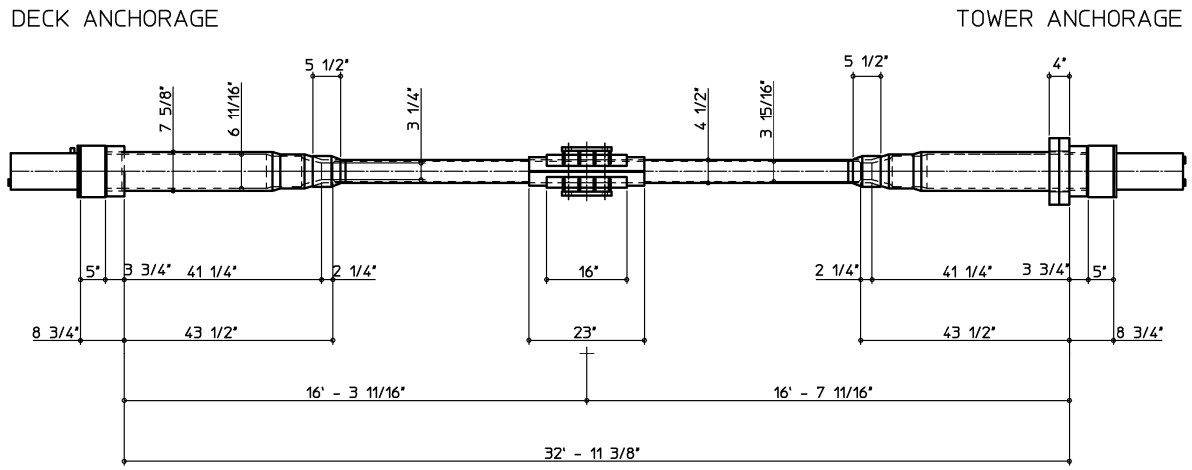

Figure 2.5 Dimensions of Cable-Stay Specimens (Phase 1)

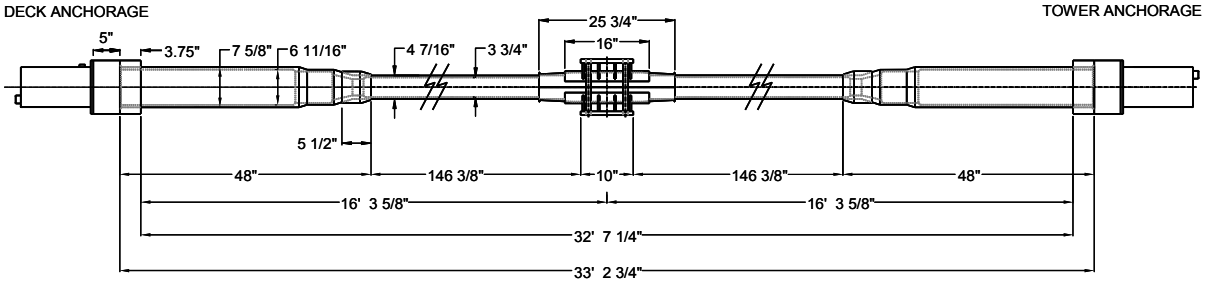

Figure 2.6 Dimensions of Cable-Stay Specimens (Phase 2)

The strands were parallel in the middle section of each specimen (between the tension rings) and fanned out between the tension ring and anchor head at each end to permit stressing. The inside diameter of the PE transition pipe at the anchor heads was 6 11⁄16 in. and the inside diameter of the PE pipe along the free length of the specimen was 3¾ in. The smallest inside diameter of the PE pipe was 3¼ in. and occurred within the tension ring, 45″ from the inside face of the anchor head. A helical spacer wire was positioned inside the PE pipe along the free length to ensure that all strands were encased in at least ¼″ of grout.

The test specimens were tested in a horizontal position, and transverse loads were applied at midspan of the self-reacting frame (Figure 2.7). A steel clamp was designed to connect the hydraulic actuator to the stay-cable specimen.

Figure 2.7 Test Setup for Stay-Cable Specimens

Because the anchorage region in the test specimens was essentially the same as in the prototype, the results from the first series of tests could be used to identify the locations along the prototype stay cables that are most susceptible to fatigue damage. Areas of interest include: (1) immediate vicinity of anchor head due to high bending stresses, (2) wedges due to local stresses, (3) tension ring due to fretting between strands, (4) along free length due to fretting between outer strands and spiral spacer wire, (5) within grout voids due to susceptibility to corrosion, and (6) any location where strands are inadvertently crossed due to fretting between strands.

2.1.2 Experimental Parameters

Six parameters were selected for investigation in the experimental program: (1) number of strands in the cross section, (2) type of strand, (3) amplitude of the displacements during the fatigue test, (4) configuration of the specimen (extent of grouting), (5) live end during stressing, and (6) construction defects. The configuration of each test specimen is summarized in Table 2.1, and the experimental parameters are summarized below.

2.1.2.1 Number of Strands

The anchor heads could accommodate nineteen strands, and eleven of the twelve specimens were constructed with nineteen strands. Specimen 6 was constructed with only thirteen strands to investigate the relationship between the number of strands and the stiffness of the test specimens.

Table 2.1 Experimental Parameters for Cable-Stay Specimens

Phase	Specimen	Number of Strands	Type of Strand	Displacement Amplitude (in.)	Configuration	Stressing End	Defects
1	1	19	A	±1.6	Grouted	Tower	Grout Void
	2	19	A	±1.6	Grouted	Tower	
	3	19	A	±1.6	Grouted	Deck	Crossed Strands
	4	19	A	±1.1	Grouted	Deck	
2	5	19	A	±1.6	Ungrouted	Tower	
	6	13	A	±1.6	Grouted	Tower	
	7	19	B	±1.6	Grouted	Tower	
	8	19	B	±1.6	Ungrouted	Tower	Misaligned Strand
	9	19	B	±1.6	Grouted	Tower	Grout Void
	10	19	B	±1.1	Grouted	Tower	
	11	19	B	±1.1	Hybrid	Tower	
	12	19	B	±1.6	Grouted	Tower	

2.1.2.2 Type of Strand

Two types of 0.6-in. strand were used in the experimental program and the properties of the strand are described in Appendix A. Strand A was used to construct the first six test specimens and Strand B was used to construct the second six test specimens. Strand B was fabricated specifically for cable-stay applications and the diameter of the center wire was slightly larger (Table A.2). Both types of strand satisfied the strength requirements in ASTM A416.

2.1.2.3 Amplitude of Displacements

During the fatigue tests, the displacements at midspan varied ±1.6 in. from the neutral position for nine of the specimens. This displacement amplitude was selected to induce a stress range of 35 to 45 ksi in the strand at the anchor head of the grouted specimens, based on the initial analyses of the test specimens (Dowd 2001). However, the strain in the strand was not measured during the fatigue tests of the cable-stay specimens, so the target stress range could not be confirmed. Three of the specimens were tested using a displacement range of ±1.1 in. to investigate the sensitivity of the fatigue life to the amplitude of the imposed displacements.

2.1.2.4 Specimen Configuration

Nine test specimens were grouted along their entire length and were representative of the prototype stays. Specimens 5 and 8 were grouted only in a 3-ft section at midspan where the hydraulic actuator was attached to the specimen. The ungrouted specimens were designed to investigate the contribution of the grout to the stiffness of the test specimens. Specimen 11 was grouted at both ends and in the middle. This hybrid specimen was intended to provide additional information about the contribution of the grout to the stiffness of the test specimens.

2.1.2.5 Live End for Stressing

Large differences in the number of wire breaks at the tower and deck ends were observed in Specimens 1 and 2. Both of these specimens were stressed from the tower end and grouted from the deck end. In an attempt to determine the relative importance of the stressing and grouting operations, Specimens 3 and 4 were stressed from the deck end and grouted from the deck end. The results were inconclusive, so the remaining specimens were stressed from the tower end and grouted from the deck end.

2.1.2.6 Construction Defects

Four specimens were assembled with construction defects, two were intentional and two were unintentional. An unintentional grout void was observed at the tower end of Specimen 1 at the conclusion of the fatigue test. Two factors contributed to the presence of the void: (a) six strands were positioned above the grout holes in the anchor head and (b) anti-bleed admixture was not used in the grout. In subsequent tests, the anchor heads were rotated 90° and anti-bleed admixture was used in the grout. Unintentional grout voids were not observed in any of the other specimens.

Specimen 3 was constructed with crossed strands. Two pairs of strands were intentionally crossed at both ends of the specimen between the tension ring and the anchor head. The strands were crossed to investigate the likelihood of fretting failures in the strand at locations of possible construction errors.

Specimen 8 was constructed with a misaligned strand near the tension ring at the deck end. This construction defect was not intentional. Because this specimen was ungrouted, evidence of fretting was observed during the fatigue test.

Specimen 9 was constructed with an intentional grout void at the tower end. TxDOT personnel had identified a grout void in one of the stays on the Fred Hartman Bridge. The specimen was used to investigate repair techniques and the possible impact of those techniques on the fatigue life of the stay cable.

2.1.3 Testing Program

Transverse loads were applied at midspan of the external loading frame during each fatigue test (Figure 2.7). The fatigue tests were run under displacement control, so the amplitude of the displacements did not vary as damage accumulated in the specimens. The test specimens were pushed downward and pulled upward from the neutral position. The force levels needed to impose the target displacements were monitored each day, and provided an indication of stiffness changes in the stay-cable specimens.

In the second phase of the experimental program, the static stiffness and fundamental natural frequency of the test specimens were measured at the beginning and end of each fatigue test.

2.1.4 Acoustic Monitoring

During each fatigue test, the acoustic response of the test specimens was monitored using a SoundPrint® system from Pure Technologies Ltd. This is the same type of system that is currently used to monitor the response of the stay cables on the Fred Hartman and Veterans Memorial Bridges. The acoustic sensors were set in a trigger mode, which was calibrated to detect wire breaks in the stay-cable specimens. The system provided a time stamp and location for each acoustic event.

2.1.5 Autopsy

At the conclusion of each fatigue test, the specimen was disassembled. The condition of the grout, extent of corrosion, and the number and location of wire breaks were documented. Most of the wire breaks were caused by fretting fatigue, and the fracture surface of each wire was examined to determine the source of the failure. The observed wire breaks were also compared with the wire breaks detected by the acoustic sensors to evaluate the sensitivity of the acoustic monitoring system.

2.2 BENDING FATIGUE TESTS OF SMALL-DIAMETER SPECIMENS

The small-diameter specimens were designed to be simple representations of grouted stay cables on the Fred Hartman Bridge. The specimens were constructed with two, 0.6-in. strands, which were parallel along the entire length (Figure 2.8). The dimensions of the anchor heads were the same as the anchor heads for the stay-cable specimens, except the maximum number of strands that could be accommodated was four, rather than nineteen for the cable-stay specimens (Figure C.4). The strands were assembled within post-tensioning (PT) duct, which is a blend of polyethylene and polypropylene. The strands were stressed to 50% of the minimum breaking strength of the strand. After stressing, the PT duct was filled with a portland cement-based grout. The small-diameter specimens were constructed and tested in a horizontal position.

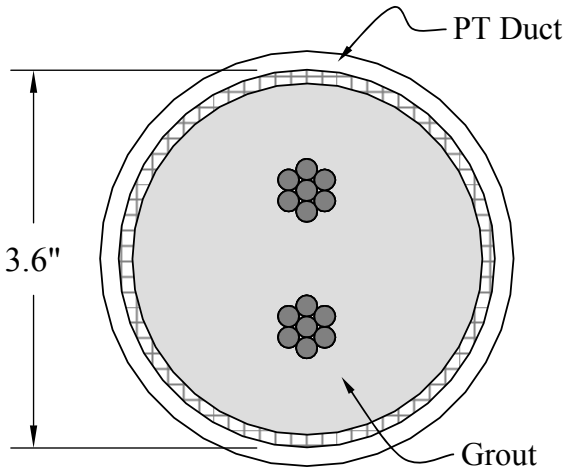

Figure 2.8 Cross-Sectional Geometry of Small-Diameter Specimens

2.2.1 Geometry

The ends of the small-diameter specimens were supported by independent reaction frames, which were bolted to the strong floor in Ferguson Laboratory (Figure 2.9). The distance between the outside faces of the load distribution plates was 49′-0″. Because the strands were parallel along the entire length, the anchor heads were positioned directly against the load distribution plates, and tension rings were not used in the small-diameter specimens.

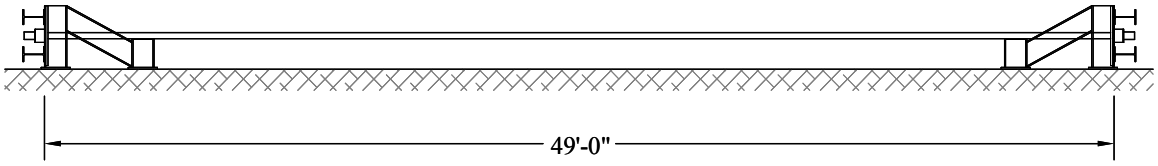

Figure 2.9 Geometry of Small-Diameter Specimens

The inner diameter of the PT duct was 3.35 in. and the wall thickness was approximately 3⁄16 in. The duct had transverse ribs and longitudinal flow channels. The outside diameter, measured to the outside of the ribs, was 4.0 in.

Initially, the transverse fatigue loads were applied at midspan of Specimen 1 (Figure 2.10). After more than forty days of testing, the location of the loading point was shifted toward the north quarter point (Figure 2.11) for the conclusion of this test and for all subsequent tests. Due to the simple geometry of the small-diameter test specimens, fatigue damage was expected to occur in the immediate vicinity of the north anchor head.

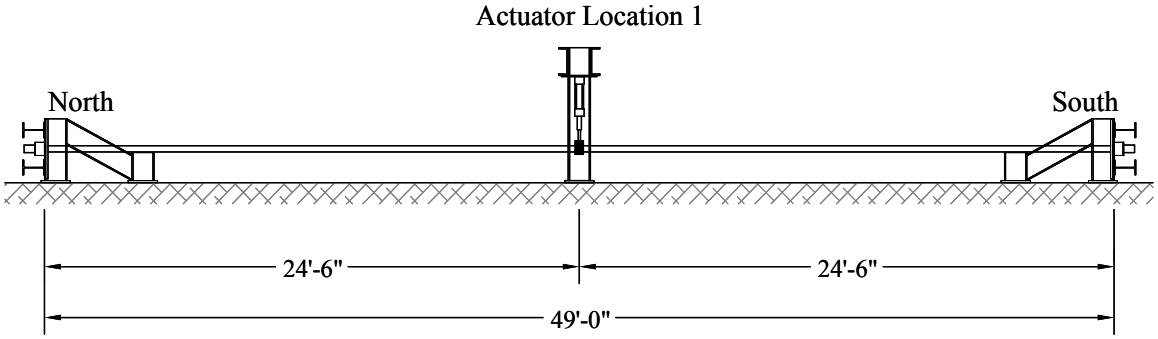

Figure 2.10 Original Loading Configuration for Small-Diameter Specimens

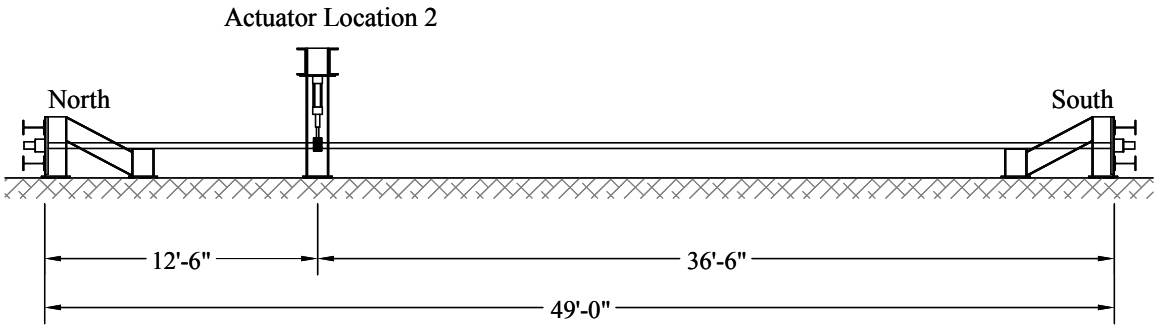

Figure 2.11 Final Loading Configuration for Small-Diameter Specimens

2.2.2 Experimental Parameters

All three test specimens were nominally identical. The primary difference was the number of strain gages used to capture the response of the strand (Table 2.2). In addition, the amplitude of the displacements during the fatigue test was slightly larger for Specimen 3.

Table 2.2 Experimental Parameters for Small-Diameter Specimens

Specimen	Number of Strain Gages	Fatigue Limits		Displacement Amplitude
		Minimum (in.)	Maximum (in.)	
1*	10	1.35	2.60	1.25
2	16	1.35	2.60	1.25
3	32	0.80	2.20	1.40

* First 3.4 million cycles for Specimen 1 were run under load control with the loads applied at midspan.

2.2.3 Testing Program

The hydraulic actuator used to test the small-diameter specimens did not have an internal displacement transducer. Therefore, the fatigue tests for Specimen 1 were started under force control. The test was not as stable as desired, so an external displacement transducer was added to the system after approximately 3.4 million cycles – the same time that the loading frame was moved near the north quarter point.

For the remainder of the fatigue test for Specimen 1 and for all subsequent tests, the fatigue test was run under displacement control. To maintain stability of the test system, the specimens were pulled upward only. The minimum displacement during each fatigue test was above the neutral position for the specimen.

Periodically during the fatigue tests of the small-diameter specimens, the static stiffness and strain response was measured. In addition, the hydraulic actuator was disconnected from the specimen and the

first six natural frequencies were measured. The objective of these periodic tests was to quantify changes in the structural characteristics of the specimens as damage accumulated.

2.2.4 Acoustic Monitoring

During each fatigue test, the acoustic response of the test specimens was monitored using a SoundPrint® system from Pure Technologies Ltd. The acoustic sensors were set in a trigger mode, which was calibrated to detect wire breaks in the small-diameter specimens. The system provided a time stamp and location for each acoustic event.

2.2.5 Autopsy

At the conclusion of each fatigue test, the specimen was disassembled. The number and location of wire breaks were documented. The observed wire breaks were compared with the wire breaks detected by the acoustic sensors to evaluate the sensitivity of the acoustic monitoring system.

CHAPTER 3: FATIGUE RESPONSE OF STAY-CABLE SPECIMENS

Each of the twelve stay-cable specimens resisted more than two million fatigue cycles during the experimental phase of this research (Figure 3.1). The criterion for stopping each fatigue test was not established in advance. In some cases, the test was terminated after a large number of wire breaks had been detected. In other cases, the test was terminated after the specimen survived a large number of fatigue cycles with relatively few wire breaks. The number of wire breaks experienced by the test specimens varied widely (Figure 3.2): zero wires fractured during the fatigue test of Specimen 5, while one hundred fifty wires fractured during the fatigue test of Specimen 12.

The results of the fatigue tests are summarized in Table 3.1. It should be noted that damage within the test specimens accumulated gradually with the number of loading cycles at the beginning of the fatigue tests (Figure 3.3). The presence of one or two wire breaks had essentially no impact on the structural integrity of the stay-cable specimens. However, the rate of damage did increase during the fatigue tests, and this increase occurred at a different number of loading cycles for different specimens and for different locations within the same specimen.

The extent of the observed damage in the stay-cable specimens is summarized in Section 3.1, the influence of the experimental parameters on the fatigue life is discussed in Section 3.2, the mechanisms that caused failure of the individual wires in the strands are discussed in Section 3.3, the relationship between the structural integrity of the test specimens and the number of wire breaks is presented in Section 3.4, and the sensitivity of the acoustic monitoring system is summarized in Section 3.5. Detailed discussions of the response of each specimen and the observed damage are documented in Appendix D.

Table 3.1 Summary of Fatigue Tests of Stay-Cable Specimens

ID	Specimen Type	Number of Strands	Displacement Amplitude (in.)	Number of Cycles	Number of Observed Wire Breaks*			
					Deck	Center	Tower	Total
1	Grouted	19	±1.6	2,808,398	0	11	14	25
2	Grouted	19	±1.6	2,865,103	1	16	52	69
3	Grouted	19	±1.6	4,961,560	13	62	9	84
4	Grouted	19	±1.1	8,775,245	3	0	28	31
5	Ungrouted	19	±1.6	5,211,106	0	0	0	0
6	Grouted	13	±1.6	6,486,024	0	11	17	28
7	Grouted	19	±1.6	2,246,869	17	65	37	119
8	Ungrouted	19	±1.6	6,200,593	2	0	2	4
9	Grouted	19	±1.6	2,634,309	3	61	12	76
10	Grouted	19	±1.1	5,614,211	8	21	23	52
11	Hybrid	19	±1.1	4,640,450	7	9	0	16
12	Grouted	19	±1.6	2,703,958	29	86	35	150

* Multiple breaks in the same wire are included in the totals.

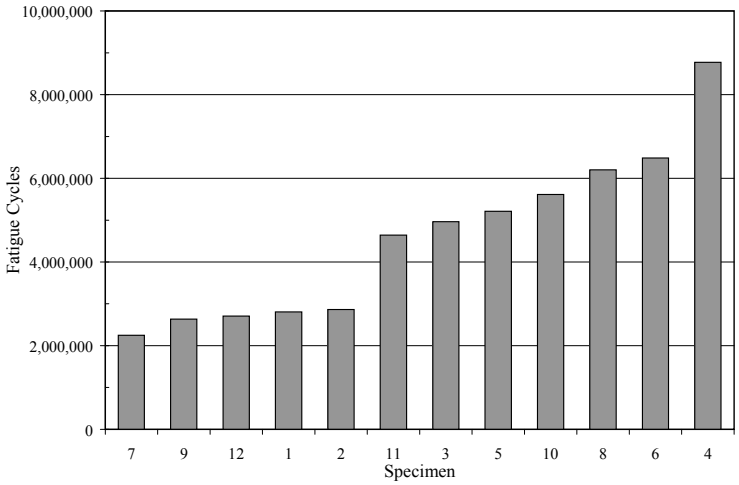

Figure 3.1 Number of Fatigue Cycles for Cable-Stay Specimens

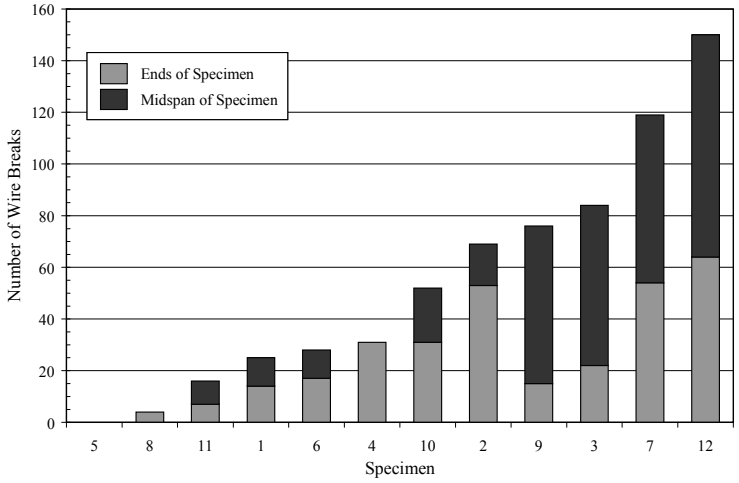

Figure 3.2 Number of Wire Breaks Observed in Cable-Stay Specimens

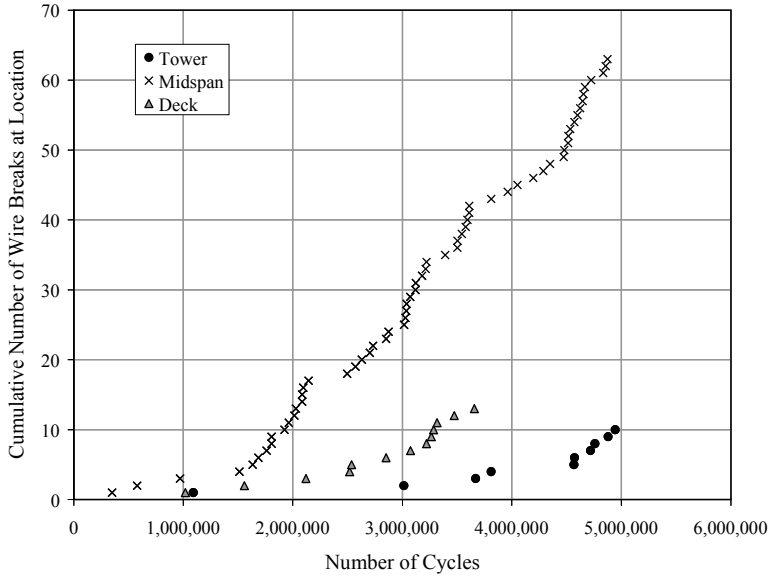

Figure 3.3 Wire Breaks Detected from Acoustic Data – Specimen 3

3.1 OBSERVED DAMAGE

At the conclusion of each fatigue test, the specimen was disassembled and the damage to the strand and grout was documented (Appendix D). The damage was concentrated near the ends of the specimens and at midspan, where the transverse loads were applied.

Three hundred eight wire breaks were identified at the ends of the cable-stay specimens. Nearly 50% of the wire breaks (Figure 3.4) occurred within the anchor head, with more than 15% within the wedges. Approximately 25% of the wire breaks were located within the threaded nut used in phase 1 or the smooth end sleeve used in phase 2. The remaining wire breaks were distributed along the transition region. All wire breaks occurred within 20 in. of the inside face of the anchor head.

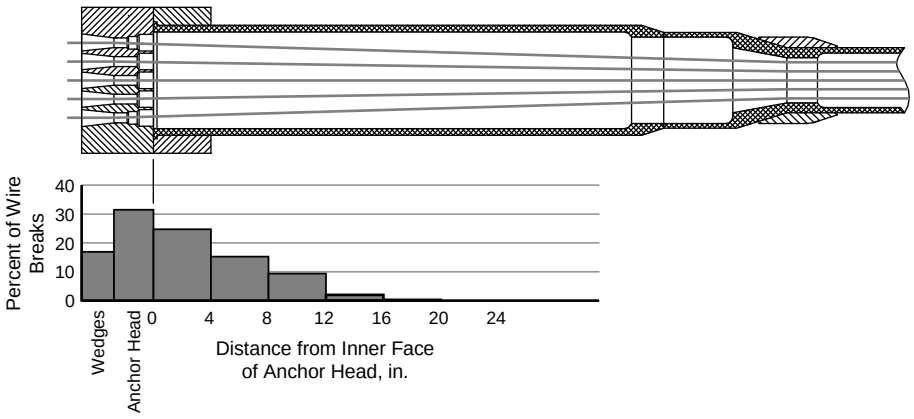

Figure 3.4 Distribution of Observed Wire Breaks at Ends of Stay-Cable Specimens

In spite of the congestion of the strands at the tension ring, no wire breaks were identified in this region. In addition, no wire breaks were identified in the vicinity of the intentionally crossed strands in Specimen 3.

Three hundred forty-two wire breaks were observed at midspan of the test specimens (Figure 3.5). Nearly 85% of the wire breaks occurred within the metal clamp used to attach the hydraulic actuator to the test specimens, with more than 50% of the wire breaks directly beneath the head of the actuator. Only 5% of the wire breaks occurred beyond the PE cushion and all wire breaks were within 20 in. of midspan.

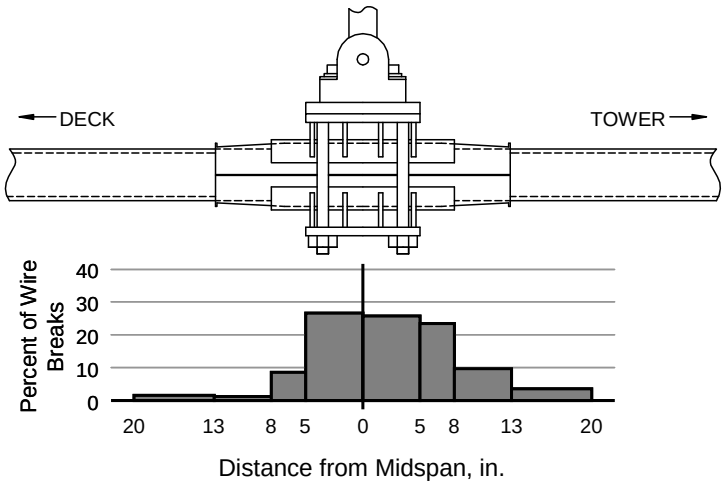

Figure 3.5 Distribution of Wire Breaks at Midspan of Stay-Cable Specimens

The distributions of wire breaks within the cross sections at each end and at midspan are summarized in Figure 3.6 through Figure 3.8. For the grouted test specimens, the wire breaks at the ends tended to occur in the layers of strand at the top or bottom of the cross section. Only in Specimens 1, 2, 6, and 12 did the wire breaks occur in an inner layer of strand. The large number of wire breaks in the top and bottom layers of Specimens 2 and 12 likely caused the damage to spread to the inner layers. However, in Specimen 1, the presence of the grout void seems to have influenced the damage pattern. Specimen 8, which was ungrouted, was the only specimen to experience wire breaks in the middle layer of strands.

At midspan, wire breaks in the inner layers of strands were more common, especially when most of the wires in the outer layer fractured. Corroded fretting product was often observed in the vicinity of the wire breaks (Figure 3.9). The amount of observed corrosion tended to increase as the number of wire breaks increased.

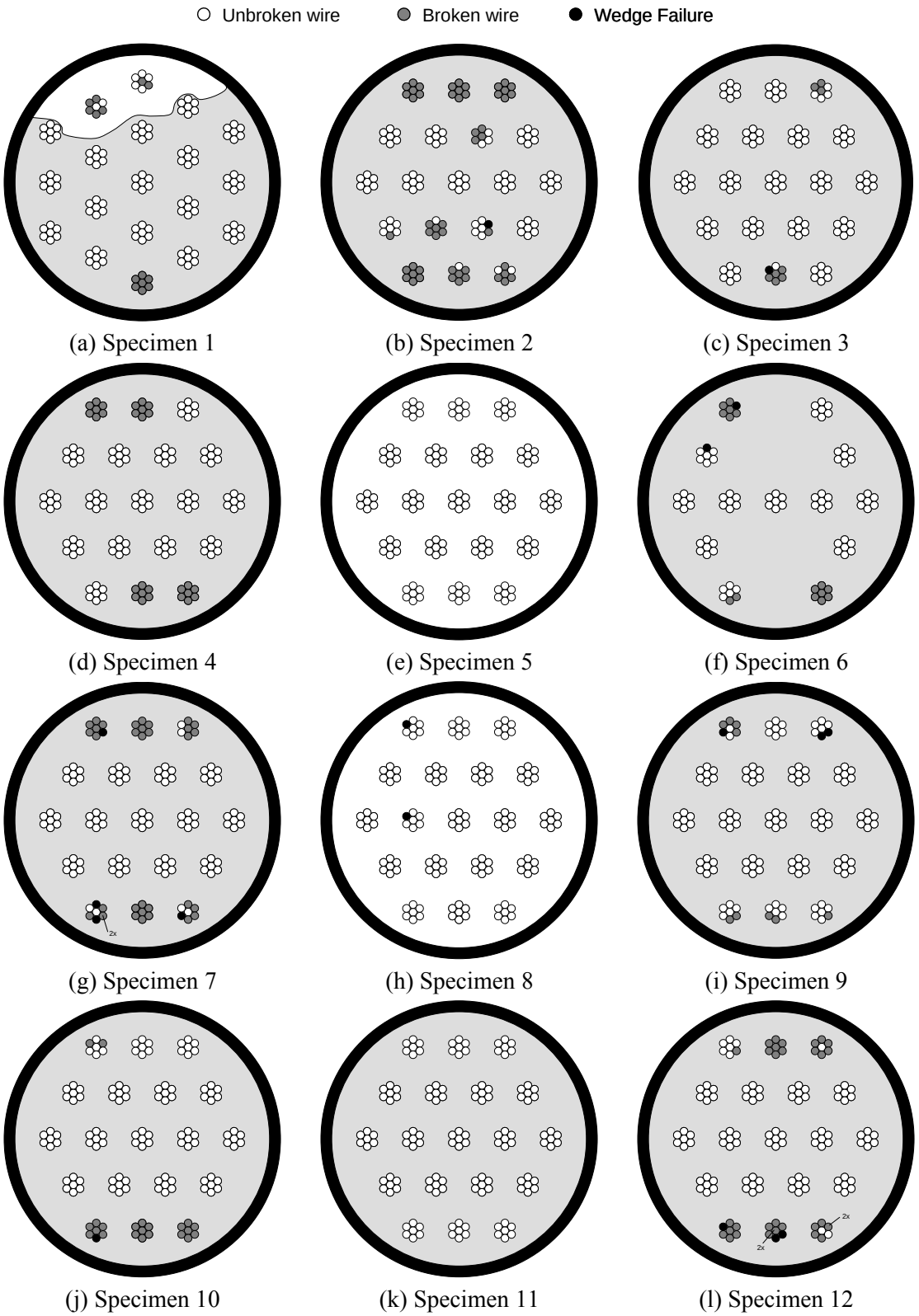

(a) Specimen 1 (b) Specimen 2 (c) Specimen 3

(d) Specimen 4 (e) Specimen 5 (f) Specimen 6

(g) Specimen 7 (h) Specimen 8 (i) Specimen 9

(j) Specimen 10 (k) Specimen 11 (l) Specimen 12

Figure 3.6 Summary of Wire Breaks at Tower End of Stay-Cable Specimens

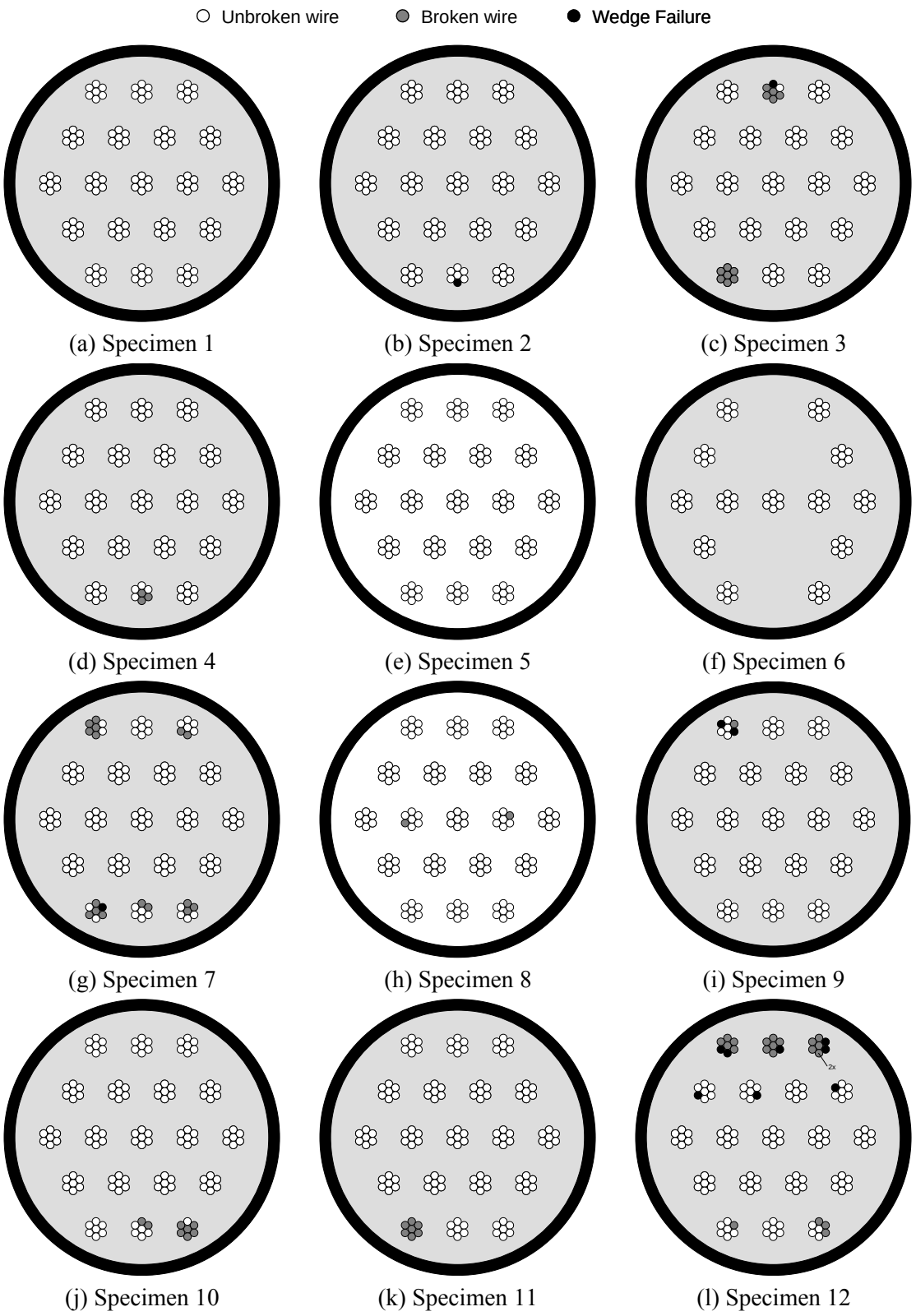

Figure 3.7 Summary of Wire Breaks at Deck End of Stay-Cable Specimens

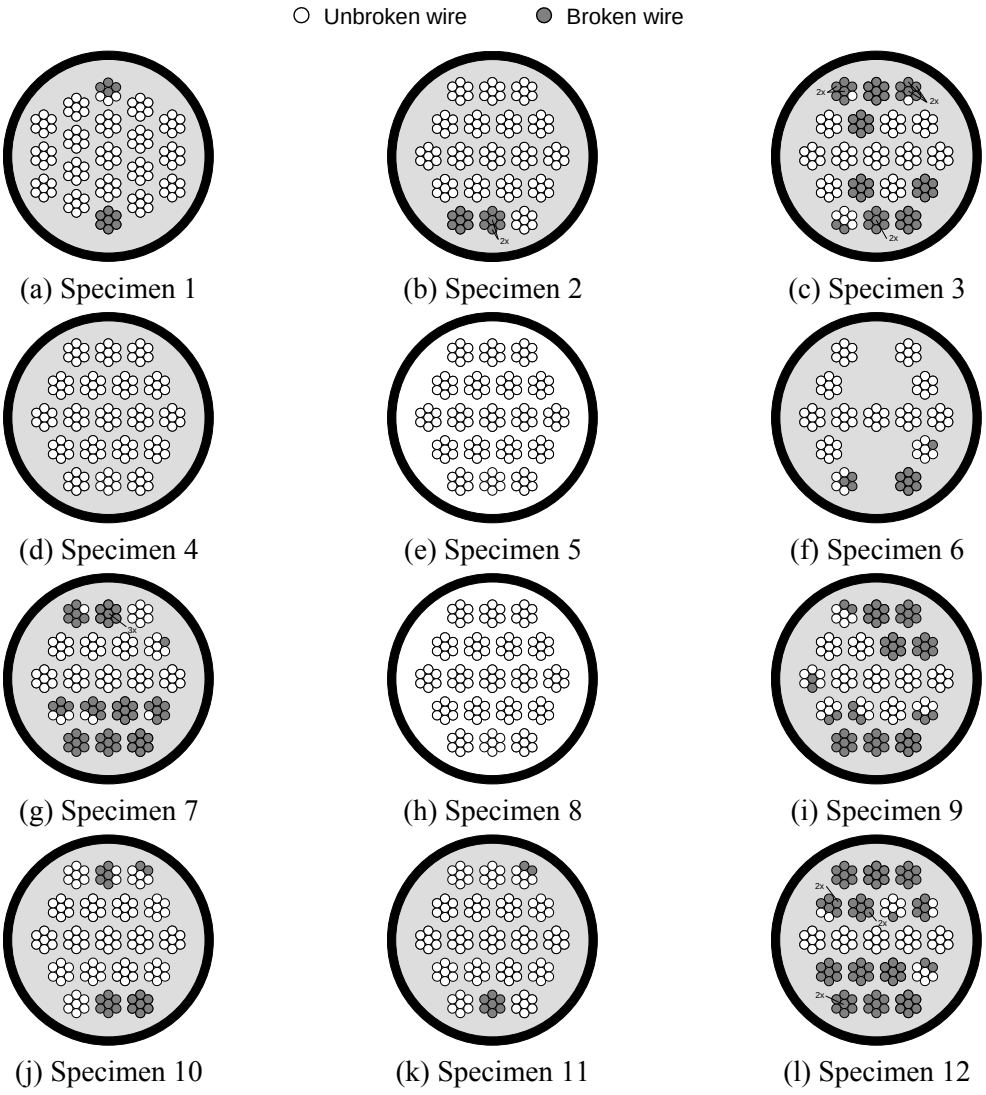

Figure 3.8 Summary of Wire Breaks at Midspan of Stay-Cable Specimens

Figure 3.9 Corroded Fretting Product on Surface of Strand at Midspan – Specimen 12

In the vicinity of wire breaks, the grout was often severely cracked (Figure 3.10 and Figure 3.11). Longitudinal cracks in the grout were characteristic of wire breaks, whereas fine circumferential cracks were observed in regions that were undamaged (Figure 3.12). These circumferential cracks were representative of cracks observed along the free length of the cables on the Fred Hartman Bridge (Figure 3.13). The width of the circumferential cracks in the test specimens tended to increase with time as the grout was exposed to the environment. These cracks were believed to be caused by shrinkage of the grout.

Figure 3.10 Condition of Grout at Deck End Immediately after Removing PE Pipe – Specimen 10

Figure 3.11 Longitudinal Cracks in Grout, Corrosion of Strand, and Wire Breaks near Midspan of Specimen 1

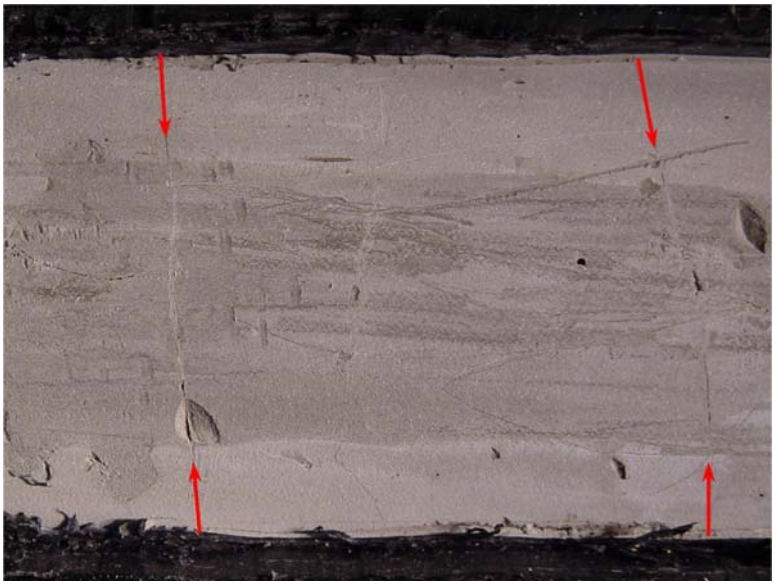

Figure 3.12 Hairline Transverse Grout Cracks – Specimen 1

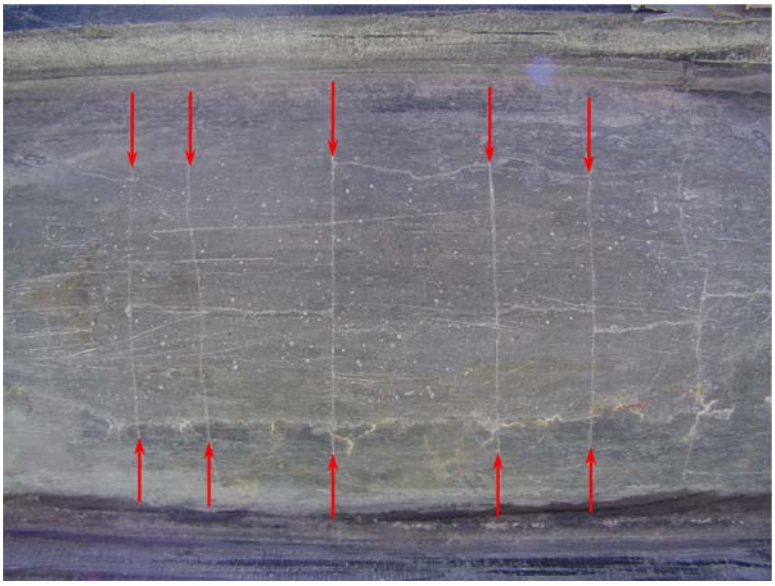

Figure 3.13 Hairline Transverse Grout Cracks - Fred Hartman Bridge

The strands were observed to be most severely congested in the vicinity of the tension ring (Figure 3.14). The strands around the perimeter of the cross section were not encased in grout at this location.

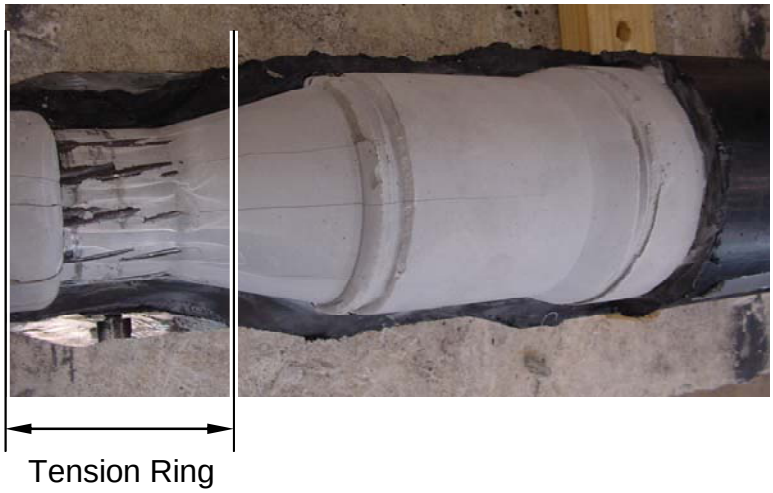

Figure 3.14 Exposed Strand at Tension Ring – Specimen 1

3.2 INFLUENCE OF EXPERIMENTAL PARAMETERS ON FATIGUE LIFE

Among the experimental parameters considered in this set of experiments, the fatigue life of the cable-stay specimens appeared to be most sensitive to two. The ungrouted specimens (Specimens 5 and 8) experienced far fewer wire breaks than the grouted specimens (Figure 3.2). In addition, the fatigue life was considerably longer for the three specimens that were subjected to lower-amplitude displacement cycles during the fatigue tests (Specimens 4, 10, and 11).

The lateral stiffness of the test specimens was used as quantitative means of comparing the fatigue response. The response of the specimens was not monitored continuously during the fatigue tests, but key data were recorded on a daily basis. The fatigue tests were run under displacement control; therefore, the applied forces necessary to achieve the target displacement levels provide an indication of the lateral stiffness. Representative data, including the variation of the peak applied loads and the occurrence or wire breaks, are plotted in Figure 3.15 as a function of the number of loading cycles. Data for all test specimens are presented in Appendix D. The average of the applied loads in the two directions divided by the peak displacement is defined as the average dynamic stiffness.

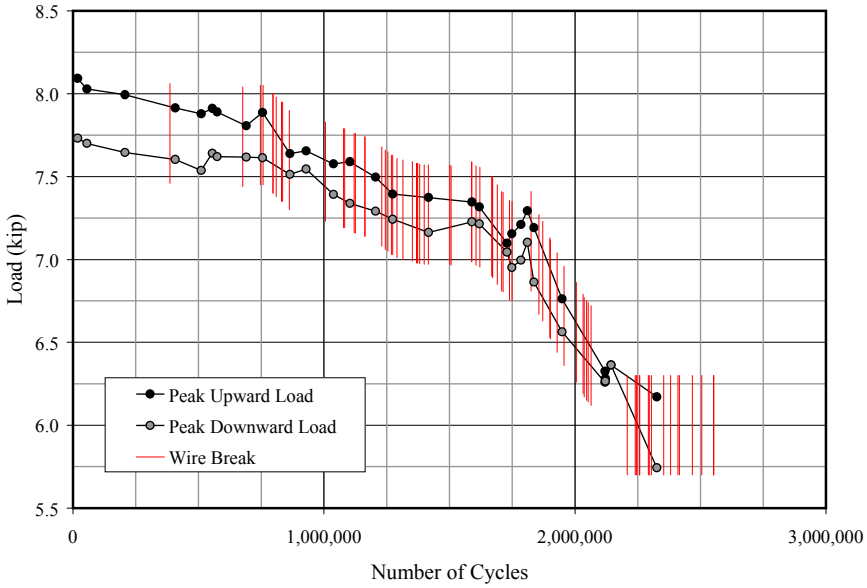

Figure 3.15 Variation of Applied Loads during Fatigue Test of Representative Cable-Stay Specimen

In order to correct for variations in the stiffness due to grouting and number of strands, the normalized dynamic stiffness was used to compare specimen response. The value of the average dynamic stiffness at any point in time was divided by the average dynamic stiffness at the beginning of the fatigue test.

The response of six grouted test specimens subjected to displacements of ±1.6 in. is plotted in Figure 3.16. During the first 500,000 cycles, the changes in stiffness were modest, but by 1.5 million cycles four of the six specimens experienced a 5% reduction in the average dynamic stiffness. The change in stiffness increased sharply between 1.5 and 2 million cycles. Three of the specimens (Specimens 7, 9 and 12) experienced between 15 and 20% reductions in stiffness by 2 million cycles. The damage accumulation was slower in Specimens 1 and 2, which experienced between 5 and 10% reductions in stiffness by 2.5 million cycles. Specimen 6 exhibited the best behavior of the group.

The reductions in dynamic stiffness for the grouted specimens seem to be closely related to the number of wire breaks experienced at midspan. Specimens 7, 9, and 12 experienced more than 60 wire breaks at midspan (Figure 3.8) and exhibited the most pronounced reductions in dynamic stiffness. In contrast, Specimens 1, 2, and 6 experienced 16 or fewer wire breaks at midspan and exhibited better fatigue performance. These trends seem to indicate that Strand A exhibited better bending fatigue performance that Strand B, but data from Specimen 3 are not available to confirm this trend.

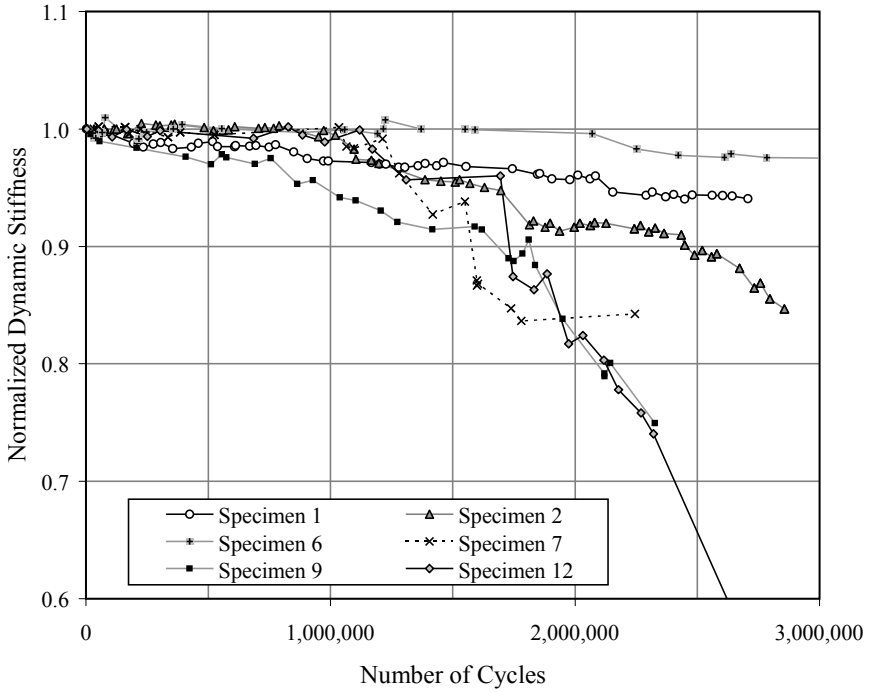

Figure 3.16 Variation in Average Dynamic Stiffness of Grouted Specimens with 1.6-in. Displacement Amplitude

The response of two grouted test specimens subjected to displacements of ±1.1 in. is plotted in Figure 3.17. The average dynamic stiffness of these specimens remained essentially constant for the first 3 million cycles. The stiffness decreased rapidly between 3.5 and 4.5 million cycles. Data from Specimen 4 are not available to evaluate the sensitivity of the fatigue response to the type of strand.

The response of the two ungrouted specimens is plotted in Figure 3.18. Both specimens experienced more than 5 million cycles with less than a 10% decrease in the average dynamic stiffness. These data also support the hypothesis that Strand A exhibited better bending fatigue performance than Strand B, but one of the strands in Specimen 8 was misaligned, and significant fretting damage was observed during the fatigue test near the tension rings (Figure 3.19). However, in spite of this observed damage, the wire breaks occurred within the anchor head for Specimen 8.

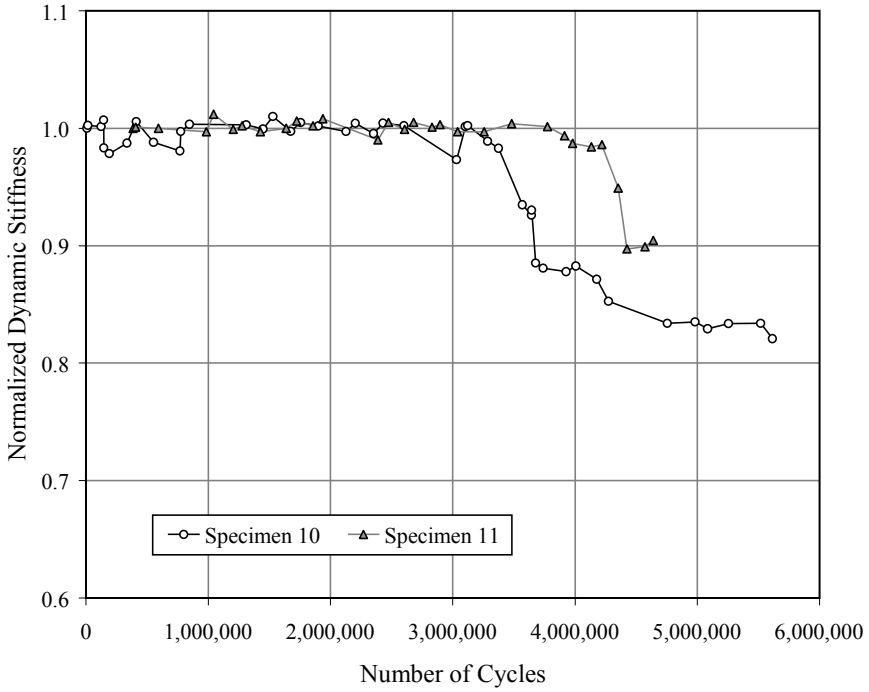

Figure 3.17 Variation in Average Dynamic Stiffness of Grouted Specimens with 1.1-in. Displacement Amplitude

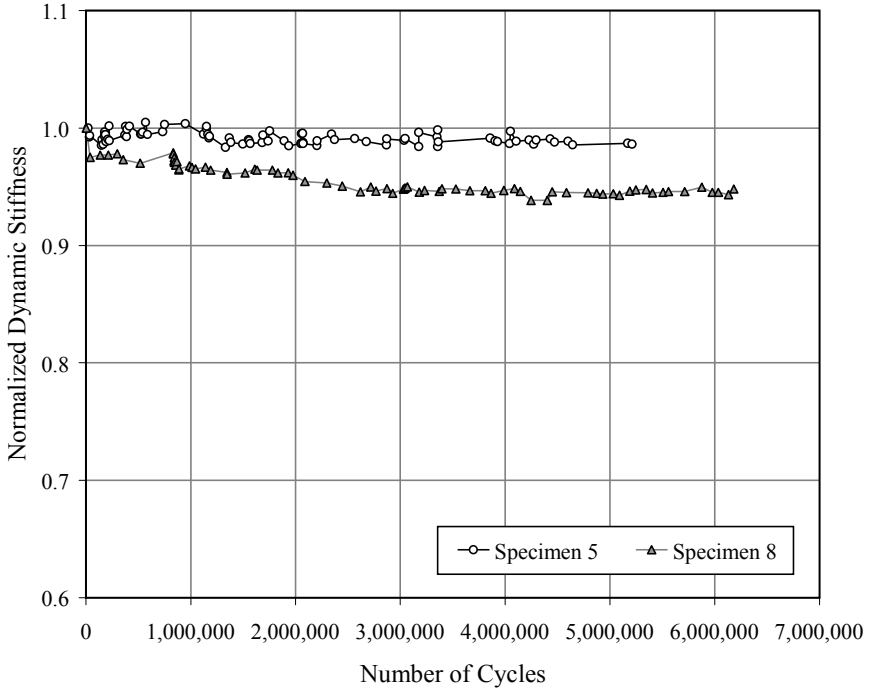

Figure 3.18 Variation in Average Dynamic Stiffness of Ungrouted Specimens

Figure 3.19 Reduction of Cross-Sectional Area of Strands Due to Fretting – Specimen 8

3.3 FAILURE MECHANISMS IN WIRES

During the autopsy of the test specimens, the fracture surface of each wire break was examined using a microscope. The wire breaks were caused primarily by fretting fatigue, which occurs when two adjacent wires rub against each other under cyclic loading. The initiation of a fatigue crack occurs at the contact point between the two wires; the fatigue crack continues to grow outward in a semi-circular manner until the loss in cross-sectional area due to the crack is sufficient to cause a tension failure.

Two types of fretting fatigue failures were most common. The first type occurred due to fretting between the center wire and an outer wire, as shown in Figure 3.20. This type of fretting can lead to fracture of the center wire, the outer wire, or both wires at the contact point. The second type of fatigue failure was due to fretting between two adjacent outer wires as shown in Figure 3.21. Failures caused by fretting of adjacent wires in the strand, center-outer and outer-outer, represented nearly 90% of the observed wire breaks.

A third, less common type of fatigue failure was observed where the fatigue crack initiated at a point that was not in contact with other wires in the strand. The point where the first tooth on the wedge engaged the strand often served as the initiation point for this type of crack (Figure 3.22 through Figure 3.24). This type of fretting failure represented approximately 6% of the total.

Occasionally fatigue failures were also observed to initiate at a point where an exterior wire was not in contact with the other wires in the strand. It is unknown what caused this type of failure, although possible sources are corrosion, defects on the wire, or fretting with the helical spacer wire (Figure 3.25). The remaining 5% of the wire breaks were in this category.

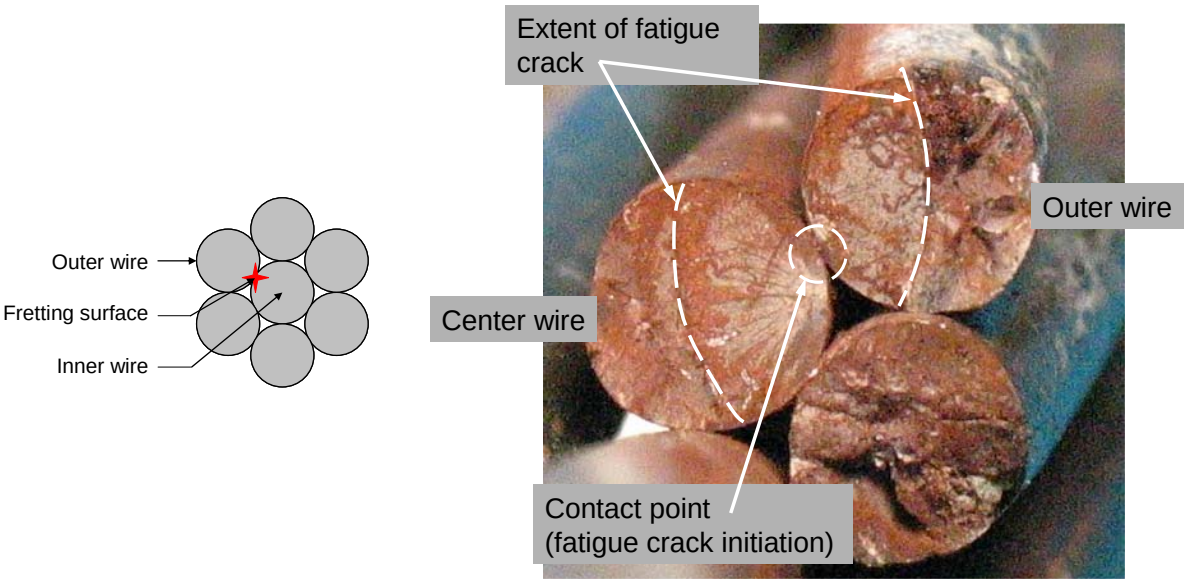

Figure 3.20 Fretting between Center Wire and an Outer Wire

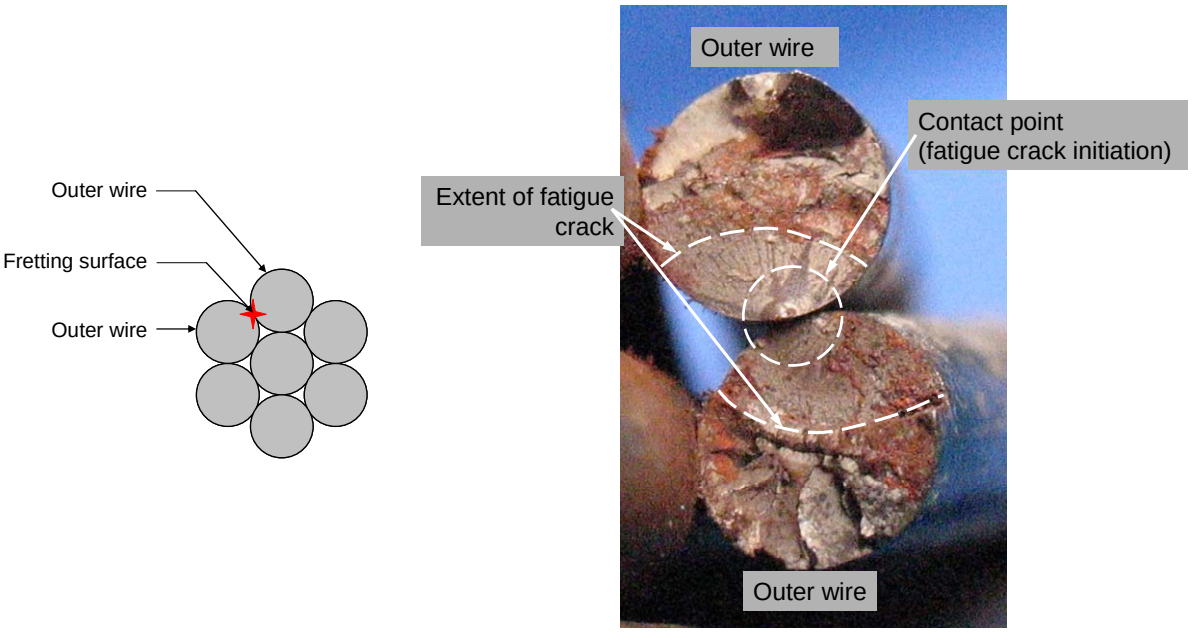

Figure 3.21 Fretting between Adjacent Outer Wires

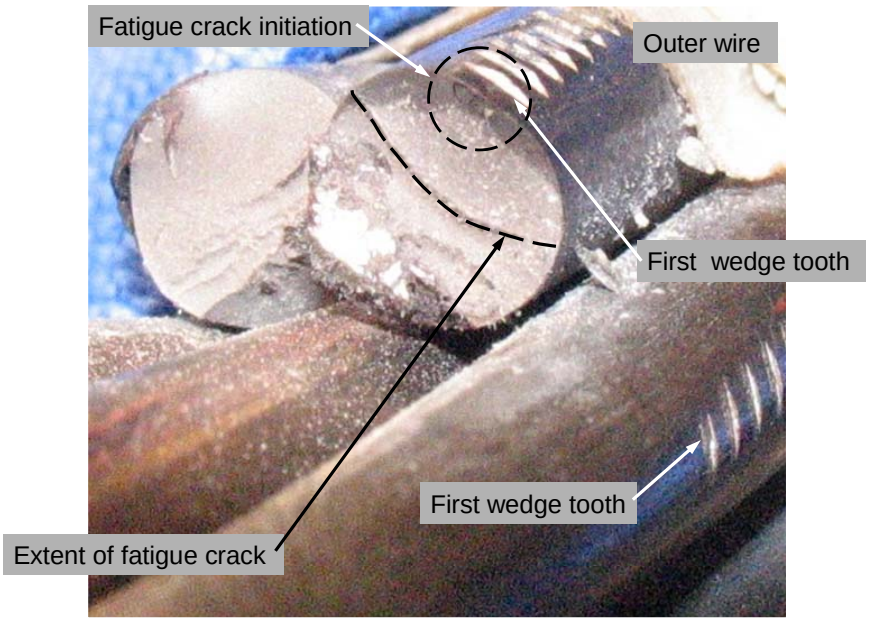

Figure 3.22 Isolated Fatigue Failure at Wedge

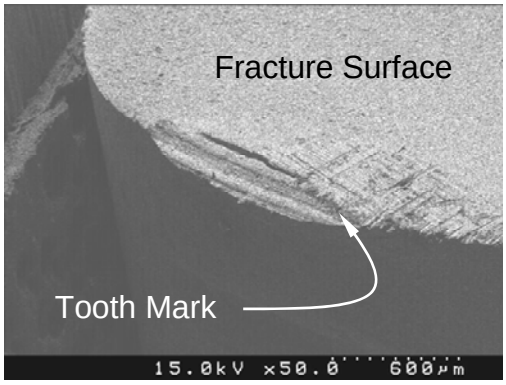

Figure 3.23 Fracture Initiation

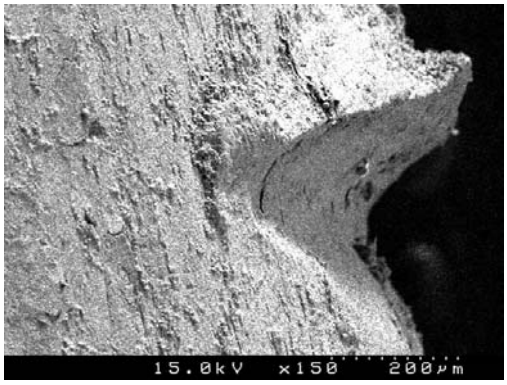

Figure 3.24 Typical Tooth Mark

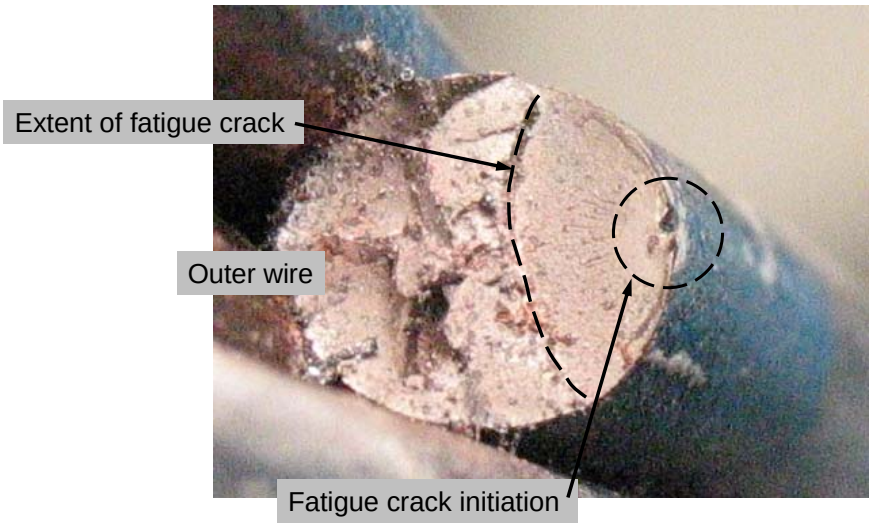

Figure 3.25 Fatigue Failure Caused by External Source

3.4 LOSS OF STRUCTURAL INTEGRITY

As discussed in Section 3.2, the average dynamic stiffness can be used to evaluate changes in the structural characteristics of the specimens as damage accumulated. The initial and final values of the average dynamic stiffness are reported in Table 3.2, as is the maximum number of wire breaks at a single location. In several of the test specimens, multiple breaks occurred in the same wire over very short distances. As discussed in Appendix D, the tension in the wire dropped to zero after the first wire break, and subsequent wire breaks did not exhibit a tensile failure, but were characterized by fatigue crack growth only. Therefore, the number of wire breaks reported in Table 3.2 for Specimens 3, 6, and 12 is less than the total number of wire breaks observed during the autopsy (Table 3.1), but represents the loss of cross-sectional area available to resist tension in the stay.

The ratio of the final average dynamic stiffness to the initial average dynamic stiffness is defined as the average dynamic stiffness ratio. The average dynamic stiffness ratio for the grouted specimens is plotted in Figure 3.26 as a function of the number of wire breaks at one location divided by the total number of wires. This parameter is of interest, because the data from the acoustic sensor systems installed on the Fred Hartman and Veterans Memorial Bridges can be used to track the number of wire breaks at a single location. Although the data are sparse, a loss of approximately 10% of the wires at a given location corresponds to a 10% loss in lateral stiffness.

Table 3.2 Summary of Variations in Stiffness and Frequency during Fatigue Tests of Cable-Stay Specimens

Specimen	Average Dynamic Stiffness		Average Dynamic Stiffness Ratio	Fundamental Frequency		Frequency Ratio	Wire Breaks at One Location*		
	Initial	Final		Initial	Final		Location	Number	Percent
	(kip/in.)	(kip/in.)		(Hz)	(Hz)				
1	4.73	4.45	0.941	—	12.0	—	Tower	14	10.5
2	4.75	4.03	0.847	12.5	11.5	0.920	Tower	52	39.1
3	—	—	—	—	—	—	Midspan	55	41.4
4	—	—	—	12.5	—	—	Tower	28	21.1
5	3.90	3.84	0.986	13.8	13.5	0.978	—	0	0
6	3.14	2.86	0.914	11.5	11.0	0.957	Tower	17	18.7
7	4.79	4.04	0.843	13.3	11.1	0.835	Midspan	63	47.4
8	4.11	3.90	0.948	13.9	13.4	0.964	Tower	2	1.5
9	4.97	3.72	0.750	12.5	10.5	0.840	Midspan	61	45.9
10	4.62	3.79	0.821	13.0	11.8	0.908	Tower	23	17.3
11	4.55	4.11	0.904	15.0	13.3	0.887	Midspan	9	6.8
12	4.75	2.70	0.568	13.1	10.0	0.763	Midspan	83	62.4

* Multiple breaks in the same wire are not included in the totals.

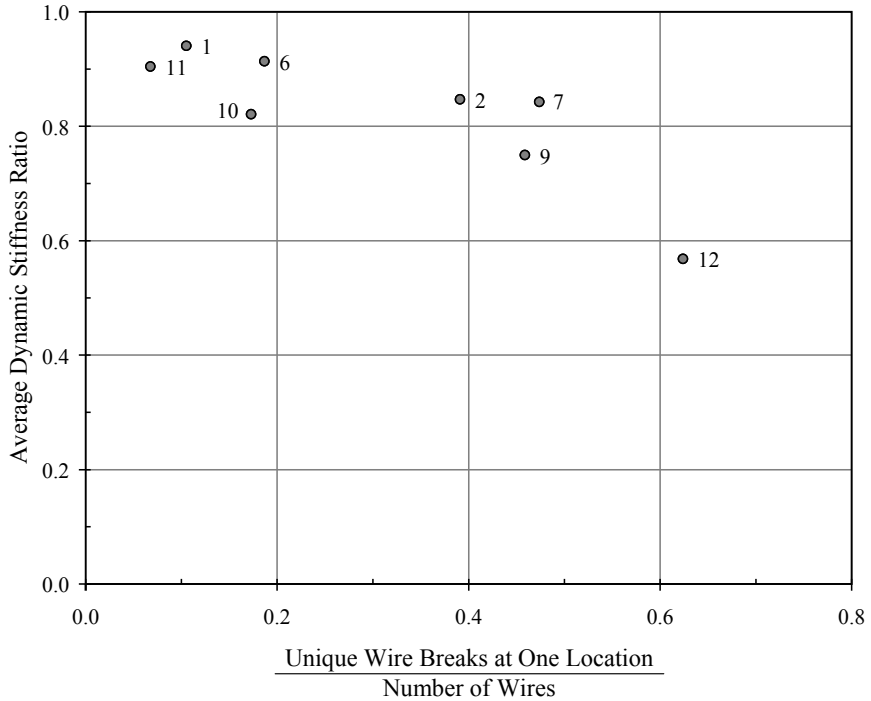

Figure 3.26 Sensitivity of Dynamic Stiffness Ratio to Number of Wire Breaks

The measured values of the fundamental natural frequency at the start and end of the fatigue tests are also reported in Table 3.2. Frequency data are much easier to measure in the field than stiffness data. However, as indicated in Figure 3.27, the natural frequencies are not as sensitive to fatigue damage as the lateral stiffness ratios. A 10% change in the fundamental frequency corresponds to between 10 and 40% loss of wires at the critical location.

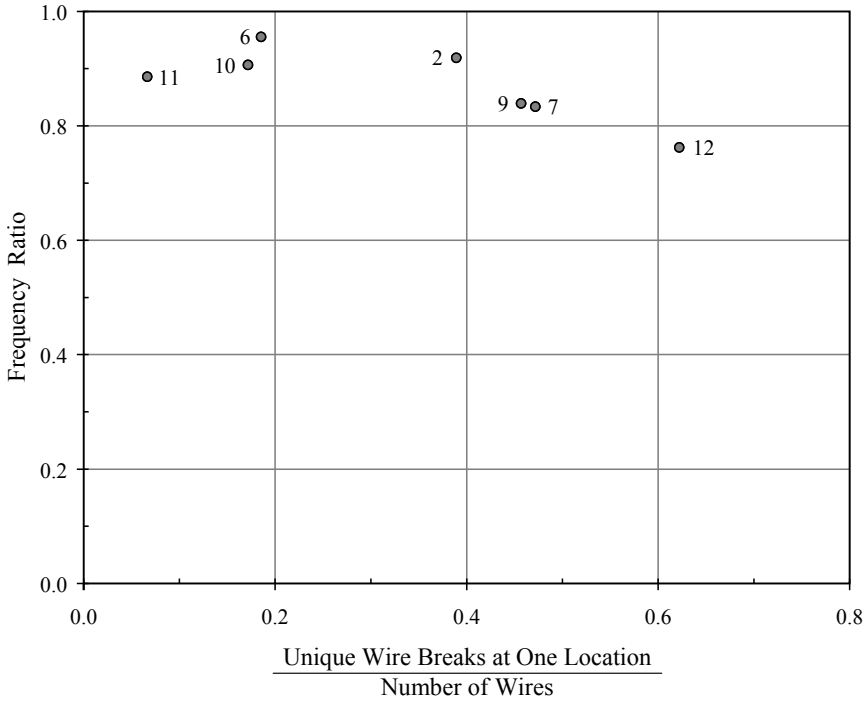

Figure 3.27 Sensitivity of Fundamental Frequency Ratio to Number of Wire Breaks

3.5 SENSITIVITY OF ACOUSTIC MONITORING SYSTEM

The acoustic monitoring system was used during the fatigue tests of all twelve specimens. As indicated in Table 3.3, the acoustic sensors provided a reasonable estimate of the number of wire breaks observed during the autopsy. The sensors used for Specimens 1 through 4 were prototypes, and the sensors used for Specimens 5 through 12 are similar to those installed on the Fred Hartman Bridge. Among the specimens in phase 2, the largest discrepancies between the observed number of wire breaks and the number of wire breaks detected by the acoustic sensors occurred in Specimens 7 and 12. These specimens experienced the largest number of wire breaks, and multiple breaks in the same wire were observed in both specimens. Therefore, the differences are not considered to be significant.

Table 3.3 Comparison of Observed Wire Breaks and Wire Breaks Detected by Acoustic Sensors

ID	Observed*				Detected by Acoustic Sensors				Difference		
	Tower	Midspan	Deck	Total	Tower	Midspan	Deck	Total	Tower	Midspan	Deck
1	14	11	0	25	14	11	0	25	0	0	0
2	52	16	1	69	49	17	1	67	-3	+1	0
3	9	62	13	84	10	63	13	86	+1	+1	0
4	28	0	3	31	26	0	1	27	-2	0	-2
5	0	0	0	0	0	0	0	0	0	0	0
6	17	11	0	28	17	11	0	28	0	0	0
7	37	65	17	119	36	62	16	114	-1	-3	-1
8	2	0	2	4	2	0	2	4	0	0	0
9	12	61	3	76	12	62	3	77	0	+1	0
10	23	21	8	52	23	20	9	52	0	-1	+1
11	0	9	7	16	0	8	7	15	0	-1	0
12	35	86	29	150	36	84	28	148	+1	-2	-1

* Multiple breaks in the same wire are included in the totals.

The longitudinal distributions of wire breaks detected by the acoustic sensors at the ends and at midspan are shown in Figure 3.28 and Figure 3.29, respectively. All the wire breaks were correctly located within 2 ft of the inside face of the anchor head; however, the reported locations of the wire breaks were nearly uniformly distributed within this region. The centroid of the actual distribution of wire breaks was closer to the inside face of the anchor head (Figure 3.4). At midspan, the reported locations of the wire breaks provided a better estimate of the actual distribution (Figure 3.5).

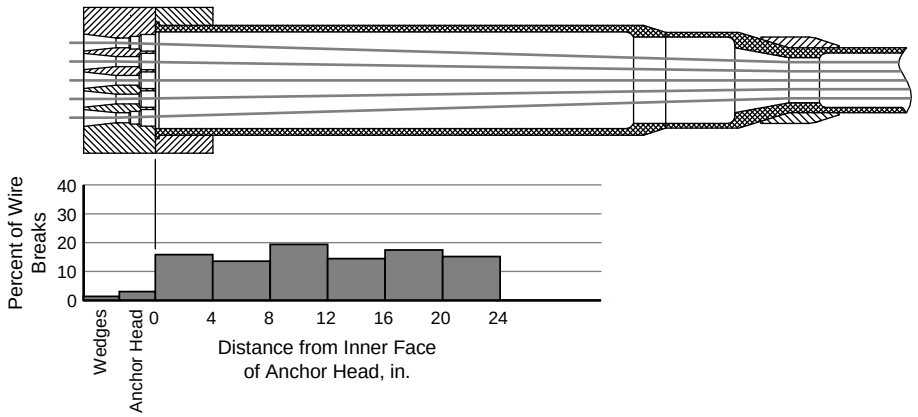

Figure 3.28 Distribution of Wire Breaks Detected by Acoustic Sensors at Ends of Stay-Cable Specimens

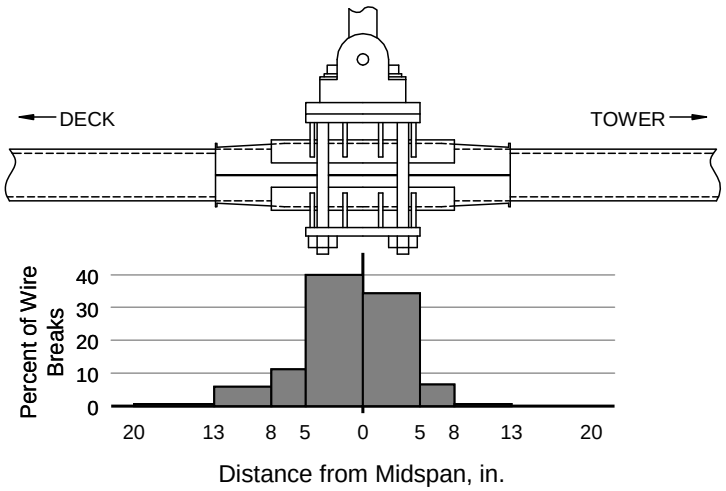

Figure 3.29 Distribution of Wire Breaks Detected by Acoustic Sensors at Midspan of Stay-Cable Specimens

CHAPTER 4: FATIGUE RESPONSE OF SMALL-DIAMETER SPECIMENS

As discussed in Chapter 2, the small-diameter specimens were designed to be simple representations of the prototype, grouted stay cables. The objective of this set of experiments was to monitor changes in stiffness, frequency, and strain as damage accumulated. The results of the fatigue tests are summarized in Table 4.1. Specimen 1 collapsed after all wires in both strands fractured at the north end. In order to avoid possible damage to the testing equipment, the fatigue tests for the other two specimens were terminated before failure.

Table 4.1 Summary of Fatigue Tests of Small-Diameter Specimens

ID	Displacement Amplitude (in.)	Number of Cycles	Number of Observed Broken Wires*			
			North End	Load Position 2†	Load Position 1†	South End
1	1.25	5,044,194	14	0	2	0
2	1.25	4,715,555	7	0	—	0
3	1.40	1,651,467	10	0	—	0

* Multiple wire breaks were not considered in the totals.

† Load Position 1 was at midspan, Load Position 2 was at the north quarter point.

The extent of the observed damage in the small-diameter specimens is summarized in Section 4.1, the measured relationships between the transverse stiffness and natural frequencies and the level of damage is discussed in Section 4.2, the measured strain response is summarized in Section 4.3, and the sensitivity of the acoustic monitoring system is summarized in Section 4.4. Detailed discussions of the response of each specimen and the observed damage are documented in Appendix E.

4.1 OBSERVED DAMAGE

Due to the location of the applied transverse loads, damage in the small-diameter specimens was concentrated near the north end (Table 4.1). At least half the wires fractured at this location in each of the test specimens, and all the wires fractured in Specimen 1. Approximately 45% of the wire breaks occurred within the north anchor head and 50% of the wire breaks occurred within 4 in. of the inside face of the anchor head (Figure 4.1). All wire breaks occurred within 8 in. of the inside face of the anchor head.

The distributions of wire breaks within the cross section are shown in Figure 4.2. Multiple wire breaks were observed in individual wires in Specimens 2 and 3. The level of damage was extremely high in all three specimens at the conclusion of the fatigue tests.

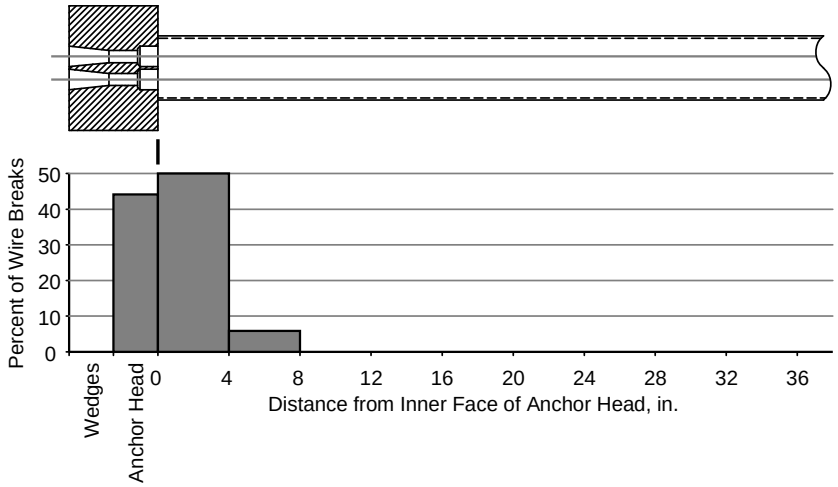

Figure 4.1 Distribution of Observed Wire Breaks at North End of Small-Diameter Specimens

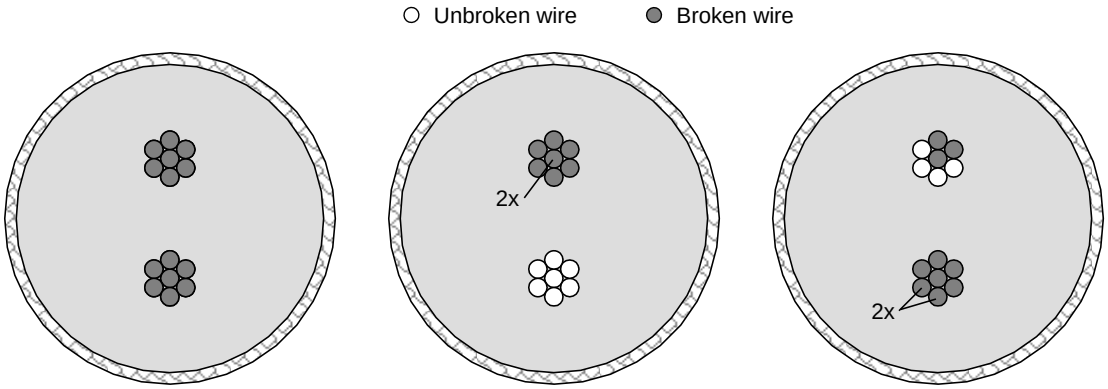

(a) Specimen 1 (b) Specimen 2 (c) Specimen 3

Figure 4.2 Summary of Wire Breaks at North End of Small-Diameter Specimens

4.2 LOSS OF STRUCTURAL INTEGRITY

The fatigue tests were stopped periodically to measure the transverse stiffness and natural frequencies of the test specimens. In many cases, these tests were conducted shortly after the acoustic monitoring system detected a wire break. With the exception of Specimen 1, all the wire breaks occurred at the north end of the specimens, so the damage may be considered to be concentrated in one area, rather than distributed, along the length of the test specimen.

4.2.1 Transverse Stiffness

The transverse stiffness was determined by applying static loads to the test specimens and measuring the resulting displacements. The variation of the stiffness reduction ratio – the measured stiffness divided by the initial stiffness – is plotted in Figure 4.3 through Figure 4.5 for Specimens 1 through 3, respectively.

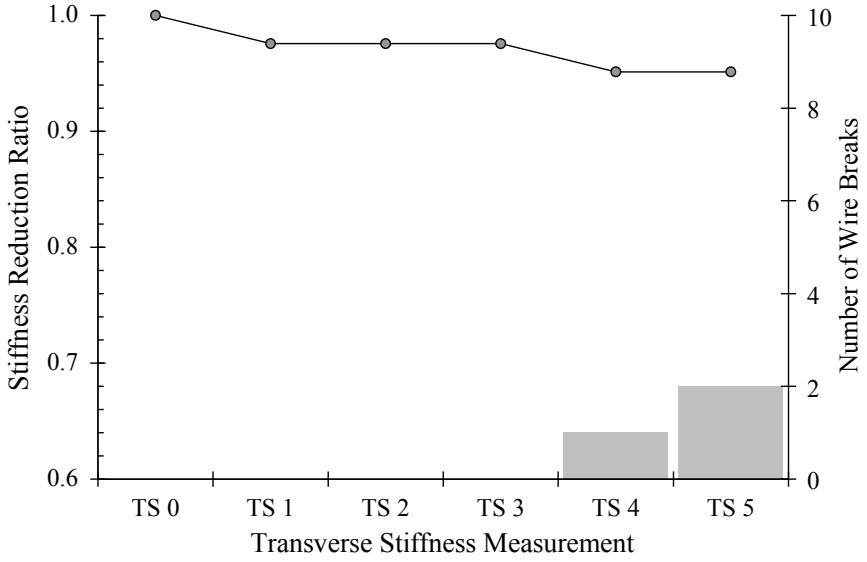

Figure 4.3 Sensitivity of Transverse Stiffness to Number of Wire Breaks – Specimen 1

For Specimen 1, the loads were initially applied at midspan, and all five stiffness measurements were taken with the actuator in this position. The two wire breaks shown in Figure 4.3 occurred near midspan, and were confirmed during the autopsy of the test specimen. The stiffness of Specimen 1 varied by less than 5% during the 3.2 million fatigue cycles documented in Figure 4.3.

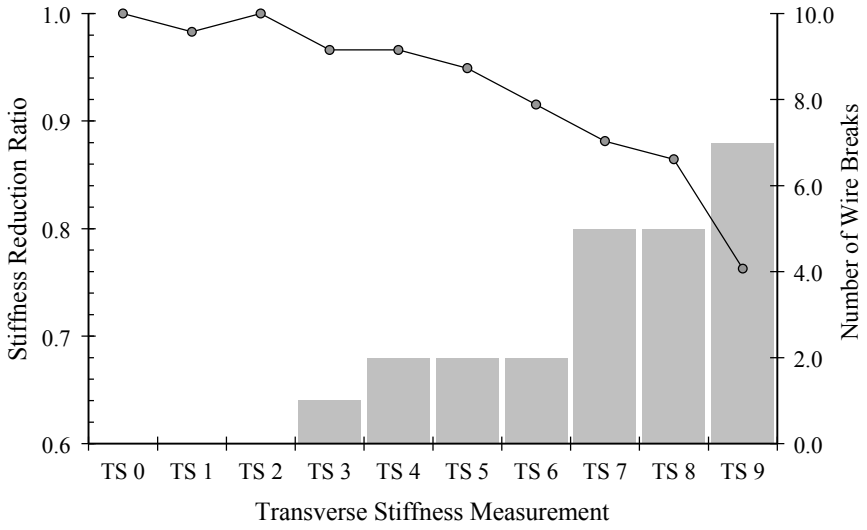

Figure 4.4 Sensitivity of Transverse Stiffness to Number of Wire Breaks – Specimen 2

For Specimen 2, the transverse stiffness was within 10% of the initial stiffness until five wire breaks had been detected (Figure 4.4). The final stiffness was measured at the conclusion of the fatigue test, when the autopsy indicated that all seven wires in the top strand had fractured. In spite of a 50% loss in the cross-sectional area of the strand, the transverse stiffness decreased by only 25%.

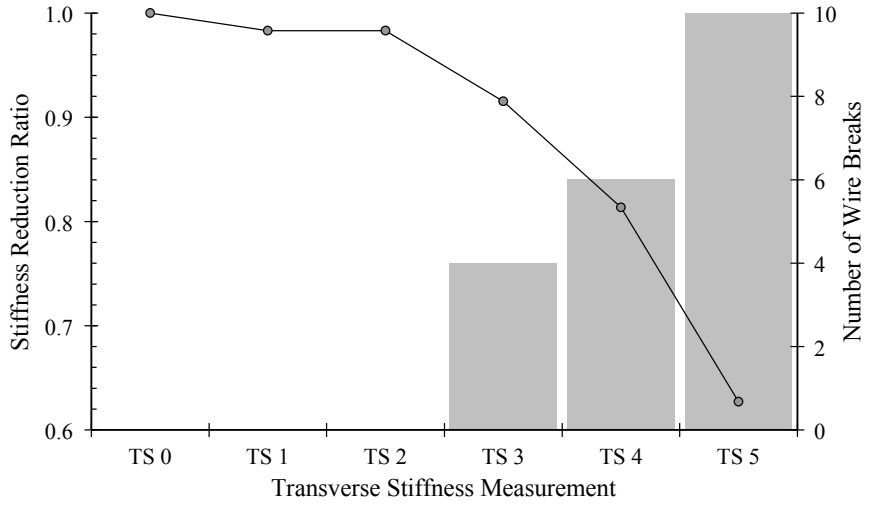

Figure 4.5 Sensitivity of Transverse Stiffness to Number of Wire Breaks – Specimen 3

Specimen 3 exhibited a 20% reduction in stiffness after the sixth wire break had been detected (Figure 4.5). At the conclusion of the fatigue test, the autopsy indicated that 10 individual wires had fractured at the north end, and the stiffness decreased by less than 40%. For this condition, only four wires were intact (less than 30% of the total number of wires).

4.2.2 Natural Frequency

The natural frequencies of the first six modes of vibration were also measured periodically during the fatigue tests. The variation of the frequency reduction ratios – the measured natural frequency divided by the initial natural frequency – is plotted in Figure 4.6 through Figure 4.8 for Specimens 1 through 3, respectively.

For Specimen 1 (Figure 4.6), the first three natural frequency measurements (NF 0 through NF 2) occurred before repositioning the hydraulic actuator. The two wire breaks detected during this period occurred at midspan of the specimens. While the higher frequencies exhibited modest reductions in these tests, the fundamental frequency was not sensitive to the damage.

Natural frequency measurements NF 3 and NF 4 occurred after the hydraulic actuator was positioned near the north quarter point, and all additional wire breaks occurred near the north anchor head. The first appreciable change in all six natural frequencies was observed after the sixth wire break was detected at the north end. However, the changes were less than 10% in all cases.

The last set of natural frequencies (NF 4) was obtained after approximately 4.5 million fatigue cycles. Because Specimen 1 collapsed, it was not possible to measure the natural frequencies at the conclusion of the fatigue test.

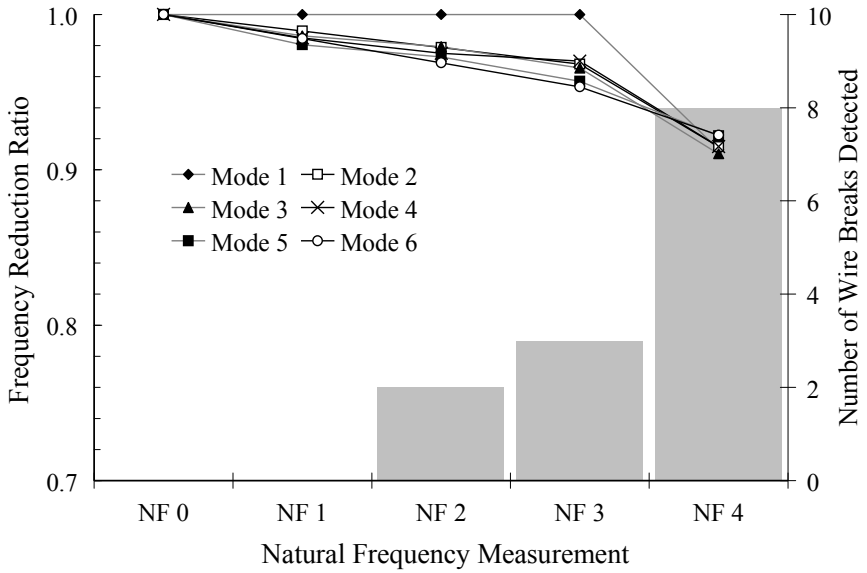

Figure 4.6 Sensitivity of Natural Frequencies to Number of Wire Breaks – Specimen 1

Specimen 2 also exhibited very slight changes in the natural frequencies with the first two wire breaks (Figure 4.7). The changes in natural frequencies were less than 5% until the fifth wire break was detected. In spite of the fact that all seven wires in the top strand had fractured at the time of NF 8, the changes in natural frequency only slightly exceeded 10% in the first two modes of vibration and were less in the higher modes.

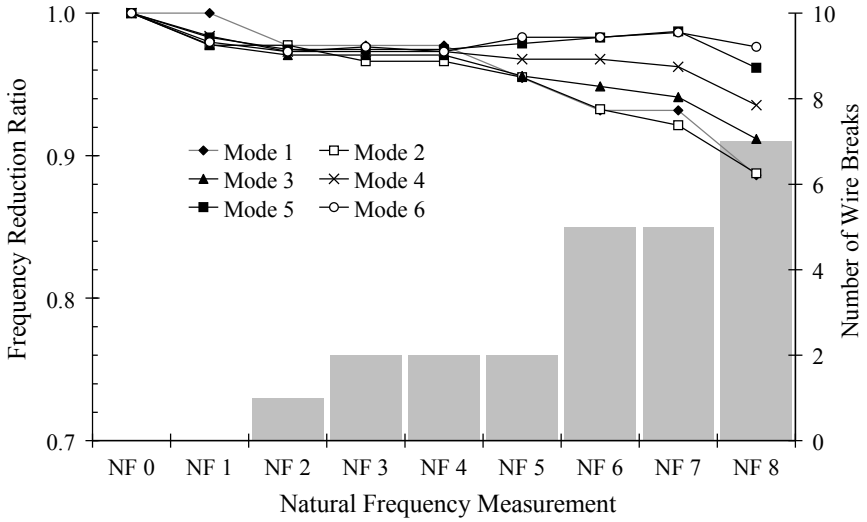

Figure 4.7 Sensitivity of Natural Frequencies to Number of Wire Breaks – Specimen 2

Specimen 3 exhibited the most pronounced relationship between natural frequency and damage (Figure 4.8). By the time that six wire breaks were detected, all six modes exhibited a 10% reduction in frequency. At the conclusion of the fatigue tests, ten of fourteen wires were fractured, and the lower modes exhibited a change of nearly 20%.

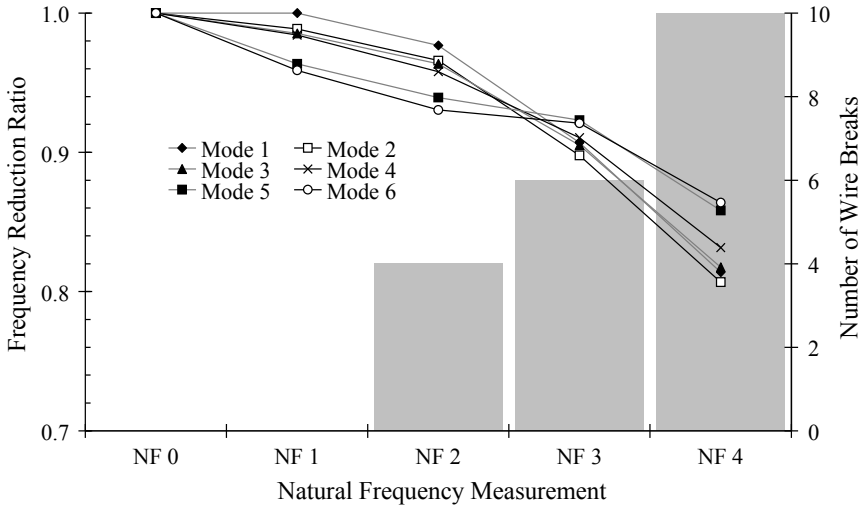

Figure 4.8 Sensitivity of Natural Frequencies to Number of Wire Breaks – Specimen 3

4.3 STRAIN MEASUREMENTS

Strains were measured at various locations along all three, small-diameter specimens. In order to capture the maximum strain response, gages were positioned within 2 in. of the north anchor head in all cases. These gages tended to exhibit nonlinear trends with increasing load (Figure 4.9). It is believed that cracking of the grout caused these trends.

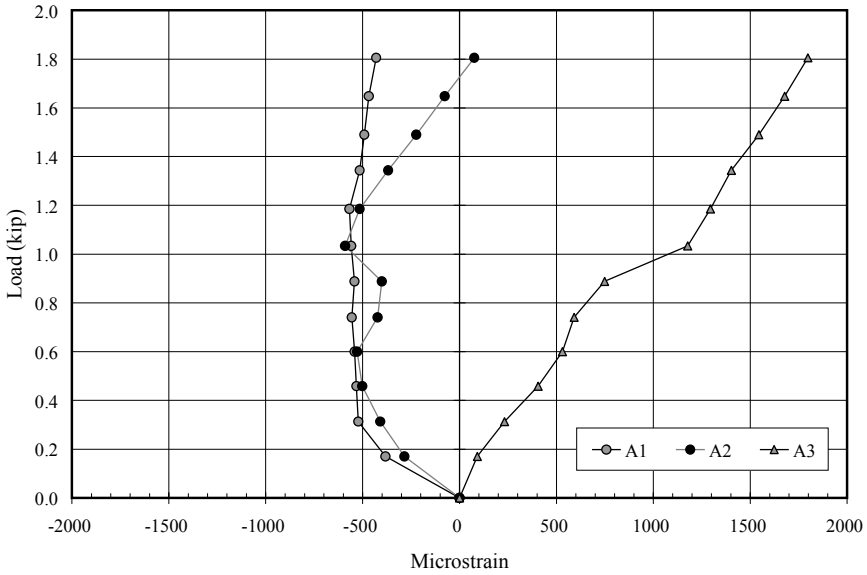

Figure 4.9 Strains Measured at North Anchor Head – Specimen 2

The most complete set of data was obtained for Specimen 3 (Section E.3.2). The data indicated that the highest stresses occurred near the north anchor head (Figure 4.10), as expected. However, for closely-spaced gages, the magnitude of the stress did not always decrease with distance along the span. These trends were also believed to be caused by cracking of the grout.

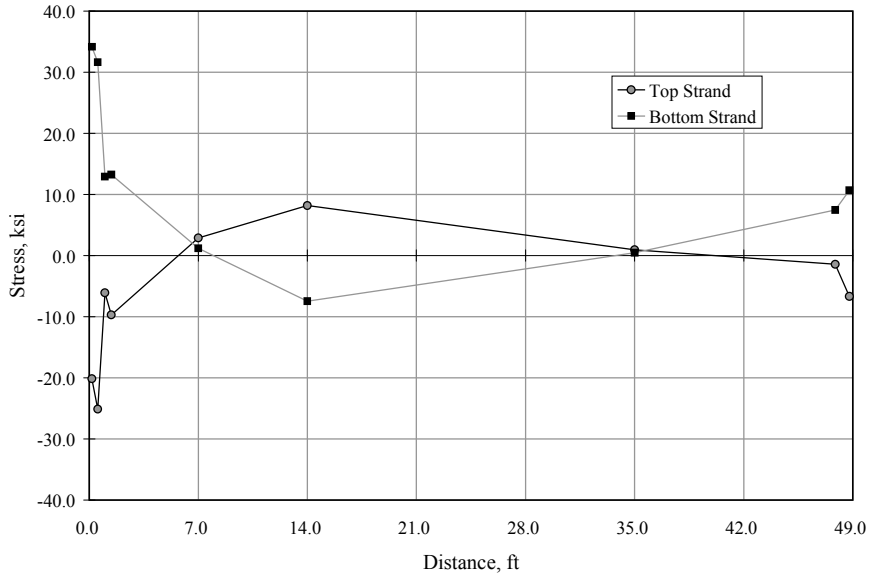

Figure 4.10 Variation of Maximum Stress along Length of Specimen 3 after 2,000 Fatigue Cycles

The gages in the immediate vicinity of the anchor heads tended to fail after several hundred thousand fatigue cycles. Therefore, it was not possible to monitor changes in these stress levels as damage accumulated. However, the stresses at other locations did not vary considerably with the number of cycles (Figure 4.11).

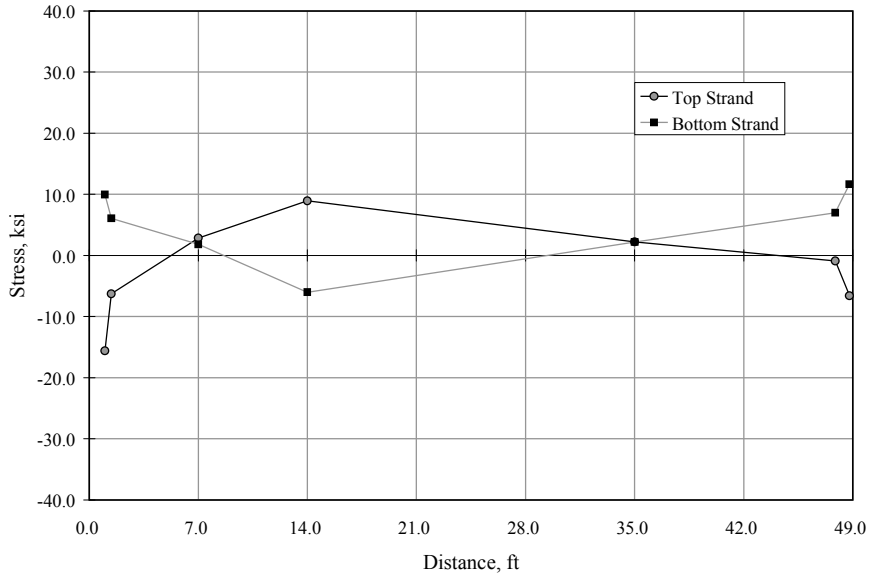

Figure 4.11 Variation of Maximum Stress along Length of Specimen 3 after 750,000 Fatigue Cycles

The stress data plotted in Figure 4.10 indicate a maximum bending stress of approximately 35 ksi in the strand near the north anchor head. The first wire break in Specimen 3 was detected after 415,000 fatigue cycles. This fatigue life is consistent with the range observed for strand tested in air at this stress range (Appendix A).

4.4 SENSITIVITY OF ACOUSTIC MONITORING SYSTEM

The acoustic monitoring system was used during the fatigue tests of all small-diameter specimens. As indicated in Table 4.2, the acoustic sensors provided a reasonable estimate of the number of broken wires observed during the autopsy. Because the total number of broken wires at the north end of the test specimens was such a high fraction of the total number of wires (Figure 4.2), it is not surprising that the number of breaks detected by the acoustic sensors was slightly less than observed.

Table 4.2 Comparison of Observed Wire Breaks and Wire Breaks Detected by Acoustic Sensors

ID	Observed Broken Wires*				Detected by Acoustic Sensors				Difference		
	North	Midspan	South	Total	North	Midspan	South	Total	North	Midspan	South
1	14	2	0	16	12	2	0	14	-2	0	0
2	7	0	0	7	6	0	0	6	-1	0	0
3	10	0	0	10	8	0	0	8	-2	0	0

* Multiple wire breaks were not considered in the totals.

The longitudinal distribution of wire breaks detected by the acoustic sensors at the north end is shown in Figure 4.12, respectively. All the wire breaks were reported within 3 ft of the inside face of the anchor head; however, the centroid of the actual distribution of wire breaks was closer to the inside face of the anchor head (Figure 4.1).

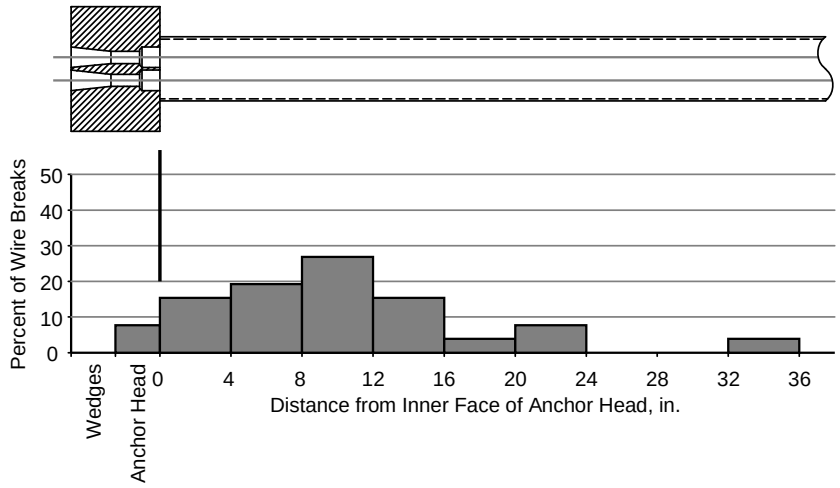

Figure 4.12 Distribution of Wire Breaks Detected by Acoustic Sensors at North End of Small-Diameter Specimens

CHAPTER 5: EXPECTED LOCATIONS OF FATIGUE DAMAGE IN GROUTED STAY CABLES

At the beginning of this project, the research team identified six locations where they considered the likelihood of fatigue damage in the prototype stay cables to be high: (1) immediate vicinity of the anchor head due to high bending stresses, (2) wedges due to high local stresses and crack initiation during stressing, (3) tension ring due to fretting between adjacent strands, (4) along free length due to fretting between outer strands and helical spacer wire, (5) within grout voids due to the increased chance of corrosion, and (6) at the location of inadvertently crossed strands due to fretting between strands. While it was not possible to evaluate each location under prototype conditions, the bending fatigue tests of the stay-cable specimens provided valuable information about the fatigue performance of grouted stay cables and the locations where fatigue damage is expected.

In the test specimens, fatigue damage was concentrated in two areas: the ends of the specimens and the immediate vicinity of the applied loads. These are the areas of highest calculated moment – and bending stress in the strand. Therefore, it is not surprising that damage was concentrated in these areas. At first glance, the damage near the applied loads is not representative of the prototype response. However, the clamps used to attach the hydraulic dampers to the stay cables on the Fred Hartman Bridge (Figure 5.1) are very similar to the clamp used to attach the hydraulic actuator to the test specimens. A large fraction of the wire breaks detected on the Fred Hartman Bridge to date have been located in the lower 25 ft of the cables. Therefore, the possibility of wire breaks in the vicinity of the dampers must be considered.

Figure 5.1 Hydraulic Damper Installed on the Fred Hartman Bridge

5.1 HIGH BENDING STRESSES

As shown in Figure 3.4, approximately 50% of the wire breaks observed at the ends of the stay-cable specimens occurred within the anchor head. In most cases, the failures in this region were caused by fretting of adjacent wires within the strand. The teeth of the wedges initiated only 6% of the total number of wire breaks. All wire breaks occurred within 16 in. of the inside face of the anchor head. Near the loading clamp, more than 50% of the wire breaks were within ± 5 in. of the centerline of the actuator and all wire breaks were within ± 20 in. of the centerline (Figure 3.5). Less than 10% of the wire breaks occurred beyond the PE cushion used as a transition between the PE pipe and the steel clamp.

These observations indicate that the wire breaks are rather tightly distributed in the regions of highest calculated bending stress. In addition, the cross sections shown in Figure 3.6 through Figure 3.8 indicate that the strands positioned near the extreme fibers of the cross section are most likely to be damaged due to fatigue. This observation is consistent with the calculated locations of maximum bending stresses if the cross section is idealized as a composite section and strains are assumed to vary linearly with depth throughout the cross section.

In the laboratory, it was easy to identify the presence of wire breaks at the completion of the fatigue test by opening the PE pipe. Longitudinal cracks in the grout accompanied wire breaks in all cases (Figure 3.10 and Figure 3.11). However, TxDOT is cautioned that opening the PE pipe may cause damage – due to the formation of shrinkage cracks – and compromise the corrosion protection system for the cable. Therefore, it is recommended that openings in the PE pipe not be cut unless a large number of wire breaks have been detected in a localized area and the possibility of stay replacement is being considered seriously.

5.2 OTHER FACTORS

Evidence of congestion of the strands near the tension ring was observed in the laboratory tests. Grout cover was negligible (Figure 3.14) under the tension ring, and relatively large reductions in the cross-sectional area of the strands (Figure 3.19) due to fretting of an ungrouted specimen (Specimen 8) in this region. However, the large confining stresses in this region did not appear to influence the fatigue performance of the strand. No wire breaks were observed near the tension rings. It is believed that the stress ranges in the strand are sufficiently low at this location that the fatigue life is not a concern.

Similarly to the prototype stays, a helical spacer wire was used along the free length of the test specimens to center the strands within the PE pipe. Very few wire breaks were caused by fretting between the strand and the spacer wire. While there is a possibility of this type of damage near the connection between the hydraulic dampers and the stay cables, the risk is considered to be low.

Two of the specimens were constructed with grout voids. The void in Specimen 1 was only detected at the conclusion of the fatigue test. The void in Specimen 9 was intentionally created during construction and was filled before beginning the fatigue test. The distribution of damage in Specimen 9 was not unique, and there was no indication that the filled void had an influence on the fatigue performance. However, in Specimen 1, the wire breaks tended to occur within the grout void and the strands exposed within the void appeared to be more vulnerable to fatigue damage. No evidence of

corrosion was observed within the grout void in Specimen 1. The risk of corrosion is considered to be much greater, however, on the Fred Hartman and Veterans Memorial Bridges. Therefore, if voids are detected near the tower anchorages of either bridge, it is recommended that they be filled with grout to reduce the likelihood of corrosion damage.

Given the length of the stay cables on the Fred Hartman and Veterans Memorial Bridges, it is likely that some of the strands in some of the stays were inadvertently crossed during construction. The fatigue response of Specimen 3 demonstrated that the risk of fretting fatigue due to crossed strands is also low.

5.3 SUMMARY

Based on the results of the bending fatigue tests of twelve, large-scale, stay-cable specimens, the fatigue damage is expected to be concentrated in the regions of highest bending stress: the ends of the stay cables and any location where a damper or restrainer is attached to the stay.

The saddle detail used at the pylon of the Veterans Memorial Bridge was not evaluated experimentally in this investigation; therefore, no information was provided about the susceptibility of bending fatigue failures at the saddle.

CHAPTER 6: EFFECTIVENESS OF NONDESTRUCTIVE METHODS IN IDENTIFYING FATIGUE DAMAGE IN STAY CABLES

The use of grouted cables for cable-stay bridges is most appropriate when corrosion of the strand is the primary serviceability limit state considered in the design of the bridge. The grout provides a high pH environment, which promotes the development of a passive layer on the surface of the strand and reduces the risk of corrosion. However, both the Fred Hartman and Veterans Memorial Bridges experienced large-amplitude cable vibrations during their service lives, and the fatigue limit state must also be considered when evaluating the remaining service life of these bridges. Unfortunately, the grout eliminates the possibility of conducting a visual inspection for fatigue damage and greatly increases the complexity and cost of replacing a cable. In the laboratory, the presence of longitudinal cracks in the grout proved to be an excellent indicator of wire breaks in the strands. However, in order to inspect the grout, the PE pipe, which is a critical component of the corrosion protection system, must be compromised. Given the harsh environmental conditions that both these bridges experience, the risk of corrosion can not be neglected. Therefore, the possibility of fatigue damage in grouted stay cables must be evaluated using non-visual means.

The usefulness of two nondestructive methods for evaluating fatigue damage in grouted stay cables is discussed in this chapter. Natural frequencies are often used as a global indicator of damage, while acoustic sensors have been installed on both the Fred Hartman and Veterans Memorial Bridges to identify local damage as it occurs. When faced with the task of maintaining cable-stayed bridges that have experienced large-amplitude vibrations in the past, two issues must be addressed: (1) how much fatigue damage was induced by the fatigue cycles that occurred before the dampers and restrainers were installed? and (2) can future fatigue damage be detected in a reliable manner as it occurs?

6.1 NATURAL FREQUENCIES

Due to their long length and relatively small cross section, stay cables are often idealized as strings for a preliminary analysis. One of the advantages of this idealization is the simple relationship between the fundamental frequency and the tension in the stay:

$$f_1 = \frac{1}{2L}\sqrt{\frac{T}{m}} \tag{6.1}$$

where f_1 is the fundamental frequency in Hz, L is the length of the stay, T is the applied tension, and m is the mass per unit length. Ideally, as wires break in the strands, the tension decreases and the natural frequency decreases, although at a slower rate. Therefore, changes in the natural frequency can be related to changes in the tension in the cable caused by fatigue damage.

However, the tension in a grouted stay cable is not directly related to the minimum cross-sectional area of the wires along the length. Consider, for example a strand where all the wires have the same initial stress. When a wire break occurs in a seven-wire strand due to fatigue damage, the stress in the damaged wire drops to zero at the location of the break, but the stresses in the other wires increases,

such that the strand is carrying nearly the same tension force. Due to the spiral configuration of the wires in the strand, the stress in the damaged wire increases with distance from the wire break. Although this research did not determine this critical distance, at some point, the stresses are again evenly distributed among all the wires. In addition to the ability to redistribute stresses among wires, some tensile force can be carried through the grout. The pronounced longitudinal cracks in the grout are an indication of these tensile forces. Because the tension in the stay cable does not decrease in proportion to the number of wire breaks, the measured natural frequencies are not sensitive to the number of wire breaks at a single location.

The fundamental natural frequency was measured at the beginning and end of seven bending fatigue tests of grouted cable-stay specimens (Figure 3.26) and the lowest six natural frequencies were measured periodically during the fatigue tests of the three small-diameter specimens (Figure 4.6 though Figure 4.8). In all cases, large number of wire breaks occurred – 25 to 50% of the wires at a given location – before the natural frequencies changed by more than 10%. Therefore, natural frequencies can not be considered to be a reliable indicator of damage in grouted stay cables. In addition, even if fatigue damage did occur during the large-amplitude vibrations of the stay cables in the past, it is unlikely that the natural frequencies could be used to assess this damage. The initial level of tension is not known reliably in the cables. Therefore, it would be inappropriate to measure the frequency in a stay, note that it is less than the frequency obtained by calculation using the nominal properties of the materials, and attribute the change in frequency to fatigue damage in the stay. The changes in frequencies are not sufficiently sensitive to detect fatigue damage in a reliable manner.

6.2 ACOUSTIC MONITORING

The same acoustic monitoring system that has been installed on both the Fred Hartman and Veterans Memorial Bridges was used to monitor the fatigue performance of the cable-stay and small-diameter test specimens. Slight differences between the number of wire breaks detected by the acoustic sensors and the number of wire breaks observed during the autopsy of the specimens were observed, but primarily in test specimens that experienced a large number of wire breaks and multiple wire breaks in the same wire (Table 3.3 and Table 4.2).

Because the geometry of the cable-stay specimens more closely models that of the prototype stays, the discussion will focus on those specimens. All the observed wire breaks in the cable-stay specimens occurred within 16 in. of the inner face of the anchor head (Figure 3.4). The acoustic sensors provided an excellent estimate of the total number of wire breaks at the ends of the specimens; however, the estimated locations of those breaks tended to be further from the anchor head than observed (Figure 3.28). This is not surprising, due to the large volume of steel at the ends of the specimens, the location of the acoustic event is more difficult to pinpoint. Therefore, when wire breaks are reported on the Fred Hartman or Veterans Memorial Bridges within 3 ft of the anchor head, the possibility that the wire break is within the anchor head should be considered.

In contrast, the acoustic sensors provided a better estimate of the locations of the wire breaks near midspan of the test specimens. The actual damage was observed to be distributed within ±20 in. of the

centerline of the loading clamp (Figure 3.5). This distribution was similar to that from the acoustic sensors (Figure 3.29).

6.3 SUMMARY

The research conducted during this project did not identify a reliable means of assessing the extent of existing fatigue damage in a grouted stay cable. A nondestructive method of detecting the presence of longitudinal cracks in the grout is one potential option, but an ultrasonic method has not been validated for this application.

The acoustic monitoring systems installed on the Fred Hartman and Veterans Memorial Bridges provide a reliable means of detecting wire breaks as they occur. Given the history of large-amplitude displacements in these cables in the past, it is strongly recommended that the acoustic monitoring be continued. Acoustic monitoring can not provide information about the level of damage that occurred before the sensors were installed. However, given the susceptibility of the grouted stay cables to fretting fatigue damage after the first wire breaks, the acoustic monitoring system does provide a means of detecting an accumulation of damage.

TxDOT should be cautioned, however, that the actual locations of a wire break may be 2 to 3 ft from the location identified by the acoustic sensors. If multiple wire breaks are detected at the same end of a stay, or near the connection to a damper, it would be prudent to assume that these breaks have occurred at the same location, even if the acoustic sensors indicate that the wire breaks are separated by several feet.

CHAPTER 7: SUMMARY AND CONCLUSIONS

Large-amplitude vibrations of the stay-cables on both the Fred Hartman and Veterans Memorial Bridges have been observed during their service lives. Although dampers and restrainers have been installed to minimize the likelihood of large-amplitude vibrations in the future, the risk of fatigue damage to the stays remains a concern. Complicating matters is the fact that visual inspection of the grouted stay cables for fatigue damage can not be accomplished without severely compromising the corrosion protection system for the stays. Given the harsh environmental conditions that these bridges face, this option is not recommended unless a threshold amount of fatigue damage has occurred.

Faced with these challenges, the Texas Department of Transportation elected to install an acoustic monitoring system on both bridges. The system provides the ability to monitor the formation of wire breaks in near real time.

The results of the bending fatigue tests conducted during this research project provide TxDOT with the basis for evaluating the acoustic data from the stay cables and making decisions regarding maintenance and repair strategies. The conclusions most closely tied to this decision-making process are summarized below.

7.1 LOCATION OF FATIGUE DAMAGE

The fatigue damage is expected to be concentrated in the regions of high bending stresses: the ends of the cables and any location where a damper or restrainer induces local bending in the stay. The laboratory tests indicated that the risk of fatigue damage was low at the tension rings, along the free length of the stays, and in the vicinity of unintentionally crossed strands. While grout voids at the tower end of the test specimens had only a slight influence on the fatigue performance, these voids have the potential to be a source of corrosion if the PE layer of the corrosion protection system is compromised. Therefore, it is recommended that any grout void detected during routine maintenance of the stay cables be filled.

The bending fatigue characteristics of stay cables passing through a saddle at a pylon – which is the case on the Veterans Memorial Bridge – were not evaluated in this program. Therefore, no information is available about special fatigue concerns in the vicinity of the saddle details. However, it is reasonable to assume that the risk of fatigue damage is higher within the saddle than along the free length of the stay.

7.2 PARAMETERS THAT INFLUENCE FATIGUE LIFE

Reducing the amplitude of the displacements had the largest influence on increasing the fatigue life of grouted stay cables of the parameters studied (Figure 7.1). Reducing the displacement amplitude by 30% increased the number of loading cycles corresponding to a 10% reduction in stiffness from approximately 1.5 million to approximately 4 million in the test specimens. TxDOT has already accomplished much larger reductions in displacement amplitude on the Fred Hartman Bridge by installing dampers and cable restrainers. While the local bending issues identified in Section 7.1 are introduced by

these vibration mitigation methods, the risk of fatigue damage due to low-amplitude, local bending is much lower than the risk of fatigue damage due to large-amplitude vibrations.

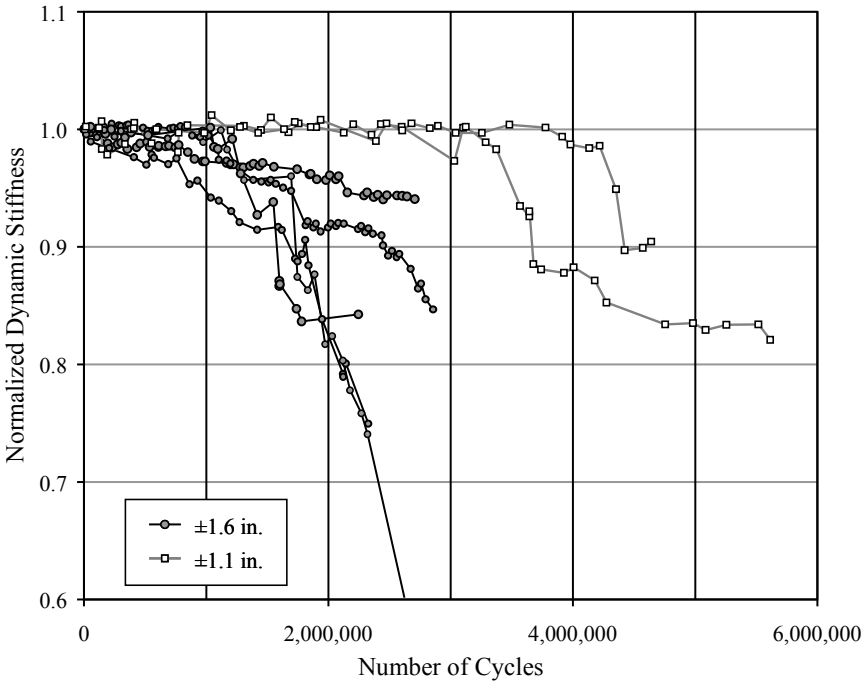

Figure 7.1 Sensitivity of Average Dynamic Stiffness for Grouted Specimens with Nineteen Strands to Displacement Amplitude during Fatigue Tests

7.3 MECHANISMS THAT CONTRIBUTE TO FATIGUE FAILURE OF THE STRAND

Approximately 95% of the wire breaks that were identified in the laboratory tests were caused by fretting fatigue: 90% were caused by fretting between adjacent wires in the same strand and 5% were caused by fretting at the wedges. The remaining 5% of the wire breaks were attributed to local defects in the strand and fretting between the strand and the spacer wire. These mechanisms are inherent to a grouted stay-cable system with parallel strands and the risk of this type of fatigue damage can only be reduced by reducing the amplitude of the vibrations, as discussed in Section 7.2.

The presence of corroded fretting product did appear to accelerate the formation of wire breaks in the test specimens. Corroded fretting product was most prevalent where the hydraulic actuator was attached to the test specimens, which corresponds to locations where the dampers and restrainers are connected to the stay cables.

7.4 STRUCTURAL INTEGRITY OF A GROUTED STAY CABLE WITH FATIGUE DAMAGE

Accumulation of fatigue damage in a grouted stay cable is a slow process, and occurs one wire break at a time. Many wire fractures can be tolerated before there is a detectible change in the transverse stiffness of the stay cable. Due to the helical configuration of the strand, the stress originally carried in the broken wire is redistributed among the other wires in the strand; therefore, changes in the tension in the cable are not proportional to the number of wire breaks.

The recommended threshold for taking corrective action is 10% of the total number of wires in the stay cable. If the number of wire breaks at one location reaches this threshold, that area of the stay should be examined. For the nineteen-strand specimens considered in this investigation, the formation of thirteen wire breaks corresponded to approximately a 10% loss in lateral stiffness (Figure 3.26).

7.5 EFFECTIVENESS OF NONDESTRUCTIVE METHODS

The acoustic monitoring systems installed on the Fred Hartman and Veterans Memorial Bridges provided a reliable means of detecting wire breaks in the laboratory specimens. Slight differences between the number of wire breaks detected by the acoustic sensors and the number of wire breaks observed during the autopsy of the specimens occurred, but these were primarily in test specimens that experienced a large number of wire breaks and multiple wire breaks in the same wire. However, the actual location of a wire break may be 2 to 3 ft from the location identified by the acoustic sensors. Therefore, if multiple wire breaks are detected at the same end of a stay, or near the connection to a damper or restrainer, it is suggested that these breaks be assumed to have occurred at the same location.

The acoustic monitoring system provides information about the accumulation of fatigue damage as it occurs, but it does not provide information about the extent of fatigue damage that occurred in the past. Studies were conducted to determine if natural frequencies could be used to determine the extent of existing damage in the stay cables. However, this method is not recommended. The measured natural frequencies are not sufficiently sensitive to localized damage to detect existing fatigue damage in a reliable manner.

jThe presence of longitudinal cracks in the grout was a good indicator of the presence of wire breaks in the strand. However, for grouted stay cables, cracks in the grout can not be observed without compromising the corrosion protection system. Therefore, visual inspection of grout damage is not recommended unless the threshold number of wire breaks has been reached. The development of a nondestructive method to detect the presence of longitudinal cracks in the grout has the potential of providing information about the extent of existing fatigue damage, but to date methods have not been validated for grouted stay-cable applications.

7.6 VARIATION OF STRESS WITHIN CROSS SECTION AND ALONG STAY

For a given cross section, the observed wire breaks tended to be concentrated in the outer layers of strand, which would experience the highest bending stresses in a composite cross section. In general, variations of stress along the length of the specimen were consistent with the calculated variation of moments. However, cracking of the grout led to local inconsistencies. In the small-diameter specimens, higher strains were measured further from the anchor head in several cases.

7.7 CONCLUSIONS

The Texas Department of Transportation has taken two important steps toward ensuring a safe service life for the Fred Hartman and Veterans Memorial Bridges: (1) dampers and restrainers have been installed to minimize cable vibrations and (2) acoustic monitoring systems have been installed to monitor the formation of fatigue damage in near real time. It is not possible with current non-destructive

technologies to determine the extent of fatigue damage that occurred during the large-amplitude vibrations of the stay cables. However, the accumulation of fatigue damage is a slow process and many wire breaks can be accommodated in grouted stay cables before a loss in strength or stiffness is detected. The most critical regions for fatigue damage are the ends of the stays and locations where dampers and restrainers are connected to the stays.

It is essential that the acoustic monitoring systems be maintained, as this provides the only reliable means of tracking fatigue damage. If the number of wire breaks detected at any location exceeds 10% of the total number of wires in the stay, that area should be examined. The PE pipe and grout should be removed to expose the strand and the number of wire breaks verified. Wire breaks within a 3-ft region should be assumed to have occurred at the same location. The cause of the fatigue failures should also be determined so that remedial action can be taken to prevent additional wire breaks in other stays.

References

American Association of State Highway and Transportation Officials (2004). *LRFD Bridge Design Specifications,* Third Edition with 2005 Interim Revisions. Washington, D.C.

American Society for Testing Materials (2002). *Standard Specification for Steel Strand, Uncoated Seven-Wire for Prestressed Concrete*, ASTM A 416. West Conshohocken, PA.

American Society for Testing Materials (2002). *Standard Test Methods for Tension Testing of Metallic Materials*, ASTM E 8. West Conshohocken, PA.

Andersen, H., Hommel, D.L., and Veje, E.M. (1999). "Emergency Rehabilitation of the Zarate-Brazo Largo Bridges, Argentina." *IASBE Conference, Malmo 1999: Cable-Stayed Bridges – Past, Present, and Future*.

Bean, M.J. (2006). "Bending Fatigue Performance of Small-Scale Stay Cables," M.S. Thesis, Department of Civil, Architectural and Environmental Engineering, University of Texas at Austin. (Available at http://fsel.engr.utexas.edu/publications)

Dowd, J.A. (2001). "Response of Stay Cables to High-Amplitude Vibration," M.S. Thesis, Department of Civil Engineering, University of Texas at Austin. (Available at http://fsel.engr.utexas.edu/publications)

Eggers, J.C. (2003). "Cable Stay Fatigue Analysis for the Fred Hartman Bridge," M.S. Thesis, Department of Civil Engineering, University of Texas at Austin. (Available at http://fsel.engr.utexas.edu/publications)

Frank, K. H. (1990). "Fatigue Test of Second 55-Strand Stay Cable Specimen for the Baytown Bridge," Phil M. Ferguson Structural Engineering Research Report, University of Texas at Austin.

Frank, K. H. and Burkett, W.R. (1989). "Fatigue and Static Tests of 55-Strand Stay Cable Specimen for the Baytown Bridge," Phil M. Ferguson Structural Engineering Research Report, University of Texas at Austin.

Frank, K. H., Moore, J.A., and Burkett, W.R. (1989). "Fatigue and Static Tests of 43-Strand Stay Cable Specimen for the Baytown Bridge," Phil M. Ferguson Structural Engineering Research Report, University of Texas at Austin

Gimsing, N.J. (1997). Cable Supported Bridges: Concept and Design. 2d ed. Chichester: John Wiley and Sons.

Gimsing, N.J. (1999). "History of Cable-Stayed Bridges," *IASBE Conference, Malmo 1999: Cable-Stayed Bridges – Past, Present, and Future.*

Hamilton, H.R., Breen, J.E., and Frank, K.H. (1998). "Bridge Stay Cable Corrosion Protection. I: Grout Injection and Load Testing," ASCE, *Journal of Bridge Engineering,* Vol. 3, No. 2, pp. 64-71.

Hamilton, H.R., Breen, J.E., and Frank, K.H. (1998). "Bridge Stay Cable Corrosion Protection. II: Accelerated Corrosion Tests," ASCE, *Journal of Bridge Engineering,* Vol. 3, No. 2, pp. 72-81.

Hamilton, H.R. (1995). "Investigation of Corrosion Protection Systems for Bridge Stay Cables," Ph.D. Dissertation, Department of Civil Engineering, University of Texas at Austin. (Available at http://fsel.engr.utexas.edu/publications)

Heller, B.E. (2003). "Fatigue Response of Pretensioned Concrete Beams," M.S. Thesis, Department of Civil Engineering, University of Texas at Austin. (Available at http://fsel.engr.utexas.edu/publications)

Ito, M. (1999). "Stay Cable Technology: Overview," *IASBE Conference, Malmo 1999: Cable-Stayed Bridges – Past, Present, and Future.*

Kesner, K., and Poston, R.W. (1999). "Progress Report No. 2: Evaluation and Repair of Stay Cable Vibrations, Fred Hartman Bridge, Veterans Memorial Bridge," Whitlock Dalrymple Poston Project No. 06-95114B, Report to TxDOT.

Lee, J.K. (2007). "Evaluation of External Post-Tensioned Tendons using Vibration Signatures," Ph.D. Dissertation, Department of Civil, Architectural and Environmental Engineering, University of Texas at Austin. (Available at http://fsel.engr.utexas.edu/publications)

Menn C. (2000). "As Simple As Possible, But Not Simpler," *Challenges & Solutions*. Finley Mc Nary. July/August Edition.

Miki, C., Endo, T., and Okukawa, A. (1990). "Full-Size Fatigue Test of Bridge Cables," *Report of IASBE Workshop El Paular, Madrid*, pp. 167-178.

Miyazaki, M. (1999). "Aerodynamic and Structural Dynamic Control System of Cable-Stayed Bridge for Wind Induced Vibration," *IASBE Conference, Malmo 1999: Cable-Stayed Bridges – Past, Present, and Future.*

Moore, J.A. (1989). "Stay Cable Anchorage System Tests," M.S. Thesis, Department of Civil Engineering, University of Texas at Austin. (Available at http://fsel.engr.utexas.edu/publications)

Paulson, C., Frank, K.H., and Breen, J.E. (1983). "A Fatigue Study of Prestressing Strand," Research Report 300-1, Center for Transportation Research, University of Texas at Austin.

Pebley, A.J. (2005). "Bending Stresses in Stay Cables during Large-Amplitude Vibrations – A Fred Hartman Bridge Case Study," M.S. Thesis, Department of Civil, Architectural and Environmental Engineering, University of Texas at Austin. (Available at http://fsel.engr.utexas.edu/publications)

Poser, M. (2001). "Full-Scale Bending Fatigue Tests of Stay Cables," M.S. Thesis, Department of Civil, Architectural and Environmental Engineering, University of Texas at Austin. (Available at http://fsel.engr.utexas.edu/publications)

Post-Tensioning Institute (2001). *PTI Guide Specification: Recommendations for Stay Cable Design, Testing and Installation*, Fourth Edition with Addendum 1, Phoenix, AZ.

Poston, R. W. 1998. "Cable-Stay Conundrum," *Civil Engineering*, Vol. 68, No. 8, pp. 58-61.

Ridd, J.E. (2004). "Fatigue Performance of Stay Cables," M.S. Thesis, Department of Civil, Architectural and Environmental Engineering, University of Texas at Austin. (Available at http://fsel.engr.utexas.edu/publications)

Tabatabai, H., Ciolko, A.T., and Dickson, T.J. (1995). "Implications of Test Results from Full-Scale Fatigue Tests of Stay Cables Composed of Seven-Wire Prestressing Strand," *Proceedings of the Fourth International Bridge Engineering Conference,* pp. 266-277.

Witthoft, S.; Wouters, J.P.; and Poston, R.W. (2001). "Final Report – Progress Report No. 3: Evaluation and Repair of Stay-Cable Vibrations: Fred Hartman Bridge and Veterans Memorial Bridge," Whitlock Dalrymple Poston Project No. 06-95114B, Report to the Texas Department of Transportation.

Wood, S.L.; Hagenberger, M.J.; Heller, B.E. and Wagener, P.J. (2007). "Evaluation of Serviceability Requirements for Load Rating Prestressed Concrete Bridges." Technical Report 0-1895-1, Center for Transportation Research, University of Texas at Austin.

Virlogeux, M. (1998). "Cable Vibrations in Cable-Stayed Bridges," *Bridge Aerodynamics*, Ed. Larsen and Esdahl, pp. 213-233.

Yamaguchi, H. and Fujino, Y. (1998). "Stayed Cable Dynamics and Its Vibration Control," *Bridge Aerodynamics,* Ed. Larsen and Esdahl, pp. 235-253.

Zuo, D. and Jones, N.P. (2005). "Stay-Cable Vibration Monitoring of the Fred Hartman Bridge (Houston, TX) and the Veterans Memorial Bridge (Port Arthur, Texas)," Technical Report 0-1401-2, Center for Transportation Research, University of Texas at Austin.

APPENDIX A: AXIAL RESPONSE OF STRAND

Three types of axial tests were conducted to characterize the mechanical properties of the 0.6-in. strand used to construct the bending fatigue specimens: (a) cyclic tests to determine the fatigue life, (b) static tests to determine the breaking strength, and (c) static tests to determine the modulus of elasticity. This appendix describes the test program and summarizes the results. Two types of strand were tested: Strand A (used to construct stay-cable Specimens 1 through 6), and Strand B (used to construct stay-cable Specimens 7 through 12 and the three, small-diameter specimens).

The results of the axial fatigue tests were used to determine the fatigue life of the strand under conditions of uniform stress. The tension tests were used to determine if the strand satisfies the requirements for Grade 270 strand in ASTM A 416. Due to the helical geometry of the strand, strains can only be measured along the local axes of the wires, rather than the longitudinal axis of the strand. Therefore, the apparent modulus of elasticity of the strand must be determined to relate the measured strains to the axial stresses in the strand.

A.1 FATIGUE TESTS

The fatigue tests were conducted in three phases: Eggers (2003) tested Type A strand, Ridd (2004) tested Type B strand, and Bean (2006) tested both types of strand. A 220-kip MTS load frame with hydraulically-controlled clamps (Figure A.1) was used in all three phases of the research; however, shortly after Eggers (2003) and Ridd (2004) completed their tests, a problem was discovered with the controller used to maintain the force limits throughout the fatigue tests. Therefore, Bean (2006) repeated the fatigue tests after the controller had been replaced to verify the response of the strand. The results from the three phases were similar; however, only the results reported by Bean (2006) are included in this appendix.

Fatigue tests were conducted using a nominal stress range of 20 ksi, 30 ksi, or 40 ksi. These stress ranges were considered to be representative of the stress ranges experienced during the bending fatigue tests of the stay cables (Dowd 2001). All tests were conduced under load control. The testing frequency was as fast as possible to achieve a stable loading history (Table A.1). Based on the testing procedures in the PTI Guide Specifications (2001), a maximum stress of 0.45 f_s' was used in all tests, where f_s' is the minimum ultimate tensile stress of the strand. The stress in the strand was calculated using the cross-sectional area of Strand B reported on the mill certificate (Table A.2).

The test set-up for the fatigue tests is shown schematically in Figure A.2. Each specimen was approximately 60 in. long. Solid copper wires and aluminum clamps were used at both ends of the specimens so that the strand was not crushed in the MTS testing machine (Figure A.3). The resulting free length of the specimens was approximately 48 in. The clamps are discussed in more detail in Ridd (2004), Bean (2006), and Lee (2007).

Figure A.1 220-kip MTS Load Frame

Table A.1 Parameters Used for Axial Fatigue Tests

Stress Range (ksi)	Frequency (Hz)	Maximum Load (kip)	Minimum Load (kip)
20	6.5	27.09	22.63
30	6.5	27.09	20.40
40	5.0	27.09	18.17

Table A.2 Area of Prestressing Strand

Area	Strand A		Strand B		ASTM A 416
	Measured	Mill Certificate	Measured	Mill Certificate	
Total	0.2200 $in.^2$	0.2185 $in.^2$	0.2230 $in.^2$	0.2204 $in.^2$	0.217 $in.^2$
Outer Wire	0.0311 $in.^2$	—	0.0313 $in.^2$	—	—
Center Wire	0.0334 $in.^2$	—	0.0352 $in.^2$	—	—

Each fatigue test was concluded when one of the following events occurred: (a) a single wire break along the free length of the specimen, (b) a single wire break within the grips, or (c) run-out (the specimen survived more than 2 million cycles). Data corresponding to wire breaks within the grips were not included when evaluating the fatigue life of the strand; therefore, those data are not included in this appendix.

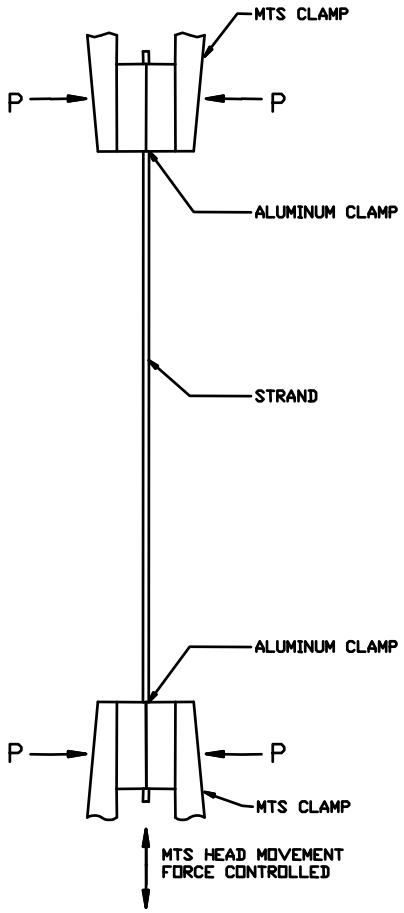

Figure A.2 Test Set-Up for Axial Fatigue Tests

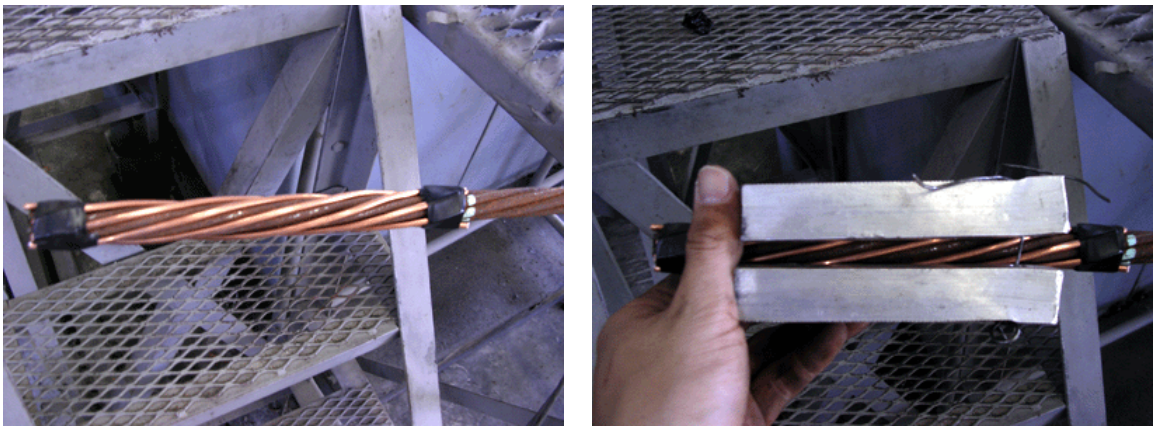

(a) Copper wires (b) Aluminum blocks

Figure A.3 Copper Wires and Aluminum Blocks Used to Grip Ends of Strand

A.1.1 Measured Fatigue Life of Strand

The results of the axial fatigue tests for Strand A are summarized in Table A.3 and the results for Strand B are summarized in Table A.4. For each test, the mean tensile stress and nominal stress range are reported. For tests that were terminated following a wire break, the number of cycles corresponds to the fatigue life of the strand. For tests that were terminated before failure (run-out), the number of cycles corresponds to the total number of applied cycles. The reason that the test was terminated is also indicated in the tables.

Table A.3 Measured Fatigue Response of Strand A

Specimen ID	Mean Stress (ksi)	Nominal Stress Range (ksi)	Number of Cycles	Reason for Terminating Test
A-1	104	40	408,528	Wire break
A-2	104	40	224,965	Wire break
A-3	104	40	245,637	Wire break
A-4	108	30	547,314	Wire break
A-5	108	30	2,345,514	Run-out*
A-6	108	30	2,375,834	Run-out*
A-7	114	20	3,308,952	Run-out*
A-8	114	20	2,477,752	Run-out*

* Test terminated before wire break.

Table A.4 Measured Fatigue Response of Strand B

Specimen ID	Mean Stress (ksi)	Nominal Stress Range (ksi)	Number of Cycles	Reason for Terminating Test
B-1	103	40	815,018	Wire break
B-2	103	40	667,259	Wire break
B-5	103	40	2,153,379	Run-out*
B-6	108	30	2,306,750	Run-out*
B-8	108	30	2,149,275	Run-out*
B-9	113	20	2,318,197	Run-out*
B-10	113	20	2,677,051	Run-out*
B-11	113	20	2,164,075	Run-out*

* Test terminated before wire break.

A.1.2 Comparison with Previous Data

Heller (2003) compiled a database of more than 650 finite-life fatigue tests of prestressing strands. More than 200 of the tests were conducted by VSL Corporation to certify strand used to construct cable-stay bridges around the world. Fatigue data from this investigation are compared with the database in Figure A.4. The stress ranges selected for study in this investigation were lower than the majority of the tests in the database. Based on this comparison, the fatigue life of Strand B appears to be near the mean of the database, while the fatigue life of Strand A appears to be lower than the majority of the strand tested in the database.

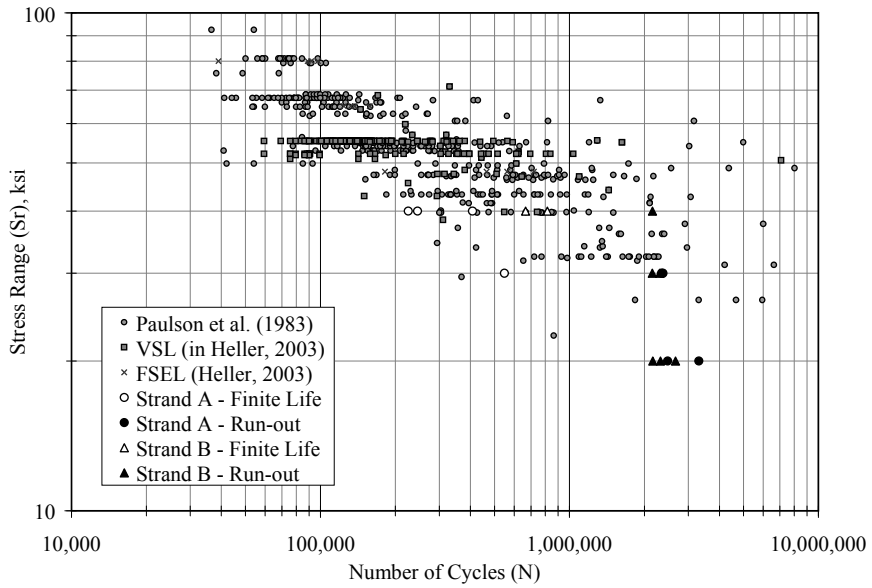

Figure A.4 Comparison of Fatigue Characteristics of Strand with Previous Data

During Project 1985, Wood et al. (2007) noted that the fatigue model for Detail Category B in the AASHTO LRFD Bridge Design Specifications (2004) provides a reasonable lower bound to the fatigue life of prestressing strand. As shown in Figure A.5, both types of 0.6-in. strand used in this investigation exhibited fatigue characteristics that exceeded the fatigue life model for Detail Category B.

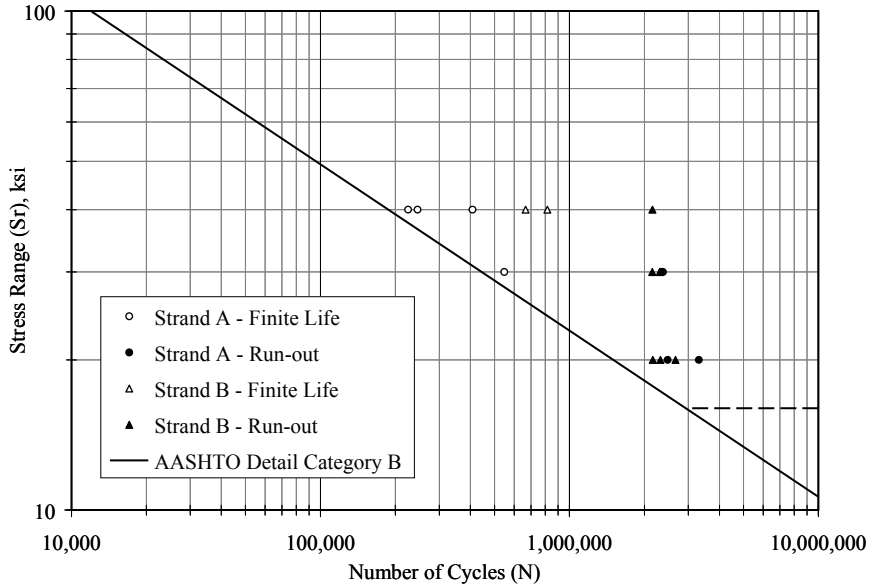

Figure A.5 Comparison of Fatigue Characteristics of Strand with Lower Bound

A.1.3 Comparison with PTI Guide Specifications

The PTI Guide Specifications (2001) include quality control tests for cable-stay bridges. An acceptance fatigue model is defined for strand, which is considerably more stringent than the lower bound model corresponding to AASHTO Detail Category B (Figure A.6). For stress ranges below 50 ksi, the PTI Guide Specification is also more stringent than the mean fatigue life model developed by Paulson et al. (1983).

Fatigue and static testing of representative samples of strand are recommended in the PTI Guide Specifications. Stress ranges for the fatigue tests are not defined explicitly; however, for each stress range selected, the corresponding minimum fatigue life can be determined from the acceptance fatigue model shown in Figure A.6.

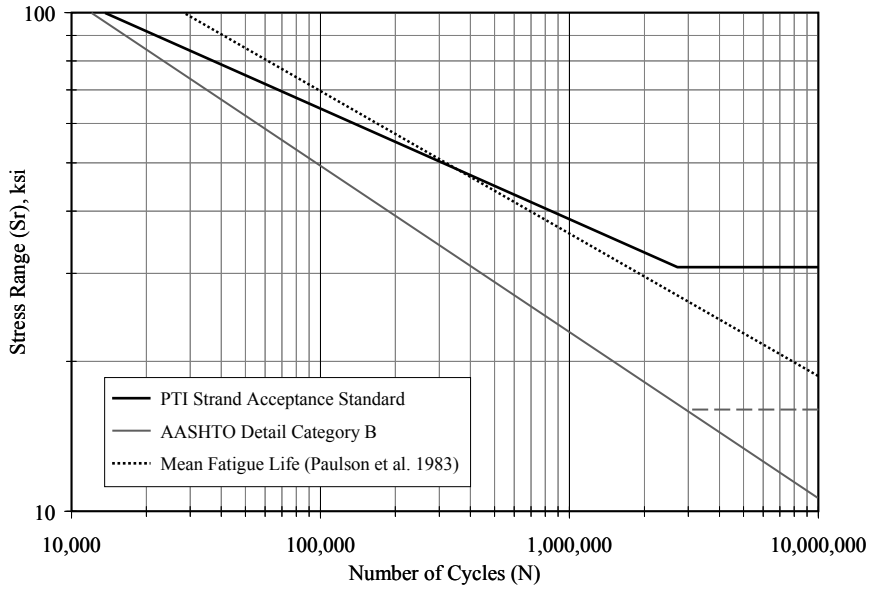

Figure A.6 Acceptance Standard for Strand from PTI Guide Specification

To satisfy the PTI recommendations, each sample of strand must resist the number of cycles corresponding to the minimum fatigue life from the acceptance fatigue model (tested using a maximum stress of 0.45 f_s') and then withstand a static load of at least 0.95 f_s' before failure. At least 5% of the strand fatigue tests must be subjected to 2 million fatigue cycles before the static test. For the acceptance fatigue model, a stress range of 33 ksi corresponds to a fatigue life of 2 million cycles.

In this investigation, the strand was subjected to fatigue loading to failure or run-out, rather than to a specified number of cycles. In addition, the strand specimens that were subjected to fatigue loads were not tested statically to failure. Therefore, it is not possible to compare the measured data directly with the PTI recommendations. However, the fatigue data are plotted with the acceptance fatigue model in Figure A.7.

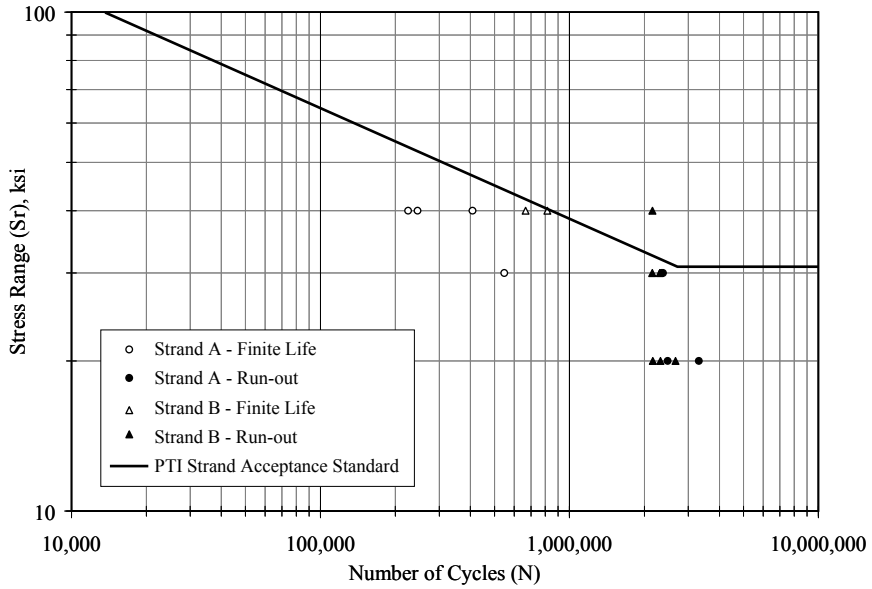

Figure A.7 Comparison of Fatigue Characteristics of Strand and PTI Strand Acceptance Model

The fatigue life of Strand A is clearly less than the PTI acceptance fatigue model at a stress range of 40 ksi. In contrast, the fatigue life of Strand B is closer to the requirements in the PTI Guide Specifications. For a stress range of 40 ksi, specimen B-5 exceeded the required number of loading cycles (847,000) and specimen B-1 was within 5%. However, based on the available data, neither strand satisfies the acceptance fatigue requirements in the PTI Guide Specifications.

A.2 BREAKING STRENGTH OF STRAND

Ridd (2004) conducted direction tension tests to verify that the strand used in this investigation satisfied the provisions in ASTM A 416 for breaking strength and to verify the values reported on the mill certificates for the strand. Tensile tests were conducted in accordance with the provisions in ASTM E 8. Three, 48-in. long specimens were tested from each type of strand. The specimens were tested in the same load frame used for the fatigue tests under displacement control at a rate of 0.04 in./sec.

The results of the tension tests are reported in Table A.5. All specimens exceeded the minimum breaking strength required by ASTM A 416 for Grade 270, 0.6-in. strand. In addition, the breaking strength reported on the mill certificates represented a lower bound to the measured data.

Table A.5 Breaking Strength of Strand

Specimen	Strand A		Strand B		ASTM A 416
	Measured	Mill Certificate	Measured	Mill Certificate	
1	59.2 kip	—	60.4 kip	—	—
2	59.5 kip	—	60.3 kip	—	—
3	59.4 kip	—	60.5 kip	—	—
Average	59.4 kip	59.0 kip	60.4 kip	60.3 kip	58.6 kip

A.3 MODULUS OF STRAND

Additional tension tests were conducted by Bean (2006) to measure the modulus of elasticity and the apparent modulus of elasticity of the strand. Three samples of Type B strand were tested. Each specimen was subjected to two cycles of loading to a maximum of 30 kip. Data measured during the second loading cycle are reported.

A.3.1 Elastic Modulus

The elastic modulus of the specimens was determined from the measured axial load and longitudinal displacement of the strand. Longitudinal displacements were measured using the apparatus designed by Heller (2003). Two aluminum blocks were attached to the strand with a gage length of 24 in. Two displacement transducers with a range of ± 0.05 in. were threaded into a third aluminum block which was not attached to the strand, but was connected to the top block by two unstressed rods. The transducers measured the relative displacement between the two blocks attached to the strand (Figure A.8).

The stress in the specimen was calculated by dividing the measured load by the area of the strand reported on the mill certificate (Table A.2). The longitudinal strain in the strand was calculated by dividing the average longitudinal displacement from the two transducers by the gage length of 24 in.

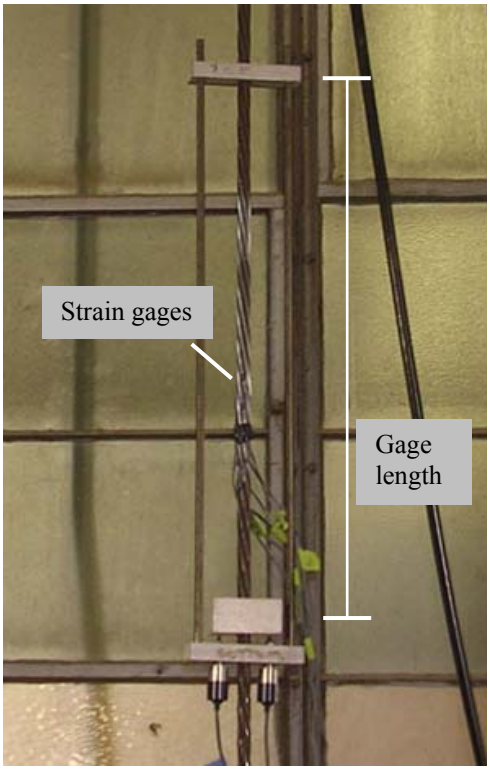

(a) Overall

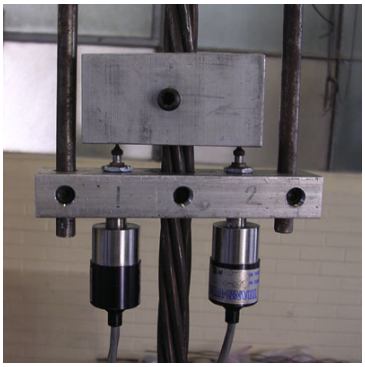

(b) LVDTs

(c) Strain gages

Figure A.8 Instrumentation Used to Measure Longitudinal Displacement and Local Strain

Test results are summarized in Table A.6 and representative data are plotted in Figure A.9. The elastic modulus was taken as the slope of the best-fit line between the stress and the longitudinal strain data. The measured elastic modulus exceeds the requirements given in ASTM A 416.

Table A.6 Elastic Modulus of Strand

Specimen	Strand B		ASTM A 416
	Measured	Mill Certificate	
1	29,500 ksi	—	—
2	29,100 ksi	—	—
3	29,500 ksi	—	—
Average	29,400 ksi	28,300 ksi	27,500 ksi

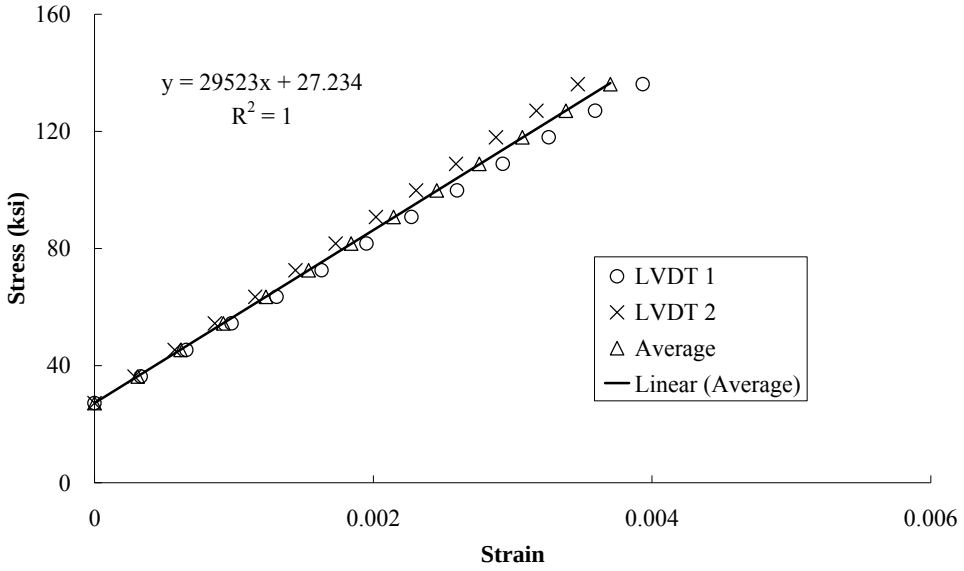

Figure A.9 Relationship between Axial Stress and Longitudinal Strain for Specimen 3

A.3.2 Apparent Modulus of Elasticity

For the 0.6-in. diameter strand used in this investigation, the local axes of the outer wires were rotated approximately 10º from the longitudinal axis of the strand (Figure A.10). Three-mm strain gages were attached to the outer wires of the strand and aligned along the axes of the individual wires (Figure A.11). The number of strain gages varied from two for specimen 2 to six for specimen 1.

The apparent modulus was taken as the slope of the best-fit line between the axial stress and the strains measured along the local axes of the wires. The results are summarized in Table A.7 and representative data are plotted in Figure A.12.

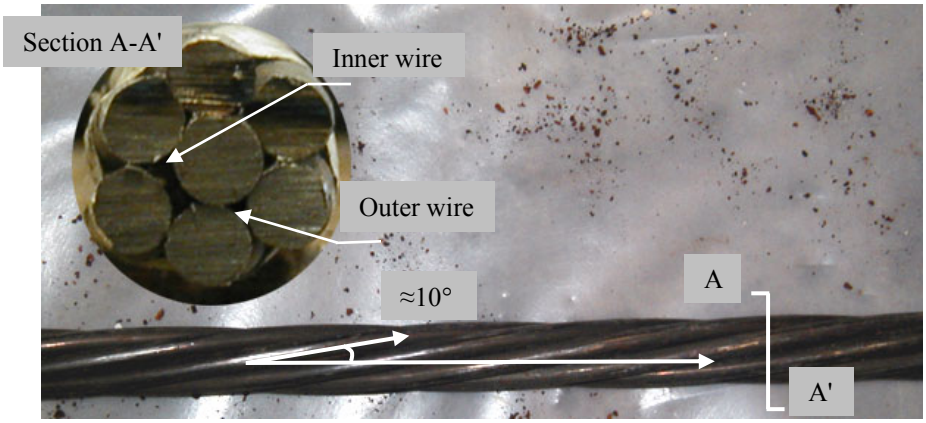

Figure A.10 Geometry of 0.6-in. Strand

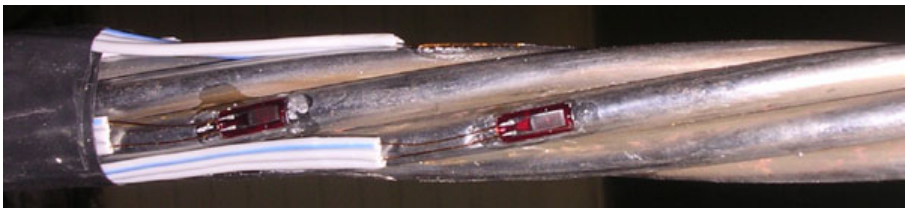

Figure A.11 Strain Gages Positioned along Local Axes of Wires

Table A.7 Apparent Modulus of Elasticity of Strand

Specimen	Gage	Apparent Modulus (ksi)
1	1	31,030
	2	30,950
	3	29,500
	4	30,480
	5	30,880
	6	31,380
2	1	32,020
	2	30,570
3	1	31,140
	2	30,500
	3	30,430
Average		30,800

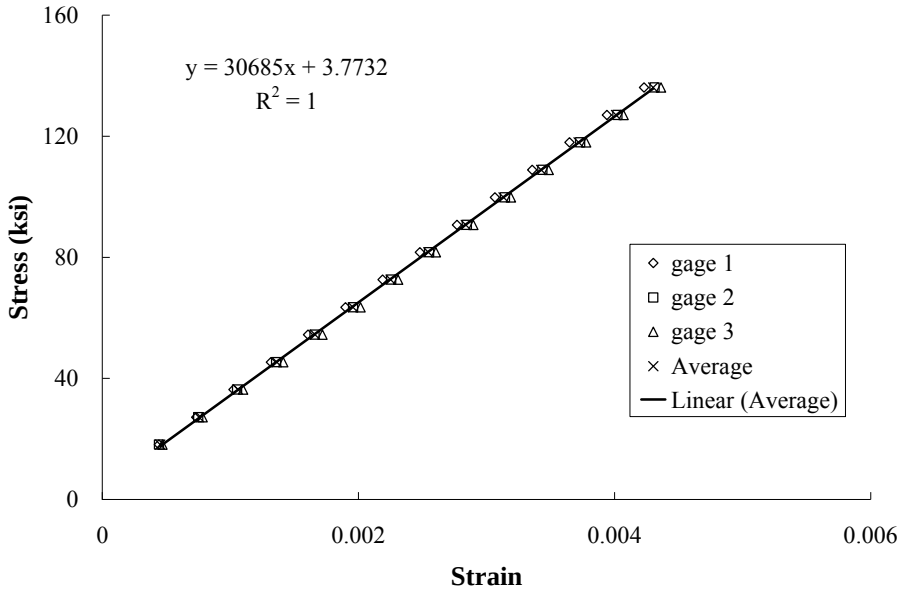

Figure A.12 Relationship between Axial Stress and Local Strain for Specimen 3

Based on the test results from the three specimens, the average modulus of elasticity was determined to be 29,400 ksi and the apparent modulus of elasticity was determined to be 30,800 ksi. The apparent modulus is approximately 5% larger than the modulus of elasticity.

A.4 SUMMARY

Based on the tests discussed in this appendix, the prestressing strand used to construct the bending fatigue specimens satisfied the strength and modulus requirements in ASTM A 416. While the fatigue characteristics of both types of strand exceeded lower-bound models for fatigue life, the strand did not satisfy the fatigue model for acceptance using the PTI Guide Specifications (2001).

APPENDIX B: CONSTRUCTION OF STAY-CABLE SPECIMENS

Twelve, large-scale, cable-stay specimens were constructed and subjected to fatigue loads during this investigation. The procedures used to construct the specimens are summarized in this appendix. The research was divided into two phases, and several of the components used to construct the specimens were different in the two phases. Specimens 1 through 4 were constructed and tested in the first phase (Poser 2001). VSL International, the cable supplier for the Fred Hartman Bridge, fabricated the anchorage components used to construct these specimens. Specimens 5 through 12 were constructed and tested during the second phase of the research (Ridd 2004). Several of the components were simplified for the second series of tests and most of the anchorage components were fabricated at a local machine shop. However, cable-stay wedges produced by VSL International were used to construct all twelve cable-stay specimens.

This appendix is divided into five sections. The moveable reaction frame used to resist the prestress within the stay-cable specimens is discussed in Section B.1. The configurations of the specimens tested in both phases of the research are summarized in Section B.2. An overview of the construction process is presented in Section B.3 and the unique characteristics of seven specimens are summarized in Section B.4. Additional information about the specimens is available in Poser (2001) and Ridd (2004). The acoustic system used to monitor the response of the test specimens, and the stay cables on the Fred Hartman and Veterans Memorial Bridges, is discussed in Section B.5

Although the stay-cable specimens were tested horizontally, the terms “deck anchorage” and “tower anchorage” are used throughout this appendix. The tower end of the specimen was elevated during the grouting procedure; therefore, a distinction is made between the two ends of the specimen. In addition, the two ends of the specimens were not symmetric in the first phase of the investigation: two shims were used at the tower end, but not at the deck end. This detail is consistent with the stay cables in the Fred Hartman Bridge, but was eliminated in the second phase of the investigation.

B.1 REACTION FRAME

A steel frame consisting of two longitudinal wide flange columns and built-up crossbeams at both ends was used to resist the initial stressing force in the stay-cable specimens and the forces induced during the fatigue tests (Figure B.1). W14x90 sections were used as the longitudinal members and the built-up crossbeams were fabricated using two W18x97 beams with welded stiffeners and a load distribution plate with an opening for the stay cable. The load distribution plate is in direct contact with the anchorage zone of the stay-cable specimens. Vertical shear forces were transferred into the laboratory floor using a T-section with anchor bolts as shown in Figure B.2.

Figure B.1 Steel Reaction Frame

The geometry of the reaction frame was selected such that the webs of the T-sections were spaced 32 ft apart to be compatible with the strong floor in Ferguson Laboratory. Because the load distribution plates and the shims were positioned outside the crossbeams, the reaction frame could accommodate specimens with an overall length of 32 ft 11⅜ in. in the first phase, when shims were used, and specimens with an overall length of 32 ft 7¼ in. in the second phase, when the shims were not used. The shims are shown at the right (tower) end of the specimen in Figure B.2 and will be discussed in more detail in Section B.2.

The reaction frame was designed to be movable with a tensioned cable-stay specimen. This characteristic was necessary because the specimens were grouted in an inclined position, whereas the bending fatigue tests were conducted in a horizontal position.

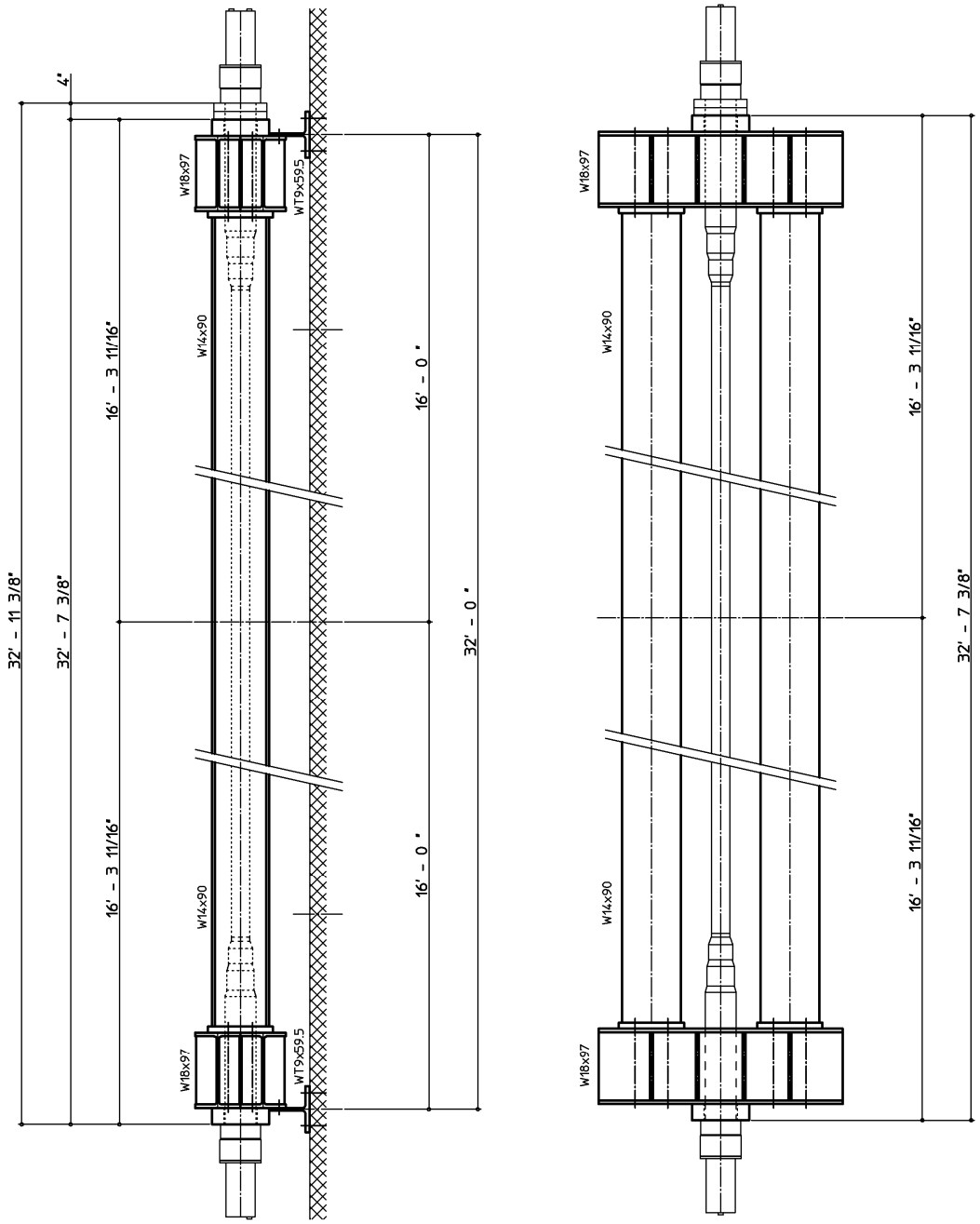

Figure B.2 Geometry of Reaction Frame

B.2 CONFIGURATION OF TEST SPECIMENS

The test specimens were modeled after the smallest-diameter stay cables on the Fred Hartman Bridge. The anchor heads and tension rings used to construct the specimens were nominally identical to those used on the bridge. However, the test specimens were considerably shorter than the prototype stay cables. As summarized in Table B.1, the primary experimental variables in the bending fatigue tests were the type of strand, the number of strands, the presence of grout near the anchor heads, and the end of the specimen that was stressed.

The anchor heads could accommodate a maximum of nineteen, 0.6-in. strands. The strands were parallel in the middle section of each specimen (between the tension rings) and fanned out between the tension ring and the anchor head at each end to permit stressing. The dimensions of the cross section at the anchor head and along the free length are given in Figure B.3 and Figure B.4, respectively.

The stay cables on the Fred Hartman Bridge were constructed with two types of corrosion protection. The strands were enclosed within polyethylene pipe, which was filled with a portland cement-based grout. Nine of the twelve test specimens were constructed in the same manner. The PE pipe is shown in Figure B.3 and Figure B.4, and the inside of the pipe is filled with grout.

Table B.1 Summary of Experimental Parameters for Cable-Stay Specimens

Specimen ID	Number of Strands	Type of Strand	Grout	Stressing End	Unique Characteristics
1	19	A	Grouted	Tower	Unintentional grout void.
2	19	A	Grouted	Tower	
3	19	A	Grouted	Deck	Intentionally crossed strands.
4	19	A	Grouted	Deck	
5	19	A	Ungrouted	Tower	Strain gages attached to four strands
6	13	A	Grouted	Tower	
7	19	B	Grouted	Tower	
8	19	B	Ungrouted	Tower	Misaligned strand near tension ring.
9	19	B	Grouted	Tower	Intentional grout void.
10	19	B	Grouted	Tower	Amplitude of fatigue cycles decreased after 2,200 cycles.
11	19	B	Hybrid	Tower	Frequency of fatigue cycles varied during first 400,000 cycles.
12	19	B	Grouted	Tower	

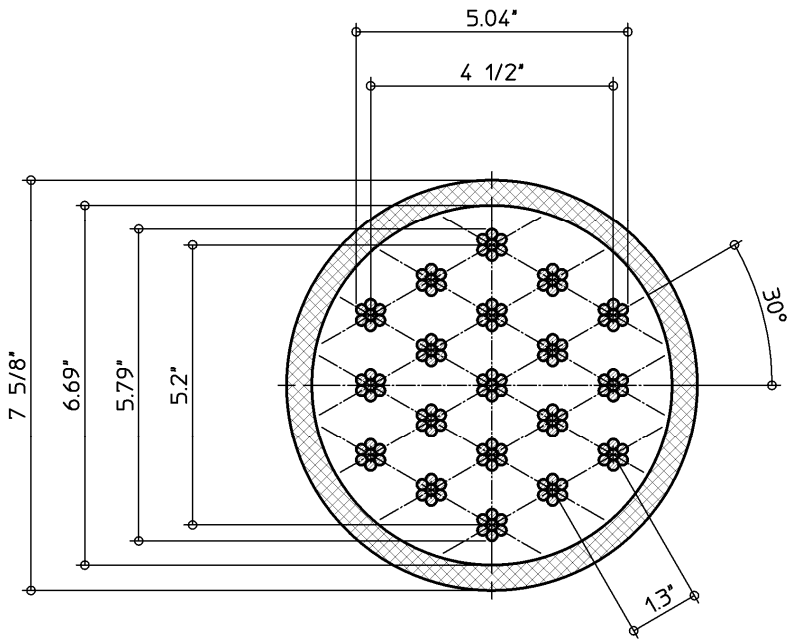

Figure B.3 Cross-Sectional Geometry of Stay-Cable Specimen at Anchor Head

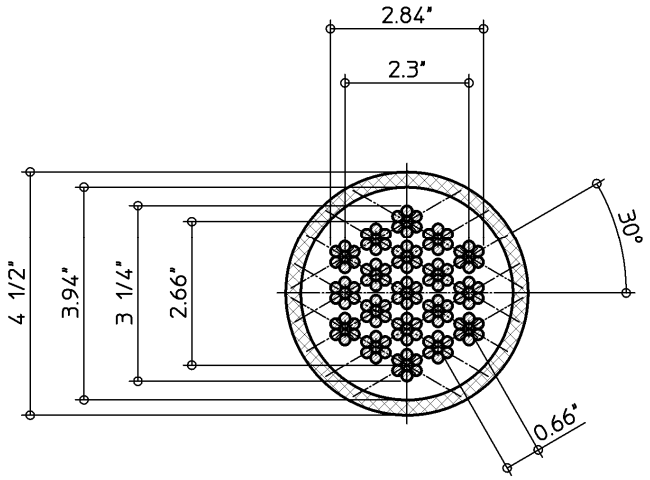

Figure B.4 Cross-Sectional Geometry of Stay-Cable Specimen along Free Length

The transition from the two limiting cross sections occurred within the anchorage zone. Exploded views of the anchorage elements used in both phases of the research are shown in Figure B.5 and Figure B.6. The components used in the first phase were supplied by VSL International and were fabricated based on the construction drawings for the Fred Hartman Bridge. In this design, the end of the PE transition pipe screws into the large-diameter nut, which was bolted to the anchor head. This connection was simplified in the second phase of the research. The PE transition pipe was fabricated with a flange. The smooth end sleeve engaged this flange and was bolted to the anchor head. These changes were considered to be minor and were not expected to influence the fatigue performance of the test specimens. The changes, however, did reduce the cost of machining the anchorage components.

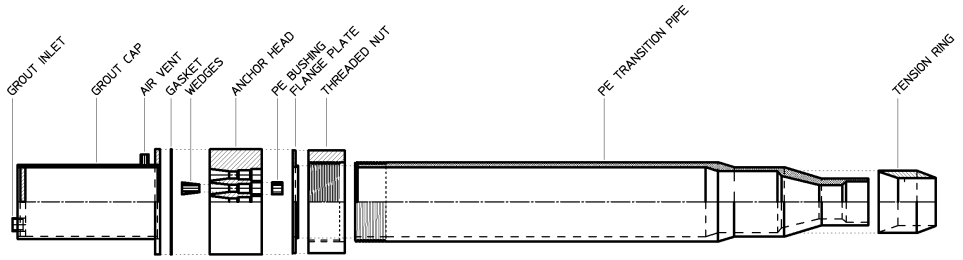

Figure B.5 Exploded View of Deck Anchorage Elements (Phase 1)

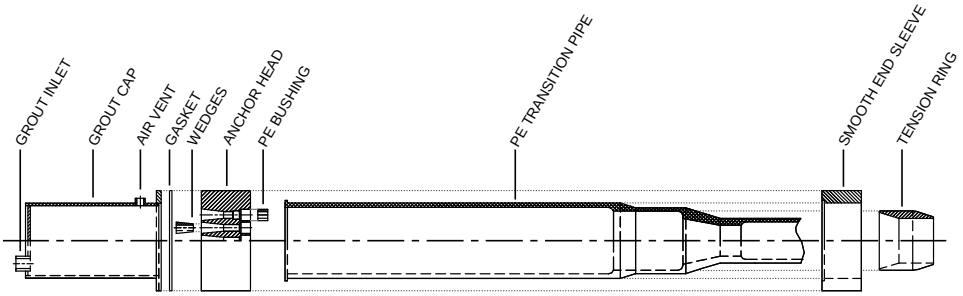

Figure B.6 Exploded View of Deck Anchorage Elements (Phase 2)

Sketches of the assembled anchorage components are shown in Figure B.7 for specimens tested in the first phase and in Figure B.8 for specimens tested in the second phase. In the first phase of the research, the two ends were not symmetric: the tower end included two shims that were not used at the deck end. The shims were necessary to construct the stay cables on the Fred Hartman Bridge, but were not required to construct the test specimens due to their shorter length. Therefore, the shims were not used in the second phase of the research. The two ends were nominally identical in this configuration.

The overall dimensions of the nine grouted test specimens are shown in Figure B.9 and Figure B.10. Transverse loads were applied at the middle of the steel reaction frame in all cases. Due to the presence of the shims in the first phase of the reserach, the anchor head at the tower end was 4 in. further from the location of the applied load than the anchor head at the deck end. The test specimens were symmetrical in the second phase.

In order to investigate the influence of the grout on the stiffness and fatigue life of the stay-cable specimens, three specimens in the second phase of the research were not grouted along their entire length. The overall dimensions for these specimens are shown in Figure B.11.

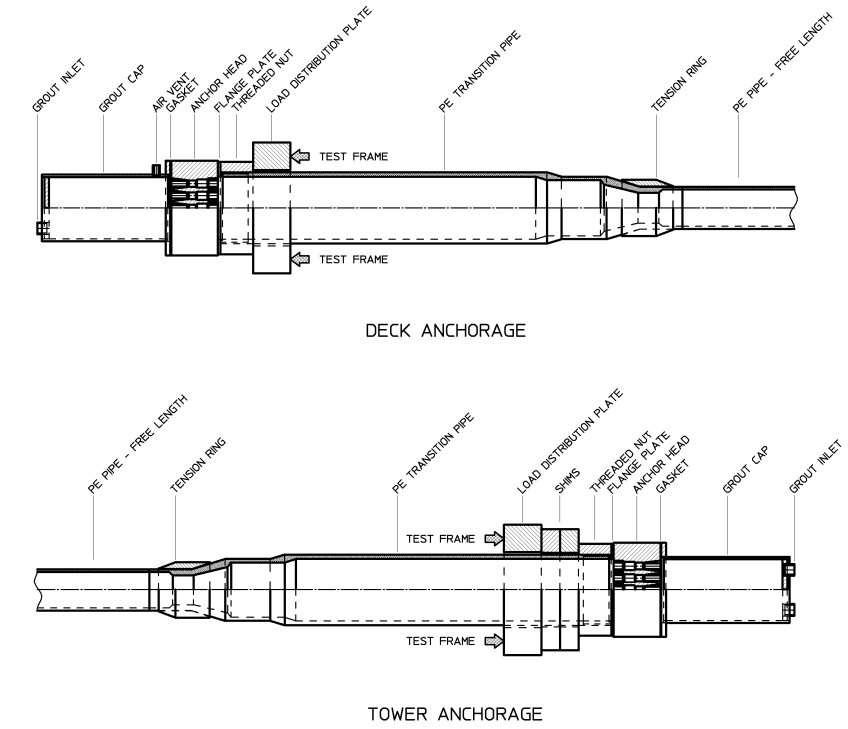

Figure B.7 Anchorage Elements of the Stay-Cable Specimens (Phase 1)

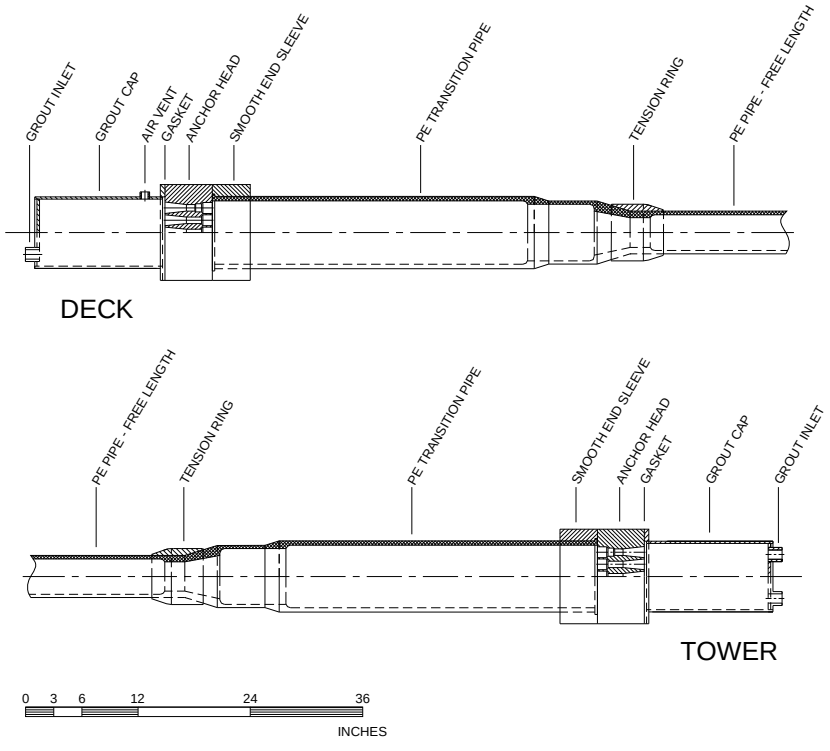

Figure B.8 Anchorage Elements of the Stay-Cable Specimens (Phase 2)

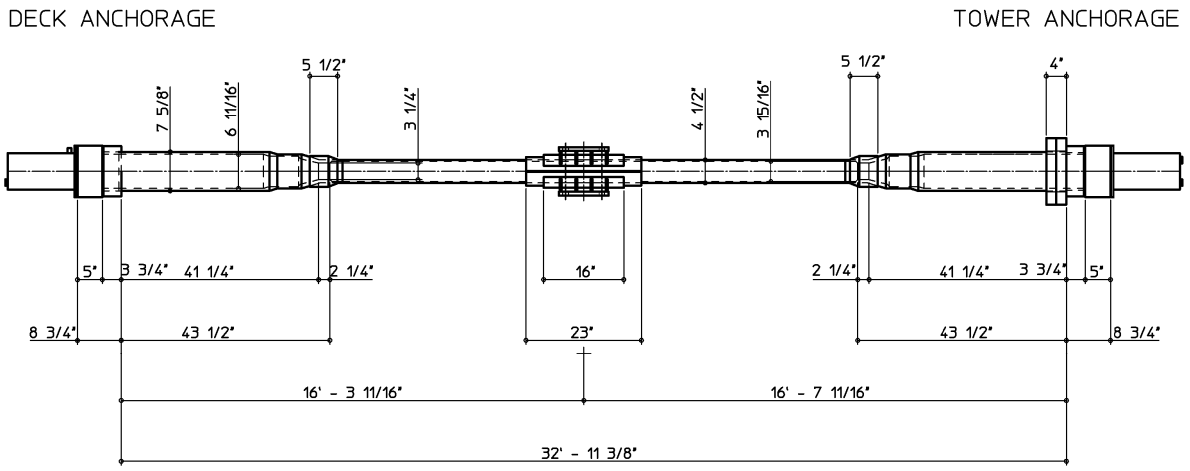

Figure B.9 Dimensions of Grouted Test Specimens (Phase 1)

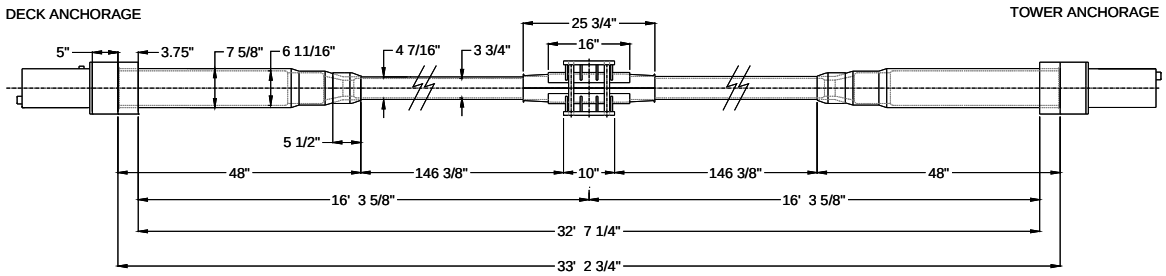

Figure B.10 Dimensions of Grouted Test Specimens (Phase 2)

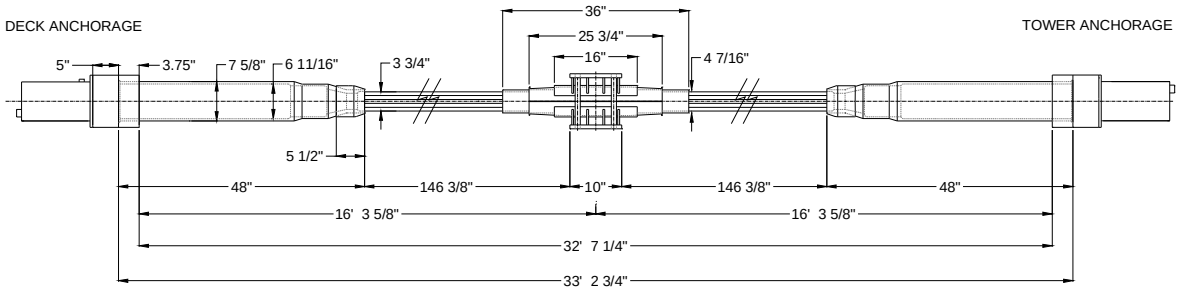

Figure B.11 Dimensions of Ungrouted and Hybrid Test Specimens (Phase 2)

A clamp was designed to connect the hydraulic actuator to the test specimens. Due to the concentrated load and localized deformations, relatively large stresses were induced in the specimens in the vicinity of the clamp and a large portion of the wire breaks occurred in this region. In order to minimize the stress concentrations, the transition region between the clamp and the free length of the specimens was designed several times. None of the designs was successful in eliminating the stress concentrations near midspan, however.

The initial design of the clamp and transition region is shown in Figure B.12 and Figure B.13. The width of the steel clamp is 16 in. and an extra layer of polyethylene (22-in. long) was positioned at midspan in attempt to cushion the stay cable (Poser 2001). In the second phase of the research, the length of the extra layer of polyethylene was increased to 26 in. and the thickness was tapered over a length of 6 in. from each end (Figure B.14 and Figure B.15).

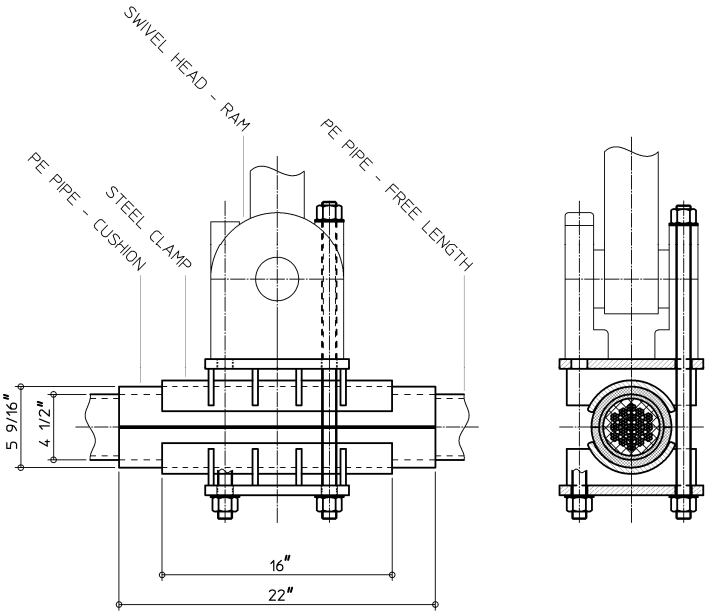

Figure B.12 Geometry of Clamp and Transition Region (Phase 1)

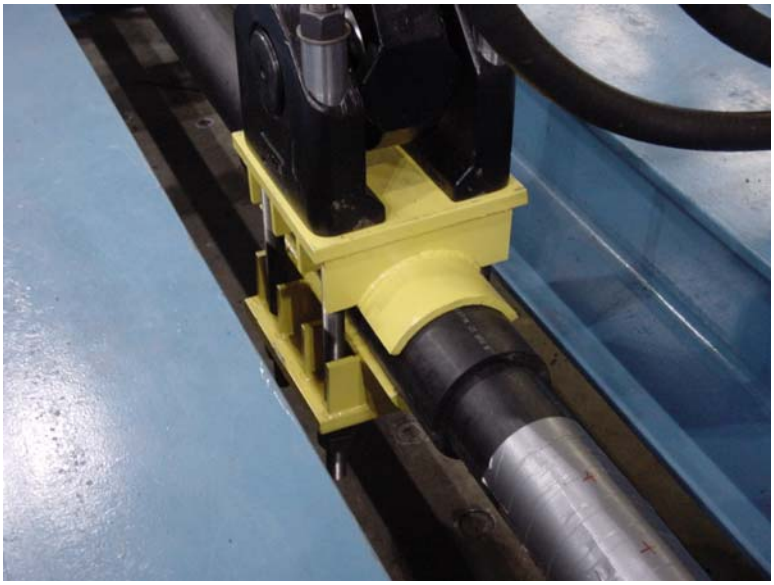

Figure B.13 Photograph of Clamp (Phase 1)

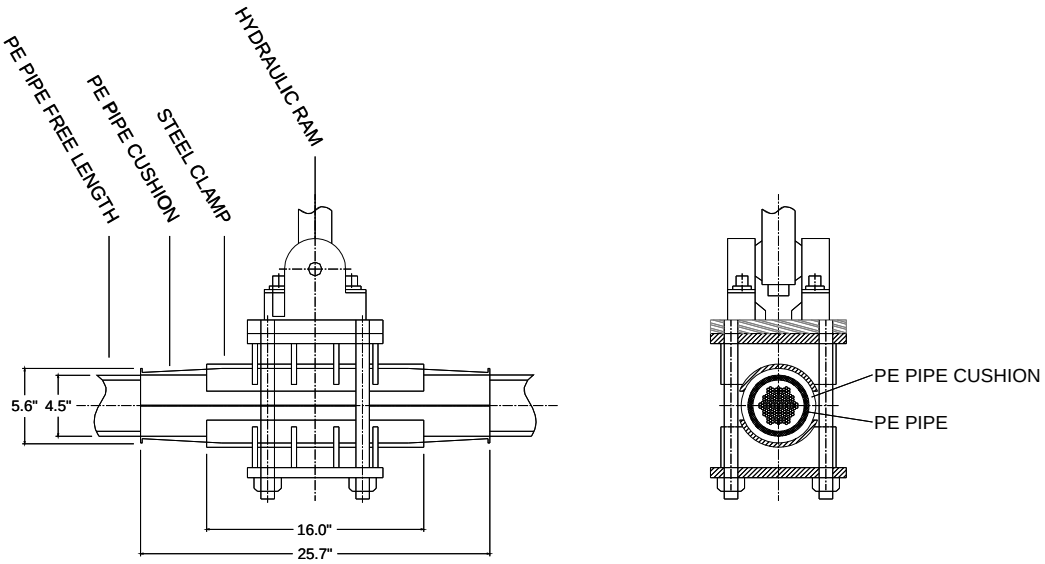

Figure B.14 Geometry of Clamp and Transition Region (Phase 2)

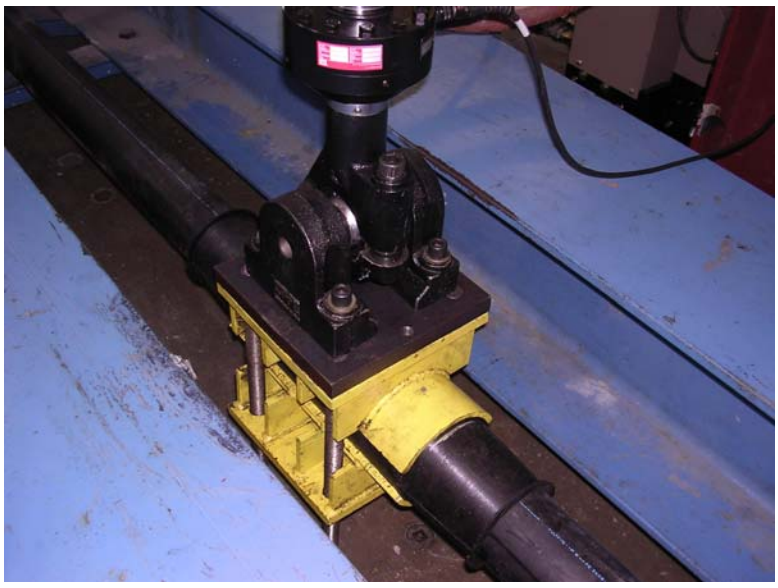

Figure B.15 Photograph of Clamp (Phase 2)

B.3 CONSTRUCTION OF STAY-CABLE SPECIMENS

The construction process for the stay-cable, bending fatigue specimens may be divided into three basic steps: (1) assembly of the components within the reaction frame, (2) stressing the strands, and (3) grouting the specimen. Section B.3.1 summarizes the procedures used to assemble the components and Section B.3.2 summarizes the procedures used to stress the strands. The procedures used to grout the grouted, ungrouted, and hybrid specimens are summarized in Sections B.3.3, B.3.4, and B.3.5, respectively. Additional details are given in Poser (2001) and Ridd (2004).

B.3.1 Assembly of Components

Prior to assembling the components, 48-ft long sections of prestressing strand were cut. Although the overall length of the test specimens was approximately 36 ft, the additional length was required for prestressing. All the strands in a given test specimen were taken from the same spool of strand. Strand A was used to construct Specimens 1 through 6 and Strand B was used to construct Specimens 7 through 12.

As shown in Figure B.16, the anchorage elements were assembled and one unit was positioned in the steel reaction frame. The individual strands were then inserted into the anchor head and pulled along the length of the reaction frame (Figure B.17). Care was taken to ensure that the strands remained parallel and did not cross along the length of the specimen. This was particularly important at the location of the tension ring, where the inside diameter of the PE transition pipe was the smallest and the strands were the most congested.

The center section of PE pipe, including the helical spacer wire, was then inserted into the reaction frame and pulled into position (Figure B.18). The spacer wire was fabricated from 0.25-in. plain steel wire and was used to center the strand within the PE pipe (Figure B.19).

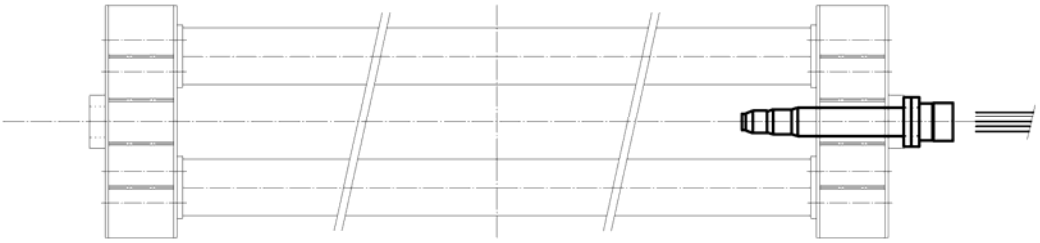

Figure B.16 Placement of First Anchorage Assembly in Steel Reaction Frame

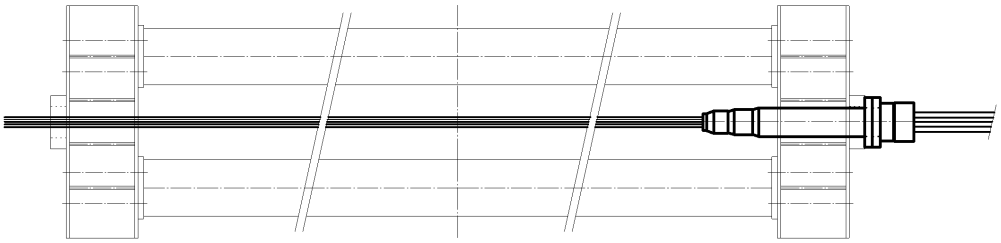

Figure B.17 Initial Position of Strand in Steel Reaction Frame

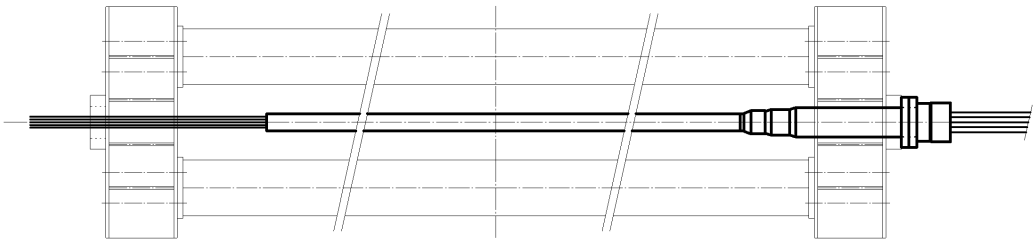

Figure B.18 Placement of PE Pipe

Figure B.19 Helical Spacer Wire inside PE Pipe along Free Length of Specimen

The second anchorage assembly was then positioned in the reaction frame (Figure B.20), and finally the second anchor head was put in place (Figure B.21). Care was taken to ensure that each strand was in the same position in the anchor heads at both ends of the test specimen.

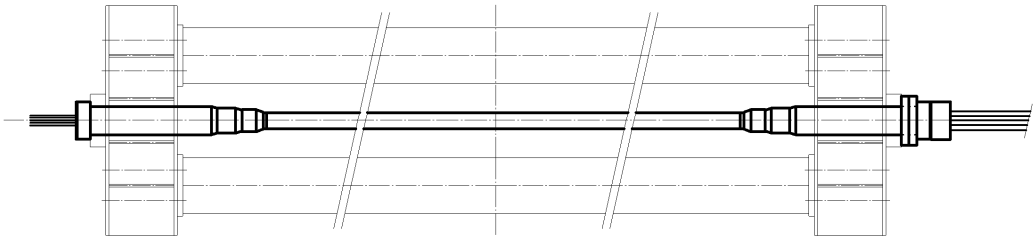

Figure B.20 Placement of Second Anchorage Assembly

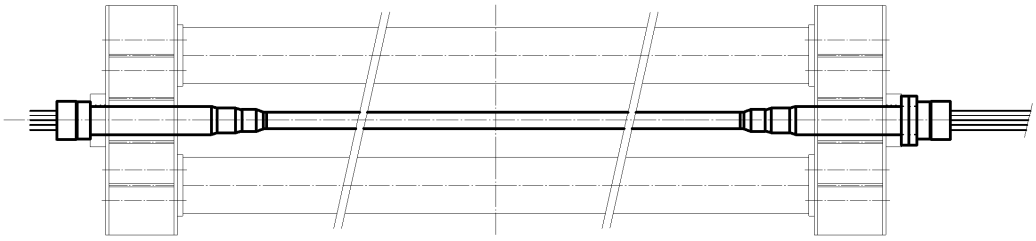

Figure B.21 Installation of Second Anchor Head

For the ungrouted and hybrid specimens, the construction process was the same; however, the PE pipe did not extend the entire free length of the specimen. A short section of PE pipe (36 to 39 in.) was positioned at midspan and the helical spacer was not used in this section. The PE transition pipes were used at both ends of all specimens.

B.3.2 Stressing the Strand

As shown in Figure B.22, the wedges were installed around each strand in both anchor heads. Each of the VSL wedges comprises two halves that fit into the tapered opening in the anchor head (Figure B.23). After being anchored with the wedges, a prestress of approximately 2 kip was applied to each strand individually, starting with the center strand. This initial prestress was applied to straighten the strands and seat the wedges. The seating force was applied using a mono-strand ram (Figure B.24).

Figure B.22 Installed Wedges

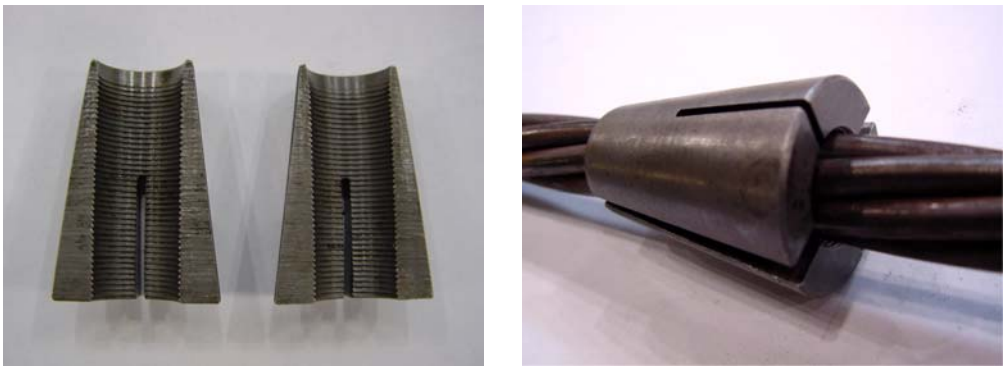

Figure B.23 Wedges

Figure B.24 Application of Initial Prestress to Individual Strands

After the components were straightened, all of the strands were pulled together to prestress the stay-cable specimen. The prestressing ram was inserted over the extra length of cable at stressing end. An extra anchor head was installed behind the ram, which was used to react against during the stressing operation (Figure B.25). A spring plate was placed between the ram and the anchor head (Figure B.26) to ensure that equal pressure was applied to all strands and that the wedges were seated evenly.

Figure B.25 Hydraulic Ram Used to Stress the Cable-Stay Specimen

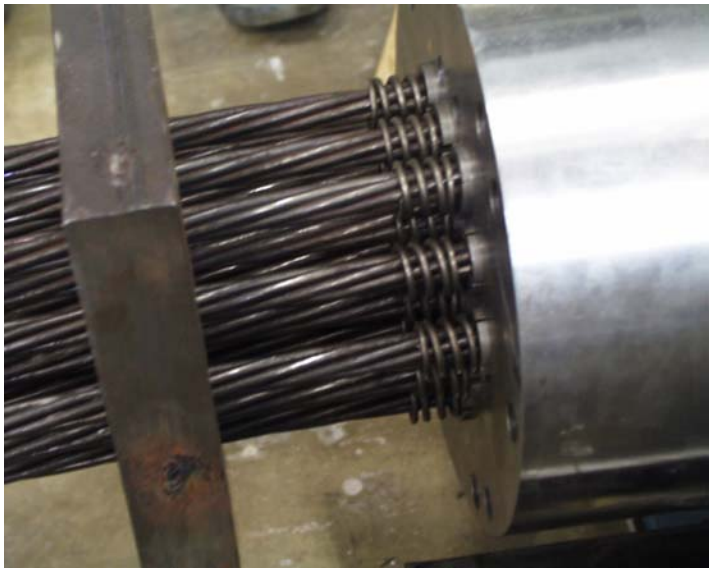

Figure B.26 Spring Plate Used during Stressing

The load was applied to the specimen in five to seven increments to minimize prestress losses. During each step, the force in the ram was increased to a maximum level, and then released to a minimum level, with the value of the maximum and minimum force increasing in subsequent steps. The nominal value of the full tension applied to the cable was 40% of the guaranteed ultimate tensile strength of the strand. This nominal value was 450 kip for the 19-strand specimens and 308 kip for the 13-strand specimen (Specimen 6).

For most of the test specimens, the tower end was the live end for stressing and the deck end was the dead end. However, for Specimens 3 and 4, the deck end was the live end for stressing. Following stressing, the PE transition pipes were welded to the PE pipe along the free length of the specimen using a commercially available plastic welder.

B.3.3 Grouting the Grouted Specimens

The reaction frame was inclined approximately 30 degrees for grouting (Figure B.27). A combined grout mixer and pump was used to fill the tensioned cable with grout, which consisted of Type I portland cement and tap water with a water-to-cement ratio of 0.42. An anti-bleed admixture (Sikament 300 SC) was also added in the recommended proportion of 2.2% by weight of cement.

After mixing the grout thoroughly, the grout was pumped into the grout cap at the deck end and through the stay. Pumping of the grout continued until gout flowed out grout cap at the tower end. The maximum pressure during grouting was limited to 70 psi to prevent the hoses and PE from rupturing.

Figure B.27 Grouted Specimen in the Inclined Position for Grouting

B.3.4 Grouting the Ungrouted Specimens

For the ungrouted specimens, only a 3-ft section of PE pipe at midspan was grouted (Figure B.11). This detail was necessary to provide a sound connection between the hydraulic actuator and the test specimen. PVC end caps were used at the ends of the PE pipe and were caulked to prevent leakage of the grout (Figure B.28).

Figure B.28 PE Pipe and PVC End Caps used at Midspan of Ungrouted Specimens

The reaction frame was propped on concrete blocks (Figure B.29), resulting in an inclination of approximately 10 degrees. The grout was pumped into the specimen at the lower end of the center section and exited at the upper end.

Figure B.29 Ungrouted Specimen in the Inclined Position for Grouting

B.3.5 Grouting the Hybrid Specimen

The hybrid specimen was grouted at the center and both ends, but ungrouted between the tension ring and midspan at each end (Figure B.30). As with the ungrouted specimens, PVC end caps were used to seal the ends of the PE pipe (Figure B.31). The specimen was grouted in three stages: (1) the tower end was elevated to grout the deck end, (2) the deck end was elevated to grout the tower end, and (3) the center section was grouted with the specimen in a horizontal position.

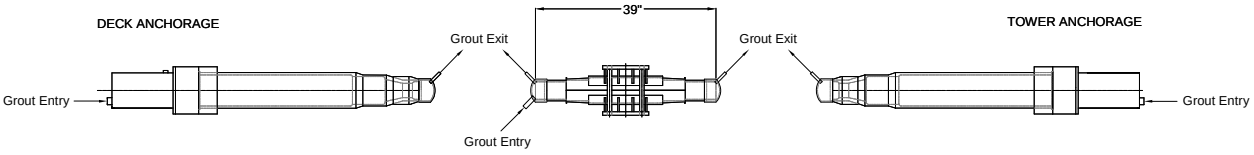

Figure B.30 Grout Ports for Hybrid Specimen

Figure B.31 PVC Cap in Position Adjacent to Tension Ring in Hybrid Specimen

B.4 CONSTRUCTION DETAILS FOR INDIVIDUAL SPECIMENS

Several of the construction details were unique for individual specimens. In some cases, these details influenced the fatigue response of the specimens; therefore, the unique characteristics are summarized below. Only four specimens identified in Table B.1 are discussed.

B.4.1 Specimen 1

During the construction of Specimen 1, three decisions were made that were changed in subsequent specimens. The decisions, and ramifications, are summarized below.

The anchor heads were fabricated with four grout inlets, as shown in Figure B.32. During the construction of Specimen 1, the grout inlets were oriented horizontally. This orientation of the anchor head caused the formation of an unintentional grout void at the tower end of the specimen. In all subsequent tests, the anchor heads were positioned such that the grout inlets were oriented vertically (Figure B.33) and these grout voids were avoided. However, there are no mechanical aids on the bridge anchorage that ensure correct orientation of the anchor heads and the orientation was not indicated on the construction drawings for the Fred Hartman Bridge. Furthermore, the anchor heads used for some of the larger stays on the Fred Hartman Bridge had grout outlets within the strand pattern, which means that it is common to have strands positioned above the grout inlet.

The grout used to construct Specimen 1 did not include the anti-bleed admixture. The bleed water likely contributed to the presence of the grout void at the tower end of Specimen 1.

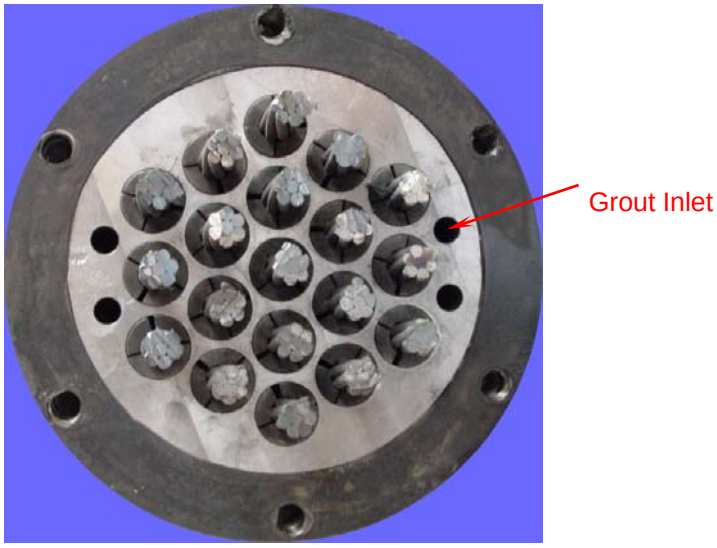

Figure B.32 Anchor Head Orientation for Specimen 1

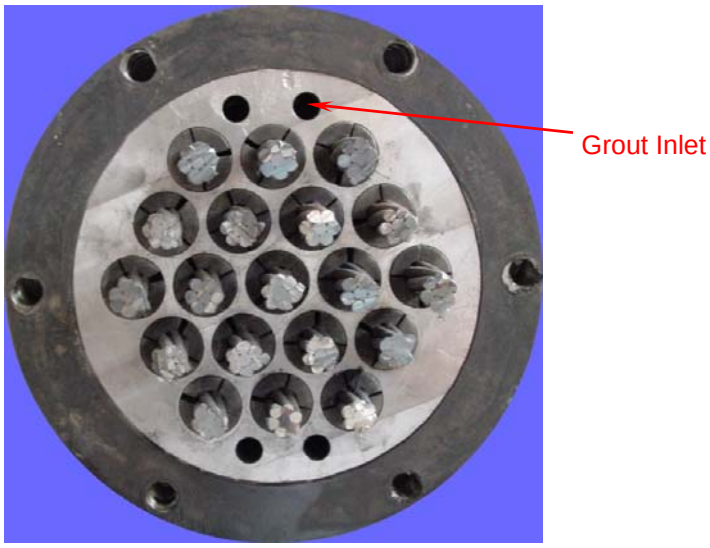

Figure B.33 Anchor Head Orientation for Specimens 2 through 12

The spring shown at the end of the mono-strand ram in Figure B.24 was not used during the initial stressing of each strand for Specimen 1. As a result, the wedges for some of the strands were seated unevenly at the deck end (Figure B.34). The wedges were marked after the initial stressing, and no movement of the wedges was observed during the final stressing or the fatigue test. Using the spring during the initial stressing provided even seating of the wedges in subsequent specimens.

Figure B.34 Unequally Seated Wedges at the Deck End of Specimen 1

B.4.2 Specimen 3

Two pairs of strands (one pair at the top and one pair at the bottom of the anchor head) were intentionally crossed at both ends between the tension ring and the anchor head in Specimen 3. Because the strands were crossed in two locations, the strands were in the correct locations at the anchor head at the deck and tower ends. Figure B.35 shows an arrangement of crossed strands that was obtained in a preliminary experiment, where the PE pipe was not present. Only the strands at the top and bottom were crossed in Specimen 3 (red and green strands) and not the strands on the side in Figure B.36 (yellow and white strands).

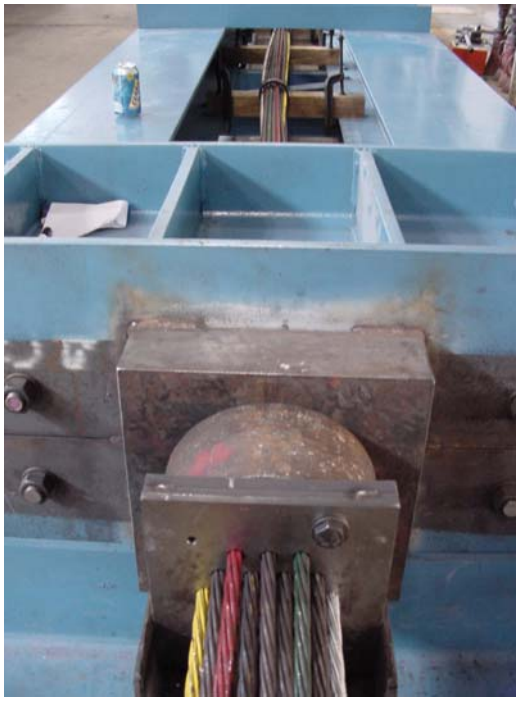

Figure B.35 Crossed Strands

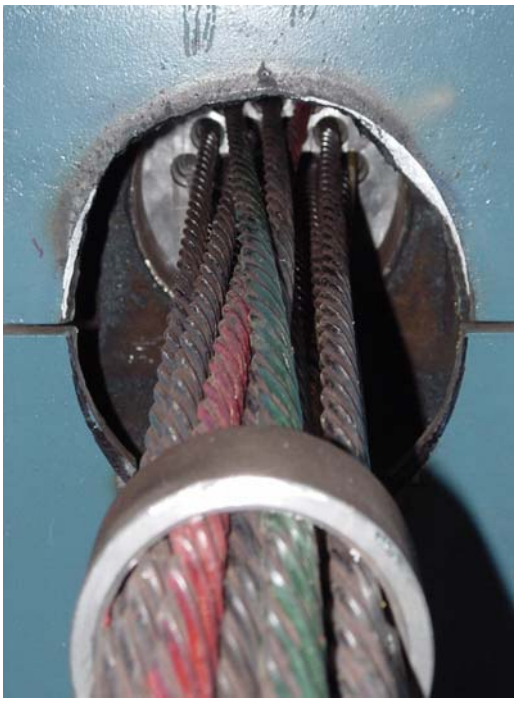

Figure B.36 Contact Point

B.4.3 Specimen 5

Specimen 5 was ungrouted. The absence of grout in the stay allowed for the use of strain gages to monitor strand stresses near the anchor head. Eight strain gages were applied at the deck end of the stay, two each on strands 1, 3, 17, and 19 as shown in Figure B.37. The distance between each gage and the inside face of the anchor head is listed in Table B.2. However, due to the presence of the PE transition pipe, it was only possible to measure these distances before the strands were stressed. Therefore, these locations must be considered as approximate. Gages were attached to the extreme exterior wire of the strand at the point of application; therefore, the two strain gages attached to each strand were not necessarily applied to the same wire.

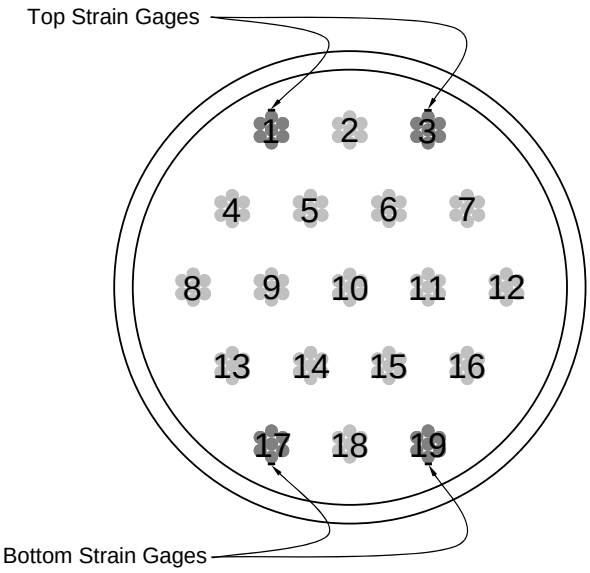

Figure B.37 Strain Gages used to Monitor the Response of Specimen 5

Table B.2 Location of Strain Gages used to Monitor the Response of Specimen 5

Gage	Strand	Location* (in.)
1	1	2.8
2	1	4.3
3	3	2.7
4	3	4.3
5	17	2.0
6	17	3.7
7	19	2.3
8	19	3.8

* Distance from inside face of anchor head to strain gage was measured before strands were stressed.

B.4.4 Specimen 8

Specimen 8 was ungrouted, but strain gages were not attached to the strands. During construction, one of the interior strands from the middle row was caught between two of the exterior strands near the tension ring at the deck end (Figure B.38). The strands were not crossed, but the misalignment caused extensive fretting between adjacent strands near the tension ring.

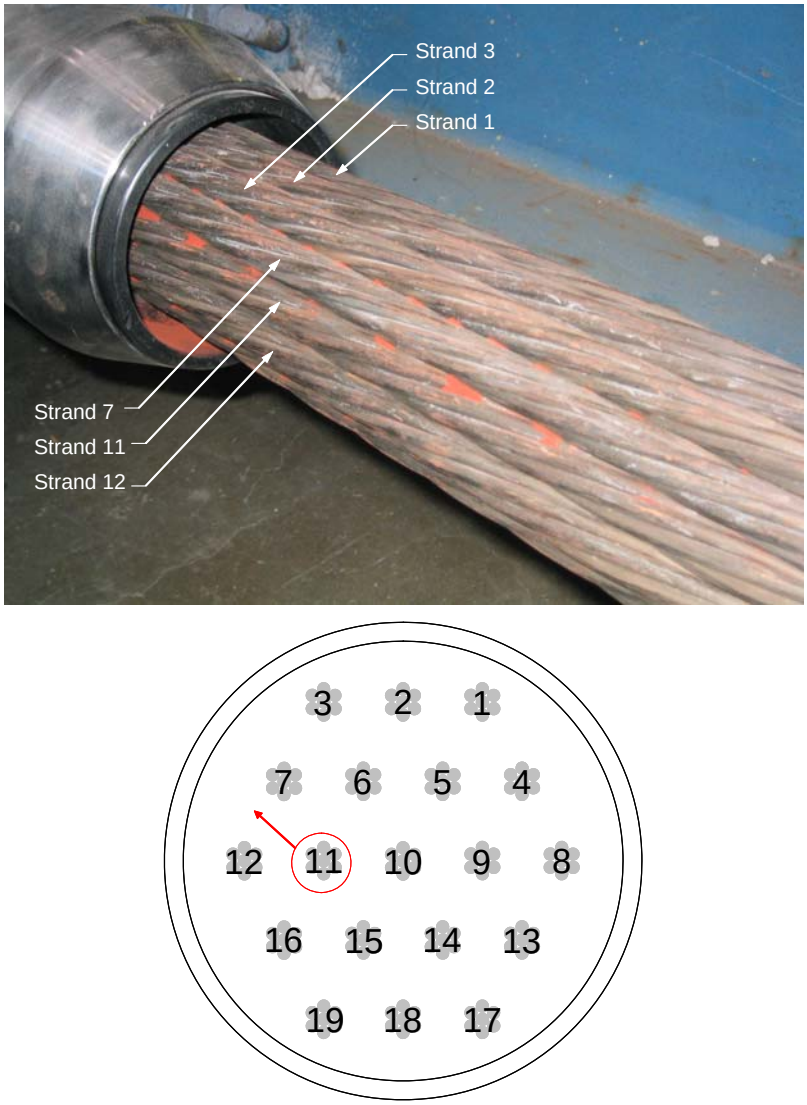

Figure B.38 Misalignment of Strands at Deck Tension Ring – Specimen 8

B.4.5 Specimen 9

Specimen 9 was grouted along the entire length; however, a grout outlet was deliberately placed approximately 2 ft from the tower anchor head. This was done to generate a grout void in the specimen. A void had been identified near the tower anchor head of one stay on the Fred Hartman Bridge. TxDOT personnel were interested in testing the efficacy of a proposed method to fill the void and determining if the added grout influenced the fatigue life of the stay.

The volume of the intentional void was approximately 6 in^3. Ten days after the main grouting of the stay, this void was filled with SikaGrout 300 PT, a non-bleed, high-flow, sand-free grout mixture. The grout in this region was a mixture of SikaGrout and tap water. The ratio of water to grout mix, by weight, was 0.27, which corresponds to the highest amount of water recommended by the manufacturers. A funnel and tube system was attached to a grout inlet hole in the tower anchor head and gravity was used to fill the void as shown in Figure B.39.

Figure B.39 Procedure Used to Fill the Intentional Grout Void at the Tower End of Specimen 9

B.4.6 Specimen 10

The original displacement amplitude selected for the fatigue test of Specimen 10 was ±2.1 in. However, the test was terminated after 2,200 cycles due to excessive movement of the hydraulic actuator. The test was restarted with an amplitude of ±1.1 in. to avoid damaging the hydraulic equipment. The cycles at the higher amplitude were included in the total number of cycles reported for the specimen.

B.4.7 Specimen 11

The original frequency selected for fatigue test for Specimen 11 was 3.0 Hz, which was used to test Specimen 4 and Specimen 10. However, when testing at this frequency, the oil temperature became too high. The only option was to reduce the testing frequency to avoid damaging the hydraulic equipment. Specimen 11 was subjected to 182,620 cycles at 3.0 Hz; 160,450 cycles at 1.5 Hz; 25,000 at 2.0 Hz; 17,150 cycles at 2.25 Hz; and the remainder of the cycles at 2.5 Hz. All cycles were included in the total.

B.5 ACOUSTIC SENSORS

During each fatigue test, the response of the test specimens was monitored using a Soundprint® system from Pure Technologies, Ltd. The same type of system is currently used to monitor the response of the stay cables on the Fred Hartman and Veterans Memorial Bridges. Pure Technologies provided the transducers and the hardware (Figure B.40) necessary to detect wire breaks from the acoustic signatures of the test specimens. The data obtained during testing were downloaded over the Internet, processed, and made available to the research team on a secure web page.

Figure B.40 Soundprint® Hardware

For the grouted specimens, four transducers (Figure B.41) were attached to each specimen. The sensors were placed on both anchor heads and along the free length as shown in Figure B.42. The transducers along the free length were placed directly on the tension rings for the Specimen 1. Because of poor acoustic coupling, the sensors were placed directly on the PE pipe for subsequent tests. For the ungrouted and hybrid specimens, only two transducers were used (Figure B.43). The sensors used in the second phase of the research (Figure B.41b) are similar to those installed on the Fred Hartman Bridge.

(a) Phase 1 (b) Phase 2

Figure B.41 Acoustic Sensors

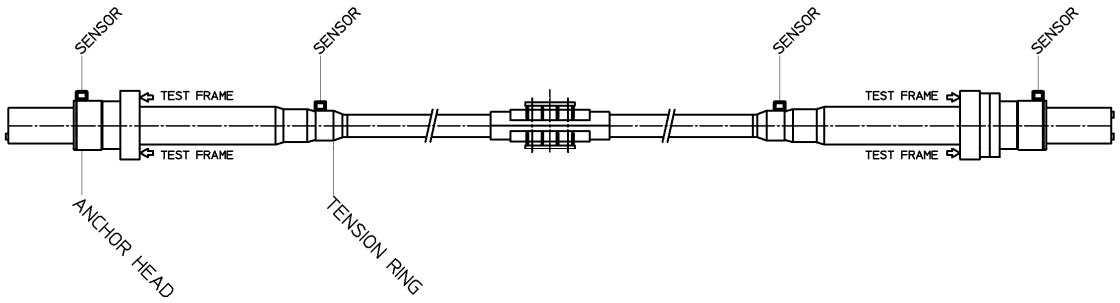

(a) Specimen 1

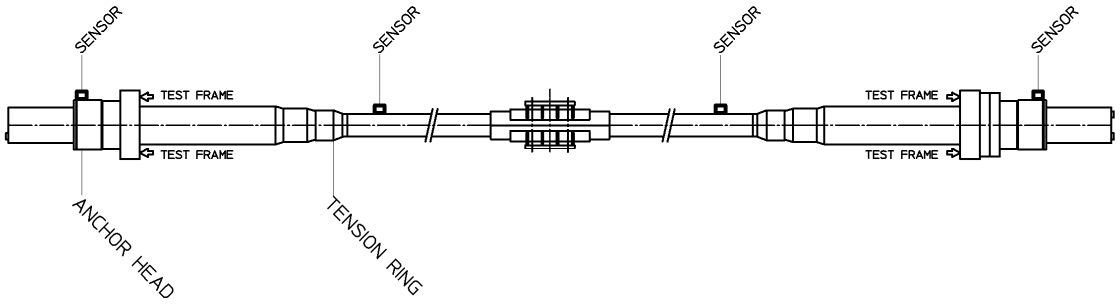

(b) Subsequent Specimens

Figure B.42 Locations of Soundprint® Sensors for Grouted Specimens

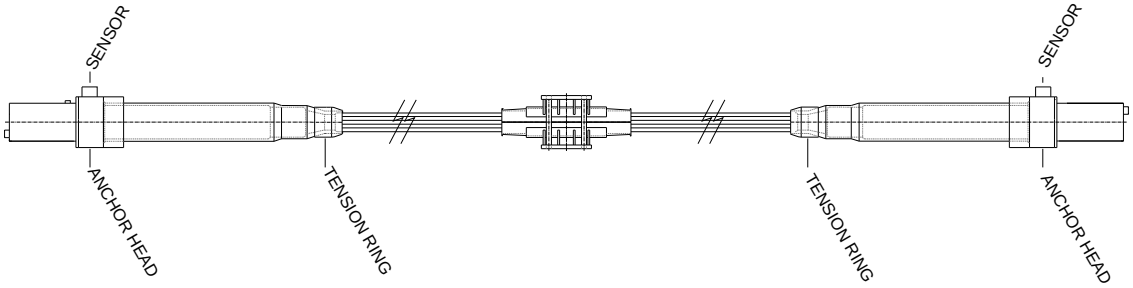

Figure B.43 Locations of Soundprint® Sensors for Ungrouted and Hybrid Specimens

The transducers were set in a trigger mode, which was calibrated to detect wire breaks on the stay cable specimen. Personnel from Pure Technologies calibrated the system for Specimen 1, and research team performed the necessary impact calibrations for all other specimens. The system provided a time stamp for each acoustic event, such as anchorage noises and wire fractures. Furthermore the location of the event was also reported. This information allowed the research team to monitor the number and location of wire breaks as the fatigue test progressed.

APPENDIX C: CONSTRUCTION OF SMALL-DIAMETER SPECIMENS

Three, small-diameter specimens were constructed and subjected to fatigue loads during this investigation. The procedures used to construct the specimens are summarized in this appendix. In contrast to the stay-cable specimens discussed in Appendix B, the small-diameter specimens were constructed and tested in the same position. External, reaction frames supported the anchor heads at each end and transferred the forces in the specimen into the strong floor (Figure C.1).

There were five primary differences between the small-diameter and the cable-stay specimens: (1) the small-diameter specimens included only two strands; (2) the small-diameter specimens did not include a tension ring, so the strands were parallel along the entire length of the specimen; (3) the length of the small-diameter specimens was longer than the length of the cable-stay specimens; (4) all small-diameter specimens were instrumented with strain gages attached to the strand; and (5) the fatigue tests were stopped periodically to measure the transverse stiffness and natural frequencies of the test specimens as damage accumulated. The first three changes were made to capture the cable-dominant behavior of the longest stays on the Fred Hartman Bridge (Pebley 2005). The fourth change was made to measure the stresses induced by transverse vibrations of the specimens, and the fifth change was made to evaluate the sensitivity of parameters that can be measured in a nondestructive manner to the damage due to wire breaks.

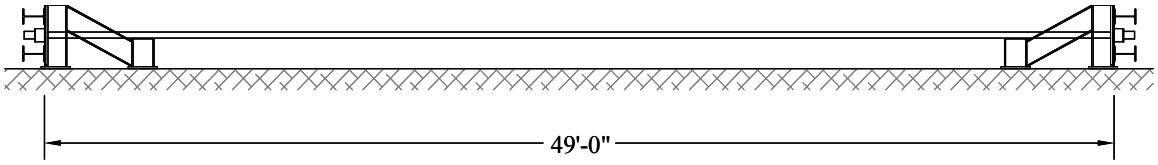

Figure C.1 Geometry of Small-Diameter Specimens

This appendix is divided into seven sections. The reaction frames used to support each specimen and resist the prestress force are discussed in Section C.1. The configuration of the specimens is summarized in Section C.2. An overview of the construction process is presented in Section C.3 and the unique characteristics of Specimen 1 are discussed in Section C.4. The procedures used to measure the transverse stiffness and natural frequencies are summarized in Section C.5. The locations of the strain gages are summarized in Section C.6, the accelerometers used to measure the frequency response are discussed in Section C.7, and the acoustic sensors used to detect wire breaks during the fatigue tests are discussed in Section C.8. Additional information about the specimens is available in Bean (2006) and Lee (2007).

C.1 REACTION FRAMES

A self-reacting frame was used to support the cable-stay specimens during the bending fatigue tests (Figure B.1). The primary advantage of this arrangement was that the specimen could be moved after the strands were stressed. The idea of constructing a self-reacting frame was abandoned for the small-diameter specimens due to the increased length. Four independent reaction frames were fabricated from W12x40 sections and attached to the laboratory strong floor (Figure C.2). A pair of reaction frames was positioned at each end of the specimen.

Figure C.2 Reaction Frame and Cross Beams

Figure C.3 Cross Beams and Plate Supporting Anchor Head

Two, W12x40 sections spanned horizontally between the reaction frames, and a 2-in. plate was bolted to the inside face of the cross beams (Figure C.3). The plate provided the reaction for the anchor heads.

Because the reaction frames were attached to the laboratory strong floor and the supports at the two ends of the specimen were independent, the specimens could not be moved after the stands were stressed. As a result, the specimens were grouted in a horizontal position.

C.2 CONFIGURATION OF TEST SPECIMENS

The anchor heads for the small-diameter bending fatigue specimens were fabricated to accommodate a maximum of four strands (Figure C.4). The spacing of the holes was selected to match that in the anchor heads for the stay-cable specimens (Figure B.3). The thickness of the anchor heads was 5 in. for both types of specimens.

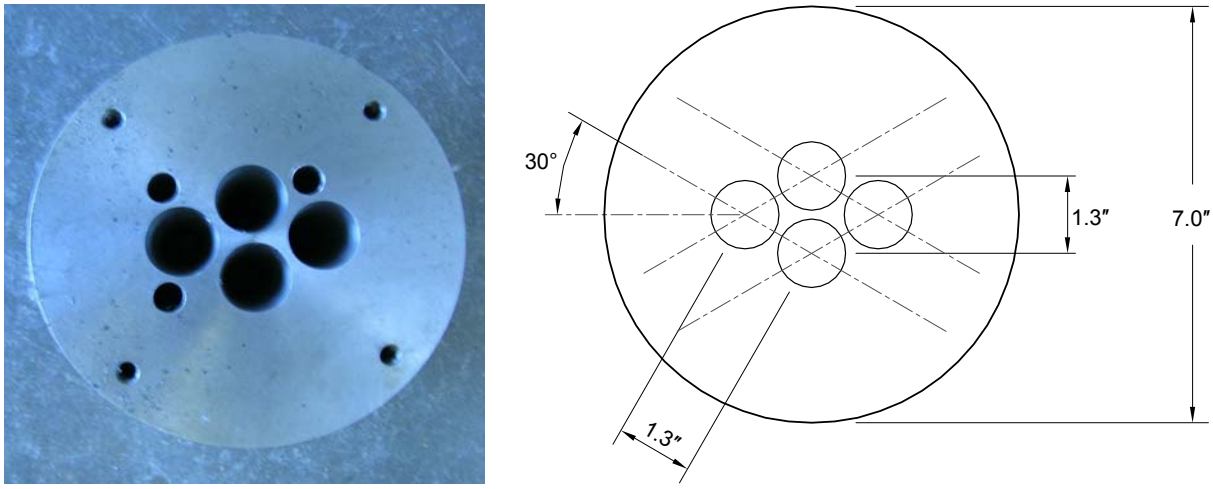

Figure C.4 Cross-Sectional Geometry of Small-Diameter Specimen at Anchor Head

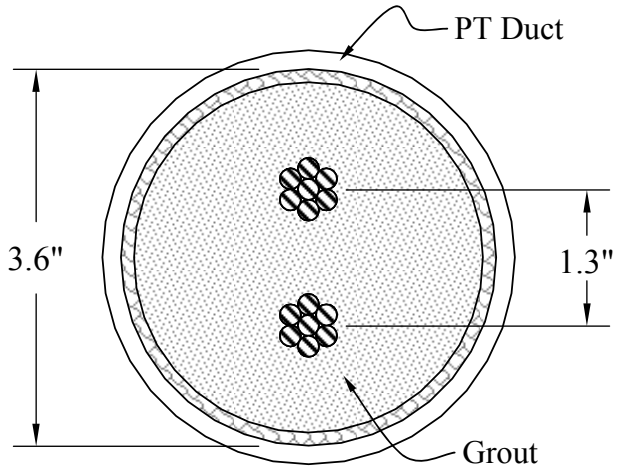

Figure C.5 Cross-Sectional Geometry of Small-Diameter Specimen along Free Length

Only two strands were used to construct the small-diameter specimens. As shown in Figure C.5, the strands were aligned vertically and the strands were parallel along the entire length of the specimen. Post-tensioning duct was selected for the small-diameter specimens to minimize the likelihood of grout voids. The post-tensioning duct is ribbed and includes three longitudinal flow channels (Figure C.6). In addition, the duct is semi-transparent, so the level of the grout can be observed during the grouting process.

The post-tensioning duct is a blend of polyethylene and polypropylene. The outside diameter is 4 in. (based on the top of the rib). The inside diameter is 3.35 in., and the wall thickness is approximately 3/16 in. The spacing of the transverse ribs is 1.5 in. (Figure C.6). Commercial couplers are available for connecting sections of duct. Using the commercial splices simplified the process of attaching strain gages to the strands, as discussed in Section C.3.4

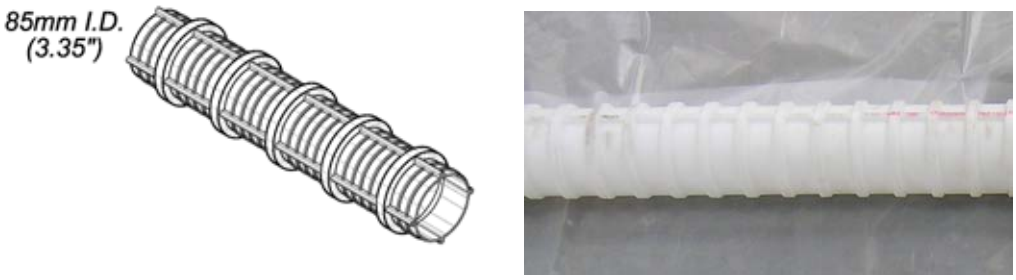

Figure C.6 Post-Tensioning Duct used to Construct Small-Diameter Specimens

The specimens were originally designed with the transverse loads applied at midspan (Figure C.7). However, the location of the actuator was shifted to the north during testing of Specimen 1 (Figure C.8), and the actuator remained in this position for the subsequent specimens.

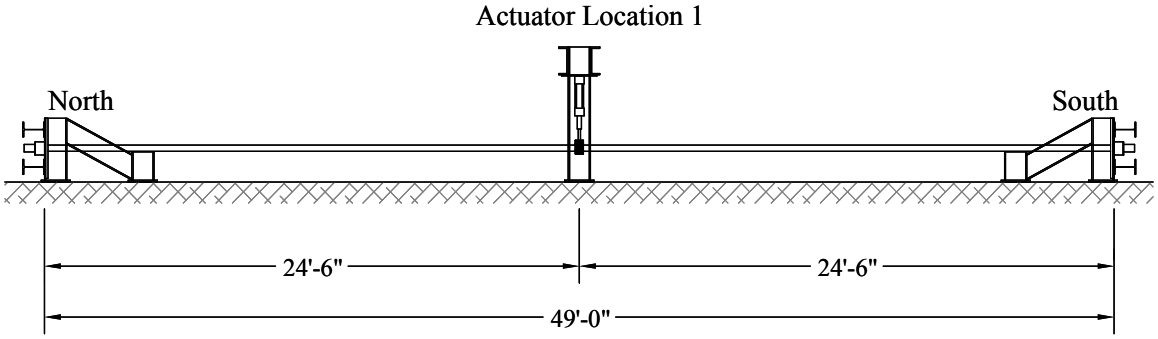

Figure C.7 Original Configuration of Small-Diameter Specimens

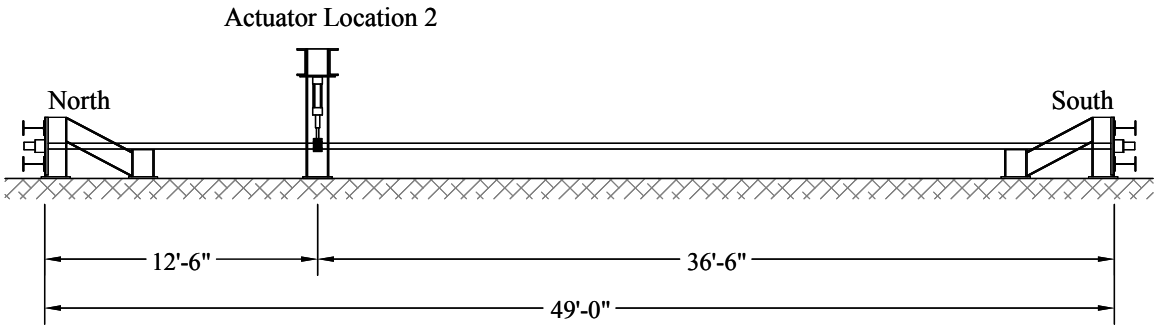

Figure C.8 Final Configuration of Small-Diameter Specimens

A 6-in. long steel clamp (Figure C.9 and Figure C.10) was designed to connect the hydraulic actuator to the test specimen. A soft, spongy styrofoam material was wrapped around the specimen as padding between the actuator grip and the duct. The styrofoam was cut into strips narrow enough to fit between the ribs on the duct. During the fatigue tests, the actuator pulled the specimen upward, but did not push the specimen downward. Therefore, the connection between the clamp and the duct could be more flexible than that for the cable-stay specimens.

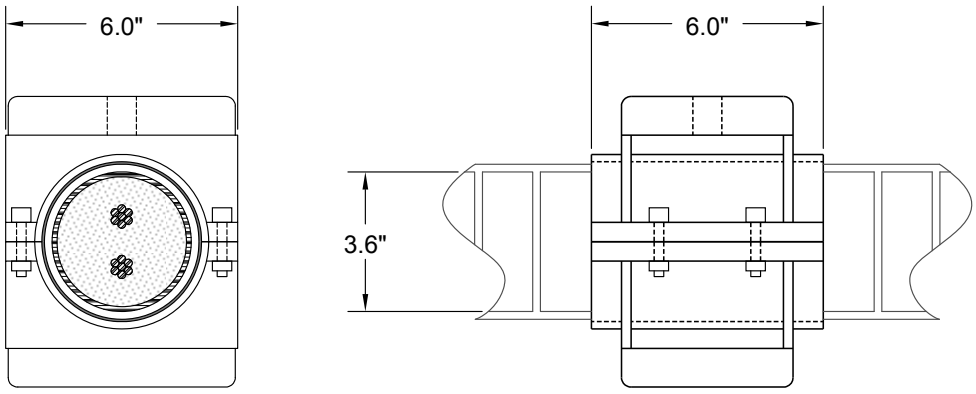

Figure C.9 Geometry of Clamp

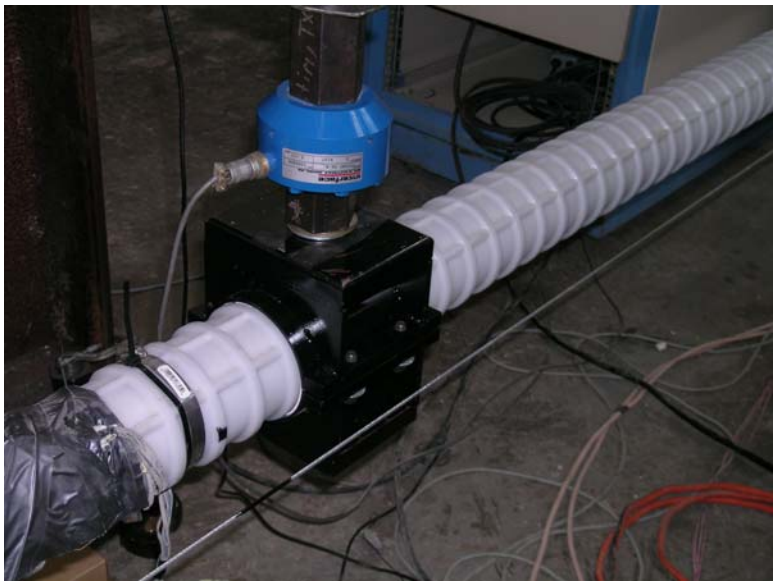

Figure C.10 Photograph of Clamp

C.3 CONSTRUCTION OF SMALL-DIAMETER SPECIMENS

The construction process for the small-diameter bending fatigue specimens may be divided into five steps: (1) assembling the components, (2) prestressing the strand, (3) installing the strain gages, (4) splicing the ducts, and (5) grouting the ducts. Each step is described briefly below.

C.3.1 Assembly of Components

Two, 55-ft sections of prestressing strand were used to construct each specimen. The strands were pushed through the holes in the anchor head at one end of the specimen. Several sections of duct and couplers were slid over the strand. The number varied depending on the number of locations that were instrumented with strain gages. The total length of the sections of duct was approximately 18 in. less than the length of the specimens.

The strands were then pushed through the holes in the anchor head at the other end of the specimen. Wedges were inserted into the south anchor head to hold the strands in place.

C.3.2 Prestressing the Strands

The strands were stressed individually from the north end (Figure C.11). The hydraulic ram used to stress the strands has a seating jack that applies uniform pressure to the wedges, which reduces the seating losses. The target stress level in each strand was 50% of GUTS (30 kip). The applied force was monitored using a pressure gage attached to the ram.

During stressing, each strand was pulled and released three times to minimize seating losses. The maximum applied force was approximately 10, 20, and 30 kip in subsequent cycles. Two springs were positioned between the anchor head and the nose of hydraulic cylinder to minimize the movement of the wedges when the applied force was released. The strand was overstressed about 5% to compensate for expected losses.

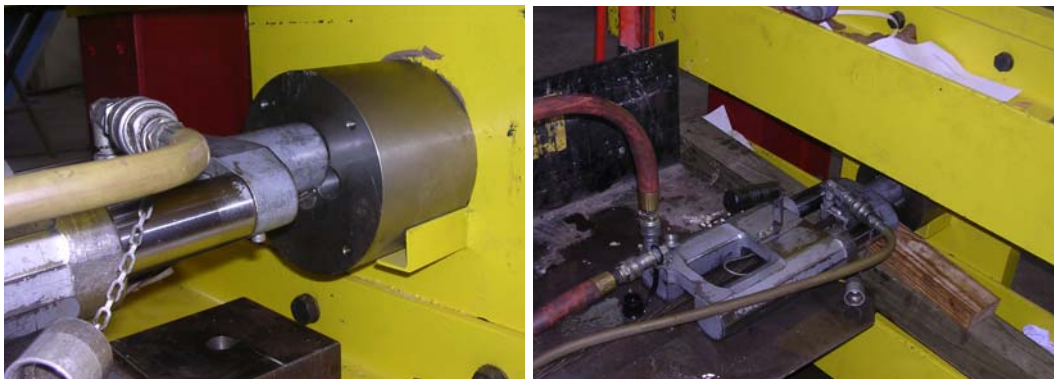

Figure C.11 Stressing of Strands Individually with Hydraulic Ram

C.3.3 Installation of Strain Gages

After stressing the strand, 3-mm strain gages were attached to the surface of the strand. Access to the desired location was obtained by sliding the sections of duct along the strands. Different locations were used for each specimen (Section C.5). Figure C.12 shows the position of the duct when the strain gages were attached to the north end of Specimen 1. Figure C.13 shows the orientation of a typical stain gage oriented along the local axis of a wire.

Figure C.12 Strain Gages Attached to Strands at North End of Specimen 1

Figure C.13 Strain Gage Oriented along Local Axes of Wire

C.3.4 Splicing the Duct

After all internal instrumentation was installed, adjacent sections of plastic ducts were connected using plastic couplers and then covered with the plastic heat shrink tubes (Figure C.14a). The space between the plastic pipe and the steel plate in the buttress was sealed with expanding foam. After the sections of duct were connected, numerous wooden supports were placed under the specimen to set the elevation of the duct (Figure C.14b).

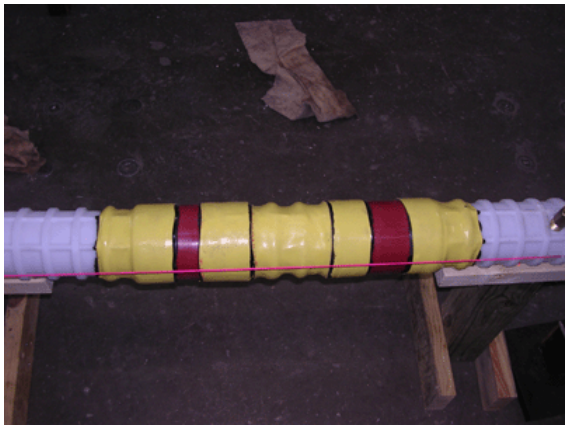

(a) Coupler and Plastic Heat Shrink Tubes

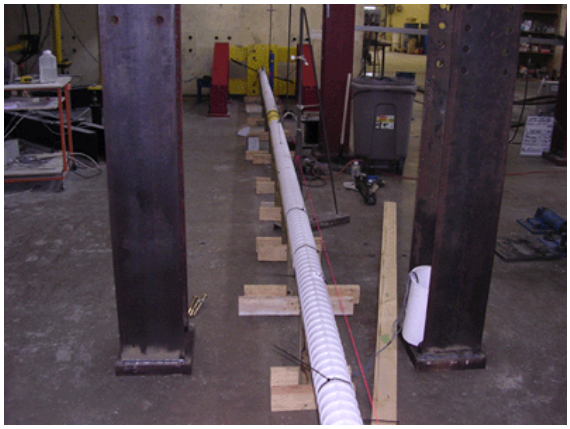

(b) Alignment before Grouting

Figure C.14 Completion of Pipe Connection

C.3.5 Grouting

A commercial, pre-packaged grout (SikaGrout 300 PT) was used to construct the specimens. Grout was pumped into the duct near the center of the specimen. Air vents were placed at several locations along the length and at each grout cap (Figure C.15). Grout was pumped continuously into the specimen flowed through each of the air vents. The ends of the hoses were then capped to prevent air from returning into the duct.

(a) Grout Hose from Pump

(b) Vent Hose after Completion of Grouting

Figure C.15 Grouting Hoses and Vents

C.4 CONSTRUCTION SEQUENCE FOR SPECIMEN 1

The actual construction sequence for Specimen 1 varied from the idealized procedure described in Section C.3. Two important differences, one intended and one unintended, are discussed in this section.

During construction of Specimen 1, four strain gages were attached to the strand before stressing. The strains were monitored during stressing to determine if the stress calculated from the pressure gage was consistent with the stress calculated from the measured strains. The pressure gage proved to be accurate.

The pre-packaged grout was mixed with almost double the recommended amount of water. The mixture had a very low viscosity and a large amount of bleed water was observed after grouting was completed. Because of the bleed water, small voids were observed at the top of the specimen along most of the length. It was possible to detect the presence of the voids through the translucent duct and vent holes before testing. However, the extent of the voids was not known until the specimen was dismantled after the conclusion of the test.

C.5 PERIODIC TESTS

The fatigue tests were interrupted periodically to conduct static tests. As damage accumulated, the transverse stiffness of the specimens was expected to decrease. The testing protocols varied slightly for the three specimens, and are summarized briefly below.

Initially, Specimen 1 was initially loaded at midspan (Figure C.7) and the fatigue tests were run under force control. During each static test, the specimen was loaded from 0 to 1.4 kip in 0.2-kip increments. After the load frame was relocated to the north end of the specimen, the static tests were discontinued. Specimens 2 and 3 were loaded near the north end (Figure C.8) and the fatigue tests were run under displacement control. During each static test, the specimen was pulled upward to a maximum displacement of approximately 2.5 in. in 0.4 to 0.6-in. increments.

After each static test, the natural frequencies of the specimen were measured. The collar used to connect the hydraulic actuator to the specimen was removed and the ram was disconnected from the test specimen. Vibrations were induced by hitting the specimen with a rubber-headed hammer. During each free-vibration test, the specimen was struck at three different locations (Figure C.16).

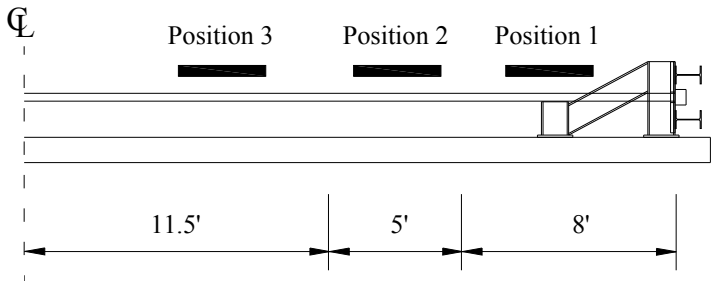

Figure C.16 Locations of Impact for Free-Vibration Tests

C.6 LOCATIONS OF STRAIN GAGES

Strain gages were used to monitor the response of the strands at various locations along the length during the fatigue tests. The number of gages varied with each specimen. Information about the locations of the strain gages is summarized below.

C.6.1 Strain Gage Positions

A two-character code is used to identify the location of each strain gage. The letter refers to the location along the length of the specimen. The number refers to the position the gage: 1 corresponds to the top of the top strand, 2 corresponds to the bottom of the top strand, 3 corresponds to the top of the bottom strand, and 4 corresponds to the bottom of the bottom strand (Figure C.17).

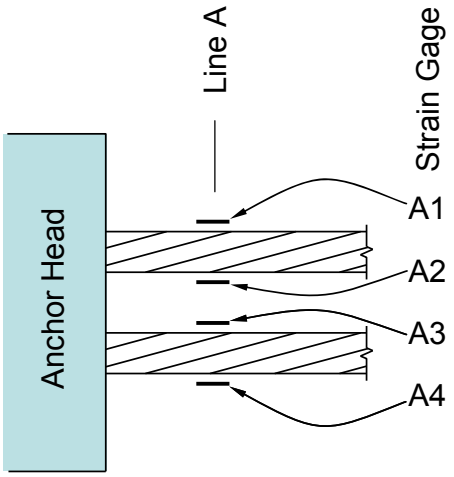

Figure C.17 Notation used to Identify Strain Gages

C.6.2 Specimen 1

Strain gages were positioned near each anchor head and near the midspan of Specimen 1. Four strain gages were positioned at each of the sections shown in Figure C.18. The midspan gages were attached to the strands before stressing and the gages near the ends were attached to the strands after stressing. Nine gages survived the grouting process.

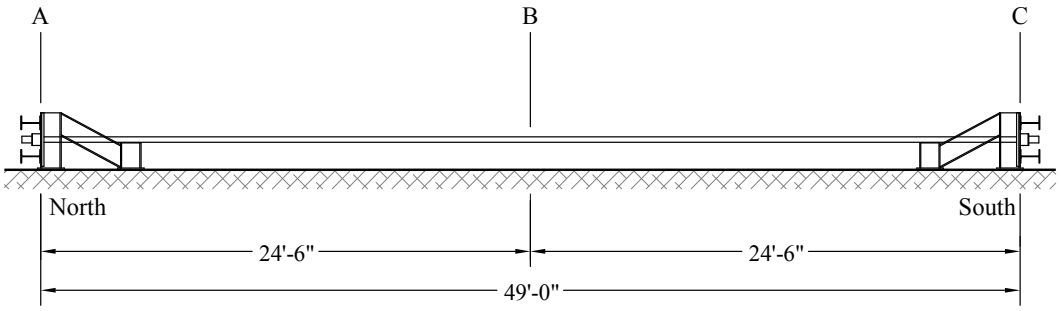

Figure C.18 Locations of Strain Gages for Specimen 1

Table C.1 Locations of Strain Gages for Specimen 1

Gage	Distance from North Anchor Head	Gage	Distance from South Anchor Head
A1	¼ in.	C1	¼ in.
A2	¼ in.	C2	¼ in.
A3	¼ in.	C3	3⁄16 in.
A4	5⁄16 in.	C4	5⁄16 in.
B1	Near center		
B4	Near center		

C.6.3 Specimen 2

Due to the location of the actuator near the north end of the specimen (Figure C.8), more strain gages were positioned near the north end of Specimen 2 that near the south end. Two sets of strain gages were positioned near the point of load application. The six locations selected for the strain gages are shown in Figure C.19 . Strain gage designations are given in Table C.2 for all sixteen gages. Fifteen gages survived the grouting process.

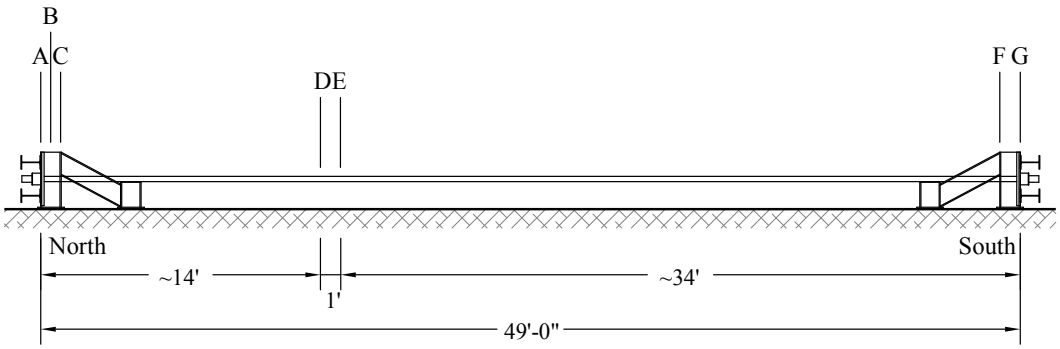

Figure C.19 Locations of Strain Gages for Specimen 2

Table C.2 Locations of Strain Gages for Specimen 2

Gage	Distance from North Anchor Head	Gage	Distance from South Anchor Head
A1	1 1/16 in.	F1	5 in.
A2	2 1/16 in.	F4	5 in.
A3	½ in.	G1	1 1/16 in.
A4	½ in.	G4	½ in.
B1	6⅛ in.		
B4	5⅞ in.		
C1	12⅜ in.		
C4	12½ in.		
D1	~14 ft		
D4	~14 ft		
E1	~15 ft		
E4	~15 ft		

C.6.4 Specimen 3

As shown in Figure C.20, strain gages were positioned at nine locations along Specimen 3. The designations used to identify the 32 gages are summarized in Table C.3. Thirty-one gages survived the grouting process.

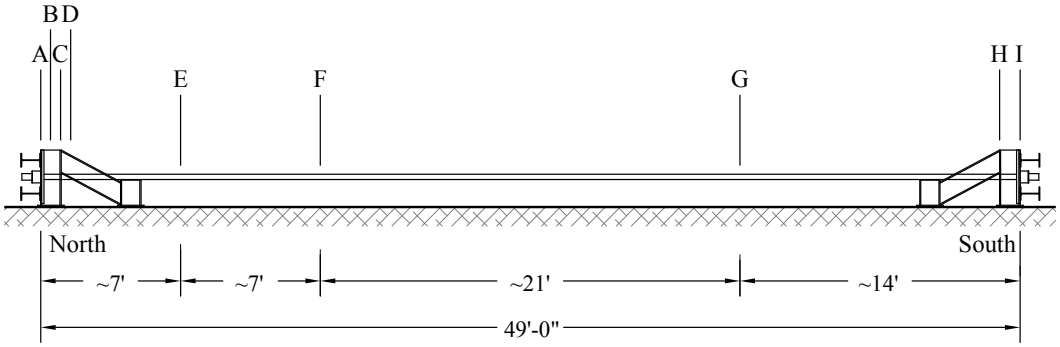

Figure C.20 Locations of Strain Gages for Specimen 3

Table C.3 Locations of Strain Gages for Specimen 3

Gage	Distance from North Anchor Head	Gage	Distance from South Anchor Head
A1	1⅝ in.	G1	14 ft 3 in.
A2	2½ in.	G4	14 ft 3in.
A3	2⅛ in.	H1	13⅞ in.
A4	2⅜ in.	H2	13⅝ in.
B1	6½ in.	H3	13⅛ in.
B2	6½ in.	H4	12⅞ in.
B3	6¼ in.	I1	2½ in.
B4	6⅝ in.	I2	2 in.
C1	12 in.	I3	2⅞ in.
C2	12 in.	I4	2½ in.
C3	12¼ in.		
C4	12¼ in.		
D1	16¾ in.		
D2	17⅝ in.		
D3	16¾ in.		
D4	17½ in.		
E1	7 ft 1 in.		
E2	7 ft 1 in.		
E3	7 ft 1 in.		
E4	7 ft 1 in.		
F1	14 ft 2 in.		
F4	14 ft 2 in.		

C.7 ACCELEROMETERS

Three accelerometers were attached to each specimen to capture the free-vibration response. Two accelerometers were positioned near the south end of the specimens and one was positioned near the north end (Figure C.21). The locations of the accelerometers were selected based on the calculated mode shapes and were sufficient to capture the first six modes of response (Lee 2007). The accelerometers were attached to the plastic ducts using hot-melt glue (Figure C.22).

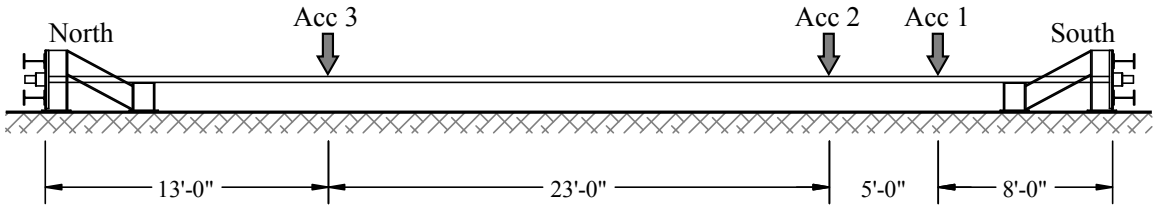

Figure C.21 Location of Accelerometers

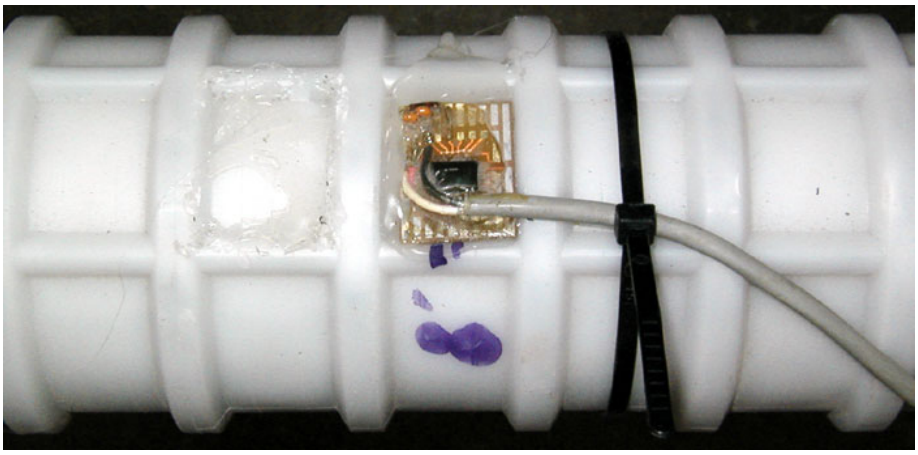

Figure C.22 Accelerometer Attached to Small-Diameter Specimens

The acceleration response was measured in the time domain during the free-vibration tests, and was converted into the frequency domain using a Fast Fourier Transform (Figure C.23). The measured vibrations indicated the same frequency components regardless of locations of sensor and impact; but the relative amplitude of each component varied.

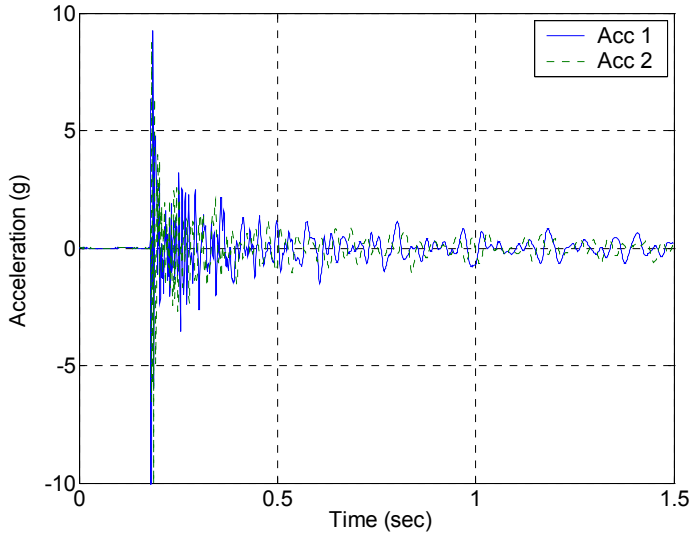

(a) Time domain

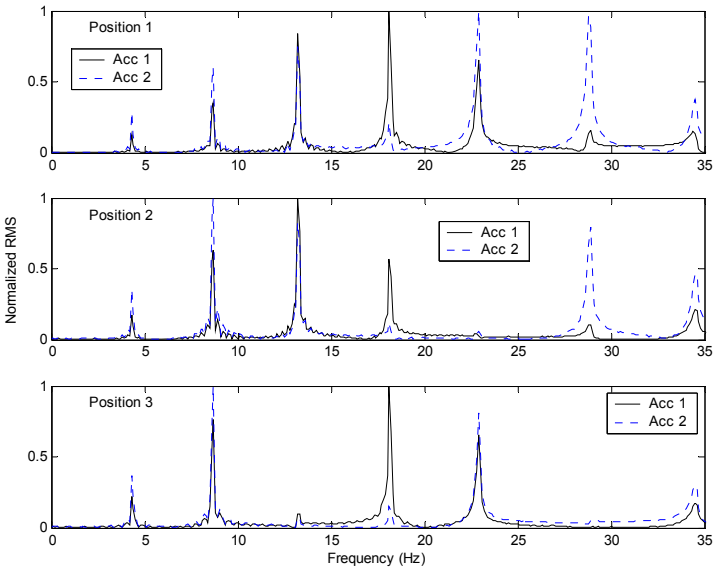

(b) Frequency domain

Figure C.23 Representative Free-Vibration Response

C.8 ACOUSTIC SENSORS

During each fatigue test, the response of the test specimens was monitored using the SoundPrint® system from Pure Technologies, Ltd. Four acoustic sensors were attached to each test specimen (Figure C.24). Sensors 0 and 3 were attached to the anchor heads and sensors 1 and 2 were attached to the plastic duct (Figure C.25). Each sensor was attached to the specimen using a cyanoacrylate adhesive and then held in place by a metal clamp.

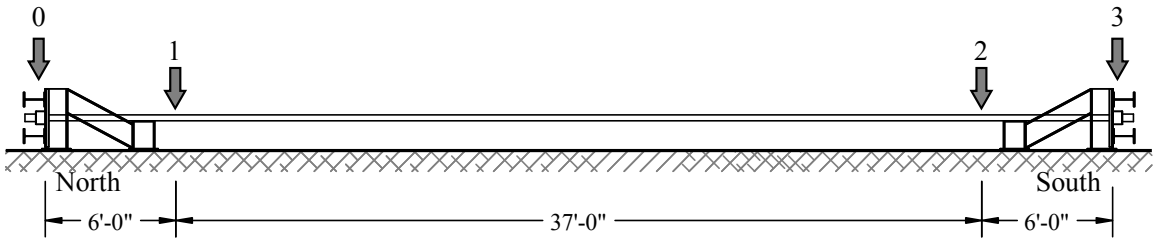

Figure C.24 Locations of Acoustic Sensors

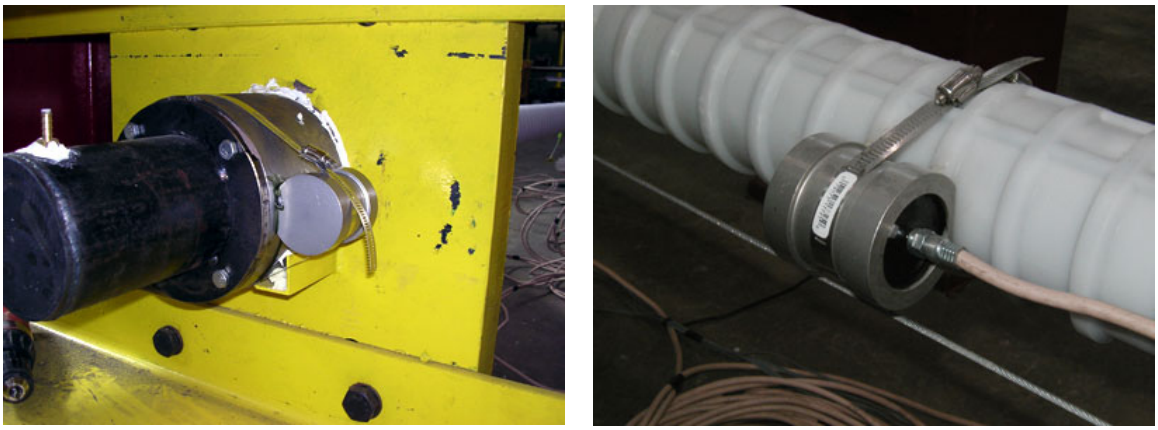

(a) Sensor Attached to Anchor Head (b) Sensor Attached to Duct

Figure C.25 Acoustic Sensors

When a wire break was detected by the sensors, the DAQ system triggered and captured the signal. These signals were stored on a local computer and transferred to Pure Technologies in Calgary once a day via an internet connection. Technical staff reviewed all signals, identified the records corresponding to wire breaks, and determined the locations of the wire breaks. Reports were available on a project website within two to four days.

APPENDIX D: FATIGUE RESPONSE OF STAY-CABLE SPECIMENS

The condition of each cable-stay specimen at the conclusion of the bending fatigue tests is documented in this appendix. Following the fatigue tests, a post-mortem investigation (autopsy) of each specimen was conducted to evaluate the condition of the grout, the extent of corrosion, and the number of wire breaks. The number of loading cycles and the observed number of wire breaks for each specimen are summarized in Table D.1.

Table D.1 Summary of Fatigue Tests

ID	No. of Strands	Specimen Type	Displacement Amplitude	Testing Frequency	Start Date	End Date	Number of Cycles	Number of Observed Wire Breaks		
			(in.)	(Hz)				Deck	Center	Tower
1	16	Grouted	±1.6	0.9	3/8/01	4/15/01	2,808,398	0	11	14
2	16	Grouted	±1.6	0.7	6/22/01	8/9/01	2,865,103	1	16	52
3	16	Grouted	±1.6	2.2	11/30/01	12/27/01	4,961,560	13	62	9
4	16	Grouted	±1.1	3.0	2/1/02	3/26/02	8,775,245	3	0	28
5	16	Ungrouted	±1.6	2.1	3/11/03	4/28/03	5,211,106	0	0	0
6	13	Grouted	±1.6	2.0	5/19/03	7/2/03	6,486,024	0	11	17
7	16	Grouted	±1.6	2.0	7/15/03	7/29/03	2,246,869	17	65	37
8	16	Ungrouted	±1.6	1.8	12/17/03	2/21/04	6,200,593	2	0	2
9	16	Grouted	±1.6	2.0	3/26/04	4/12/04	2,634,309	3	61	12
10	16	Grouted	±1.1	3.1	5/7/04	6/9/04	5,614,211	8	21	23
11	16	Hybrid	±1.1	2.5	7/12/04	8/5/04	4,640,450	7	9	0
12	16	Grouted	±1.6	1.7	8/11/04	8/30/04	2,703,958	29	86	35

In documenting the observed fatigue damage, a consistent set of notation was used. The strands were numbered from 1 to 19, beginning with the upper left strand and concluding with the lower right strand (Figure D.1). To establish the numbering pattern, the cross section is viewed from the tower end of the specimen looking toward the deck end. This pattern was used for all specimens, including Specimen 1 (cross head was rotated by 90°) and Specimen 6 (thirteen strands). Within each strand, the outer wires were numbered clockwise from 1 to 6, beginning with the top wire. The center wire was identified as 7 (Figure D.2).

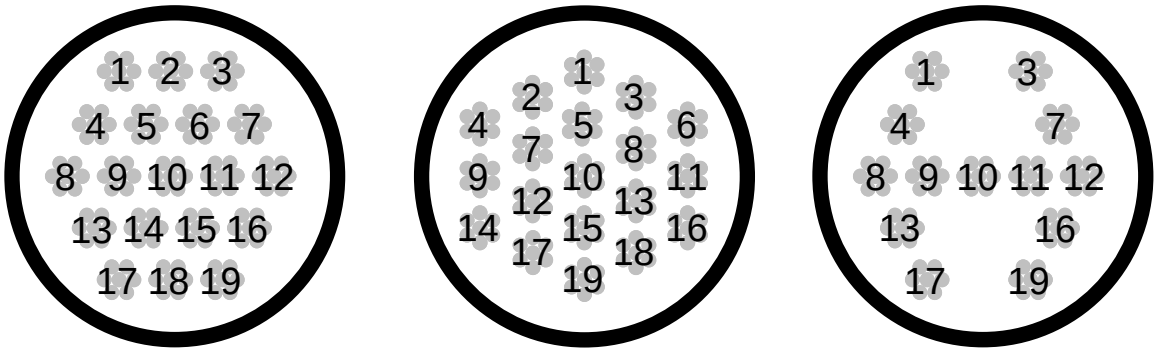

Typical Specimen Specimen 1 Specimen 6

Figure D.1 Notation Used to Identify Individual Strands

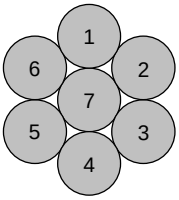

Figure D.2 Notation Used to Identify Individual Wires within a Strand

D.1 SPECIMEN 1

Specimen 1 sustained 2,808,398 loading cycles during the fatigue test. Twenty-five wire breaks were identified at the conclusion of the test: fourteen breaks occurred at the tower end and eleven breaks occurred at the center of the specimen under the load point. No breaks were identified at the deck end. Specimen 1 was stressed from the tower end and grouted from the deck end. Anti-bleed admixture was not used in the grout for this specimen, and the anchor heads were rotated 90° compared with the other specimens. As a result, six of the strands were positioned above the upper grout inlets (Figure B.32). The specimen was tested under displacement control, with an amplitude of ±1.6 in. at midspan.

D.1.1 Observed Condition of Grout and Strand

When the PE transition pipe was removed, a large grout void was observed near the anchor head at the tower end of the specimen (Figure D.3). The void was approximately 20 in. long and had a maximum depth of 1.5 in. Strands 1 and 2 were fully exposed within the grout void along a length of approximately 12 in. (Figure D.4). A very thin layer of grout covered strands 3 and 4.

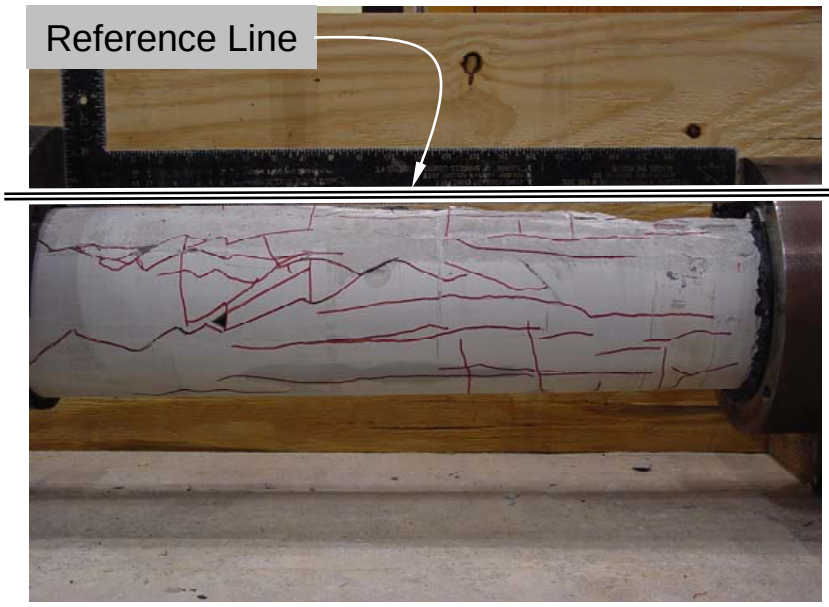

Figure D.3 Grout Void near Tower Anchorage – Specimen 1

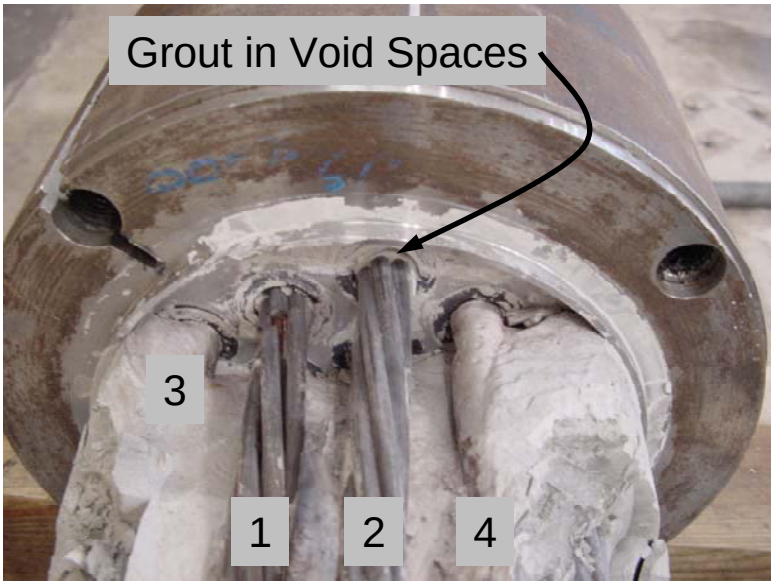

Figure D.4 Exposed Strand within Grout Void at Tower End of Specimen 1

It is unclear whether strands 1 and 2 were in contact with grout at some point during the grouting operation. The openings in the anchor head for strands 1 and 2 were fully grouted (Figure D.4), which is an indication that the entire stay cable was initially grouted and that the grout void is a result of a bleed-water concentration at the top of the specimen. Excessive bleed water was also observed on the top surface of the grout cubes. This suggests that the sections of the strand exposed within the void were at one time exposed to bleed water. However, no significant signs of corrosion were found on the exposed strands in the grout void or on the anchor head. The surface corrosion seen in Figure D.4 is light surface corrosion that was found on the shim plate.

The grout in the rest of the specimen was homogeneous and only minor surface defects were observed. The defects were often very close to the helical spacer wire as shown in Figure D.5. Orange surface corrosion was found on some locations at the very outside of the helical spacer wire where it was in contact with the PE pipe.

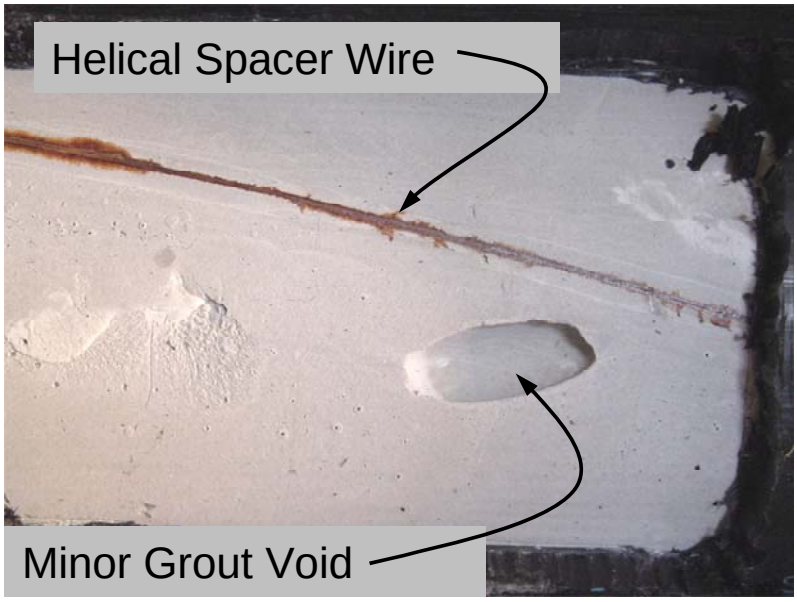

Figure D.5 Grout Surface Defect and Corrosion on Spacer Wire – Specimen 1

Several windows were cut into the PE pipe during the fatigue test of Specimen 1. Shortly after the windows were opened, fine, parallel, transverse cracks formed in the grout (Figure D.6). These hairline cracks were caused by shrinkage of the grout in the exposed area. Similar shrinkage cracks (Dowd 2001) were found in all the windows that were cut into the actual stay cables of the Fred Hartman Bridge (Figure D.7) and in a previous investigation of stay cables (Hamilton 1995).

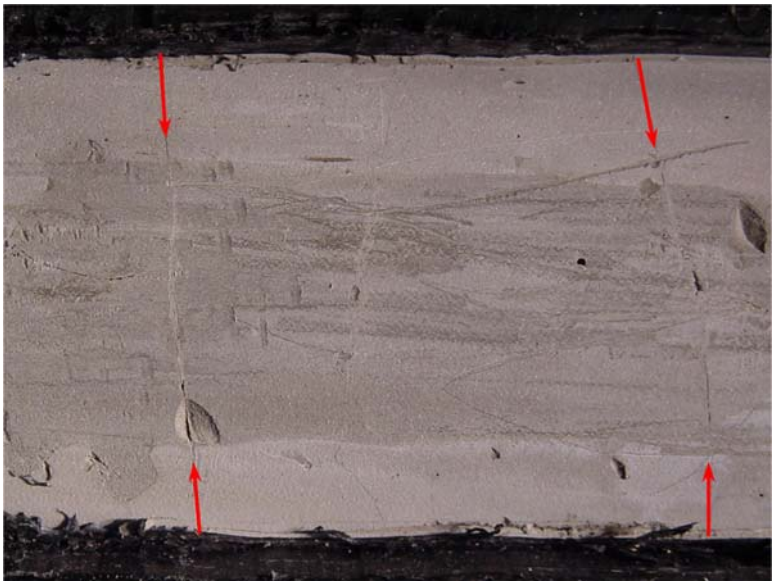

Figure D.6 Hairline Transverse Grout Cracks – Specimen 1

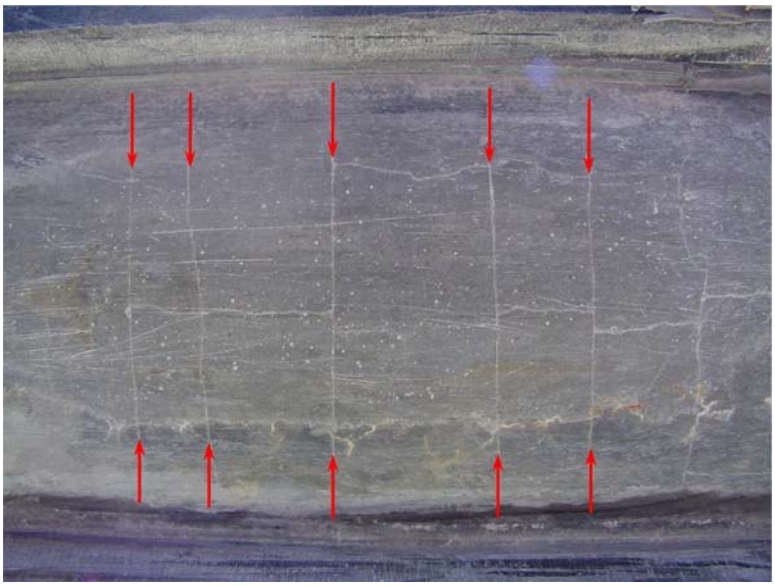

Figure D.7 Hairline Transverse Grout Cracks - Fred Hartman Bridge

Longitudinal cracks in the grout were found wherever wire breaks occurred. Figure D.8 shows two photographs of the same location near midspan of the specimen. The upper photograph was taken immediately after the PE pipe was removed, and the lower photograph was taken after some grout was chipped off. Note that these cracks were present when the PE pipe was removed, and did not develop with time due to shrinkage. As discussed in Section D.1.2, four wire breaks were observed in the top strand at this location.

Figure D.8 Longitudinal Cracks in Grout, Corrosion of Strand, and Wire Breaks near Midspan of Specimen 1

The PE pipe was also removed near the tension ring. The condition of the grout was good, and only a few longitudinal were observed (Figure D.9). However, due to the very tight spacing of the strand in this area, the surface of the strand was not covered with grout. Therefore, the potential for corrosion of the strand is higher in this region.

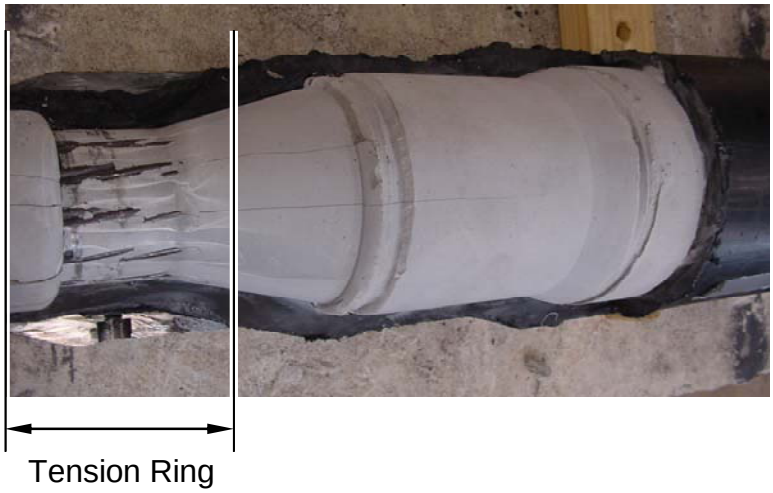

Figure D.9 Exposed Strand at Tension Ring – Specimen 1

D.1.2 Wire Breaks

Twenty-five wire breaks were identified during the autopsy of Specimen 1. Fourteen wire breaks occurred near the tower anchorage and eleven occurred near the loading point. All breaks at the tower end occurred within 14 in. of the inside face of the anchor head. The wire breaks occurred in strands positioned on the top and bottom of the cross section (Figure D.10). Six of the seven wire breaks at the top of the cross section occurred within the grout void. At the bottom of the cross section, all wire breaks occurred within 4 in. of the inside face of the anchor head (Figure D.11).

Under the loading point, the eleven wire breaks occurred in the strands at the top and bottom of the cross section (Figure D.12). Interestingly, both strands also experienced fractures in the tower anchorage region. All breaks were located in a 23-in. window, with a bias towards the deck anchorage side (Figure D.13).

The wire fractures that occurred within the grout void at the tower end did not exhibit any signs of corrosion. Figure D.14 shows the wire fractures that occurred in strand 2 at the tower end.

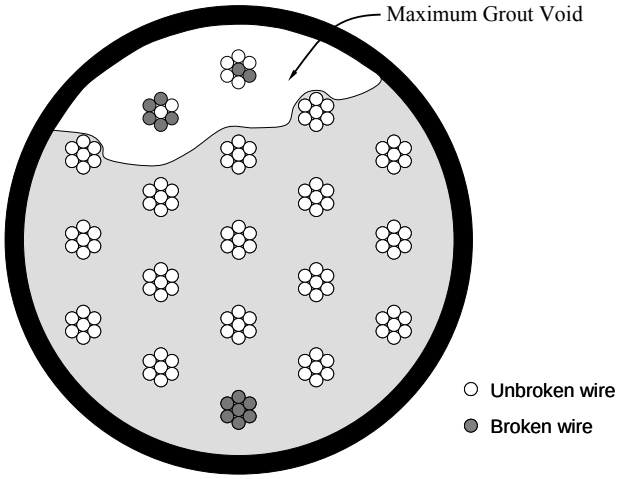

Figure D.10 Distribution of Wire Breaks near Tower End – Specimen 1

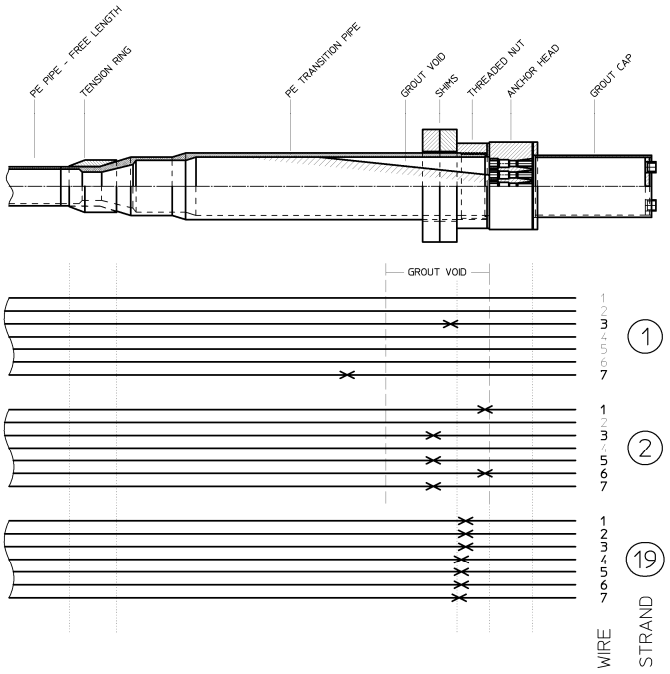

Figure D.11 Location of Wire Breaks near Tower End – Specimen 1

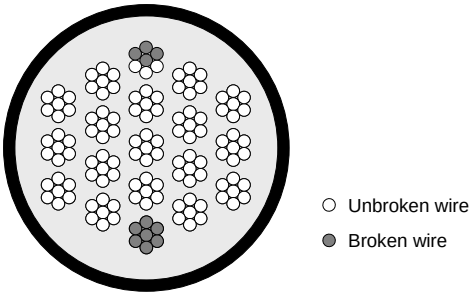

Figure D.12 Distribution of Wire Breaks near Midspan – Specimen 1

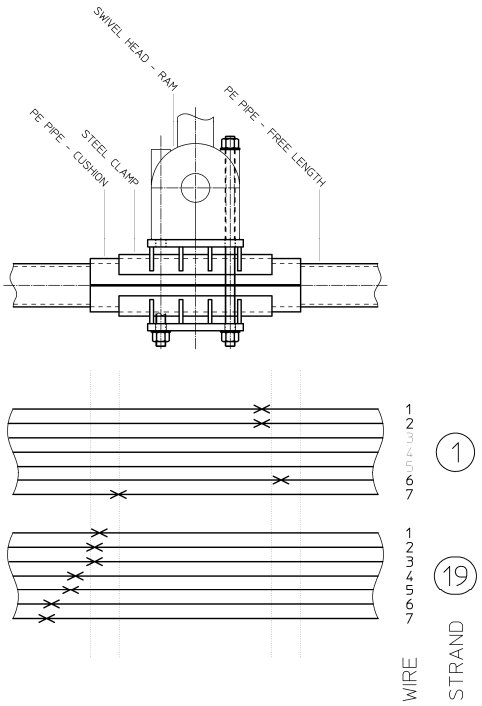

Figure D.13 Location of Wire Breaks near Midspan – Specimen 1

Figure D.14 Wire Breaks in Strand 2 near Tower End of Specimen 1

The area around the wire breaks on strand 19 at the tower end exhibited orange surface corrosion (Figure D.15) characteristic of corroded fretting product. The contact points, which served as initiation points for fretting fatigue, are clearly visible in Figure D.16. Orange surface corrosion was also observed along the contact points of strand 1 near midspan (Figure D.17).

Figure D.15 Wire Breaks in Strand 19 near Tower End of Specimen 1

Figure D.16 Fracture Surfaces for Strand 19 at the Tower End of Specimen 1

Figure D.17 Wire Breaks in Strand 1 near Midspan of Specimen 1

D.1.3 Acoustic Data

Four acoustic sensors were used to monitor the fatigue response of Specimen 1, and twenty-five wire breaks were detected (Table D.2). The number and distribution of wire breaks matched those observed during the autopsy of the test specimen. The first wire break was detected after 300,000 fatigue cycles (Figure D.18).

Table D.2 Summary of Wire Breaks – Specimen 1

Method	**Number**	**Tower**	**Midspan**	**Deck**	**Total**
Observed during Autopsy	Total	14	11	—	25
	Unique Wires*	14	11	—	25
Acoustic Sensors	Total	14	11	—	25

* Multiple wire breaks in the same wire are not included in this category.

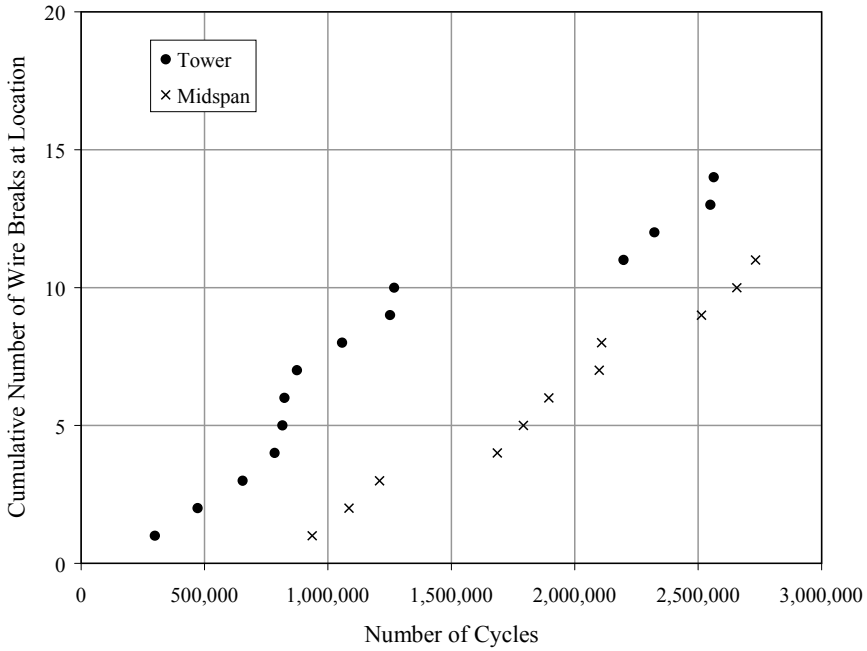

Figure D.18 Wire Breaks Detected from Acoustic Data – Specimen 1

D.1.4 Lateral Stiffness

During the fatigue test, the maximum and minimum force levels were recorded daily. The variation in the maximum and minimum applied forces needed to achieve the target displacement levels of ±1.6 in. are shown in Figure D.19. The vertical lines also indicate the approximate number of cycles corresponding to each wire break detected by the acoustic sensors.

Because the average of the applied loads divided by the displacement amplitude provides an estimate of the transverse stiffness of the specimen, the data shown in Figure D.19 can also be used to evaluate changes in the transverse stiffness during the fatigue test. The final average dynamic stiffness was approximately 6% less than the initial average dynamic stiffness (Table D.3). In addition, the initial average dynamic stiffness was within 2% of static stiffness measured at the beginning of the fatigue test.

Table D.3 Summary of Stiffness Changes during Fatigue Test – Specimen 1

	Static Stiffness	Average Dynamic Stiffness	Frequency
	(kip/in.)	(kip/in.)	(Hz)
Initial	4.8	4.73	—
Final	—	4.45	12.0
Final / Initial	—	0.941	—

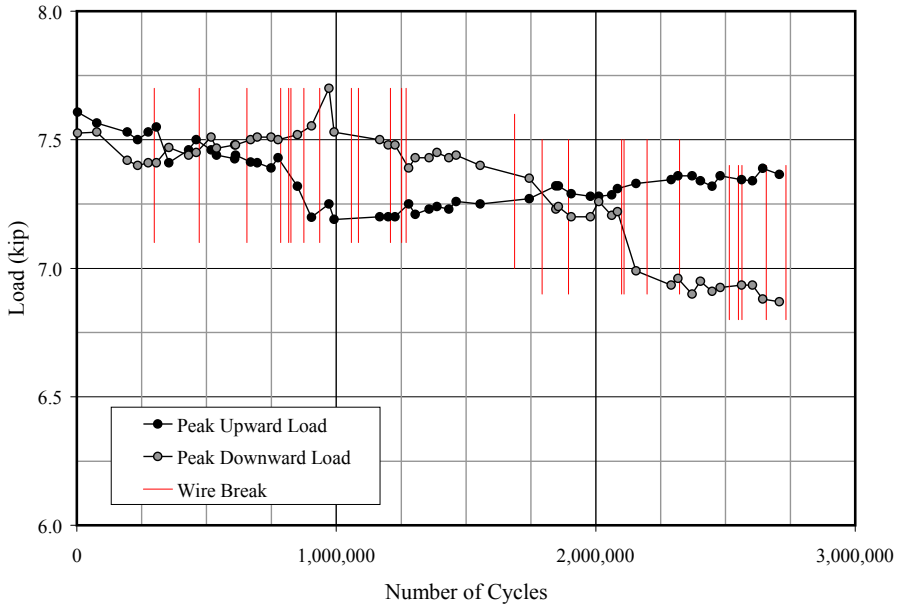

Figure D.19 Variation of Applied Loads during Fatigue Test – Specimen 1

D.2 SPECIMEN 2

Specimen 2 sustained 2,865,103 loading cycles during the fatigue test. Sixty-nine wire breaks were identified at the conclusion of the test: fifty-two breaks occurred at the tower end, sixteen breaks occurred at the center of the specimen under the load point, and one break occurred at the deck end. Specimen 2 was stressed from the tower end and grouted from the deck end. The specimen was tested under displacement control, with an amplitude of ±1.6 in. at midspan.

D.2.1 Observed Condition of Grout and Strand

An anti-bleed admixture was mixed with the grout for Specimen 2. Closely spaced air voids (Figure D.20) were observed at the deck end when the PE pipe was removed, but a grout void was not present at the tower end. The research team noted that it was much easier to chip the grout immediately after removing the PE pipe than after the grout had been exposed to the environment for several days. However, no measurements were taken to verify this observation.

There were some localized signs of orange corrosion on some intact strands, as well as some fine corrosion spots on the helical spacer wire. Figure D.21 shows a typical example of this type of corrosion from midspan of the test specimen.

Figure D.20 Air Voids in Grout near the Deck End – Specimen 2

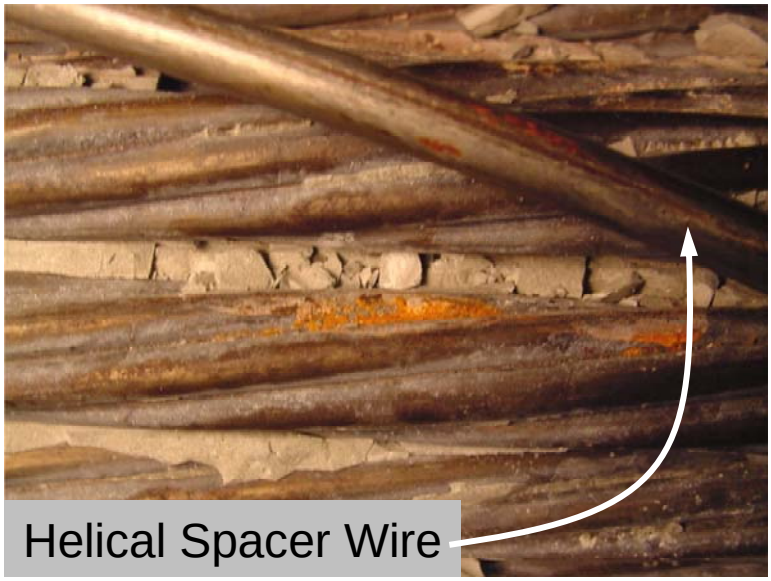

Figure D.21 Localized Corrosion on Strand and Helical Spacer Wire – Specimen 2

D.2.2 Wire Breaks

Sixty-nine wire breaks were identified during the autopsy of Specimen 2. Fifty-two wire breaks occurred near the tower anchorage, sixteen occurred near the loading point, and one occurred near the deck anchorage.

The fifty-two wire breaks near the tower end were distributed among ten different strands (Figure D.22), which were located near the top and bottom of the cross section. Figure D.23 shows the longitudinal location of the wire breaks. Most of the fractures occurred within the anchor head. All breaks occurred within 3.25 in. of the inside face of the anchor head. Representative examples of the breaks within the anchor head are shown in Figure D.24 for strand 1. The fracture surfaces, with the fatigue cracks and the points of initiation, can be clearly identified in this photograph.

Photographs of strand 2 near the tower end (Figure D.25) provide examples of the breaks that occurred just beyond the wedges. These breaks were not initiated by the teeth marks on the wires caused by the wedges, but initiated just beyond the gripping area. Figure D.26 indicates that all the breaks initiated at contact points with the center wire and none of the fractures appears to have been initiated from the outside surface of the strand.

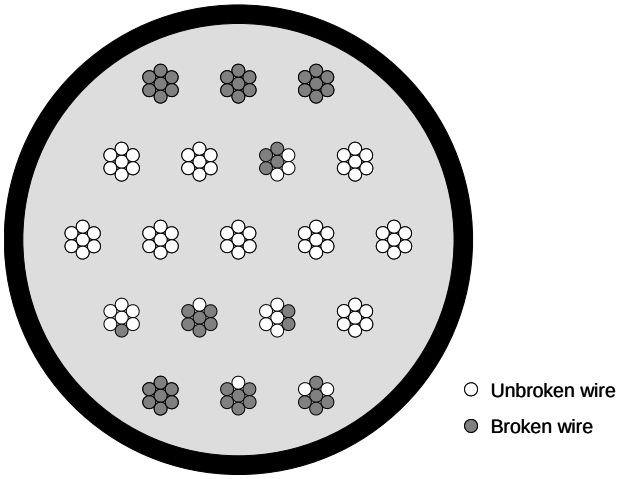

Figure D.22 Distribution of Wire Breaks near Tower End – Specimen 2

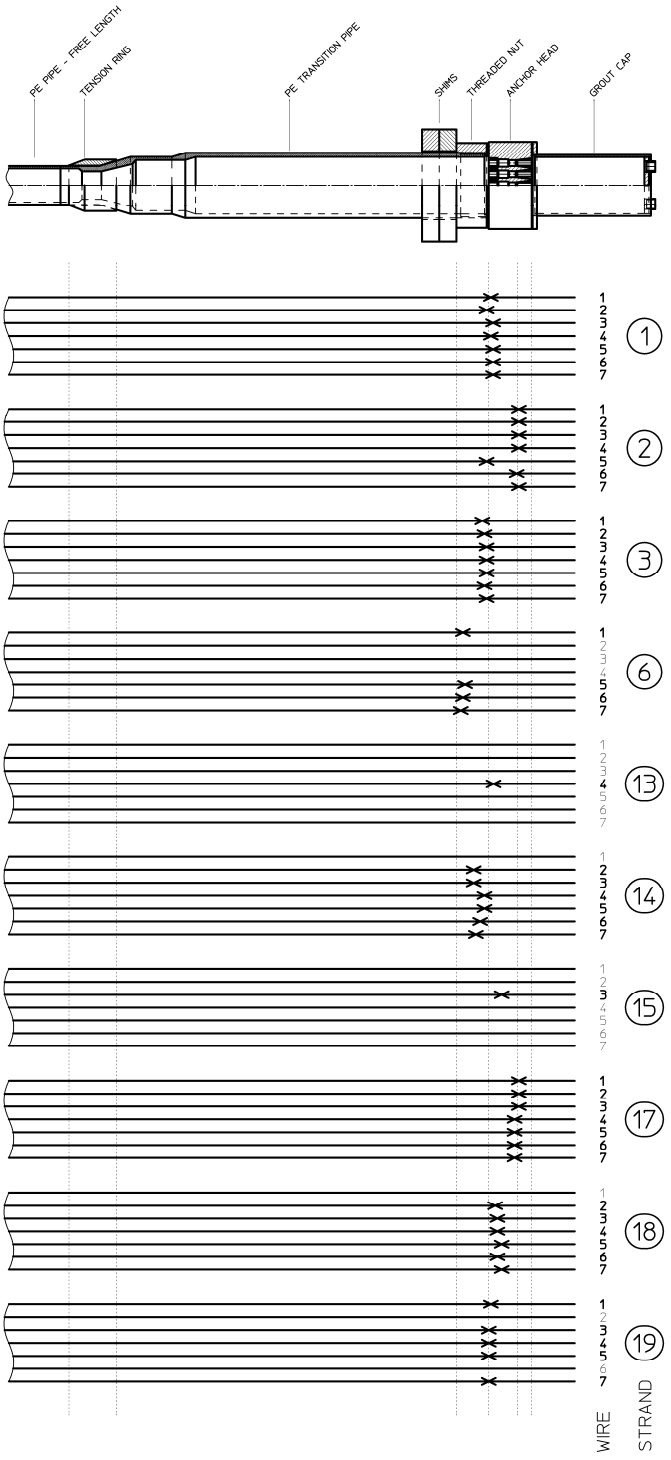

Figure D.23 Location of Wire Breaks near Tower End – Specimen 2

Figure D.24 Fracture Surfaces for Strand 1 near Tower Anchor Head – Specimen 2

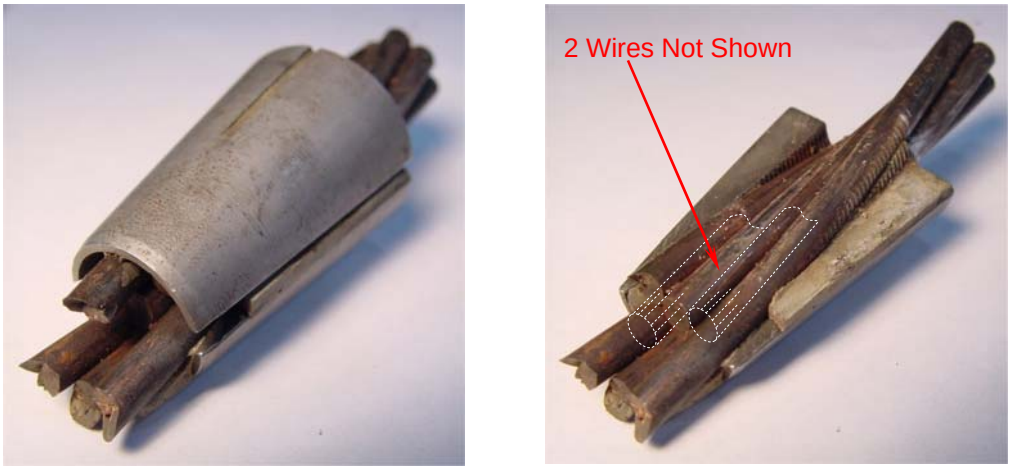

Figure D.25 Opened Wedges and Wire Fractures for Strand 2 near Tower Anchor Head – Specimen 2

Figure D.26 Fracture Surfaces for Strand 2 near Tower End – Specimen 2

Near midspan, the sixteen wire breaks occurred in strands 17 and 18, which were both in the bottom layer of strands (Figure D.27). All breaks were located in a 10-in. window, with a bias towards the deck side. Interestingly, wires 4 and 7 of strand 18 experienced two fractures within the same strand (Figure D.28).

One of the fractures in strand 18 occurred near a possible contact point with the helical spacer wire as shown in Figure D.29. The fracture surface for that wire indicates; however, that the fracture was initiated at the contact point with the center wire, which was also fractured (Figure D.30). The fatigue crack is also significantly larger than on all other failure locations, which indicates that the tension in the strand was negligible at the time of fracture. Consequently, this fracture was the second fracture that occurred on this particular wire.

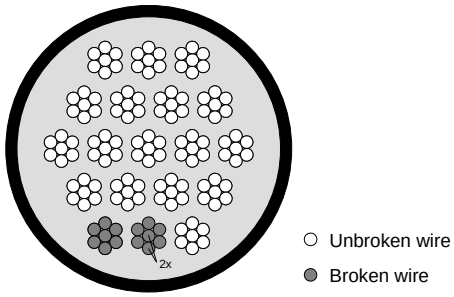

Figure D.27 Distribution of Wire Breaks near Midspan – Specimen 2

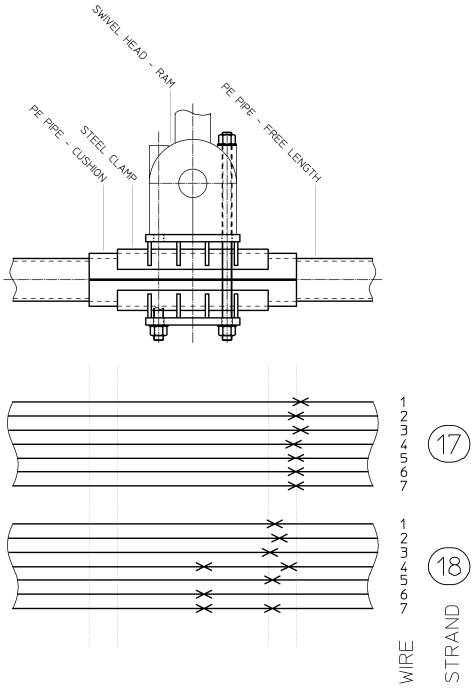

Figure D.28 Location of Wire Breaks near Midspan – Specimen 2

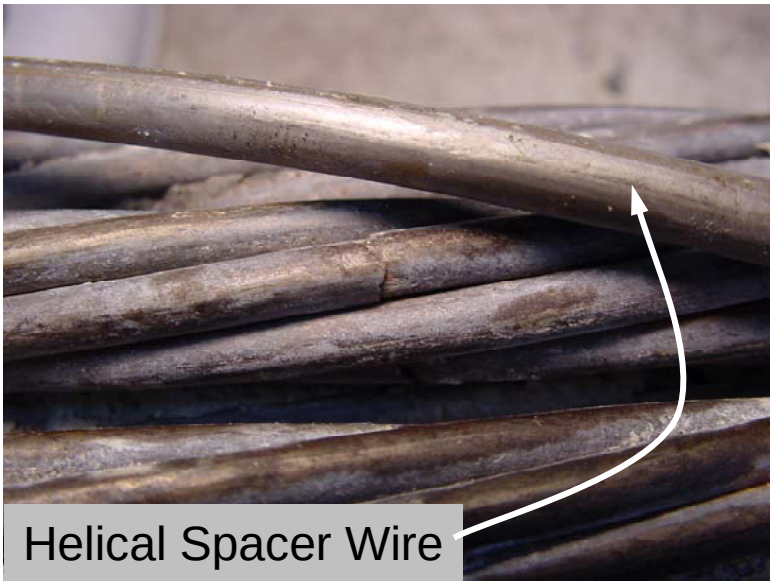

Figure D.29 Wire Break Close to Helical Spacer near Midspan – Specimen 2

Figure D.30 Detail of Fractured Wires shown in Figure D.29

The break at the deck anchorage was found in strand 17 (Figure D.31). The break was initiated at the first tooth of the wedge (Figure D.32). Figure D.33 shows a fairly rounded tooth mark on the wire.

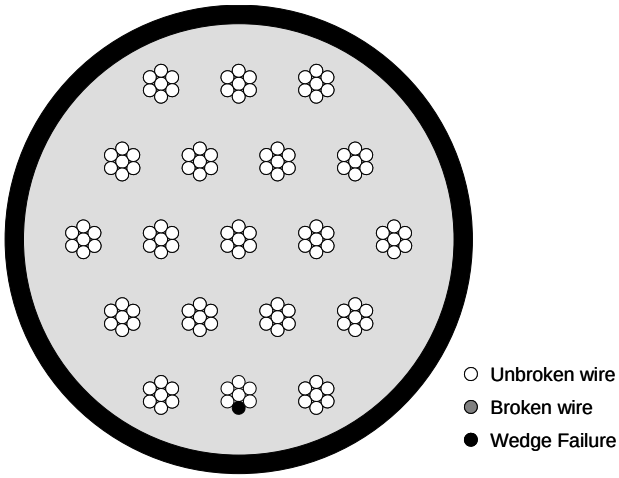

Figure D.31 Distribution of Wire Breaks near Deck End – Specimen 2

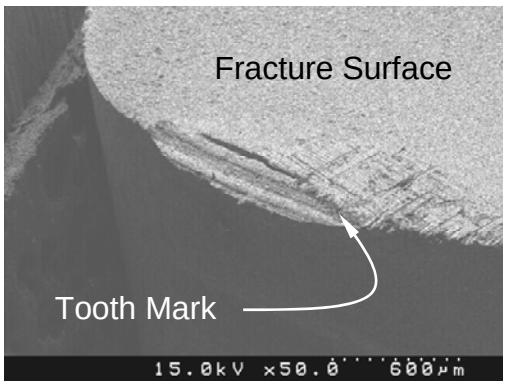

Figure D.32 Fracture Initiation

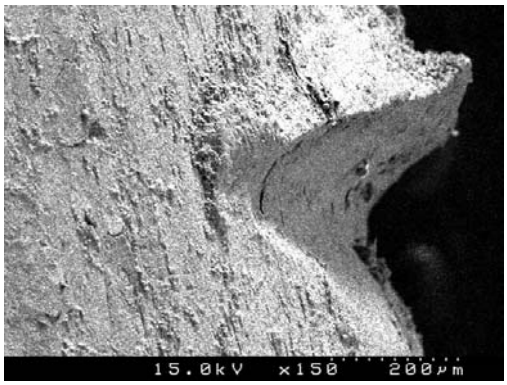

Figure D.33 Typical Tooth Mark

D.2.3 Acoustic Data

The acoustic sensors detected sixty-seven wire breaks during the fatigue test for Specimen 2 (Table D.2). Slight variations in the number and distribution of wire breaks existed between those detected by the acoustic sensors and those observed during the autopsy of the test specimen. The number of wire breaks reported at the tower end was three fewer than observed and the number of breaks reported at midspan was one more than observed. The first wire break was detected after 420,000 fatigue cycles (Figure D.34).

Table D.4 Summary of Wire Breaks – Specimen 2

Method	**Number**	**Tower**	**Midspan**	**Deck**	**Total**
Observed during Autopsy	Total	52	16	1	69
	Unique Wires*	52	14	1	67
Acoustic Sensors	Total	49	17	1	67

* Multiple wire breaks in the same wire are not included in this category.

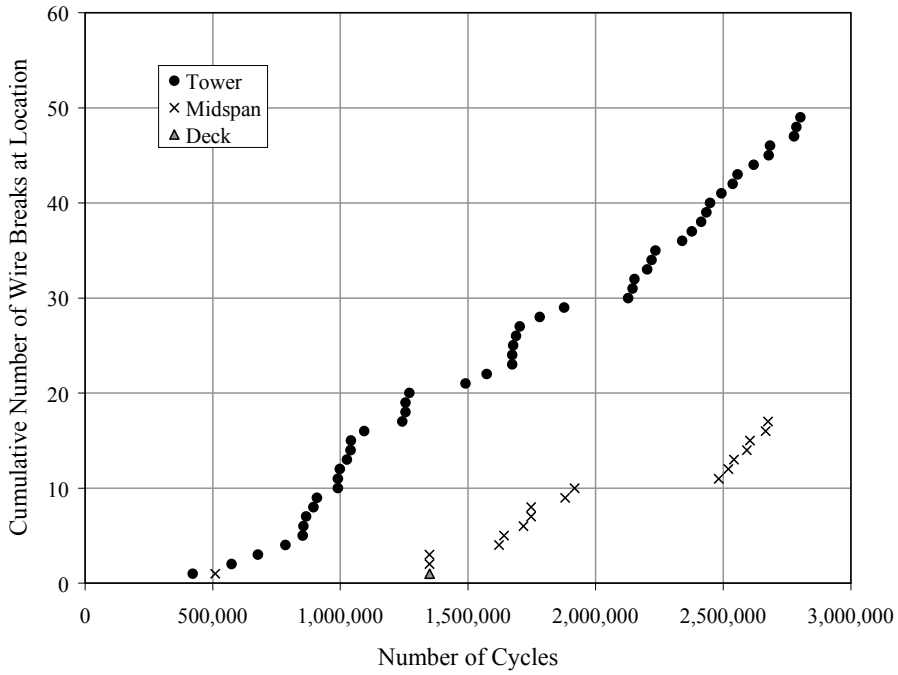

Figure D.34 Wire Breaks Detected from Acoustic Data – Specimen 2

D.2.4 Lateral Stiffness

The variation in the maximum and minimum applied forces needed to achieve the target displacement levels of ±1.6 in. are shown in Figure D.35. The vertical lines also indicate the approximate number of cycles corresponding to each wire break detected by the acoustic sensors. The final average dynamic stiffness was approximately 85% of the initial average dynamic stiffness (Table D.5). Approximately forty wire breaks were detected before the average dynamic stiffness decreased by more than 10%.

Table D.5 Summary of Stiffness Changes during Fatigue Test – Specimen 2

	Static Stiffness	Average Dynamic Stiffness	Frequency
	(kip/in.)	(kip/in.)	(Hz)
Initial	4.8	4.75	12.5
Final	—	4.03	11.5
Final / Initial	—	0.847	0.920

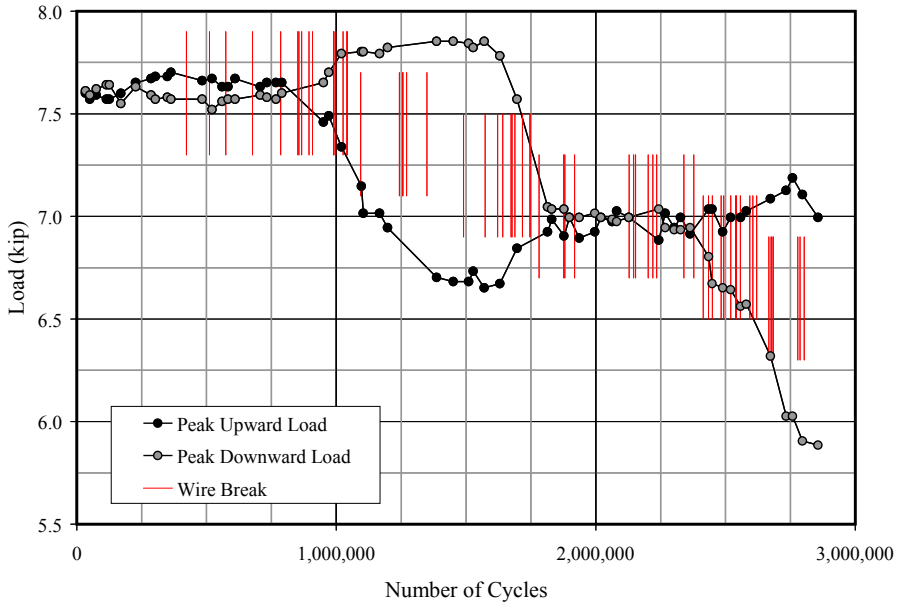

Figure D.35 Variation of Applied Loads during Fatigue Test – Specimen 2

D.3 SPECIMEN 3

Specimen 3 sustained 4,961,560 loading cycles during the fatigue test. Eighty-four wire breaks were identified at the conclusion of the test: nine breaks occurred at the tower end, sixty-two breaks occurred at the center of the specimen under the load point, and thirteen breaks occurred at the deck end. Four wires were intentionally crossed between the anchor head and tension ring at each end of the specimen (Section B.4.5). Specimen 3 was stressed from the deck end and grouted from the deck end. The specimen was tested under displacement control, with an amplitude of ±1.6 in. at midspan.

D.3.1 Observed Condition of Grout

Small grout voids, which partially exposed an opening in the anchor head, were observed at the tower end of Specimen 3 (Figure D.36). Closely spaced air voids were observed at both ends of the specimen (Figure D.37).

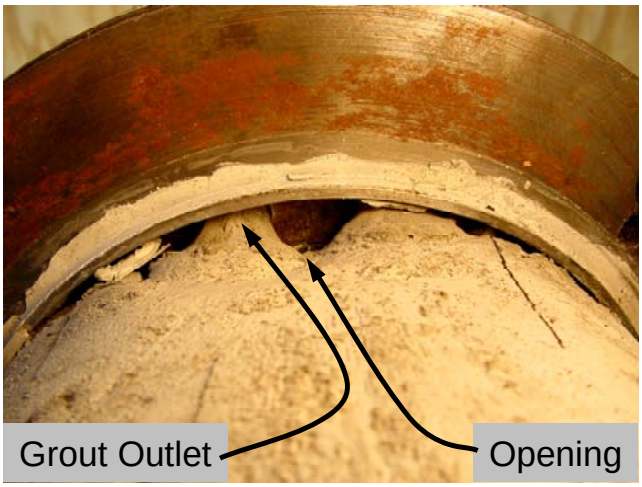

Figure D.36 Air Voids at Tower End of Specimen 3

Figure D.37 Distributed Air Voids at Tower End of Specimen 3

D.3.2 Wire Breaks

Eighty-four wire breaks were identified during the autopsy of Specimen 3. Nine wire breaks occurred near the tower anchorage, sixty-two occurred near the loading point, and thirteen occurred near the deck anchorage.

All the fractures near the tower end occurred within the anchor head and were concentrated in two strands (Figure D.38). No breaks occurred at the contact points of the intentionally crossed strands. Figure D.39 shows the longitudinal location of the wire breaks. One of the wire breaks in strand 18 initiated at the first tooth mark from the wedge. All other wire breaks initiated at the contact points between adjacent strands.

Near midspan, the sixty-two wire breaks occurred in nine different strands (Figure D.40). Six wires fractured at two locations. The distances between the multiple wire breaks varied from 5 in. in strand 1 to 16 in. in strand 18. All breaks were located in a 20-in. window under the loading point, with a slight tendency towards the tower end (Figure D.41).

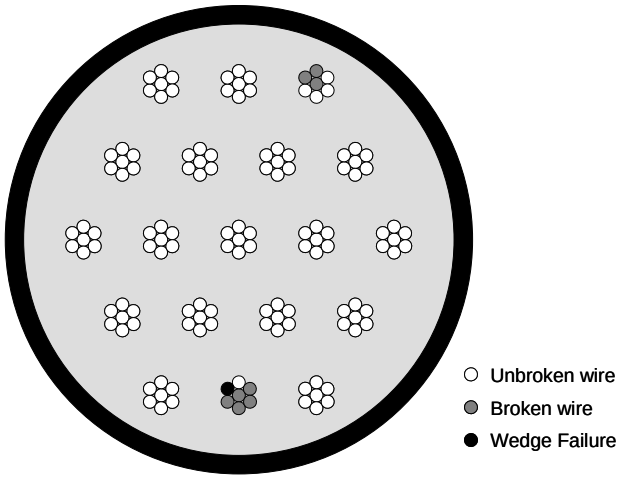

Figure D.38 Distribution of Wire Breaks near Tower End – Specimen 3

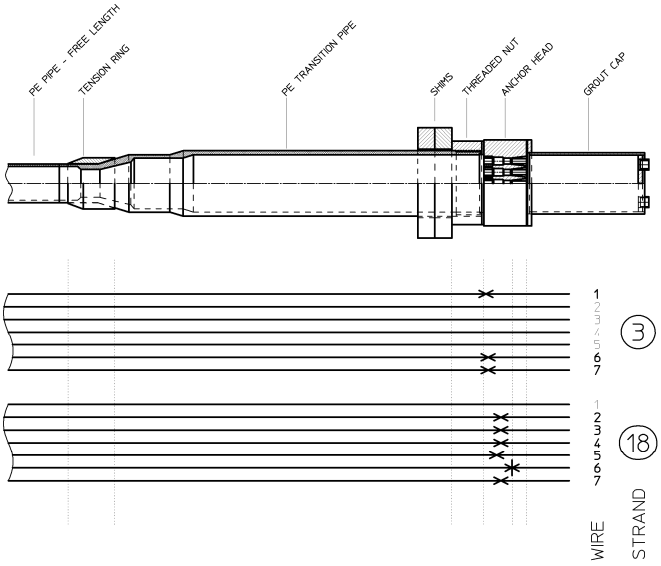

Figure D.39 Location of Wire Breaks near Tower End – Specimen 3

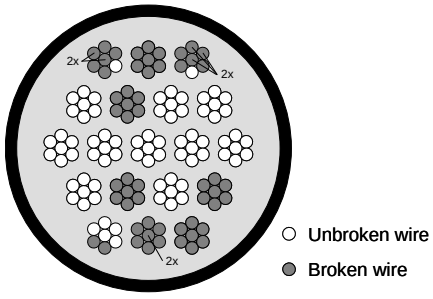

Figure D.40 Distribution of Wire Breaks near Midspan – Specimen 3

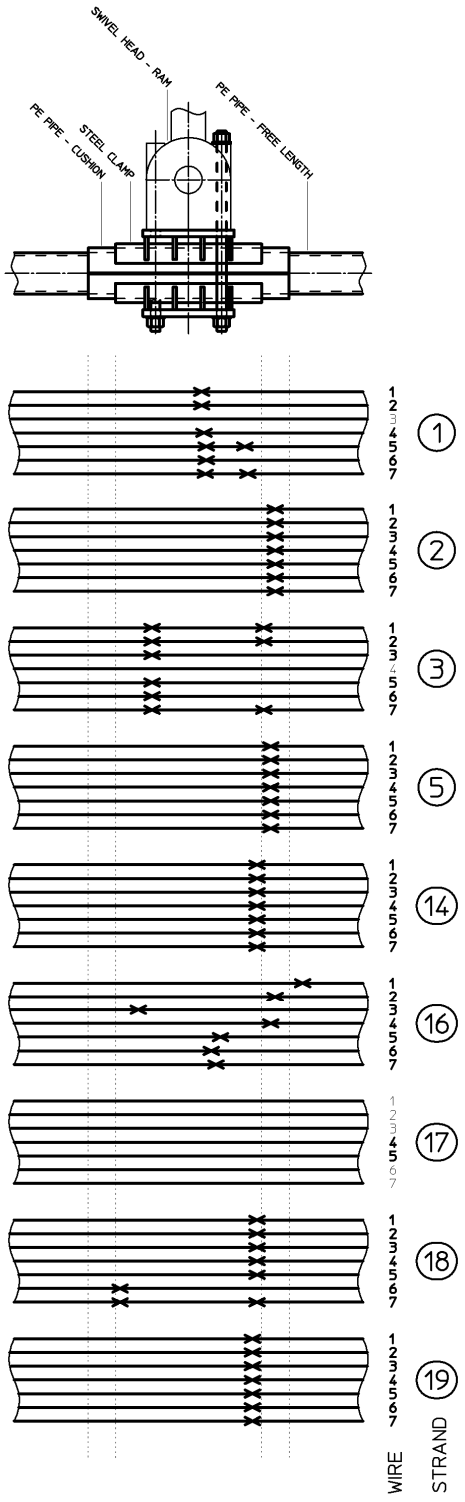

Figure D.41 Location of Wire Breaks near Midspan – Specimen 3

Near the deck end of the specimen, the fractures occurred in strands 2 and 17 (Figure D.42). Figure D.43 shows the longitudinal location of the wire breaks. The breaks in strand 17 occurred within 2 in. of the inside face of the anchor head. Five of the six breaks in strand 2 occurred within the anchor head, and one of the breaks occurred at the first tooth mark from the wedge. No wire breaks occurred at the contact points of the intentionally crossed strands.

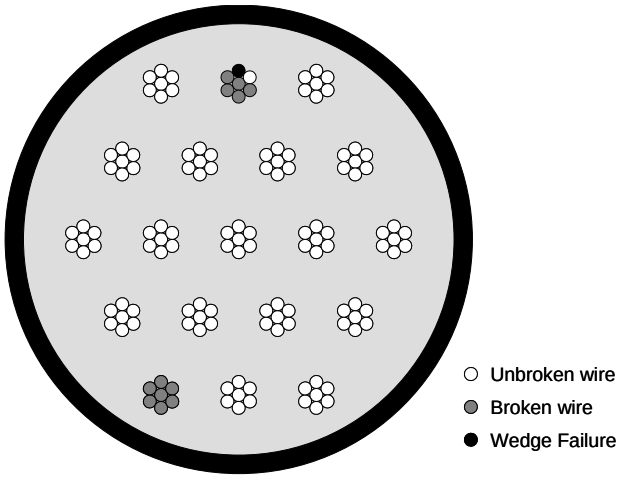

Figure D.42 Distribution of Wire Breaks near Deck End – Specimen 3

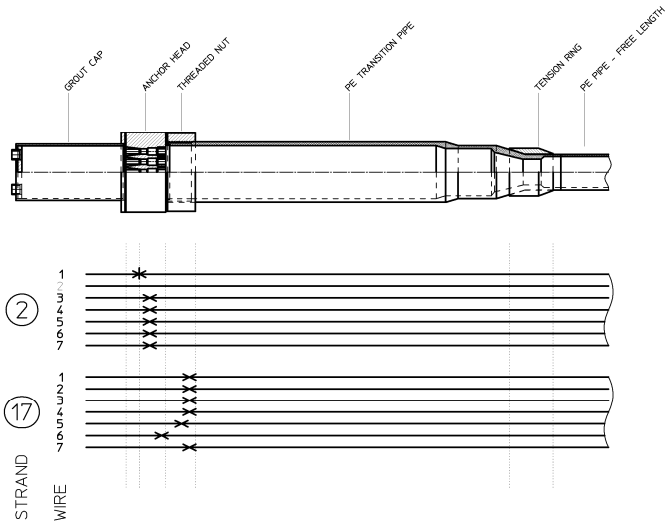

Figure D.43 Location of Wire Breaks near Deck End – Specimen 3

D.3.3 Acoustic Data

The acoustic sensors detected eighty-six wire breaks during the fatigue test for Specimen 3 (Table D.4). Slight variations in the number of wire breaks existed between those detected by the acoustic sensors and those observed during the autopsy of the test specimen. The acoustic sensors detected one more wire break at the tower end and at midspan than was observed. The first wire break was detected after 350,000 fatigue cycles (Figure D.44).

Table D.6 Summary of Wire Breaks – Specimen 3

Method	**Number**	**Tower**	**Midspan**	**Deck**	**Total**
Observed during Autopsy	Total	9	62	13	84
	Unique Wires*	9	56	13	78
Acoustic Sensors	Total	10	63	13	86

* Multiple wire breaks in the same wire are not included in this category.

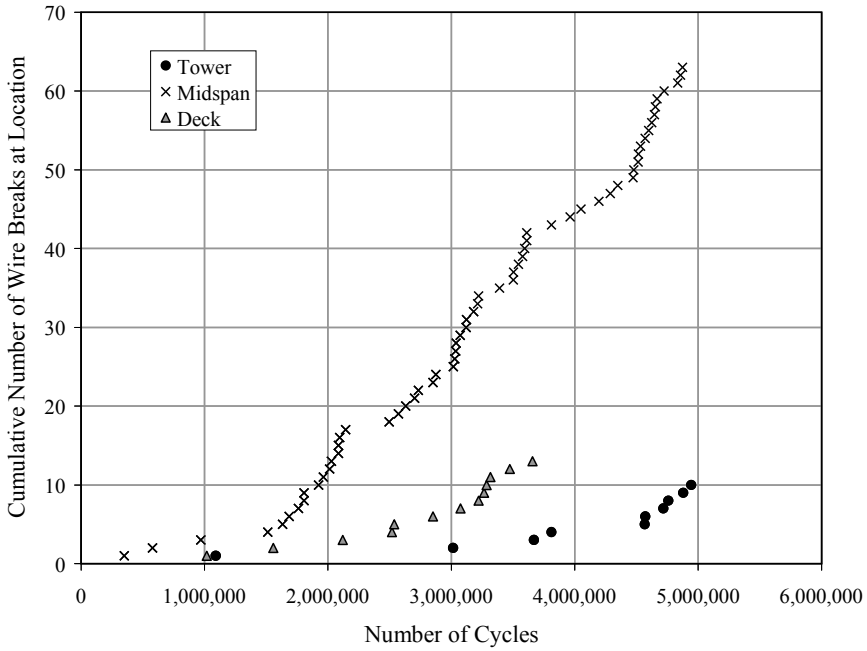

Figure D.44 Wire Breaks Detected from Acoustic Data – Specimen 3

D.3.4 Lateral Stiffness

Dynamic stiffness data are not available for Specimen 3. The initial static stiffness is reported in Table D.7.

Table D.7 Summary of Stiffness Changes during Fatigue Test – Specimen 3

	Static Stiffness	Average Dynamic Stiffness	Frequency
	(kip/in.)	(kip/in.)	(Hz)
Initial	4.7	—	—
Final	—	—	—
Final / Initial	—	—	—

D.4 SPECIMEN 4

Specimen 4 sustained 8,775,245 loading cycles during the fatigue test. Thirty-one wire breaks were identified at the conclusion of the test: twenty-eight breaks occurred at the tower end and three breaks occurred at the deck end. No wire breaks were detected near midspan. Specimen 4 was stressed from the deck end and grouted from the deck end. The specimen was tested under displacement control, with an amplitude of ±1.1 in. at midspan.

D.4.1 Observed Condition of Grout and Strand

Closely spaced air voids were observed at both anchorages. The size and distribution of the voids were similar to those observed for Specimen 2. No information is available about the condition of the strand.

D.4.2 Wire Breaks

Thirty-one wire breaks were identified during the autopsy of Specimen 4. Twenty-eight wire breaks occurred near the tower anchorage and three occurred near the deck anchorage. Near the tower end, all seven wires fractured in each of four strands (Figure D.45). All breaks occurred within ±0.5 in. of the inside face of the anchor head (Figure D.46). The three fractures near the deck end occurred in strand 18 (Figure D.47). All breaks occurred within ±0.5 in. of the inside face of the anchor head (Figure D.48).

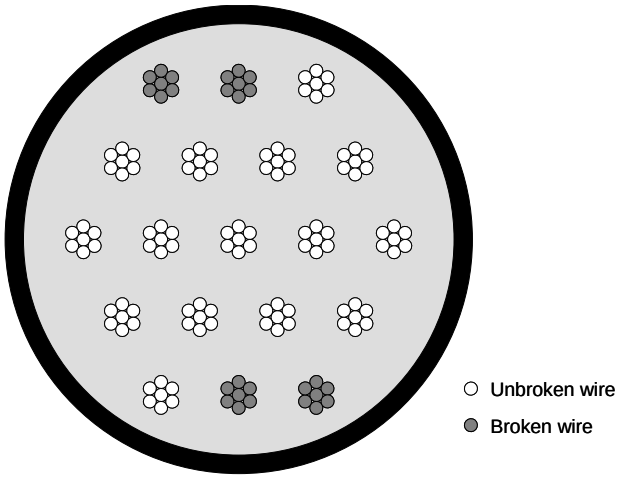

Figure D.45 Distribution of Wire Breaks near Tower End – Specimen 4

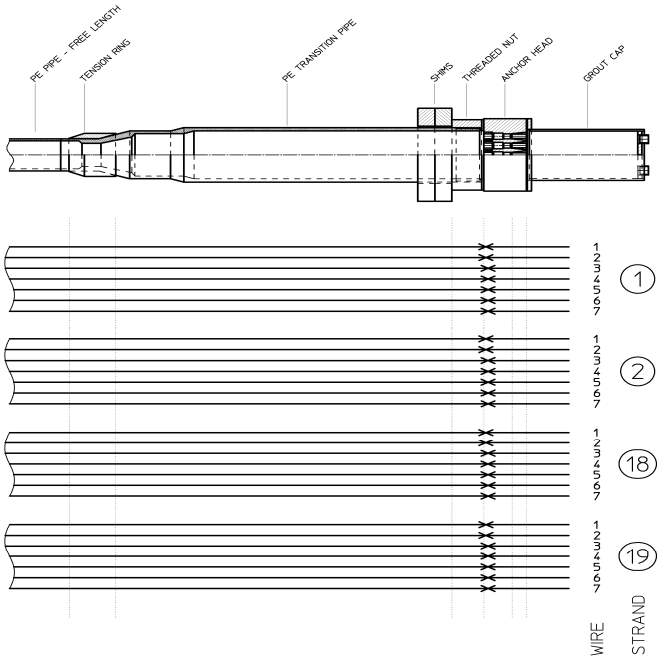

Figure D.46 Location of Wire Breaks near Tower End – Specimen 4

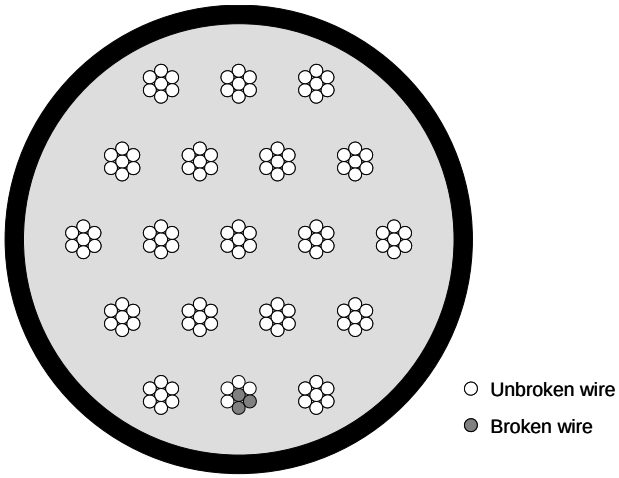

Figure D.47 Distribution of Wire Breaks near Deck End – Specimen 4

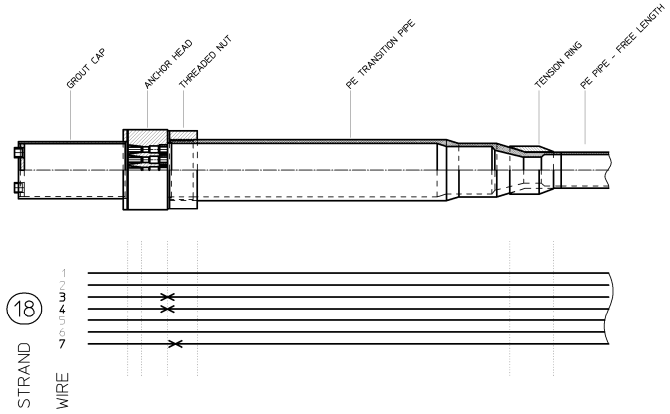

Figure D.48 Location of Wire Breaks near Deck End – Specimen 4

D.4.3 Acoustic Data

The acoustic sensors detected twenty-seven wire breaks during the fatigue test for Specimen 4 (Table D.8). The number of wire breaks detected was two less than the number observed at each end of the specimen. The first wire break was detected after 2,830,000 fatigue cycles (Figure D.49).

Table D.8 Summary of Wire Breaks – Specimen 4

Method	**Number**	**Tower**	**Midspan**	**Deck**	**Total**
Observed during Autopsy	Total	28	—	3	31
	Unique Wires*	28	—	3	31
Acoustic Sensors	Total	26	—	1	27

* Multiple wire breaks in the same wire are not included in this category.

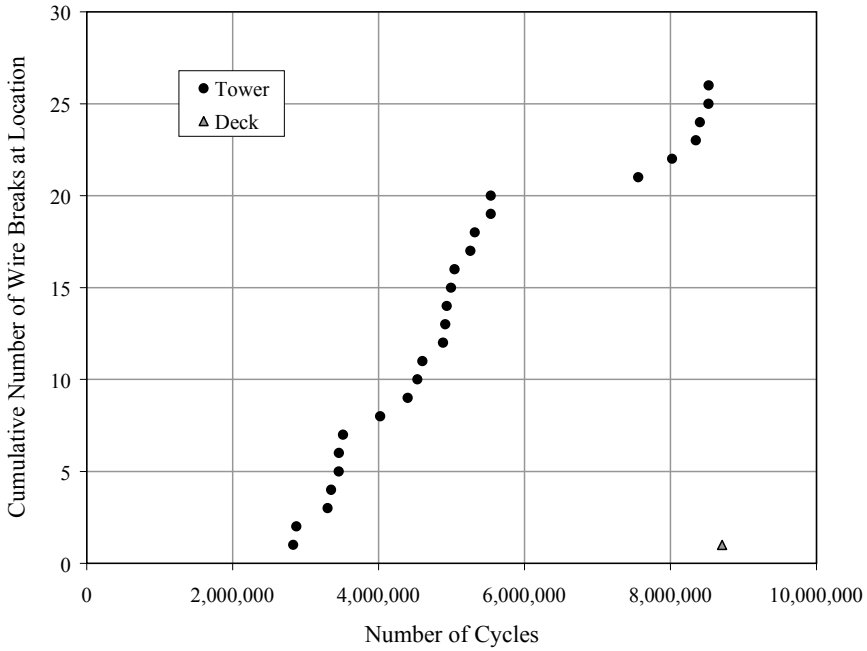

Figure D.49 Wire Breaks Detected from Acoustic Data – Specimen 4

D.4.4 Lateral Stiffness

Dynamic stiffness data are not available for Specimen 4. The initial static stiffness and the initial frequency are reported in Table D.9.

Table D.9 Summary of Stiffness Changes during Fatigue Test – Specimen 4

	Static Stiffness	Average Dynamic Stiffness	Frequency
	(kip/in.)	(kip/in.)	(Hz)
Initial	4.5	—	12.5
Final	—	—	—
Final / Initial	—	—	—

D.5 SPECIMEN 5

Specimen 5 sustained 5,211,106 loading cycles without a wire fracture. Specimen 5 was stressed from the tower end and the 3-ft center section was grouted from the deck end. The cable displacement was ±1.6 in. at midspan.

D.5.1 Observed Condition of Grout and Strand

The only portion of Specimen 5 that was grouted was a 3-ft section at the center. The grout had no appreciable voids, apart from a small defect at the location of the vent hole used for grouting, and appeared to be homogeneous. The grout appeared to be essentially uncracked immediately upon opening

the PE pipe (Figure D.50). The longitudinal cracks visible in Figure D.50 were caused by the router used to open the PE pipe. Longitudinal cracks characteristic of wire breaks were not observed. However, within minutes of opening the polyethylene pipe, circumferential shrinkage cracks began to appear and the grout began to fall away in pieces.

Corrosion was observed on the surface of the strand at the interface between the grout and caulk in the center portion of the specimen (Figure D.51). The color indicates the presence of corroded fretting product, but the source of this fretting is unclear. Very little corrosion or corroded fretting product was observed along the ungrouted portion of the specimen.

Figure D.50 Condition of Grout in Center Section of Specimen 5

Figure D.51 Corrosion Product Observed at Interface between Caulk and Grout in Specimen 5

D.5.2 Wire Breaks

Specimen 5 did not experience any wire breaks during the fatigue tests. To ensure accurate calibration of the Soundprint® monitoring system, the research team intentionally generated two wire breaks (Figure D.52). A Dremel tool was used to cut the wires, and then the cable was displaced until the damaged wire broke. The acoustic monitoring system accurately captured the simulated wire breaks.

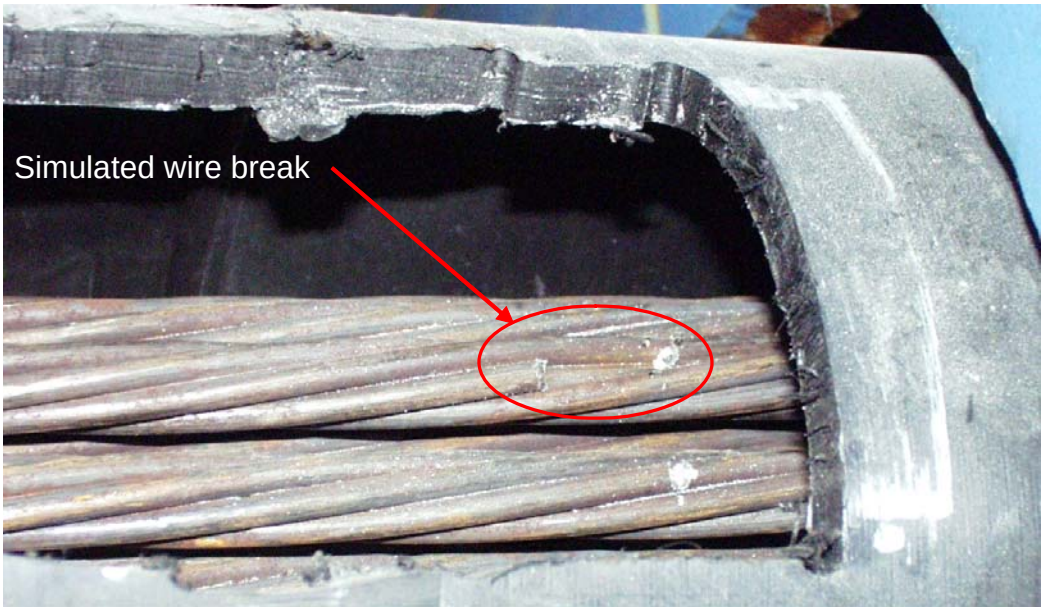

Figure D.52 Simulated Wire Break in Specimen 5

D.5.3 Lateral Stiffness

The variation in the maximum and minimum applied forces needed to achieve the target displacement levels of ±1.6 in. are shown in Figure D.35. The maximum applied load did not vary appreciably during the fatigue tests, and the final average dynamic stiffness was within 2% of the initial average dynamic stiffness (Table D.10). In the static tests (Figure D.54), the change in stiffness was less than 5%.

Table D.10 Summary of Stiffness Changes during Fatigue Test – Specimen 5

	Static Stiffness	Average Dynamic Stiffness	Frequency
	(kip/in.)	(kip/in.)	(Hz)
Initial	4.07	3.90	13.8
Final	3.90	3.84	13.5
Final / Initial	0.957	0.986	0.978

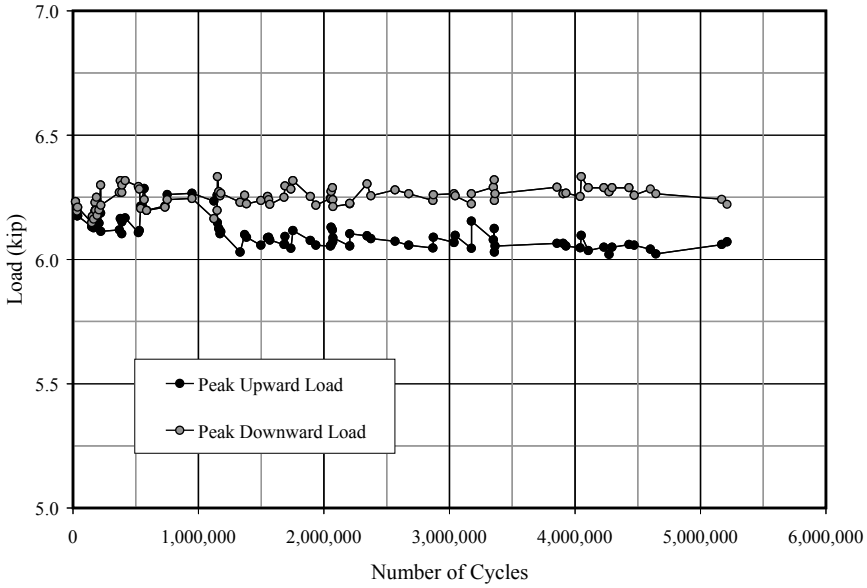

Figure D.53 Variation of Applied Loads during Fatigue Test – Specimen 5

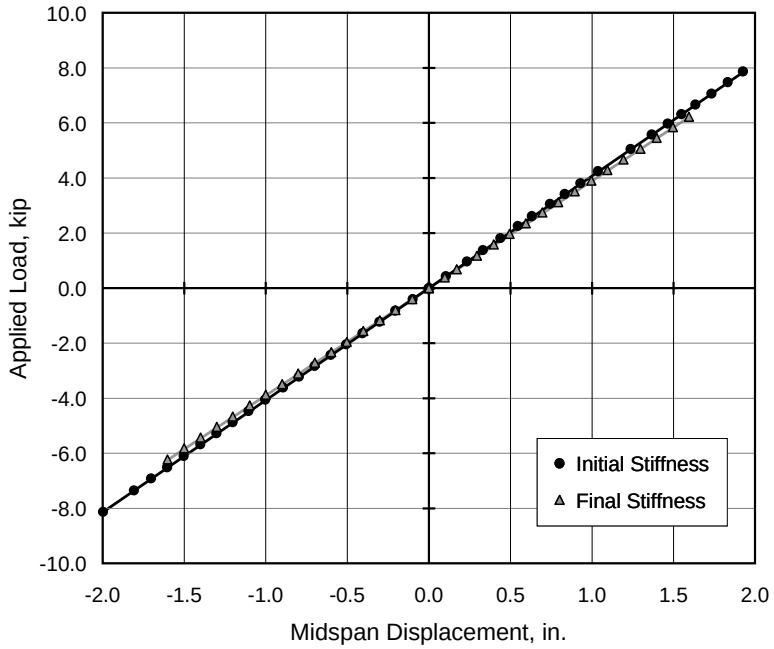

Figure D.54 Load - Displacement Response during Static Tests – Specimen 5

D.5.4 Measured Strain in Strand

Specimen 5 was instrumented with eight strain gages; therefore, it was possible to calculate the stress range in the strand near the anchor head. The locations of the strain gages were discussed in Section B.4.3.

Strain data were collected periodically during the fatigue test. Figure D.55 presents the strain data from two gages taken during a static test. Gage 2 was on the top of Strand 1 and gage 8 was on the

bottom of Strand 19. Both were approximately 4 in. from the inside face of the deck anchor head. The strain was considered to be zero when the midspan displacement of the cable was zero. Positive strain values in Figure D.55 represent an increase in tension and negative strain values represent a decrease in tension. Due to the level of prestress, the strands in the specimen did not experience net compressive strains. Based on the maximum strain reported by any gage during the test, the strand remained elastic throughout the test.

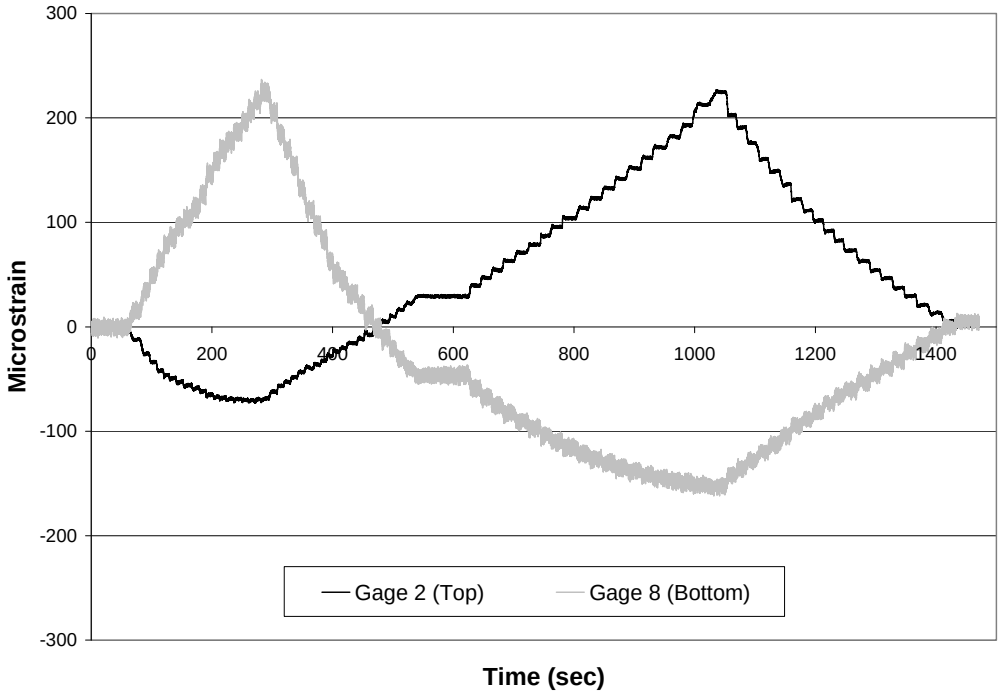

Figure D.55 Measured Strain Data from Static Test – Specimen 5

Figure D.56 shows the stress range calculated for each gage during the fatigue tests. The stress was calculated using the average apparent modulus of elasticity for the strand (Table A.7) and assuming linear-elastic behavior. The stress range measured near the bottom of the section (Gages 5 through 8) tended to be higher that that at the top (Gages 1 through 4). On any given strand, the gages farther away from the anchor head experience a lower stress range than those nearer the anchor head. In most locations, the stress range was less than 10 ksi.

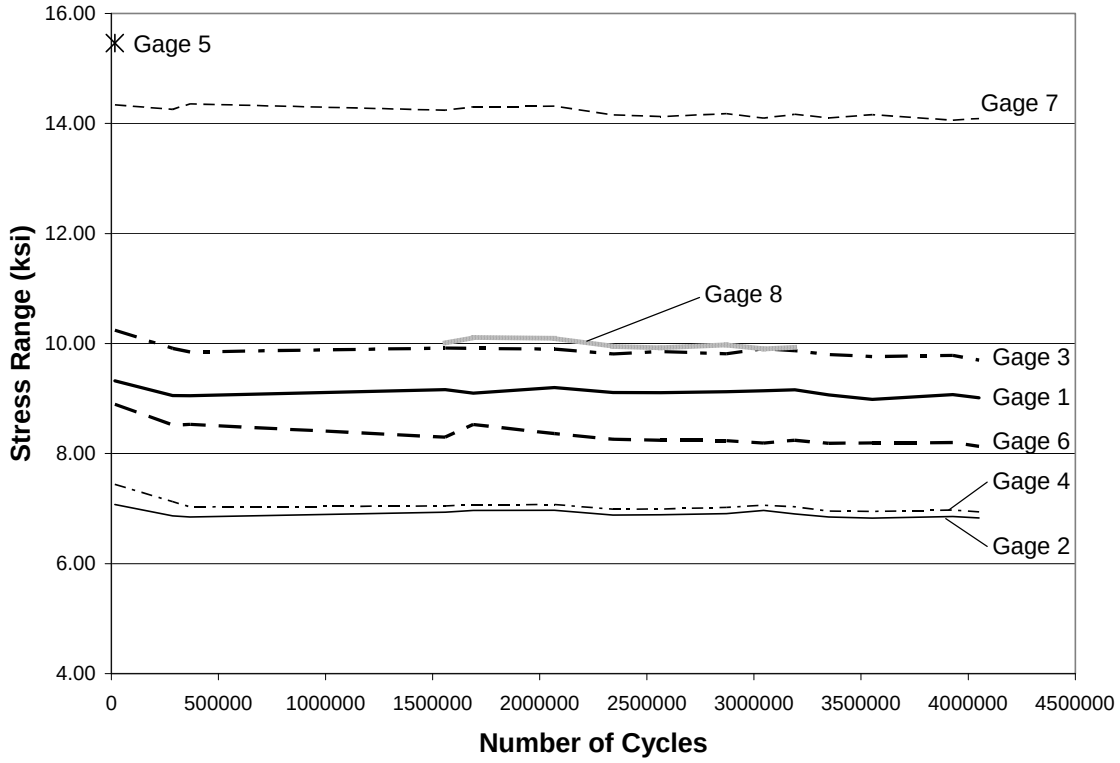

Figure D.56 Stress Range Inferred from Strain Measurements near Deck End of Specimen 5

D.6 SPECIMEN 6

Specimen 6 sustained 6,483,024 loading cycles during the fatigue test. Twenty-eight wire breaks were identified at the conclusion of the test: seventeen breaks occurred at the tower end and eleven breaks occurred at the center of the specimen under the load point. No breaks were found at the deck end. The specimen was constructed using only 13 strands. Specimen 6 was stressed from the tower end and grouted from the deck end. The specimen was tested under displacement control, with an amplitude of ±1.6 in. at midspan.

D.6.1 Observed Condition of Grout and Strand

Figure D.57 shows the condition of the grout immediately after opening the PE pipe. At the deck anchorage, a large grout crack was observed on the bottom of the specimen near the ring formed in the grout due to the weld in the polyethylene transition pipe. Several small (less than 0.25-in. diameter) air voids were also visible at the deck end.

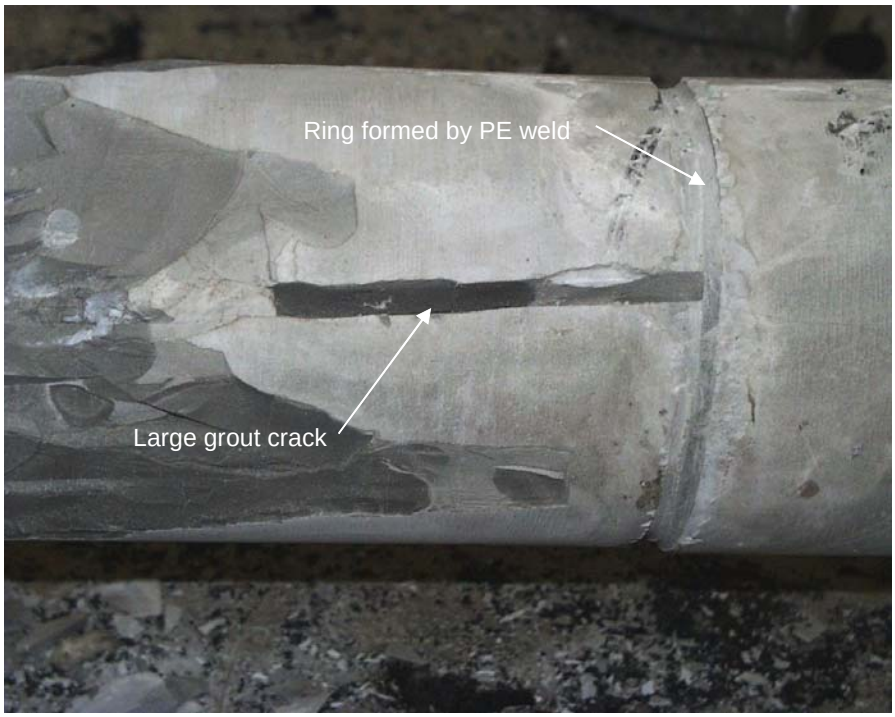

Figure D.57 Large Grout Crack near Deck Anchorage – Specimen 6

At the tower end, large longitudinal cracks characteristic of wire breaks were present immediately upon opening the PE pipe. As the grout was exposed to the environment, parallel circumferential cracks began to form and pieces of grout began to fall away, exposing two strands (Figure D.58). Apart from the cracking, the grout had no visible imperfections and appeared to be homogenous.

Figure D.58 Grout Cracking near Tower End – Specimen 6

The grout near midspan exhibited severe longitudinal cracks characteristic of wire breaks (Figure D.59). Thin, parallel circumferential cracks were also observed. As with the other portions of the stay, the cracking in the center portion of the specimen became more severe after exposure to the air.

Figure D.59 Grout near Midspan of Specimen 6

Upon opening the PE pipe, corroded fretting product was observed near the wire breaks. As wires fret against each other, microscopic particles of steel begin to rub off the wire surfaces. These particles have a very high surface area to volume ratio, thus corrode very easily to form an abrasive product that aggravates fretting (Frank 2004). In most cases, this corroded fretting product was not evident on the exterior of the strand and could only be seen by taking apart the strand and inspecting the contact surfaces between wires. An example of corroded fretting product can be seen in Figure D.60.

Figure D.60 Corroded Fretting Product on Strand 19 – Specimen 6

The abrasive nature of the corrosion product formed by fretting may initiate fatigue cracking or may be a product formed after a wire breaks. After one wire of a strand fractures, the increased relative movement between the adjacent intact wires and the sharp fracture surface may increase the surface abrasion and also the production of fretting product, thus instigating further fatigue cracking.

In the case of Specimen 6, the evidence of fretting near the wire breaks at the tower anchor head was more severe than the evidence of fretting found elsewhere. In some places, corrosion was evident on the exterior of the strand and was accompanied by a white substance that coated the strand, shown in Figure D.61. In this region, corrosion was also seen on the grout surface at the interface between the grout and the strand (Figure D.62).

Figure D.61 Corrosion on Strand 19 near Tower Anchor Head – Specimen 6

Figure D.62 Corrosion Product on Grout from Tower End of Specimen 6

D.6.2 Wire Breaks

Twenty-eight wire breaks were identified during the autopsy of Specimen 6. Seventeen wire breaks occurred near the tower anchorage and eleven occurred near the loading point. The seventeen wire breaks near the tower end were distributed among four strands (Figure D.63). Figure D.64 shows the longitudinal location of wire breaks near the tower anchorage. Nearly all breaks at the tower end of the specimen occurred within 2 in. of the inside face of the anchor head in the region confined by the smooth end sleeve. Examples of wire breaks occurring in this region are shown in Figure D.65 and Figure D.66.

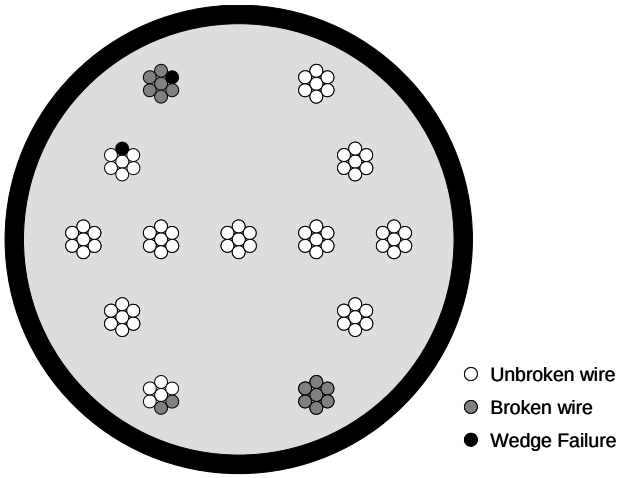

Figure D.63 Distribution of Wire Breaks near Tower End – Specimen 6

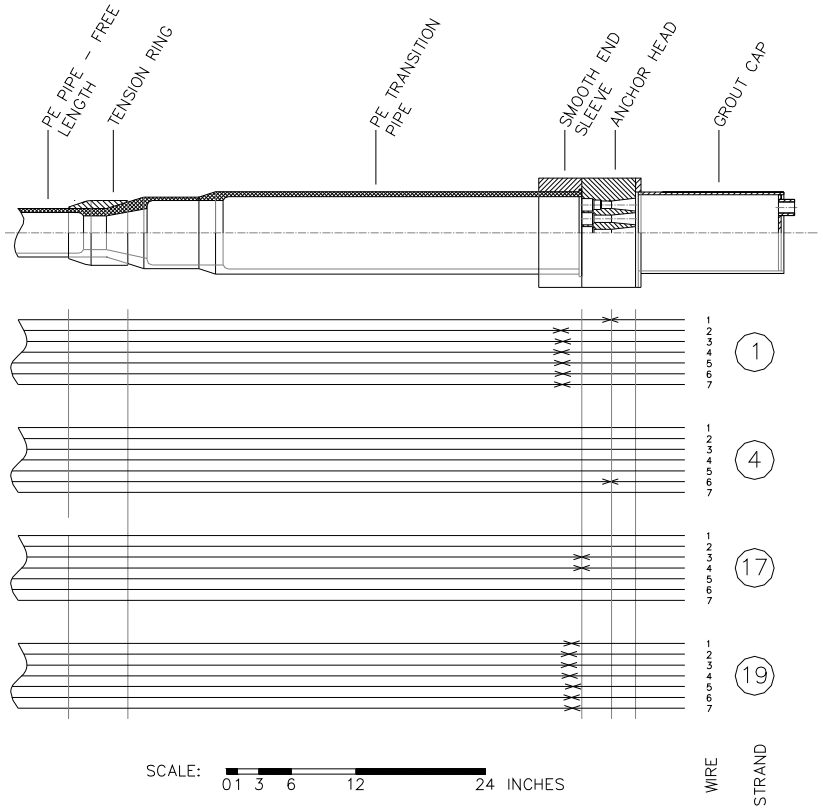

Figure D.64 Location of Wire Breaks near Tower End – Specimen 6

Figure D.65 Wire Breaks in Strand 1 near Tower End – Specimen 6

Figure D.66 Wire Breaks in Strand 17 at the Inside Face of the Tower Anchor Hear – Specimen 6

At midspan, the eleven wire breaks occurred in three strands (Figure D.67). The longitudinal distribution of the breaks is shown in Figure D.68. All breaks occurred beyond the tapered polyethylene cushioning pipe.

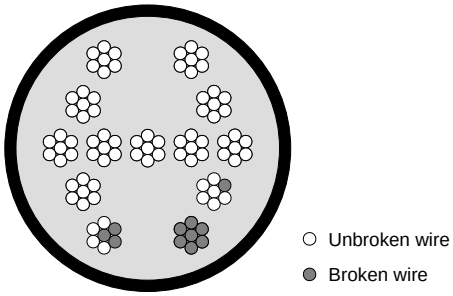

Figure D.67 Distribution of Wire Breaks near Midspan – Specimen 6

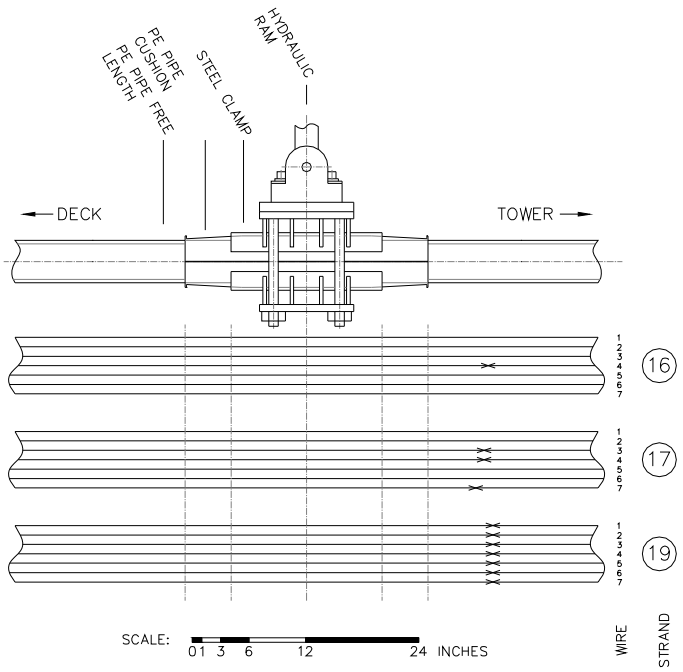

Figure D.68 Location of Wire Breaks near Midspan – Specimen 6

D.6.3 Acoustic Data

The acoustic sensors detected all twenty-eight wire breaks during the fatigue test for Specimen 6 (Table D.11). The first wire break was detected after 610,000 fatigue cycles (Figure D.69).

Table D.11 Summary of Wire Breaks – Specimen 6

Method	**Number**	**Tower**	**Midspan**	**Deck**	**Total**
Observed during Autopsy	Total	17	11	—	28
	Unique Wires*	17	11	—	28
Acoustic Sensors	Total	17	11	—	28

* Multiple wire breaks in the same wire are not included in this category.

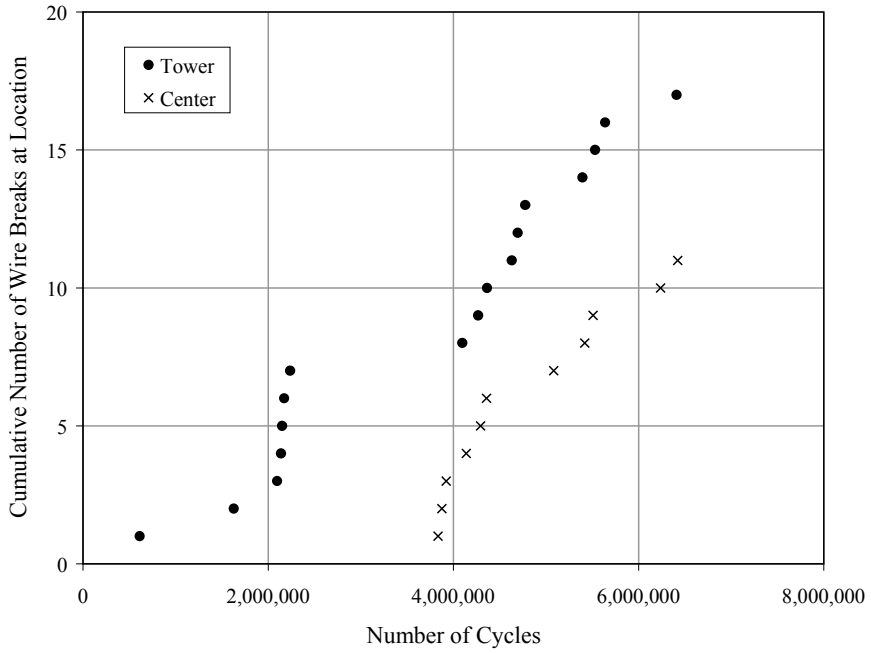

Figure D.69 Wire Breaks Detected from Acoustic Data – Specimen 6

D.6.4 Transverse Stiffness

The variation in the maximum and minimum applied forces needed to achieve the target displacement levels of ±1.6 in. are shown in Figure D.70. The vertical lines also indicate the approximate number of cycles corresponding to each wire break detected by the acoustic sensors. The final average dynamic stiffness was within 9% of the initial average dynamic stiffness (Table D.12).

The transverse stiffness was determined from the static tests by comparing the load and midspan deflection data (Figure D.71). The stiffness values determined from the static tests were slightly higher than those from the fatigue tests; however, the percent change in stiffness was nearly the same for the two types of data.

Table D.12 Summary of Stiffness Changes during Fatigue Test – Specimen 6

	Static Stiffness	Average Dynamic Stiffness	Frequency
	(kip/in.)	(kip/in.)	(Hz)
Initial	3.29	3.14	11.5
Final	3.00	2.86	11.0
Final / Initial	0.911	0.914	0.957

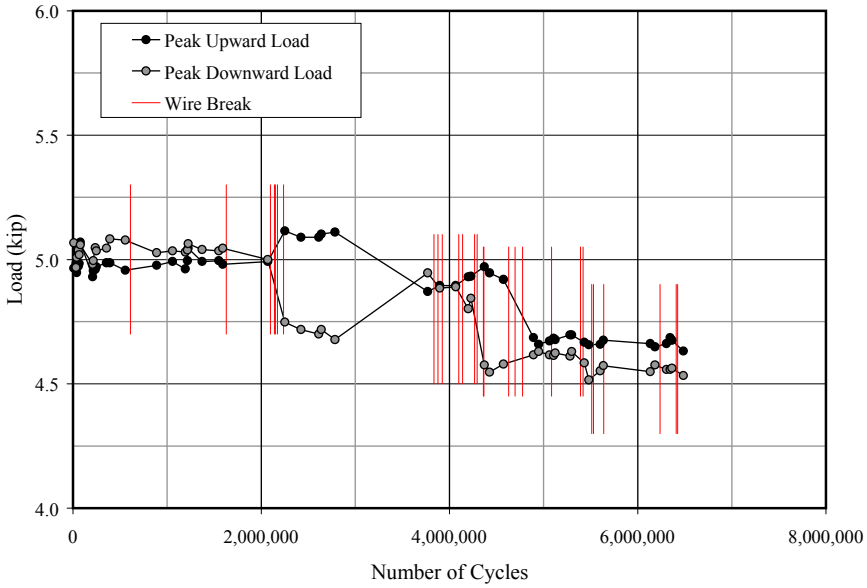

Figure D.70 Variation of Applied Loads during Fatigue Test – Specimen 6

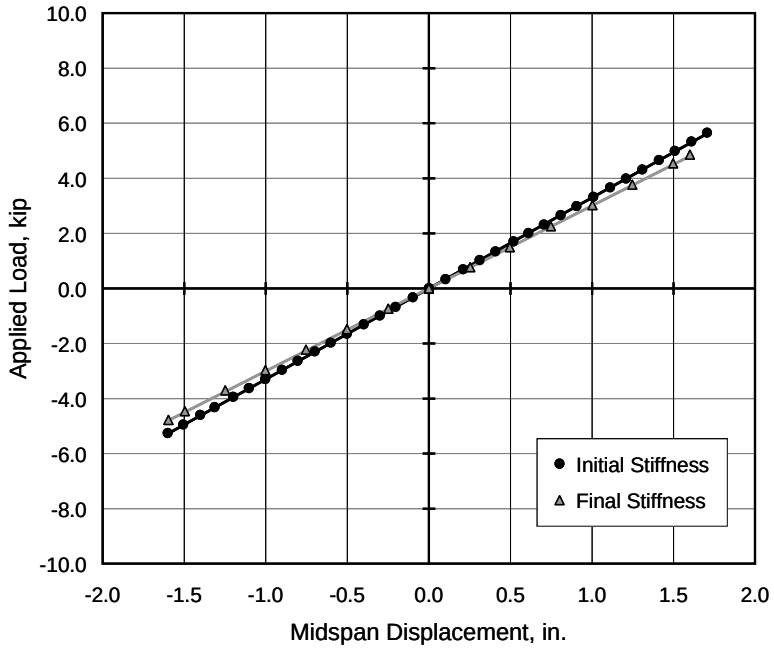

Figure D.71 Load - Displacement Response during Static Tests – Specimen 6

D.7 SPECIMEN 7

Specimen 7 sustained 2,246,869 loading cycles during the fatigue test. One hundred seventeen wire breaks were identified at the conclusion of the test: thirty-seven breaks occurred at the tower end, sixty-five breaks occurred at the center of the specimen under the load point, and seventeen occurred at the deck end. Specimen 7 was stressed from the tower end and grouted from the deck end. The specimen was tested under displacement control, with an amplitude of ±1.6 in. at midspan.

D.7.1 Observed Condition of Grout and Strand

After exposing the grout at the tower end of the stay to the atmosphere, several air voids with an approximate diameter of 0.5 in. were observed (Figure D.72). Longitudinal cracks indicative of wire breaks were also observed. Figure D.72 also shows the ring-shaped deformity in the grout caused by the weld in the polyethylene transition pipe.

Figure D.72 Condition of Grout at Tower End - Specimen 7

The grout at the deck end appeared homogeneous with no significant air voids. Some circumferential cracks were observed (Figure D.73). Despite the presence of wire breaks in the region, the grout appeared to be in good condition immediately after exposing the grout to the atmosphere (Figure D.73). However, the grout cracked significantly with time (Figure D.74).

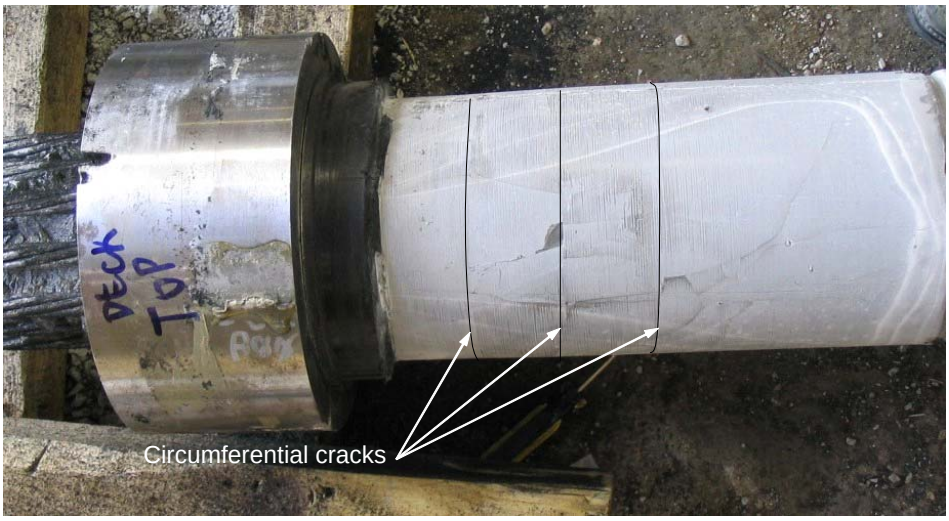

Figure D.73 Condition of Grout near Deck Anchor Head Immediately after Removing Polyethylene Pipe – Specimen 7

Figure D.74 Condition of Grout near Deck Anchor Head Several Minutes after Removing Polyethylene Pipe – Specimen 7

At midspan, serious damage to the grout was observed immediately after removing the PE pipe (Figure D.75). The extent of cracking did not increase with time at this location.

Figure D.75 Condition of Grout under Load Point – Specimen 7

Most of the corrosion and corroded fretting product observed after removing the PE pipe was in the vicinity of the wire breaks. Figure D.76 shows a typical example of the corroded fretting product found in these areas.

Figure D.76 Corrosion Observed near Tower Anchorage on Strand 18 – Specimen 7

In the center of the stay, a white substance was found near most wire breaks (Figure D.78). In addition to the white substance, red-orange corroded fretting product was typically observed between the wires in the strands in which wire breaks occurred. The corroded fretting product was often not visible on the surface of the strand.

Figure D.77 White Substance on Surface of Strand 17 at Midspan – Specimen 7

Figure D.78 Corrosion on Surface of Strand 17 at Midspan – Specimen 7

D.7.2 Wire Breaks

One hundred seventeen wire breaks were identified during the autopsy of Specimen 7. Thirty-seven wire breaks occurred near the tower anchorage, sixty-five occurred near the loading point, and seventeen occurred near the deck anchorage.

The thirty-seven wire breaks near the tower end were distributed among six strands (Figure D.79). Figure D.80 shows the longitudinal location of wire breaks near the tower anchorage. A majority of the breaks occurred within 9 in. of the inside face of the anchor head. Wire breaks in Specimen 7 occurred as far as 16 in. from the face of the anchor head.

The order of the two wire breaks in strand 17 can be determined by studying the fracture surfaces (Figure D.81). The jagged fracture surface in Figure D.81(a), which is somewhat obscured by the presence of grout on the surface, indicates that the wire was carrying tensile force at the time that this break occurred. In contrast, the smooth fracture surface in Figure D.81(b) indicates that the tensile force was essentially zero. Therefore, the break shown in Figure D.81(a) occurred before the break shown in Figure D.81(b).

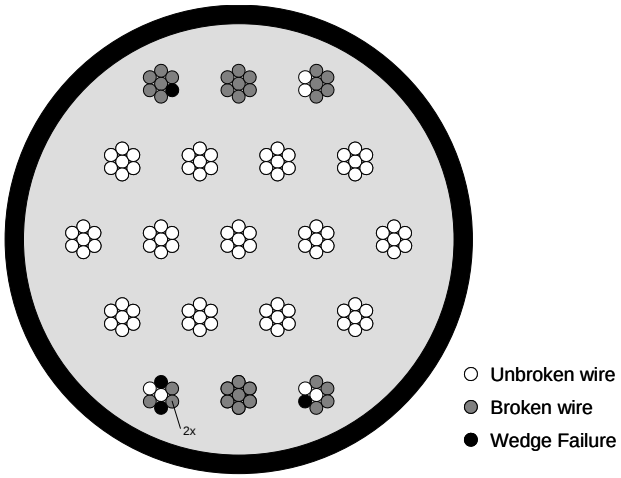

Figure D.79 Distribution of Wire Breaks near Tower End – Specimen 7

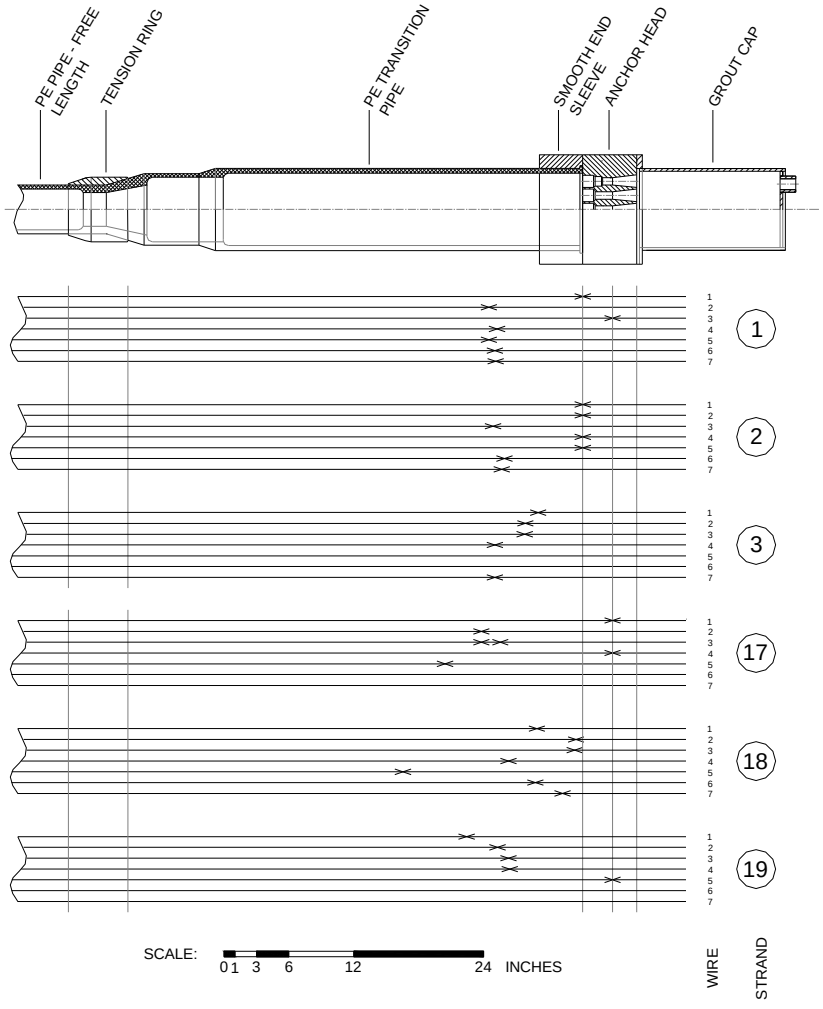

Figure D.80 Location of Wire Breaks near Tower End – Specimen 7

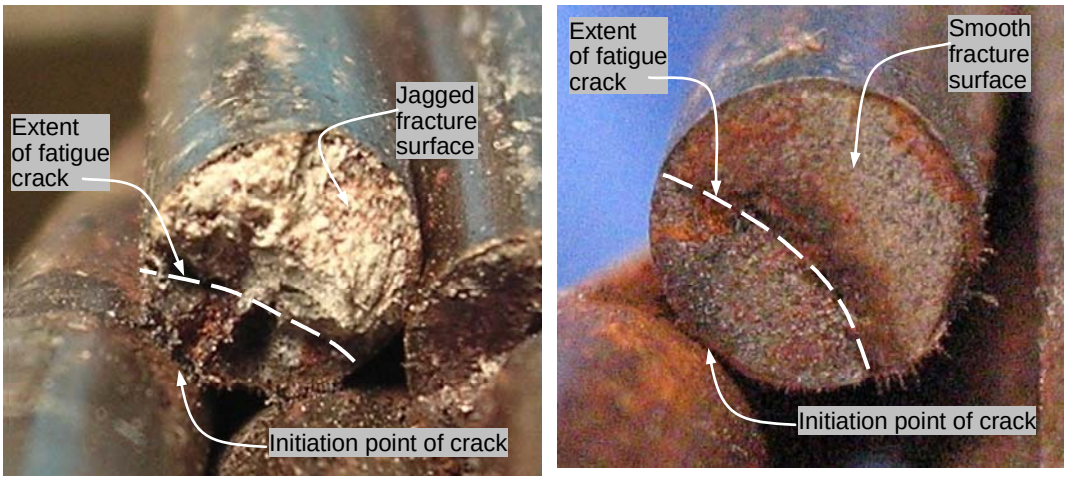

(a) First Fracture Surface **(b) Subsequent Fracture Surface**

Figure D.81 Two Wire Breaks in the Same Wire near the Tower End – Specimen 7

Figure D.82 shows the distribution of the wire breaks among ten strands at midspan. The longitudinal distribution of the breaks at midspan is shown in Figure D.83 and Figure D.84. The breaks tend to be centered near the edge of the load plate where the clamp is bolted to the cable. The center wire in strand 2 fractured in three places.

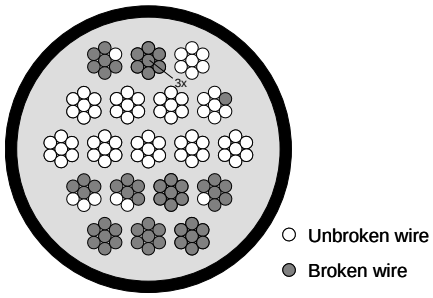

Figure D.82 Distribution of Wire Breaks near Midspan – Specimen 7

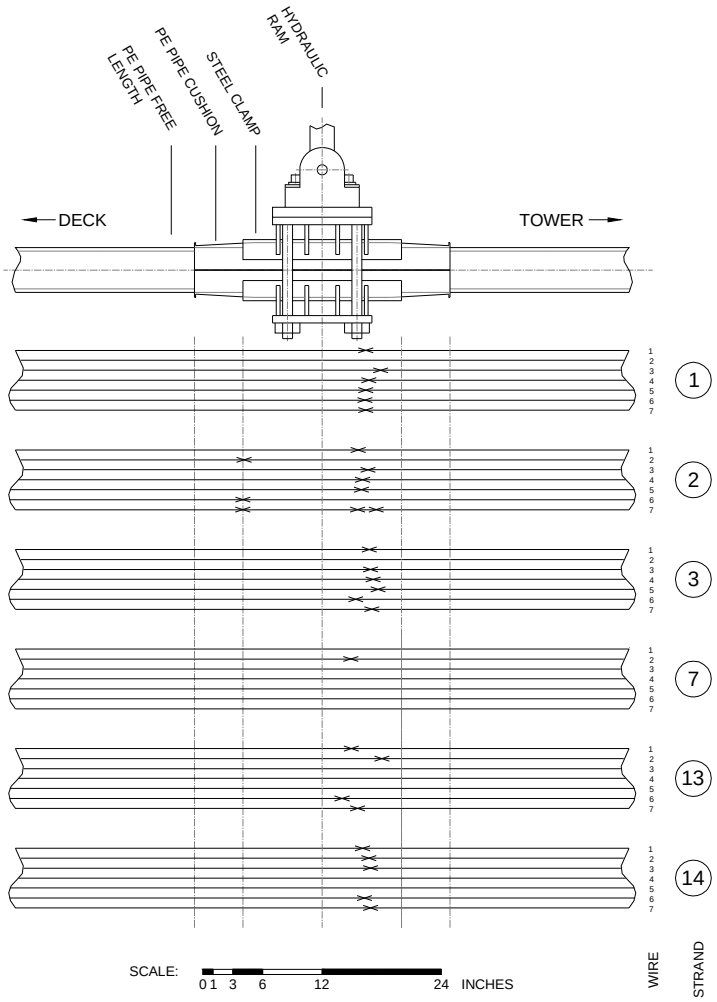

Figure D.83 Location of Wire Breaks near Midspan – Specimen 7 (Part 1)

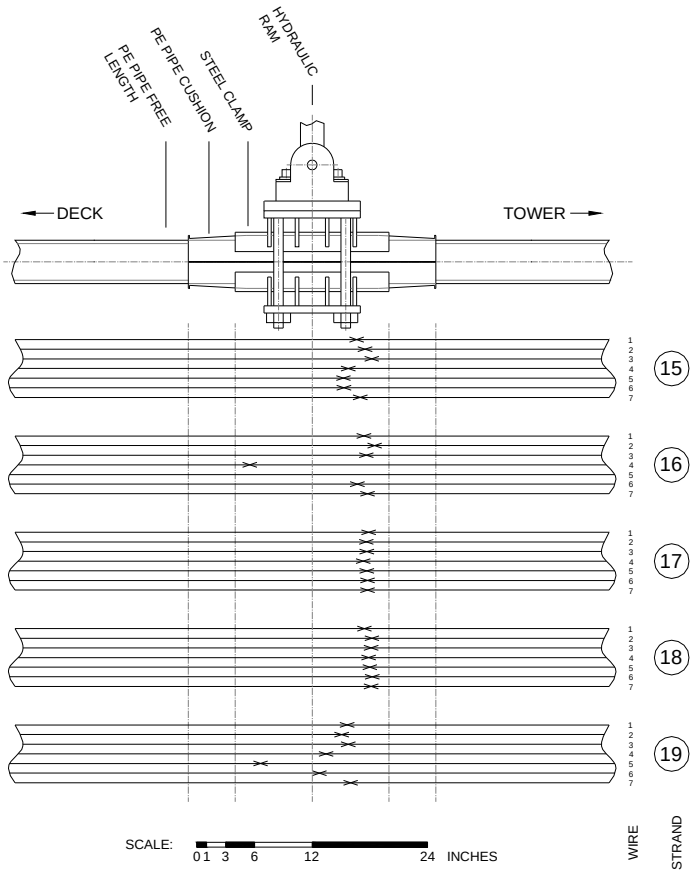

Figure D.84 Location of Wire Breaks near Midspan – Specimen 7 (Part 2)

The seventeen wire breaks near the deck end were distributed among five strands (Figure D.85). Figure D.86 shows the longitudinal location of wire breaks near the deck anchorage. Most of the wire breaks occurred within 4 in. of the inside face of the anchor head or inside the anchor head. One wire in strand 18 broke approximately 14 in. from the inside face of the anchor head.

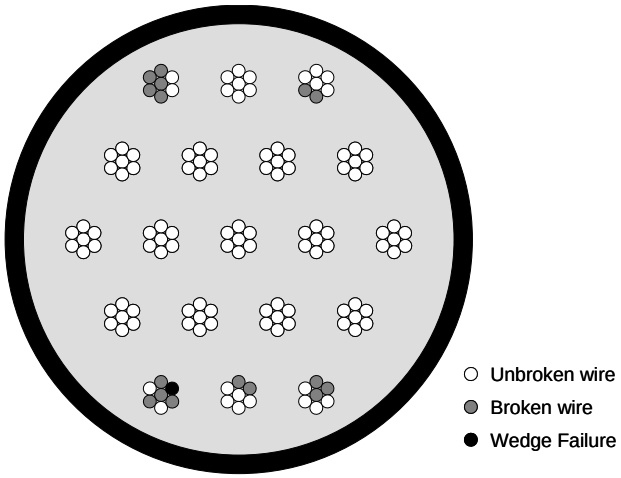

Figure D.85 Distribution of Wire Breaks near Deck End – Specimen 7

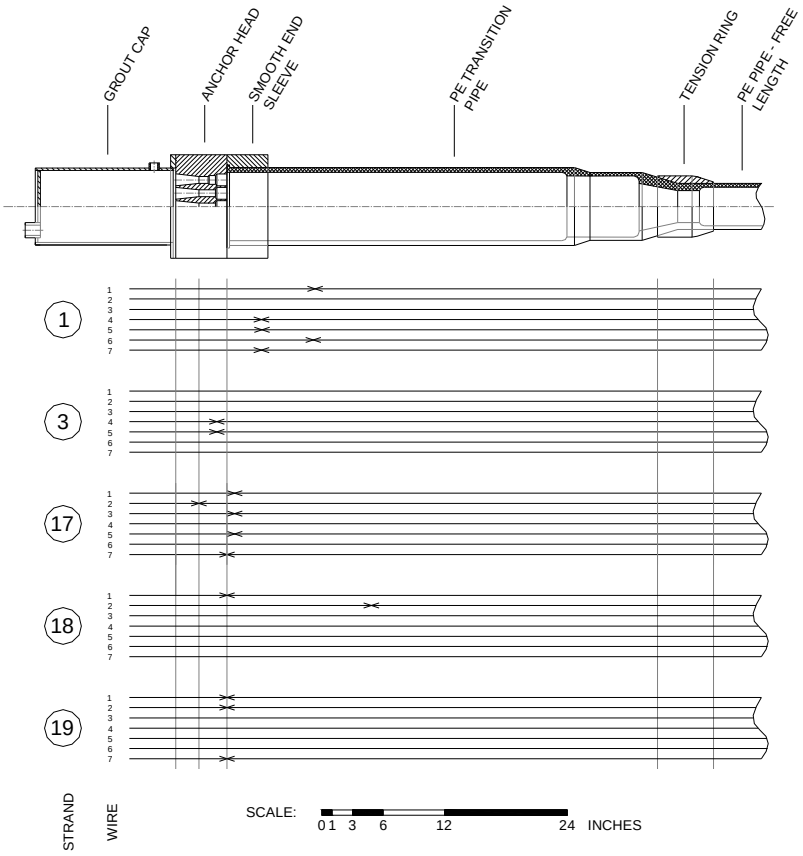

Figure D.86 Location of Wire Breaks near Deck End – Specimen 7

D.7.3 Acoustic Data

The acoustic sensors detected all twenty-eight wire breaks during the fatigue test for Specimen 7 (Table D.13). The first wire break was detected after 670,000 fatigue cycles (Figure D.87).

Table D.13 Summary of Wire Breaks – Specimen 7

Method	**Number**	**Tower**	**Midspan**	**Deck**	**Total**
Observed during Autopsy	Total	37	65	17	119
	Unique Wires*	36	63	17	116
Acoustic Sensors	Total	36	62	16	114

* Multiple wire breaks in the same wire are not included in this category.

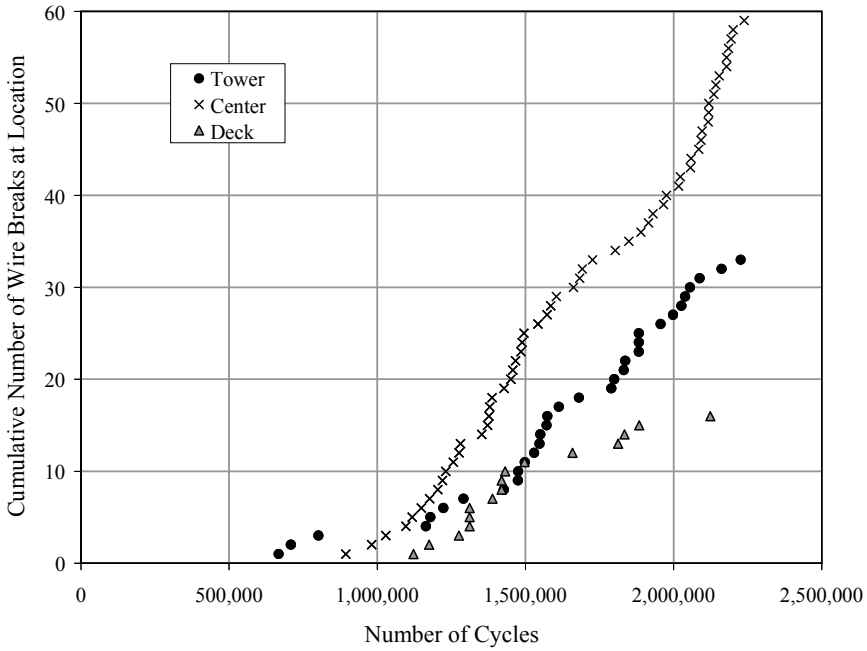

Figure D.87 Wire Breaks Detected from Acoustic Data – Specimen 7

D.7.4 Lateral Stiffness

The variation in the maximum and minimum applied forces needed to achieve the target displacement levels of ±1.6 in. are shown in Figure D.88. The vertical lines also indicate the approximate number of cycles corresponding to each wire break detected by the acoustic sensors. The final average dynamic stiffness was less than 85% of the initial average dynamic stiffness (Table D.14). Nearly fifty wires fractured before the average dynamic stiffness decreased by more than 10%.

The transverse stiffness was determined from the static tests by comparing the load and midspan deflection data (Figure D.89). The initial static stiffness was slightly higher than the average initial dynamic stiffness; however, the final static stiffness was 15% less than the average final dynamic stiffness.

Table D.14 Summary of Stiffness Changes during Fatigue Test – Specimen 7

	Static Stiffness	Average Dynamic Stiffness	Frequency
	(kip/in.)	(kip/in.)	(Hz)
Initial	5.00	4.79	13.3
Final	3.46	4.04	11.1
Final / Initial	0.691	0.843	0.835

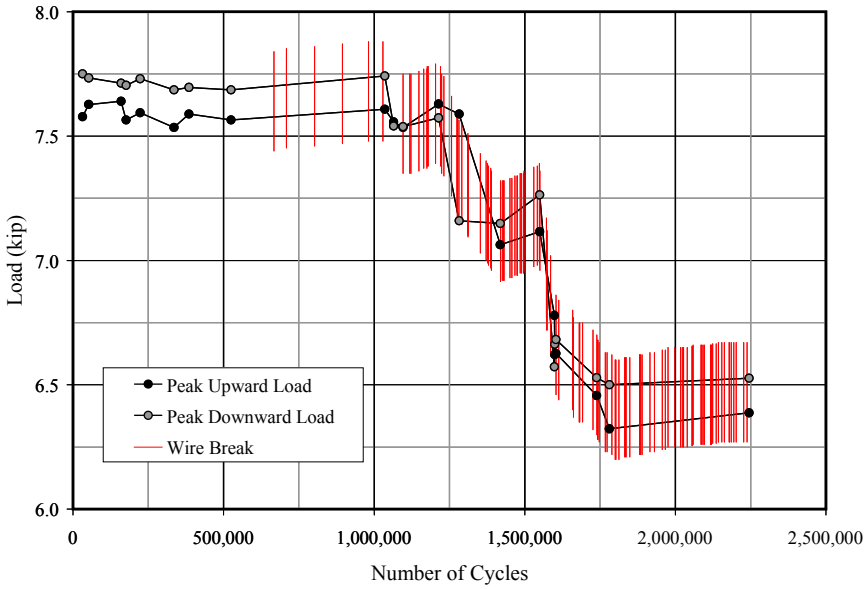

Figure D.88 Variation of Applied Loads during Fatigue Test – Specimen 7

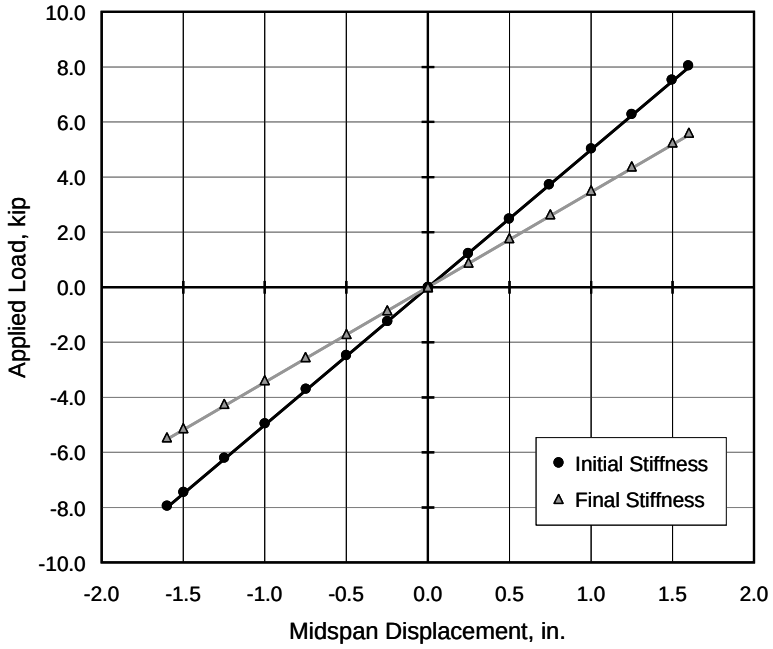

Figure D.89 Load - Displacement Response during Static Tests – Specimen 7

D.8 SPECIMEN 8

Specimen 8 sustained 6,200,593 loading cycles during the fatigue test. Four wire breaks were identified at the conclusion of the test: two breaks occurred at the tower end and two breaks occurred at the deck end. Specimen 8 was stressed from the tower end and the 3-ft center section was grouted from the deck end. The specimen was tested under displacement control, with an amplitude of ±1.6 in. at midspan.

D.8.1 Observed Condition of Grout and Strand

The only portion of Specimen 8 that was grouted was a 3-ft section at the center. The grout had no appreciable voids apart from a small defect at the location of the vent hole used for grouting, and appeared to be homogeneous. Immediately after removing the PE pipe, longitudinal cracks were observed along the entire length of the grouted section. Circumferential cracks were also present and were concentrated near the PVC end caps (Figure D.90). The cracks in the grout were more severe near the ends of the grouted section.

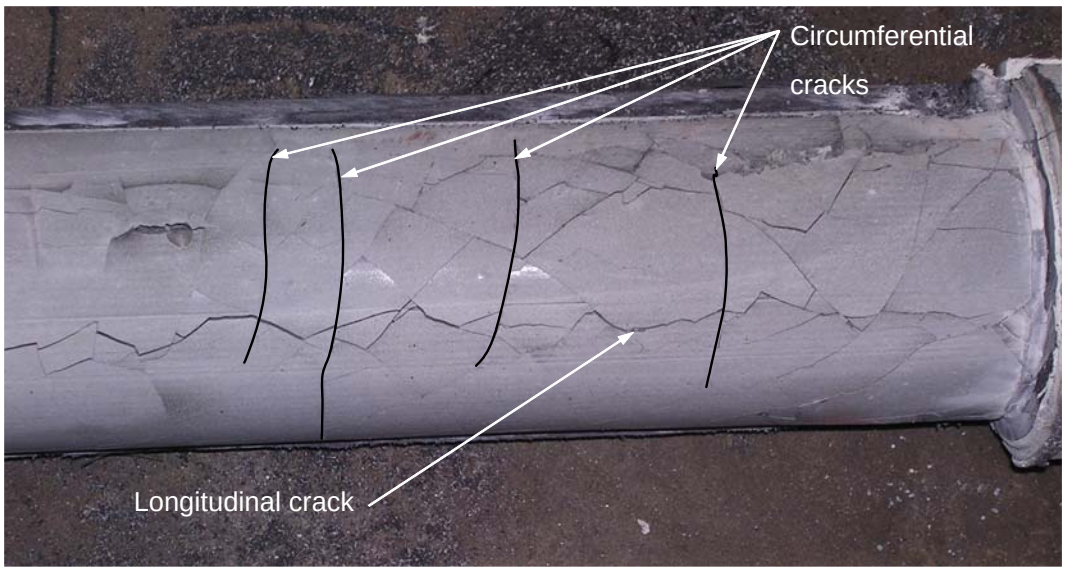

Figure D.90 Condition of Grout in Center Section of Specimen 8

Corroded fretting product was observed on the surface of the strands at both tension rings after fewer than 1,000,000 fatigue cycles. Fretting was more severe at the deck end (Figure D.91) due to a misalignment of the strands (Section B.4.5). The strands were aligned at the tower end; however, fretting was observed at this location also. Wear of the wires at the contact points due to the fretting was observed during the autopsy of the specimen (Figure D.92).

Near the tension rings, the friction due to the contact between the strands caused a noticeable temperature increase. The temperature difference between the tension ring and the free length of the cable was 20 °F at the deck end and 18 °F at the tower end.

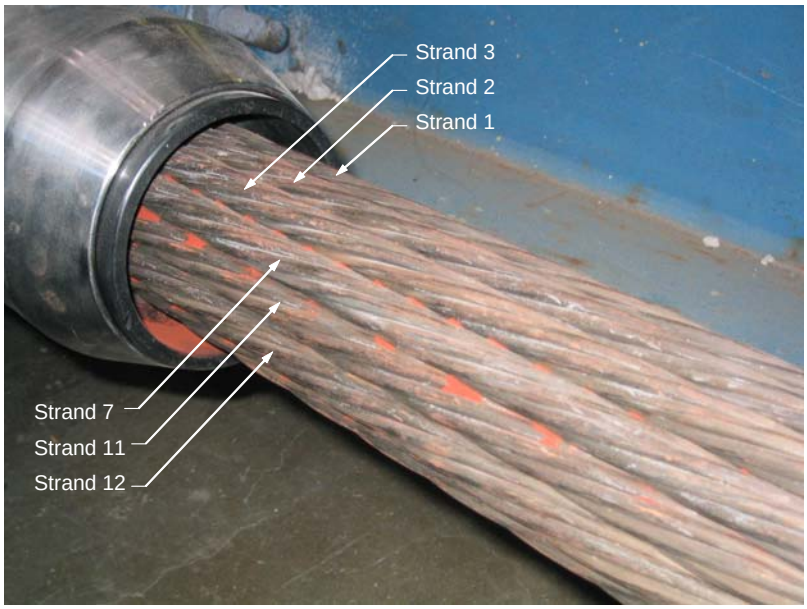

Figure D.91 Evidence of Fretting Fatigue at Deck Tension Ring – Specimen 8

Figure D.92 Reduction of Cross-Sectional Area of Strands Due to Fretting – Specimen 8

Extensive corrosion was also observed at the interface between the strand and the silicone caulk used in the PVC end caps of the grouted section (Figure D.93), although this corrosion did not appear to limit the performance of the test specimen.

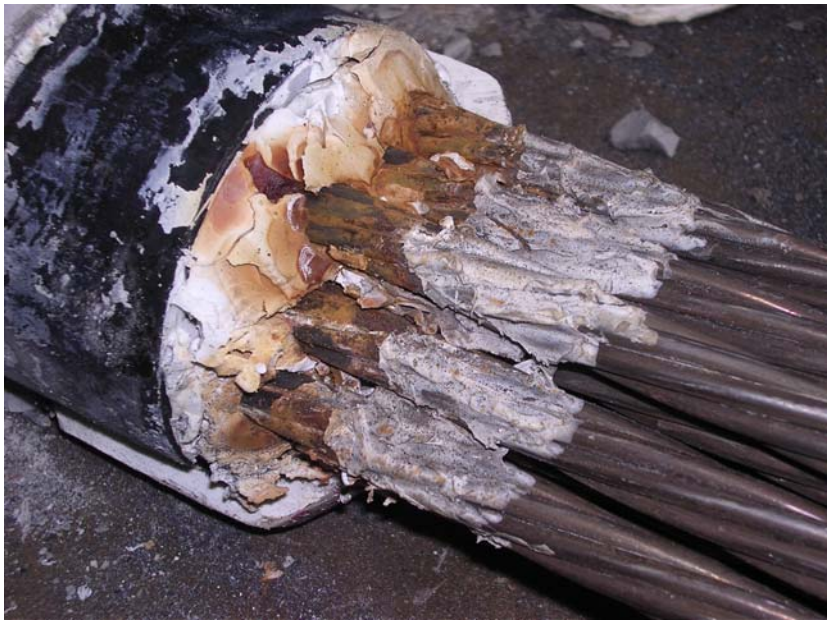

Figure D.93 Corrosion Product Observed at Interface between Caulk and Grout in Specimen 8

D.8.2 Wire Breaks

Four wire breaks were identified during the autopsy of Specimen 8. Two wire breaks occurred near the tower anchorage and two occurred near the deck anchorage. The two wire breaks near the tower end occurred in two strands (Figure D.94). Both wire breaks occurred at the contact point between the strand and the wedge (Figure D.95 and Figure D.96). Scraping was evident on the strand which is caused by the teeth as the strand is pulled through the wedge during stressing (Figure D.97).

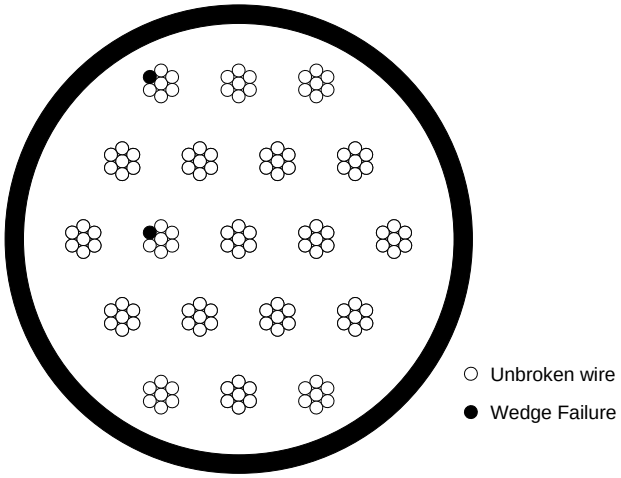

Figure D.94 Distribution of Wire Breaks near Tower End – Specimen 8

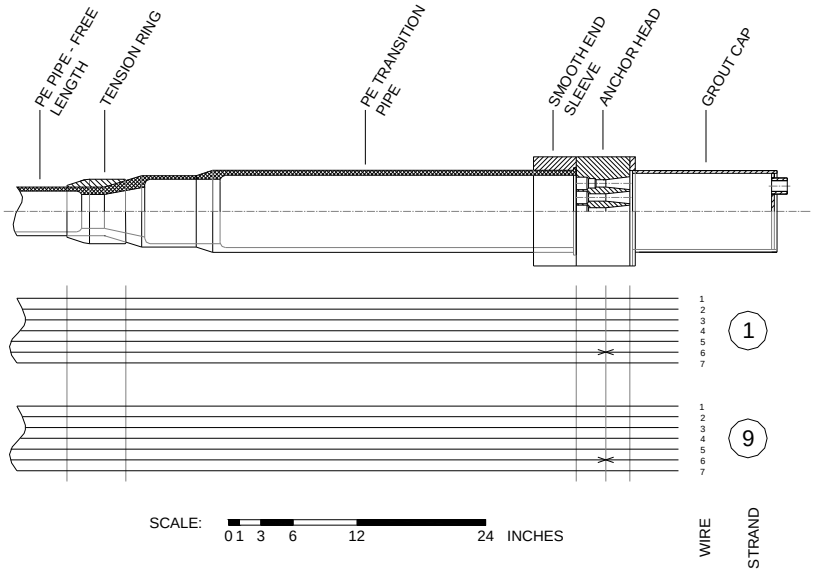

Figure D.95 Location of Wire Breaks near Tower End – Specimen 8

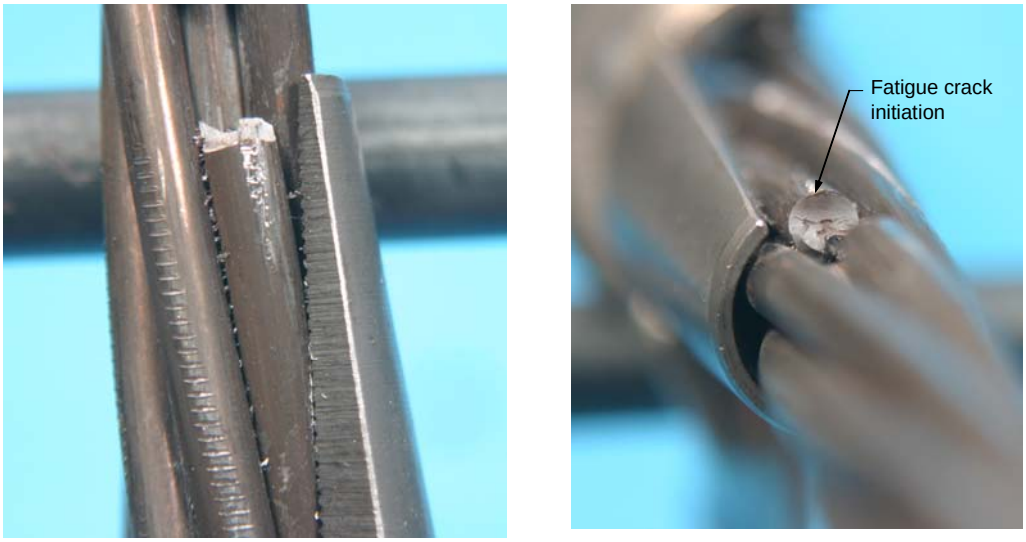

Figure D.96 Wire Breaks in Strand 9 at Wedge near Tower End – Specimen 8

Figure D.97 Scraping of Strand Due to Stressing at Tower End – Specimen 8

At the deck end, the two wire breaks were distributed in two strands (Figure D.98). Both breaks occurred in the center layer of strands. Figure D.99 shows the longitudinal location of each wire break near the deck anchorage and photographs are shown in Figure D.100 and Figure D.101. The fracture in strand 9 initiated within the wedge, but was caused by fretting against an adjacent wire.

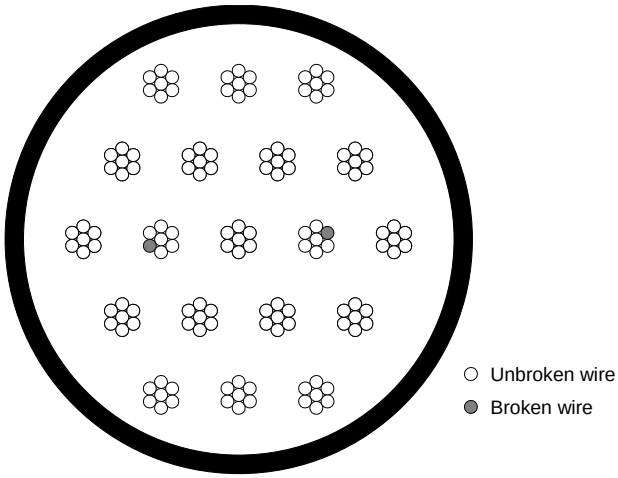

Figure D.98 Distribution of Wire Breaks near Deck End – Specimen 8

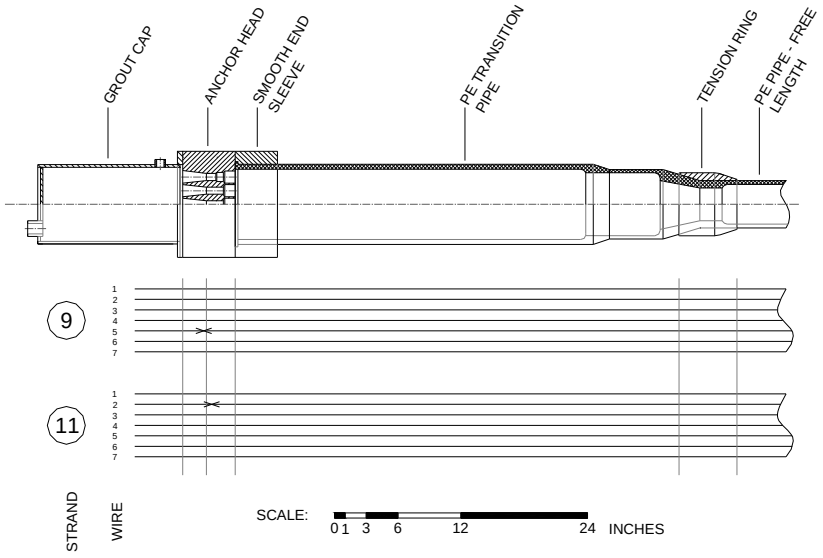

Figure D.99 Location of Wire Breaks near Deck End – Specimen 8

Figure D.100 Wire Break in Strand 9 at Deck End of Specimen 8

Figure D.101 Wire Break in Strand 11 at Deck End of Specimen 8

D.8.3 Acoustic Data

The acoustic sensors detected all four wire breaks during the fatigue test for Specimen 8 (Table D.15). The first wire break was detected after 300,000 fatigue cycles (Figure D.102).

Table D.15 Summary of Wire Breaks – Specimen 8

Method	**Number**	**Tower**	**Midspan**	**Deck**	**Total**
Observed during Autopsy	Total	2	—	2	4
	Unique Wires*	2	—	2	4
Acoustic Sensors	Total	2	—	2	4

* Multiple wire breaks in the same wire are not included in this category.

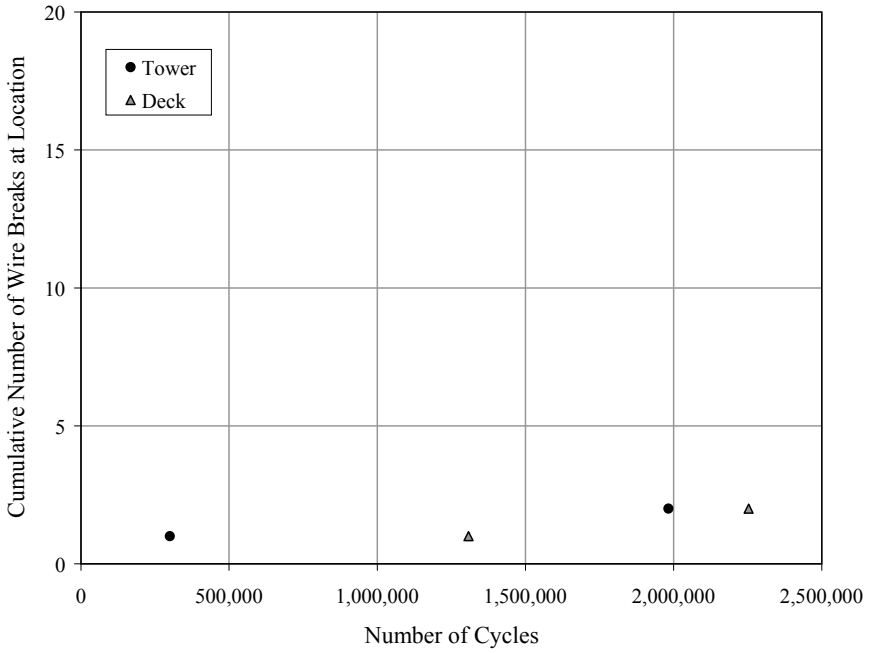

Figure D.102 Wire Breaks Detected from Acoustic Data – Specimen 9

D.8.4 Lateral Stiffness

The variation in the maximum and minimum applied forces needed to achieve the target displacement levels of ±1.6 in. are shown in Figure D.103. The vertical lines also indicate the approximate number of cycles corresponding to each wire break detected by the acoustic sensors. The final average dynamic stiffness was within 6% of the initial average dynamic stiffness (Table D.16).

The transverse stiffness was determined from the static tests by comparing the load and midspan deflection data (Figure D.104). The stiffness values determined from the static tests were slightly higher than those from the fatigue tests, but the percent change in stiffness was essentially the same.

Table D.16 Summary of Stiffness Changes during Fatigue Test – Specimen 8

	Static Stiffness	Average Dynamic Stiffness	Frequency
	(kip/in.)	(kip/in.)	(Hz)
Initial	4.17	4.11	13.9
Final	3.94	3.90	13.4
Final / Initial	0.944	0.948	0.964

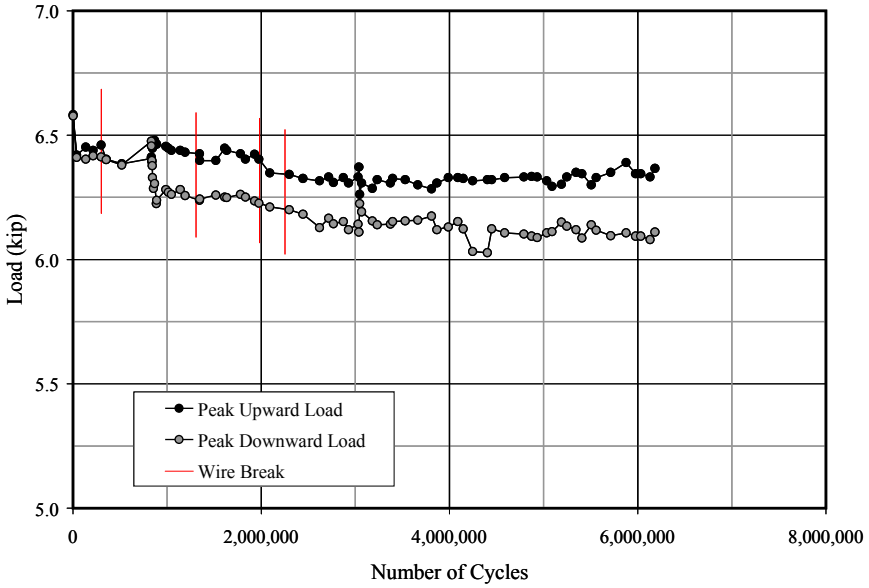

Figure D.103 Variation of Applied Loads during Fatigue Test – Specimen 8

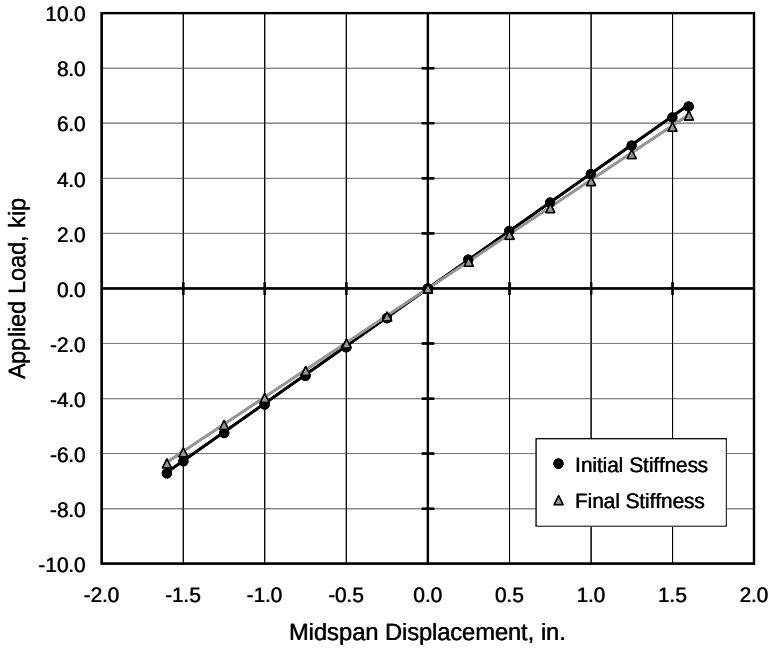

Figure D.104 Load - Displacement Response during Static Tests – Specimen 8

D.9 SPECIMEN 9

Specimen 9 sustained 2,566,126 loading cycles during the fatigue test. Seventy-six wire breaks were identified at the conclusion of the test: twelve breaks occurred at the tower end, sixty-one breaks occurred at the center of the specimen under the load point, and three occurred at the deck end. The specimen was nominally identical to Specimen 7, except an intentional grout void was created and repaired at the tower end (Section B.4.5). Specimen 9 was stressed from the tower end and grouted from the deck end. The specimen was tested under displacement control, with an amplitude of ±1.6 in. at midspan.

D.9.1 Observed Condition of Grout and Strand

An intentional grout void was created at the tower end during the initial grouting of Specimen 9. This void was filled with SikaGrout 300 PT one week later to investigate the effects of filling a grout void, which had been identified by TxDOT personnel on the Fred Hartman Bridge. The SikaGrout, identified by its darker color, formed a lens on the surface of the original grout approximately 11 in. long starting 4 in. from the anchor head (Figure D.105) and ending at the ring formed by the weld in the polyethylene transition pipe. This lens ranged from 1/16 in. thick near the anchor head to 1/32 in. thick at the far end of the lens.

Apart from the grout lens, no evidence of the grout used to repair the void was found on the exterior of the cable at the face of the anchor head. However, the repair grout was found around the grout inlet holes in the anchor heads under the surface of the original grout (Figure D.106). No strands intersected the grout void, thus no strand had contact with the repair grout.

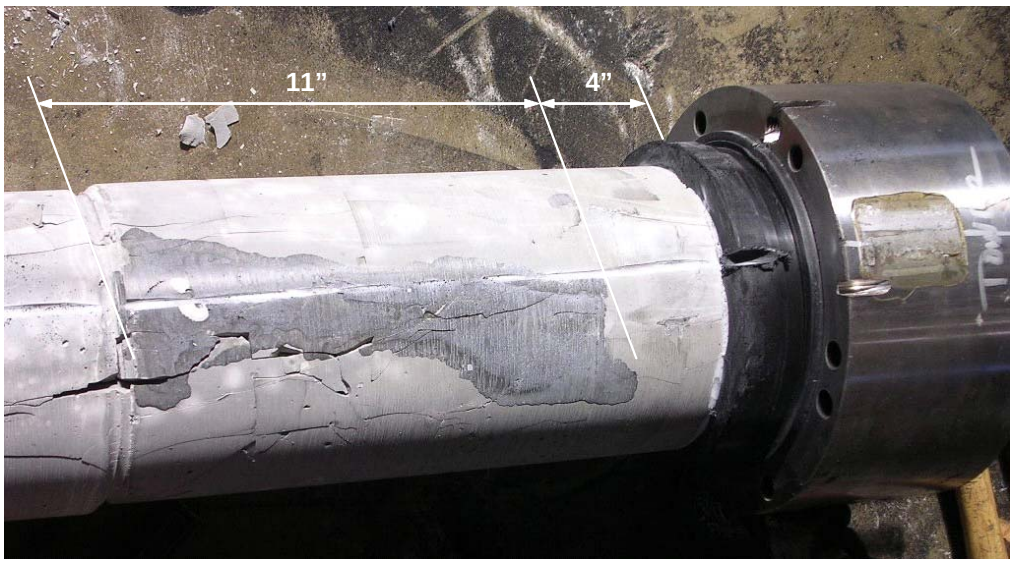

Figure D.105 Intentional Grout Lens at Tower End – Specimen 9

Figure D.106 Interface between Grout Used to Construct Specimen 9 and Grout Used to Repair Intentional Void at Tower End

The grout at the deck end of the stay was homogeneous and relatively uncracked, consistent with finding no wire breaks outside the anchor head. The grout in the center section, under the load point, was heavily damaged (Figure D.107).

Figure D.107 Condition of Grout under Load Point – Specimen 9

Near the anchorages, corrosion was generally mild and found only near wire breaks. Several spots of heavy corrosion that were unaccompanied by wire breaks were found near the tower anchorage as seen in Figure D.108. These areas were all located under the intentional grout void.

Figure D.108 Corrosion on Surface of Strand near Tower End – Specimen 9

Extensive corrosion was observed in the region near the center of the stay. Heavy, red-orange corroded fretting product near wire breaks (Figure D.109) was accompanied by black and red pitting corrosion in several places. Several breaks appeared to initiate at these points of pitting corrosion. White powder and grout coated many of the strands and obscured some fracture surfaces in this region. The amount of fretting residue tended to be more severe when all (or nearly all) the wires of a strand had fractured, which may indicate that such corrosion forms after wire breaks occur.

D.9.2 Wire Breaks

Seventy-six wire breaks were identified during the autopsy of Specimen 9. Twelve wire breaks occurred near the tower anchorage, sixty-one occurred near the loading point, and three occurred near the deck anchorage.

Figure D.109 Corrosion on Surface of Strand near Midspan – Specimen 9

The twelve wire breaks near the tower end were distributed among five strands, which were distributed along the extreme fibers of the cross section (Figure D.110). Figure D.111 shows the location of each wire break near the tower anchorage. Three wires broke inside the anchor head at the contact point between the wedge and the strand. Two wire breaks in strand 1 occurred 15 in. from the anchor head at the location of a weld in the polyethylene transition pipe.

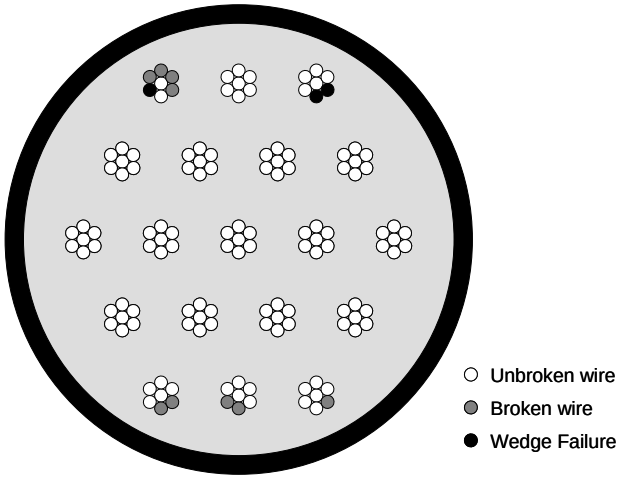

Figure D.110 Distribution of Wire Breaks near Tower End – Specimen 9

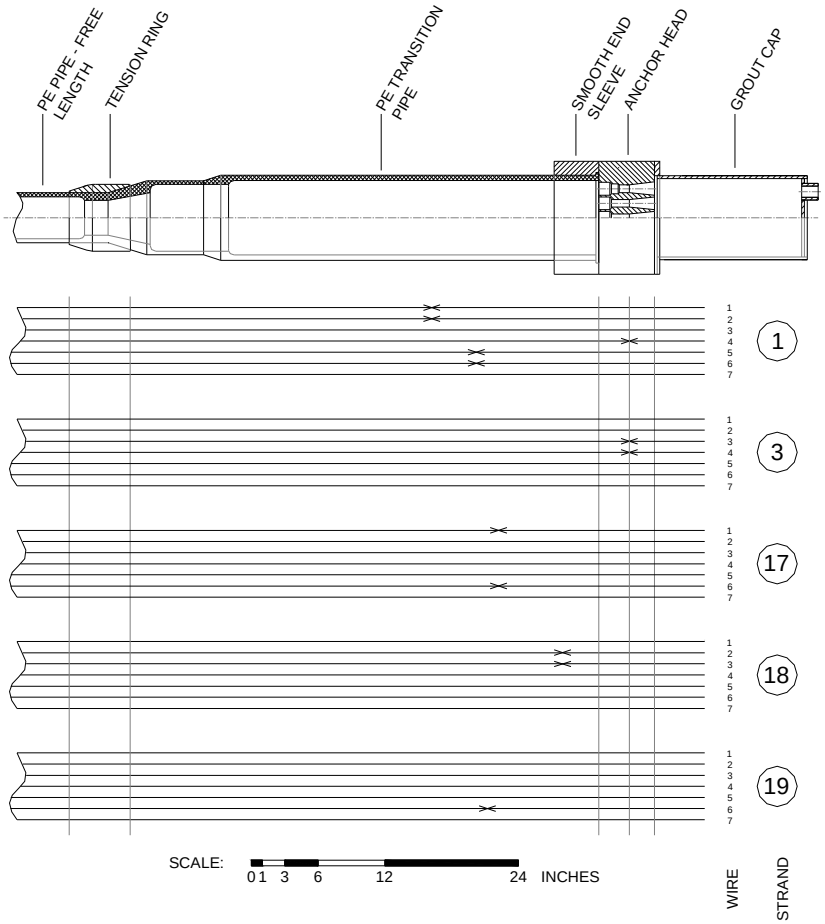

Figure D.111 Location of Wire Breaks near Tower End – Specimen 9

The distribution of wire breaks in Specimen 9 should be compared with those in Specimen 1, which was constructed with an unintentional grout void (Figure D.3). The grout void in Specimen 1 was not repaired and it was approximately four times larger than the void created in Specimen 9. Nearly half of the wire breaks at the tower end of Specimen 1 (Figure D.10 and Figure D.11) occurred in strands that were exposed in the grout void. Although no strands were in exposed in the grout void in Specimen 9, the four wire breaks in the top layer of strands that were not caused by the wedges, were considerably further from the inside face of the anchor head than was common in the other grouted test specimens.

Figure D.112 shows the distribution of wire breaks at midspan. The sixty-one breaks occurred in twelve strands. Specimen 9 was the only stay to experience wire breaks within the middle layer of strands under the load point. Figure D.113 and Figure D.114 show the location of each wire break relative to the load point.

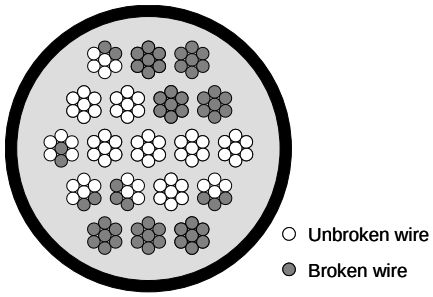

Figure D.112 Distribution of Wire Breaks near Midspan – Specimen 9

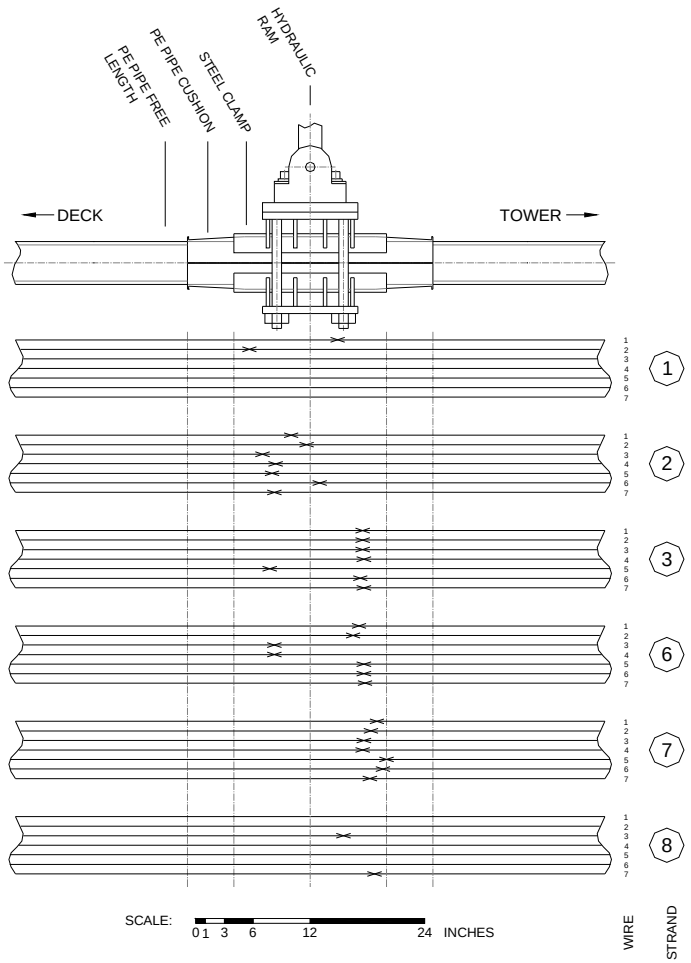

Figure D.113 Location of Wire Breaks near Midspan – Specimen 9 (Part 1)

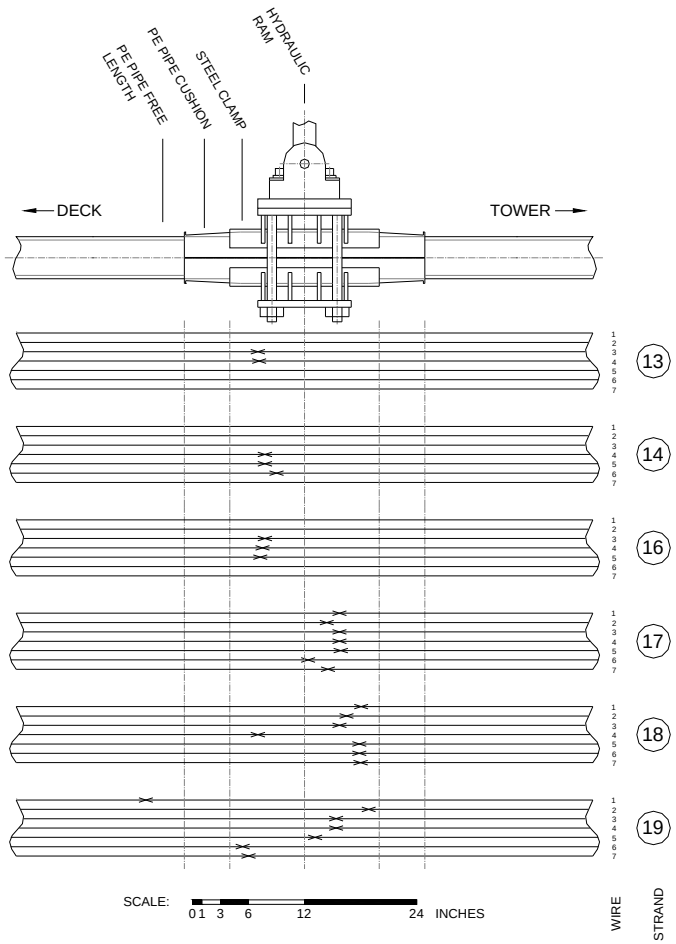

Figure D.114 Location of Wire Breaks near Midspan – Specimen 9 (Part 2)

The three wire breaks at the deck end were concentrated in a single strand (Figure D.115). As shown in Figure D.116, all three breaks occurred within the anchor head. Two breaks were initiated by the first wedge tooth and one break occurred at the front of the polyethylene bushing at the face of the anchor head.

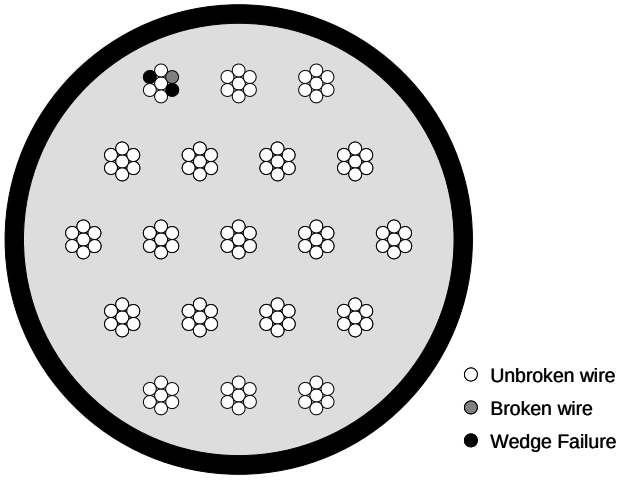

Figure D.115 Distribution of Wire Breaks near Deck End – Specimen 9

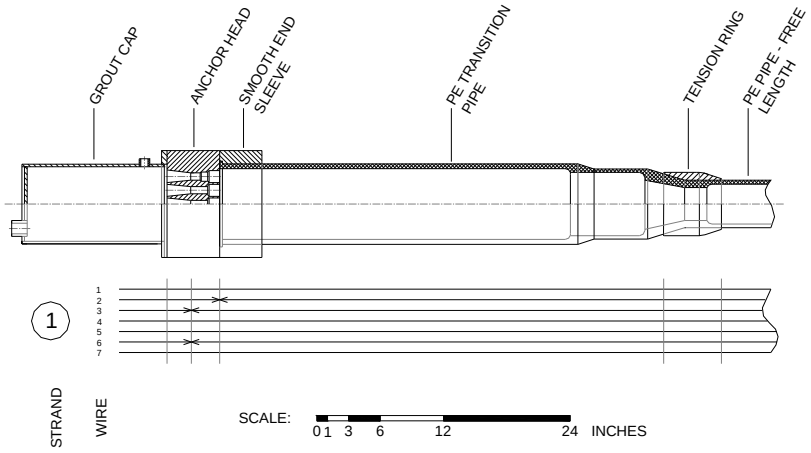

Figure D.116 Location of Wire Breaks near Deck End – Specimen 9

D.9.3 Acoustic Data

The acoustic sensors detected seventy-seven wire breaks during the fatigue test for Specimen 9 (Table D.17). The number of wire breaks detected at midspan was one larger than identified during the autopsy of the specimen. The first wire break was detected after 390,000 fatigue cycles (Figure D.117).

Table D.17 Summary of Wire Breaks – Specimen 9

Method	**Number**	**Tower**	**Midspan**	**Deck**	**Total**
Observed during Autopsy	Total	12	61	3	76
	Unique Wires*	12	61	3	76
Acoustic Sensors	Total	12	62	3	77

* Multiple wire breaks in the same wire are not included in this category.

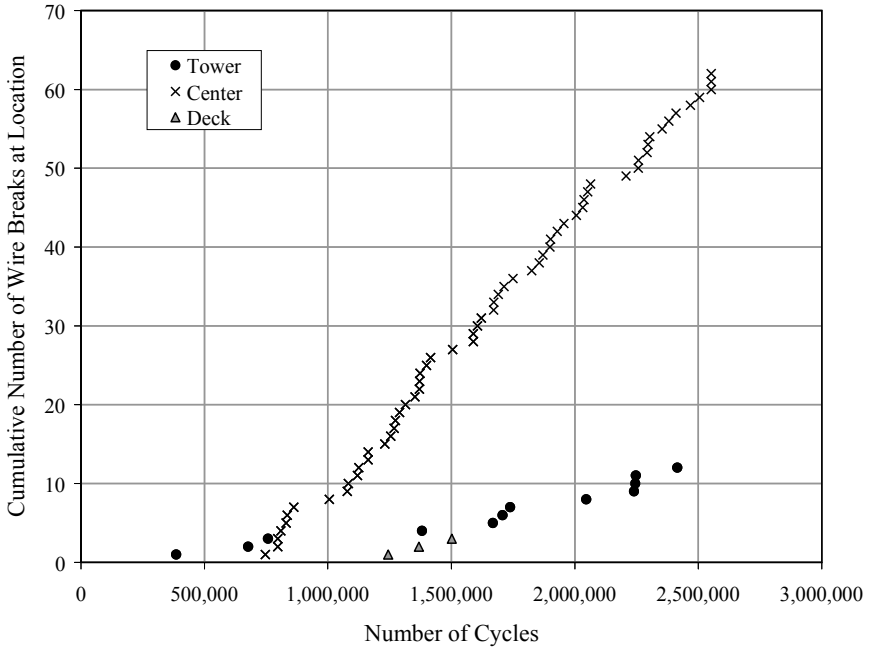

Figure D.117 Wire Breaks Detected from Acoustic Data – Specimen 9

D.9.4 Lateral Stiffness

The variation in the maximum and minimum applied forces needed to achieve the target displacement levels of ±1.6 in. are shown in Figure D.118. The vertical lines also indicate the approximate number of cycles corresponding to each wire break detected by the acoustic sensors. The final average dynamic stiffness was 75% of the initial average dynamic stiffness (Table D.18). Nearly forty wires fractured before the average dynamic stiffness decreased by more than 10%.

The transverse stiffness was determined from the static tests by comparing the load and midspan deflection data (Figure D.119). The last static test was conducted after 1,750,000 loading cycles. A static test was not conducted at the conclusion of the fatigue test for Specimen 9 due to a mechanical failure of the hydraulic actuator.

Table D.18 Summary of Stiffness Changes during Fatigue Test – Specimen 9

	Static Stiffness	Average Dynamic Stiffness	Frequency
	(kip/in.)	(kip/in.)	(Hz)
Initial	4.82	4.97	12.5
Final	4.22*	3.72	10.5
Final / Initial	0.875*	0.750	0.840

* Final static test was conducted after 1,748,000 cycles. Fatigue test was terminated after 2,634,309 cycles

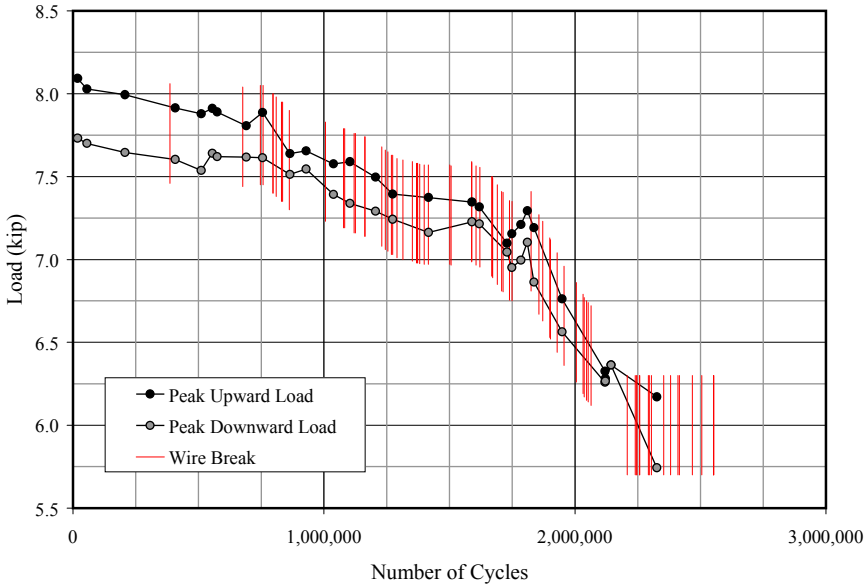

Figure D.118 Variation of Applied Loads during Fatigue Test – Specimen 9

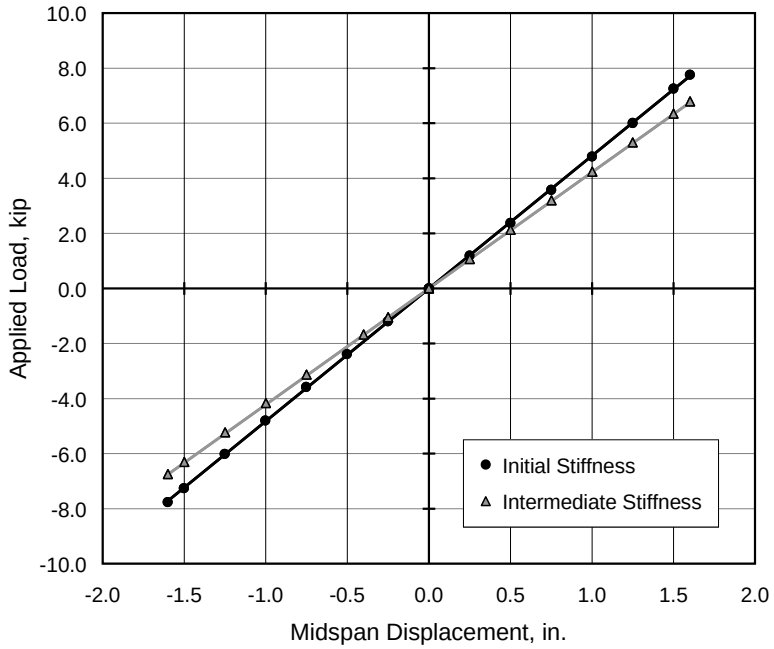

Figure D.119 Load - Displacement Response during Static Tests – Specimen 9

D.10 SPECIMEN 10

Specimen 10 sustained 5,614,211 loading cycles during the fatigue test. Fifty-two wire breaks were identified at the conclusion of the test: twenty-three breaks occurred at the tower end, twenty-one breaks occurred at the center of the specimen under the load point, and eight occurred at the deck end. Specimen 10 was stressed from the tower end and grouted from the deck end. The specimen was tested under displacement control. The amplitude of the midspan displacement was ±2.1 in. for the first 2,220 cycles and was reduced to ±1.1 in. for the remainder of the fatigue test. The maximum midspan displacement was decreased due to excessive lateral movement of the loading apparatus.

D.10.1 Observed Condition of Grout and Strand

Figure D.120 shows the condition of the grout at the tower end immediately after removing the PE transition pipe. Severe longitudinal cracks were observed, which indicate wire breaks in the region. Apart from the cracking, no other visual imperfections in the grout were observed. Figure D.121 shows the condition of the grout under the load point. The grout in this region was also severely cracked. Figure D.122 shows the condition of the grout at the deck end. Large longitudinal cracks were observed, despite the fact that no wire breaks were found outside of the anchor head. This level of cracking was not expected, and may be due to the large-amplitude cycles at the beginning of the fatigue test.

Figure D.120 Condition of Grout at Tower End Immediately after Removing PE Pipe – Specimen 10

Figure D.121 Condition of Grout at Midspan Immediately after Removing PE Pipe – Specimen 10

Figure D.122 Condition of Grout at Deck End Immediately after Removing PE Pipe – Specimen 10

Corroded fretting residue was found near the wire breaks at the tower end (Figure D.123) and under the load point (Figure D.124). The amount of fretting residue observed was less than that observed in Specimens 7 and 9. Traces of corroded residue were found in the grout at the tower end.

Figure D.123 Corroded Fretting Product near Tower End – Specimen 10

Figure D.124 Corroded Fretting Product near Midspan – Specimen 10

D.10.2 Wire Breaks

Fifty-two wire breaks were identified during the autopsy of Specimen 10. Twenty-three wire breaks occurred near the tower anchorage, twenty-one occurred near the loading point, and eight occurred near the deck anchorage.

The twenty-three wire breaks near the tower end were distributed among four strands (Figure D.125). Most of the breaks at the tower end occurred on the bottom layer of strands. In addition to the twenty-three wire breaks, a fatigue crack was found 3¾ in. from the inside face of the anchor head on wire 4 of strand 18. The wire was not fractured at this point because the wire had fractured 4¾ in. away and there was not enough tension in the wire to cause the second crack to fracture before the fatigue test was stopped. Figure D.126 shows the longitudinal location of each wire break relative to the tower anchorage.

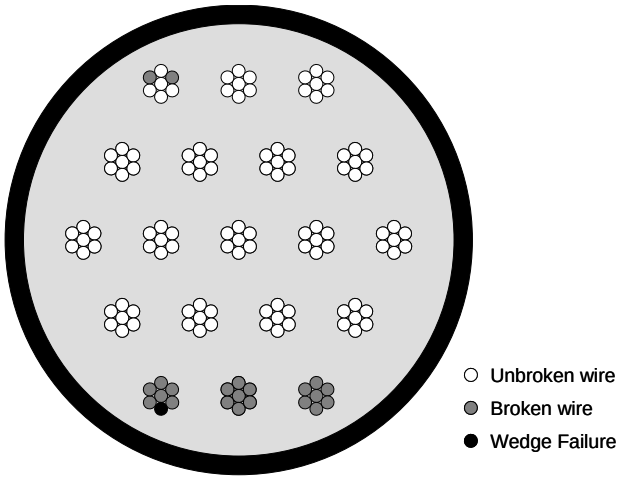

Figure D.125 Distribution of Wire Breaks near Tower End – Specimen 10

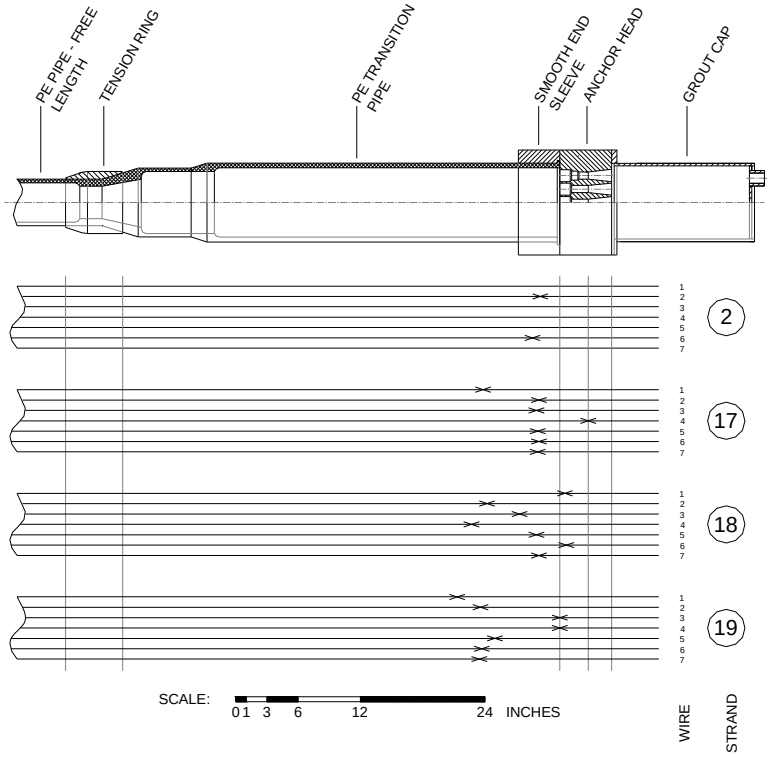

Figure D.126 Location of Wire Breaks near Tower End – Specimen 10

Figure D.127 shows the distribution of wire breaks near midspan. The twenty-one breaks occurred in four strands. Figure D.128 shows the location of each wire break relative to the load point. The breaks all occurred within the clamp region, and tended to occur between the edge of the load plate and the end of the steel clamp.

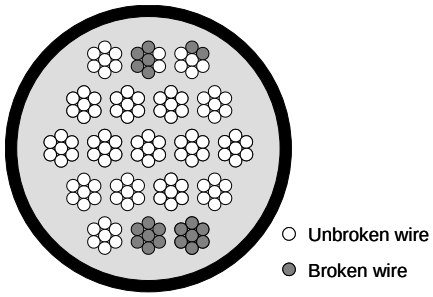

Figure D.127 Distribution of Wire Breaks near Midspan – Specimen 10

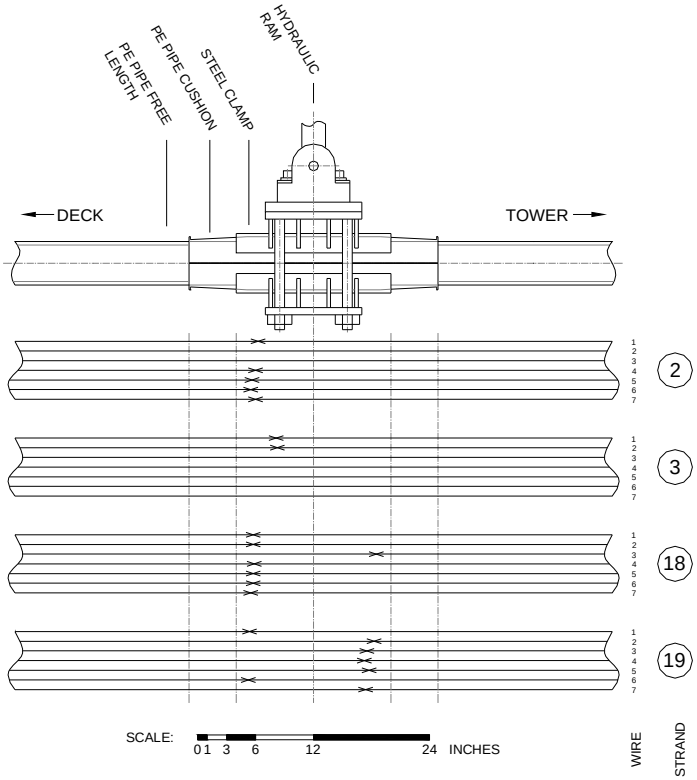

Figure D.128 Location of Wire Breaks near Midspan – Specimen 10

The eight wire breaks at the deck end were distributed in two strands (Figure D.129). All wire breaks occurred within the anchor head, but no wires fractured at the wedges (Figure D.130).

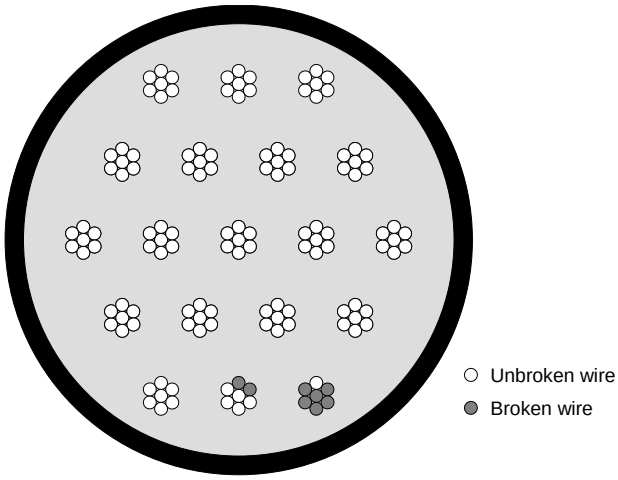

Figure D.129 Distribution of Wire Breaks near Deck End – Specimen 10

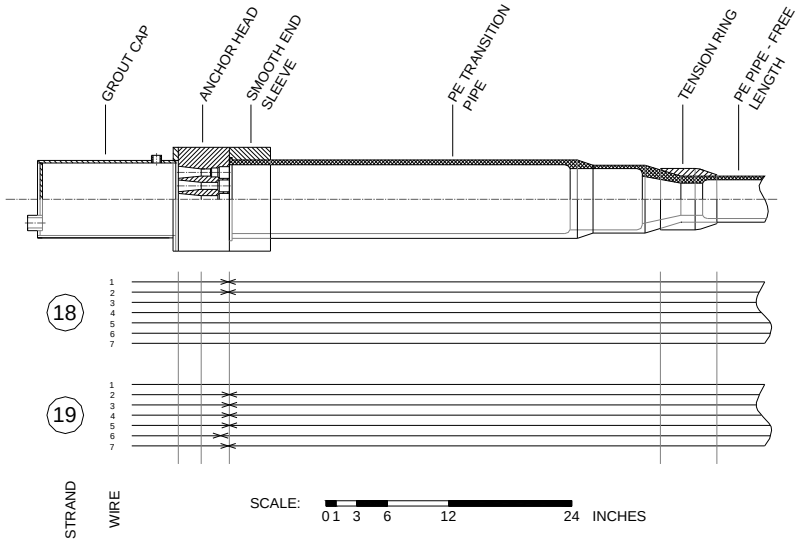

Figure D.130 Location of Wire Breaks near Deck End – Specimen 10

D.10.3 Acoustic Data

The acoustic sensors detected all fifty-two wire breaks during the fatigue test for Specimen 10 (Table D.19); however, the distribution along the specimen was slightly different from that observed during the autopsy. The number of wire break detected at midspan was one less than observed, and the number detected at the deck end was one greater than observed. The first wire break was detected after 930,000 fatigue cycles (Figure D.131).

Table D.19 Summary of Wire Breaks – Specimen 10

Method	Number	Tower	Midspan	Deck	Total
Observed during Autopsy	Total	23	21	8	52
	Unique Wires*	23	21	8	52
Acoustic Sensors	Total	23	20	9	52

* Multiple wire breaks in the same wire are not included in this category.

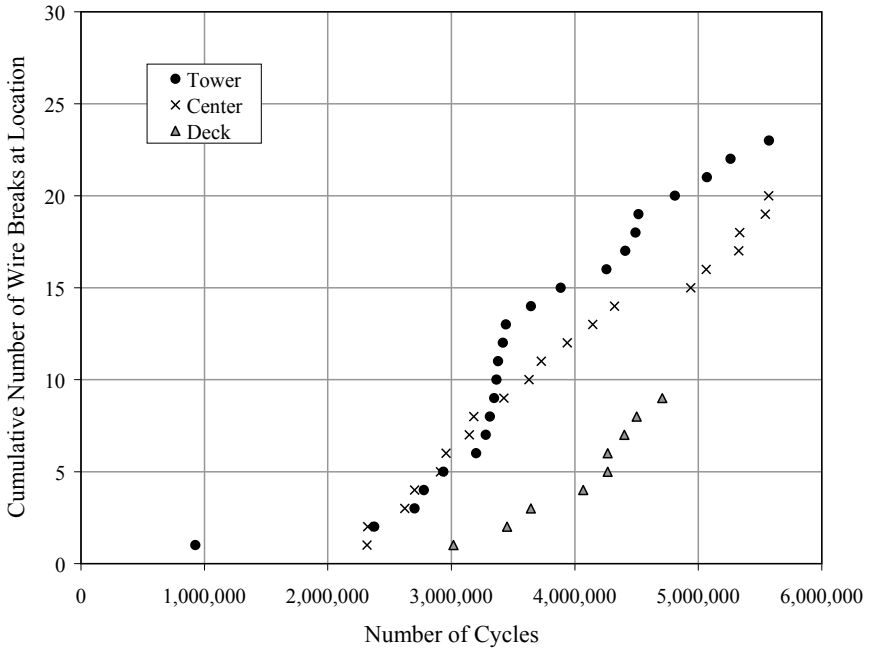

Figure D.131 Wire Breaks Detected from Acoustic Data – Specimen 10

D.10.4 Lateral Stiffness

The variation in the maximum and minimum applied forces needed to achieve the target displacement levels of ±1.1 in. are shown in Figure D.132. The vertical lines also indicate the approximate number of cycles corresponding to each wire break detected by the acoustic sensors. The final average dynamic stiffness was less than 85% of the initial average dynamic stiffness (Table D.20). Approximately twenty-five wires fractured before the average dynamic stiffness decreased by more than 10%.

The transverse stiffness was determined from the static tests by comparing the load and midspan deflection data (Figure D.133). The static stiffness values were slightly higher than the average dynamic stiffness values; however, the percent change during the fatigue test was nearly the same.

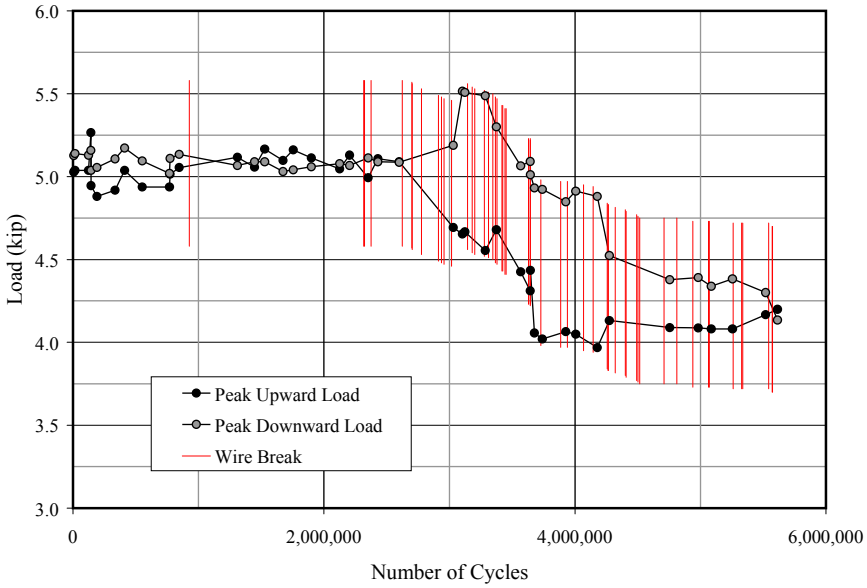

Figure D.132 Variation of Applied Loads during Fatigue Test – Specimen 10

Table D.20 Summary of Stiffness Changes during Fatigue Test – Specimen 10

	Static Stiffness	Average Dynamic Stiffness	Frequency
	(kip/in.)	(kip/in.)	(Hz)
Initial	4.79	4.62	13.0
Final	4.03	3.79	11.8
Final / Initial	0.840	0.821	0.908

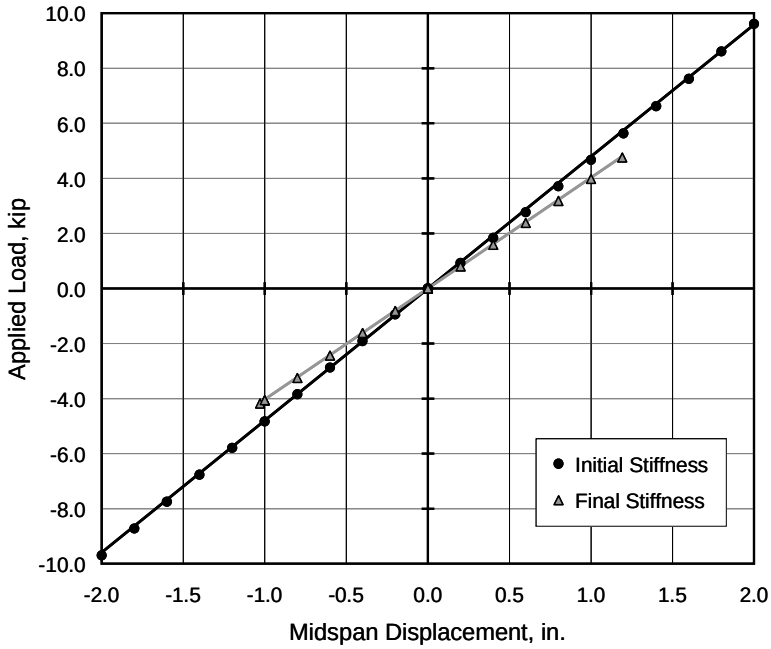

Figure D.133 Load - Displacement Response during Static Tests – Specimen 10

D.11 SPECIMEN 11

Specimen 11 sustained 4,640,450 loading cycles during the fatigue test. Sixteen wire breaks were identified at the conclusion of the test: nine occurred at the center of the specimen under the load point and seven occurred at the deck end. Specimen 11 was a hybrid specimen: both ends and the center were grouted, but the specimen was ungrouted along the free length. The specimen was stressed from the tower end. The specimen was tested under displacement control, with an amplitude of ±1.1 in. at midspan.

The test was terminated after a relatively small number of wire breaks. However, all the wires fractured in one of the strands at midspan. Because the specimen was not grouted along the free length, these broken strands pulled out of the center, grouted section and began to rub against the other strands in the specimen. This was not considered to be representative behavior, so the fatigue test was stopped.

D.11.1 Observed Condition of Grout and Strand

Distributed, small air voids were observed on the surface of the grout at the tower end of the specimen (Figure D.134). Minor longitudinal cracks were also observed. The surface of the grout exhibited similar small voids at the deck end of the specimen (Figure D.73); however, a significant longitudinal crack was present near the bottom of the cross section. At midspan, the grout appeared to be free of grout voids, but had extensive cracks in the longitudinal and circumferential directions (Figure D.75).

Like the grouted specimens, corrosion of the reinforcement was observed at the interface of the grout and the caulk (Figure D.137). Modest amounts of corroded fretting product were also observed near midspan (Figure D.138), but were not present near the deck end.

Figure D.134 Condition of Grout at Tower End – Specimen 11

Figure D.135 Condition of Grout near Deck End – Specimen 11

Figure D.136 Condition of Grout under Load Point – Specimen 11

Figure D.137 Corrosion at Interface between Grout and Caulk near Midspan – Specimen 11

Figure D.138 Corroded Fretting Product on Surface of Strand 18 at Midspan – Specimen 11

D.11.2 Wire Breaks

Sixteen wire breaks were identified during the autopsy of Specimen 11. Nine occurred near the loading point, and seven occurred near the deck anchorage. The nine wire breaks at midspan occurred in two strands (Figure D.139). Failure of all wires in strand 18 at midspan led to the termination of the fatigue test (Figure D.140).

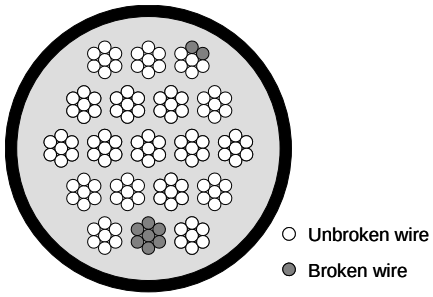

Figure D.139 Distribution of Wire Breaks near Midspan – Specimen 11

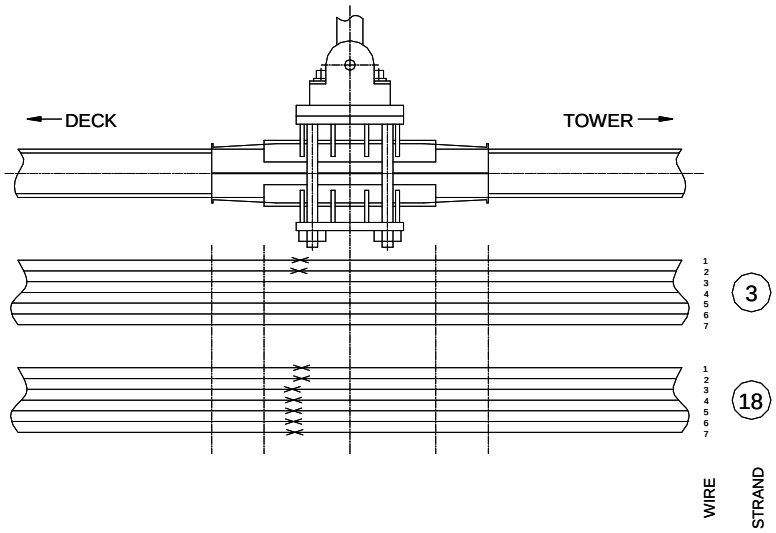

Figure D.140 Location of Wire Breaks near Midspan – Specimen 11

The seven wire breaks near the deck end were concentrated in strand 17 (Figure D.141). All wires fractured near the inside end of the smooth end sleeve (Figure D.142).

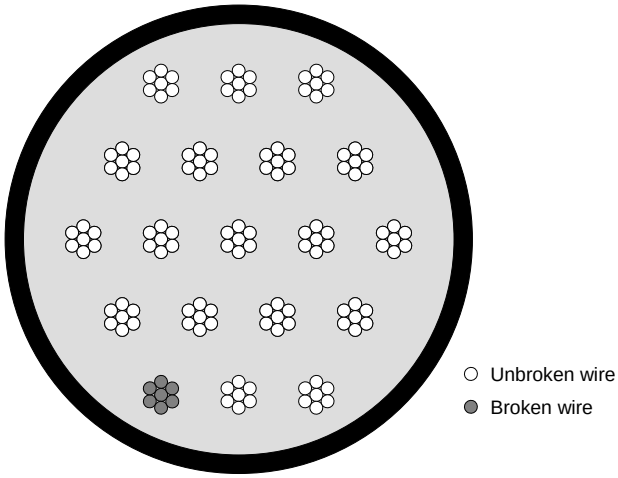

Figure D.141 Distribution of Wire Breaks near Deck End – Specimen 11

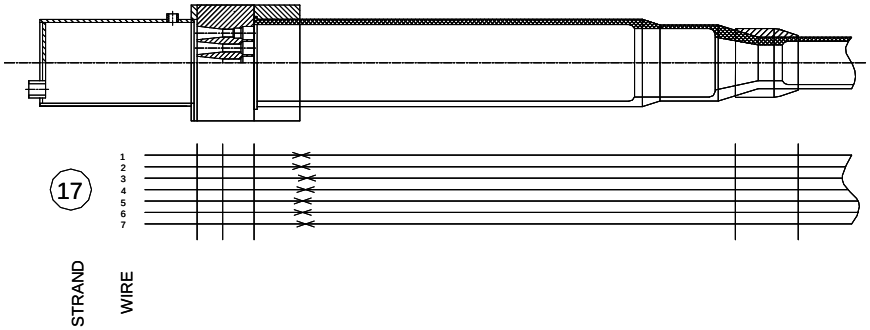

Figure D.142 Location of Wire Breaks near Deck End – Specimen 11

D.11.3 Acoustic Data

The acoustic sensors detected fifteen of the sixteen wire breaks that occurred during the fatigue test for Specimen 11 (Table D.21). The number of wire breaks detected at midspan was one less than observed. The first wire break was detected after 2,590,000 fatigue cycles (Figure D.143).

Table D.21 Summary of Wire Breaks – Specimen 11

Method	Number	Tower	Midspan	Deck	Total
Observed during Autopsy	Total	—	9	7	16
	Unique Wires*	—	9	7	16
Acoustic Sensors	Total	—	8	7	15

* Multiple wire breaks in the same wire are not included in this category.

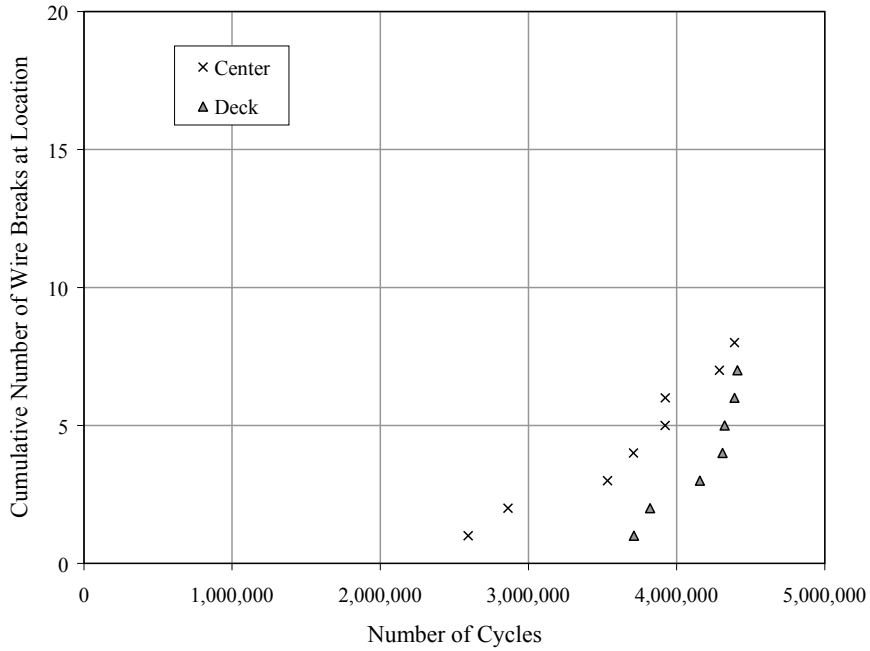

Figure D.143 Wire Breaks Detected from Acoustic Data – Specimen 11

D.11.4 Lateral Stiffness

The variation in the maximum and minimum applied forces needed to achieve the target displacement levels of ±1.1 in. are shown in Figure D.144. The vertical lines also indicate the approximate number of cycles corresponding to each wire break detected by the acoustic sensors. The final average dynamic stiffness was approximately 90% of the initial average dynamic stiffness (Table D.22).

The transverse stiffness was determined from the static tests by comparing the load and midspan deflection data (Figure D.145). The static stiffness values were slightly higher than the average dynamic stiffness values; however, the percent change during the fatigue test was nearly the same.

Table D.22 Summary of Stiffness Changes during Fatigue Test – Specimen 11

	Static Stiffness	Average Dynamic Stiffness	Frequency
	(kip/in.)	(kip/in.)	(Hz)
Initial	4.72	4.55	15.0
Final	4.21	4.11	13.3
Final / Initial	0.891	0.904	0.887

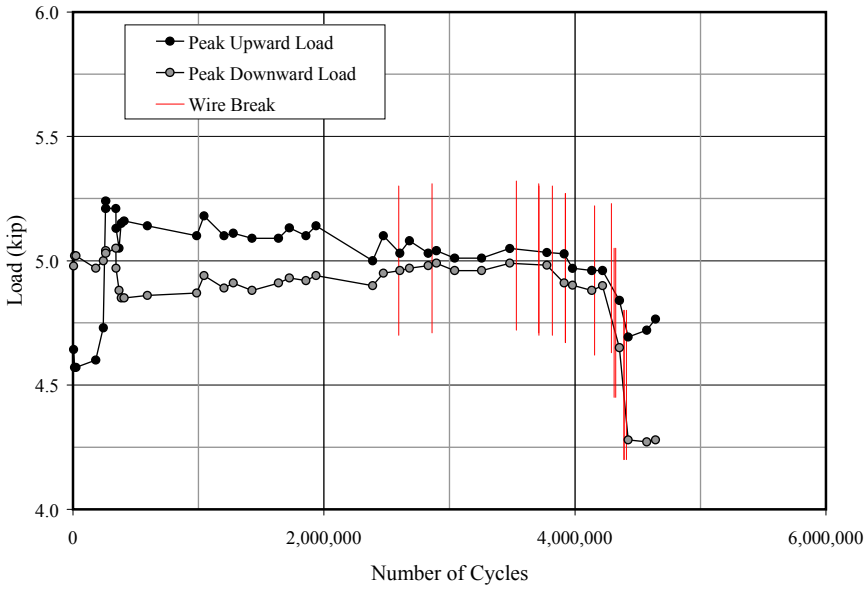

Figure D.144 Variation of Applied Loads during Fatigue Test – Specimen 11

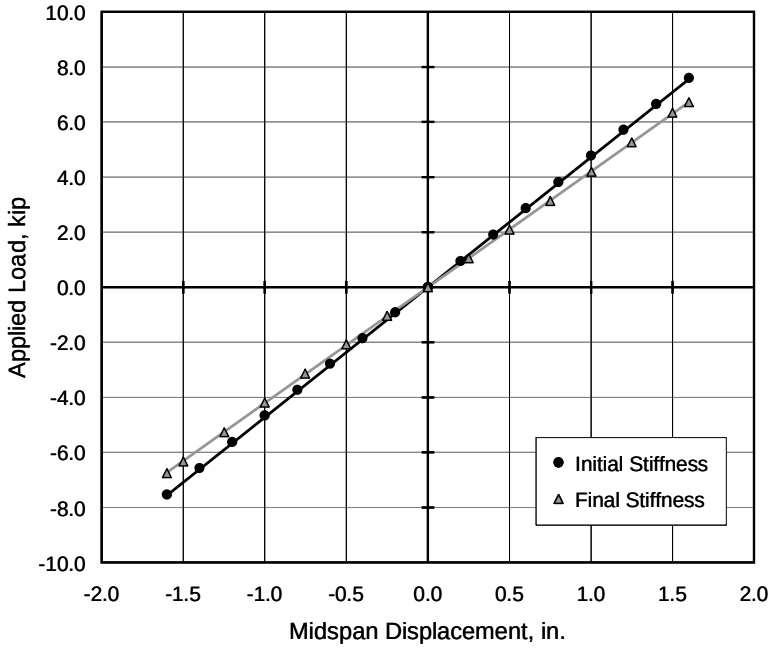

Figure D.145 Load - Displacement Response during Static Tests – Specimen 11

D.12 SPECIMEN 12

Specimen 12 sustained 2,703,958 loading cycles during the fatigue test. One hundred fifty wire breaks were identified at the conclusion of the test: thirty-five occurred at the tower end, eighty-six occurred at the center of the specimen under the load point, and twenty-nine occurred at the deck end. Specimen 12 was stressed from the tower end and grouted from the deck end. The specimen was tested under displacement control, with an amplitude of ±1.6 in. at midspan.

D.12.1 Observed Condition of Grout and Strand

Due to the large number of wire breaks, the grout was severely cracked at the conclusion of the fatigue test. Photographs of the condition of the grout at midspan and the deck end are shown in Figure D.146 and Figure D.147, respectively.

Figure D.146 Condition of Grout near Midspan – Specimen 12

Figure D.147 Condition of Grout near Deck End – Specimen 12

Large amounts of corroded fretting product were observed in the vicinity of the wire breaks near midspan (Figure D.148). The white corrosion product observed in Specimens 6 and 7 was also present on the surface of the strand. Extensive corrosion was also observed on the surface of the strand near both anchor heads (Figure D.149 and Figure D.150). Near the ends of the specimen, the corrosion was not limited to the immediate vicinity of the wire breaks. Evidence of black corrosion was observed in a few locations (Figure D.151), and all the wedges removed from the anchor heads exhibited corrosion on the surface (Figure D.152).

Figure D.148 Corroded Fretting Product on Surface of Strand at Midspan – Specimen 12

Figure D.149 Corrosion on Surface of Strand near Tower End – Specimen 12

Figure D.150 Corrosion on Surface of Strand near Deck End – Specimen 12

Figure D.151 Black Corrosion on Surface of Strand near Tower End – Specimen 12

Figure D.152 Corrosion of Wedges at Tower End – Specimen 12

D.12.2 Wire Breaks

One hundred fifty wire breaks were identified during the autopsy of Specimen 12. Thirty-five occurred near the tower anchorage, eighty-six occurred near the loading point, and twenty-nine occurred near the deck anchorage.

The thirty-five wire breaks at the tower end were distributed among six strands, and all breaks occurred in the top and bottom layers of strand (Figure D.153). Two wires in the bottom layer of strand experienced two wire breaks. Most of the wire breaks were within 12 in. of the inside face of the anchor head (Figure D.154); however, wire 2 in strand 19 fractured more than 15 in. from the face of the anchor head.

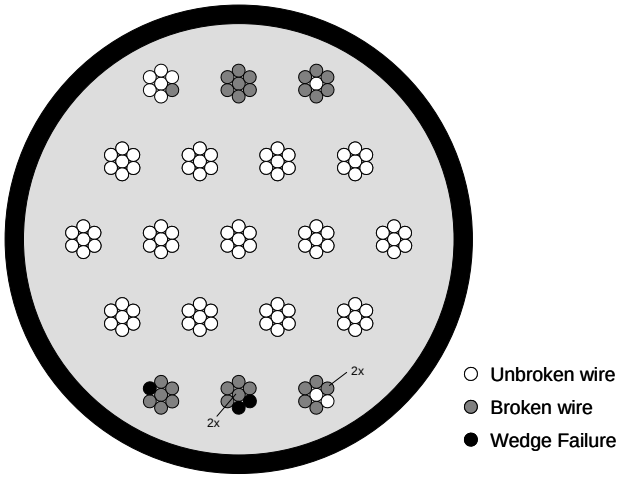

Figure D.153 Distribution of Wire Breaks near Tower End – Specimen 12

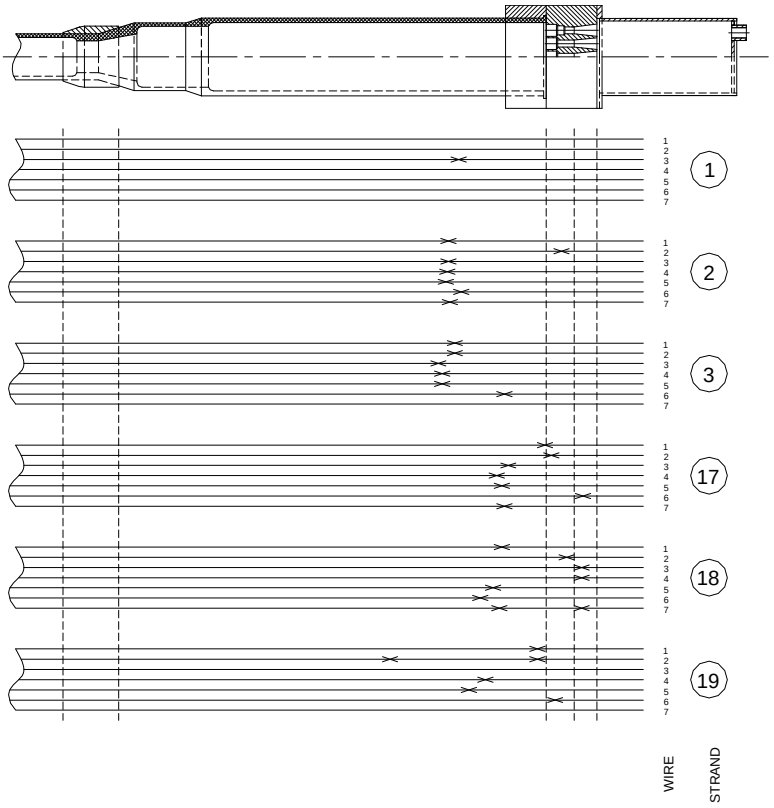

Figure D.154 Location of Wire Breaks near Tower End – Specimen 12

At midspan, the eighty-six wire breaks were distributed among fourteen strands (Figure D.155). Three wires experienced two wire breaks. Only the five strands in the middle row survived the fatigue test without a wire break. All wire breaks occurred within ±8 in. of the centerline of the hydraulic actuator (Figure D.156 and Figure D.157).

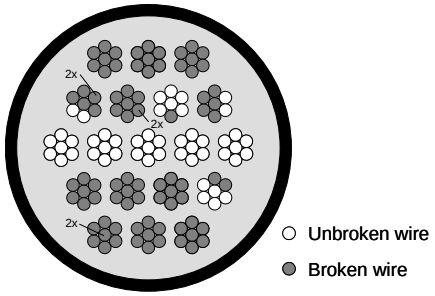

Figure D.155 Distribution of Wire Breaks near Midspan – Specimen 12

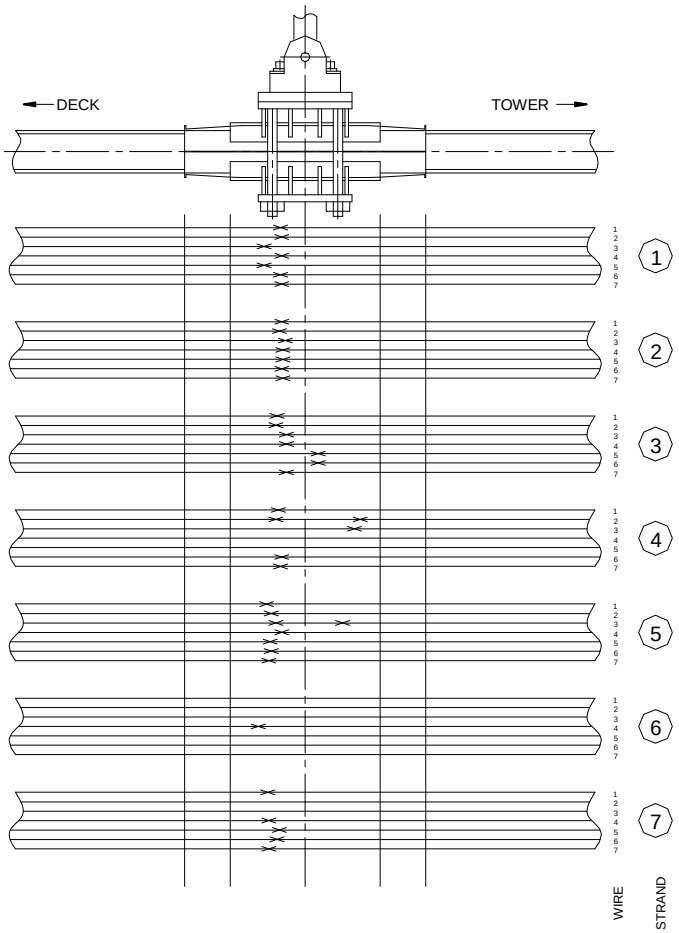

Figure D.156 Location of Wire Breaks near Midspan – Specimen 12 (Part 1)

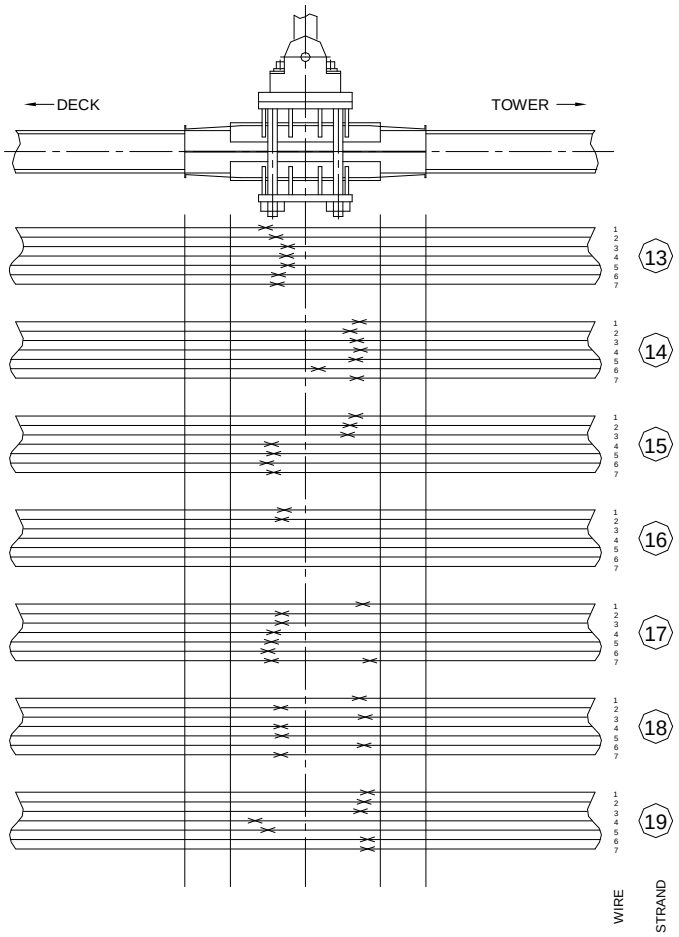

Figure D.157 Location of Wire Breaks near Midspan – Specimen 12 (Part 1)

The twenty-nine wire breaks near the deck end were distributed among eight strands (Figure D.158). The damage was concentrated near the top of the cross section. All wires fractured in the three strands along the top row and one wire experienced two wire breaks. All wires in strands 1 and 2 fractured within the anchor head (Figure D.159).

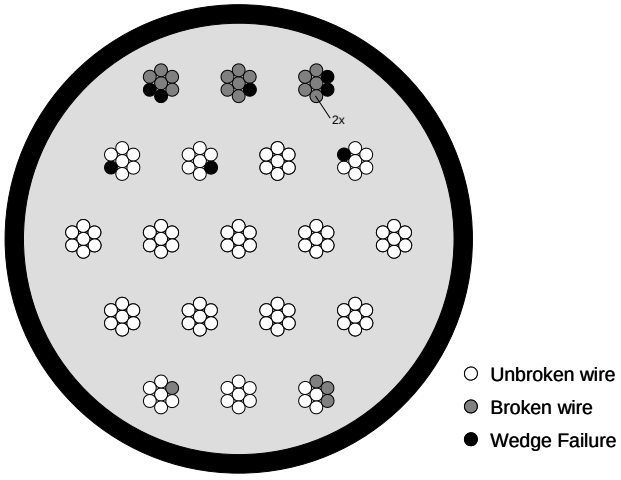

Figure D.158 Distribution of Wire Breaks near Deck End – Specimen 12

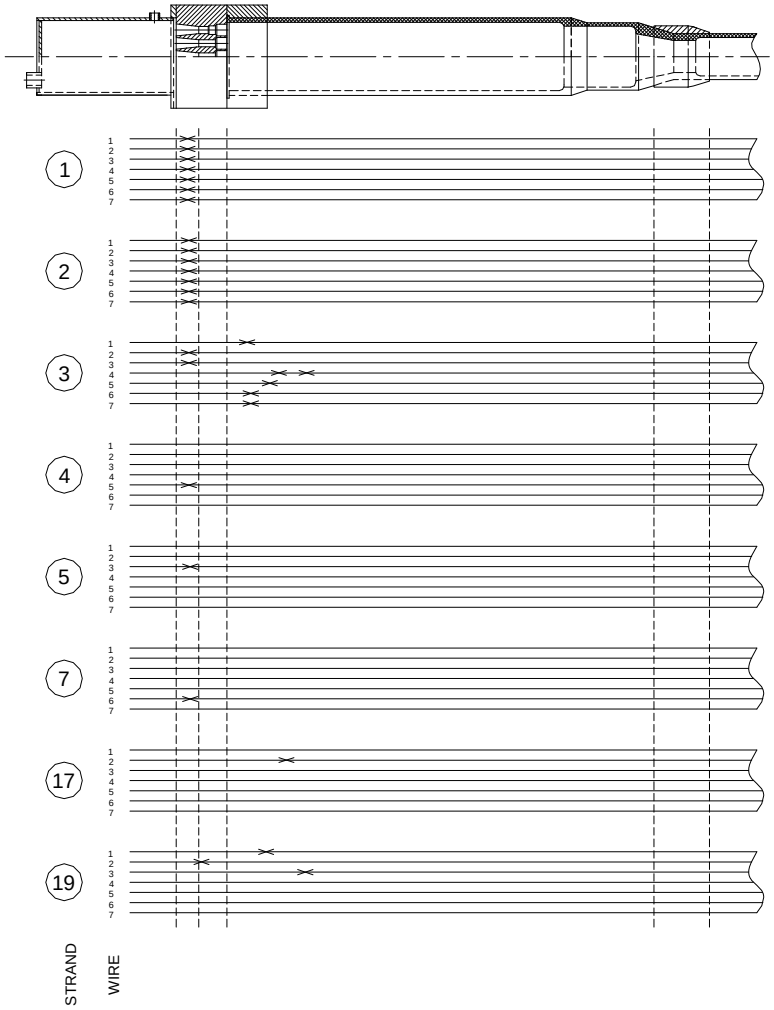

Figure D.159 Location of Wire Breaks near Deck End – Specimen 12

D.12.3 Acoustic Data

The acoustic sensors detected all but two of the one hundred fifty wire breaks that occurred during the fatigue test for Specimen 12 (Table D.23). The number of wire breaks detected was one greater than observed at the tower end, two fewer than observed at midspan, and one fewer than observed at the deck end. The first wire break was detected after 320,000 fatigue cycles (Figure D.160).

Table D.23 Summary of Wire Breaks – Specimen 12

Method	**Number**	**Tower**	**Midspan**	**Deck**	**Total**
Observed during Autopsy	Total	35	86	29	150
	Unique Wires*	33	83	28	144
Acoustic Sensors	Total	36	84	28	148

* Multiple wire breaks in the same wire are not included in this category.

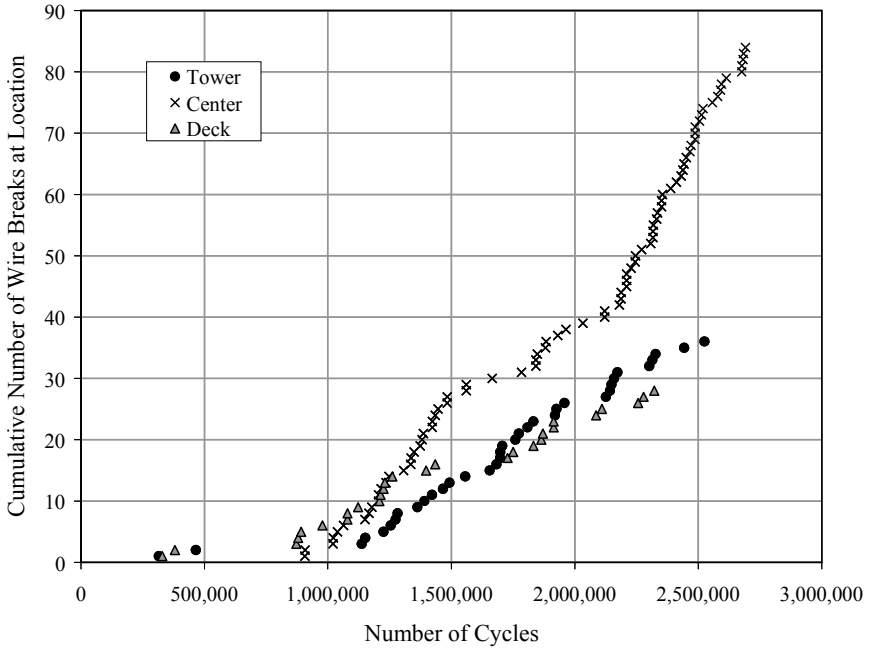

Figure D.160 Wire Breaks Detected from Acoustic Data – Specimen 12

D.12.4 Lateral Stiffness

The variation in the maximum and minimum applied forces needed to achieve the target displacement levels of ±1.6 in. are shown in Figure D.161. The vertical lines also indicate the approximate number of cycles corresponding to each wire break detected by the acoustic sensors. The final average dynamic stiffness was less than 60% of the initial average dynamic stiffness (Table D.24). More than 60 wire breaks were detected before the average dynamic stiffness decreased by more than 10%.

The transverse stiffness was determined from the static tests by comparing the load and midspan deflection data (Figure D.162). The percent changes in the static stiffness values and average dynamic stiffness values during the fatigue test were nearly the same.

Table D.24 Summary of Stiffness Changes during Fatigue Test – Specimen 12

	Static Stiffness	Average Dynamic Stiffness	Frequency
	(kip/in.)	(kip/in.)	(Hz)
Initial	4.79	4.75	13.1
Final	2.66	2.70	10.0
Final / Initial	0.555	0.568	0.763

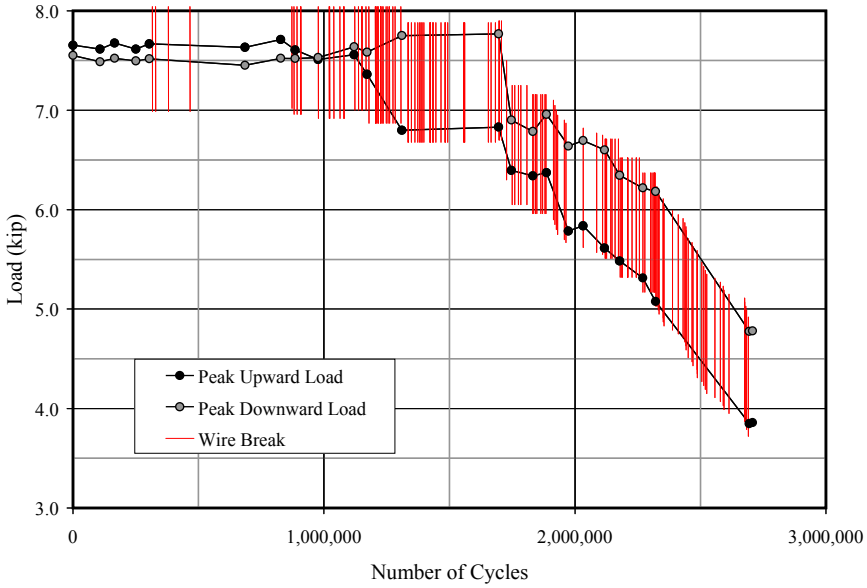

Figure D.161 Variation of Applied Loads during Fatigue Test – Specimen 12

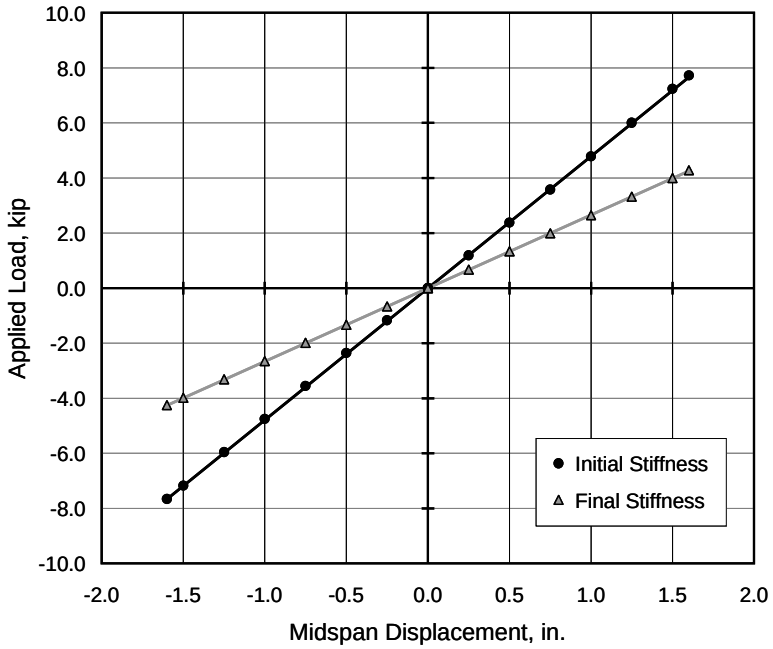

Figure D.162 Load - Displacement Response during Static Tests – Specimen 12

APPENDIX E: FATIGUE RESPONSE OF SMALL-DIAMETER SPECIMENS

The primary objective of the bending fatigue tests of the small-diameter specimens was to document changes in the transverse stiffness, frequency, and measured strains in the strand as damage accumulated. The results of the periodic measurements and the observed damage at the conclusion of the fatigue tests are documented in the following sections. Additional information, including the complete set of strain measurements, is available in Bean (2006) and Lee (2007).

E.1 SPECIMEN 1

Specimen 1 was subjected to 5 million loading cycles over a 61-day period. The fatigue test was terminated after all fourteen wires fractured at the north end of the specimen. Initially, the fatigue test was run under load control with the hydraulic actuator positioned at midspan (Figure C.7). However, only two wire breaks were detected after the first 40 days of the fatigue test. Therefore, the load frame was repositioned near the north quarter-point (Figure C.8), and the fatigue test was continued under displacement control.

The list of periodic measurements for Specimen 1 is given in Table E.1. The transverse stiffness was measured six times during the fatigue test, strain response was measured twice, and natural frequencies were measured five times.

Table E.1 Overview of Periodic Tests – Specimen 1

Date	Transverse Stiffness	Strains	Natural Frequency	Wire Breaks Reported	Notes
9/01/05	TS 0	S 0	NF 0	0	—
9/06/05	TS 1	S 1	—	0	260,000 cycles
9/16/05	TS 2	—	NF 1	0	970,000 cycles
9/27/05	TS 3	—	—	0	2,330,000 cycles
10/03/05	TS 4	—	—	1	3,120,000 cycles
10/05/05	TS 5	—	NF 2	2	3,260,000 cycles
10/14/05	—	—	—	2	Load frame repositioned
10/24/05	—	—	NF 3	3	4,150,000 cycles
10/27/05	—	—	NF 4	8	4,500,000 cycles

E.1.1 Transverse Stiffness

The six transverse stiffness measurements Specimen 1 are shown in Figure E.1 and summarized in Table E.2. Tests are designated “TS X” where “TS” refers to transverse stiffness and “X” indicates the test number. All transverse stiffness tests were conducted while the load frame was positioned at midspan.

The load-displacement relationship for Specimen 1 was linear. The transverse stiffness decreased from 0.41 to 0.39 kip/in. as the number of the loading cycles increased. Two wires breaks were reported near midspan in the 47 days between test TS 0 and TS 5.

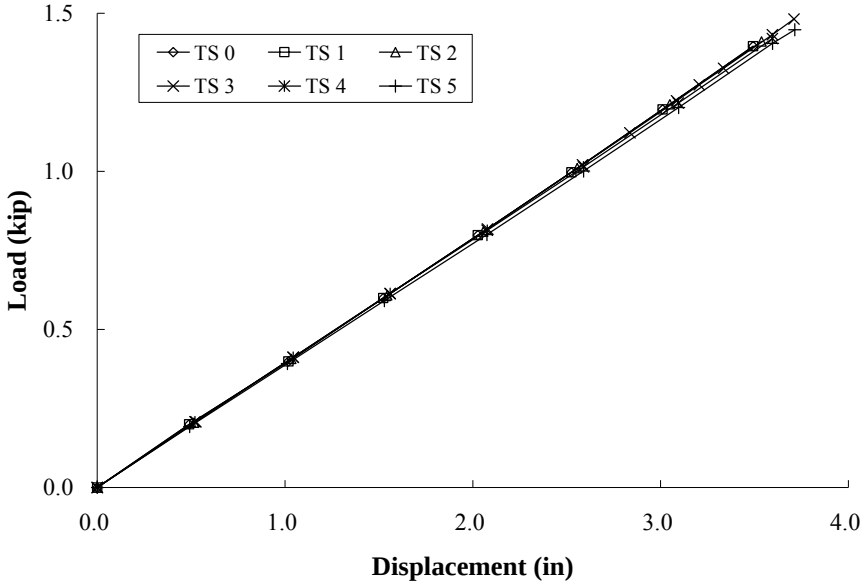

Figure E.1 Measured Transverse Stiffness of Specimen 1

Table E.2 Summary of Variation in Transverse Stiffness for Specimen 1

Measurement	Date	Stiffness (kip/in.)	Wire Breaks Reported
TS 0	8/30/05	0.41	0
TS 1	9/06/05	0.40	0
TS 2	9/16/05	0.40	0
TS 3	9/27/05	0.40	0
TS 4	10/03/05	0.39	1
TS 5	10/05/05	0.39	2

E.1.2 Distribution of Strains

Strains were measured two times during the fatigue test of Specimen 1. Tests are designated "S X" where "S" refers to strain measurements and "X" indicates the test number. Ten strain gages were positioned along the specimen, as summarized in Section C.6.2. Four strain gages were attached to the strand in the vicinity of each anchor head and two strain gages were attached at midspan. The gages were installed along the axes of individual wires. The measured strains represent the variation in strain due to the applied load and do not include the initial level of prestress.

The measured relationships between strain near the anchor heads and the applied load are presented in Figure E.2 through Figure E.5. The strains exhibited highly nonlinear trends with increasing load, and the maximum strains measured at the two ends of the specimen were significantly different. These trends were observed during both sets of strain measurements.

The maximum measured strain was approximately 470 $\mu\varepsilon$ near the north anchor head, which corresponds to a maximum variation in stress of 14 ksi. Most of the strain gages malfunctioned after test S 1; therefore, strains were not measured after the loading frame was repositioned.

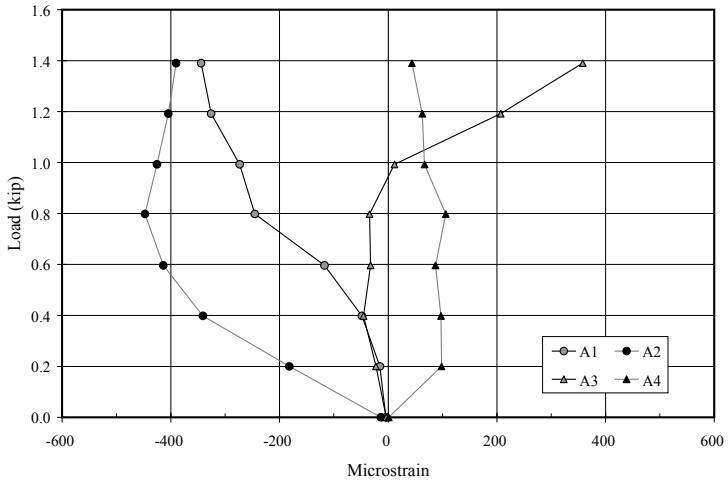

Figure E.2 Measured Strains near North Anchor Head – Test S 0 – Specimen 1

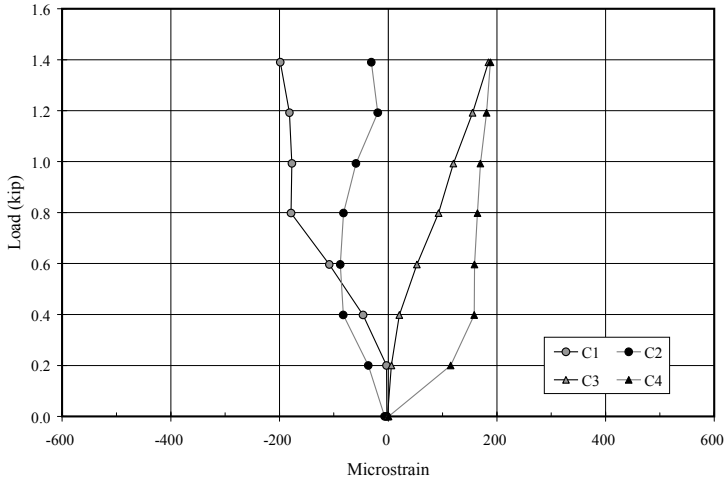

Figure E.3 Measured Strains near South Anchor Head – Test S 0 – Specimen 1

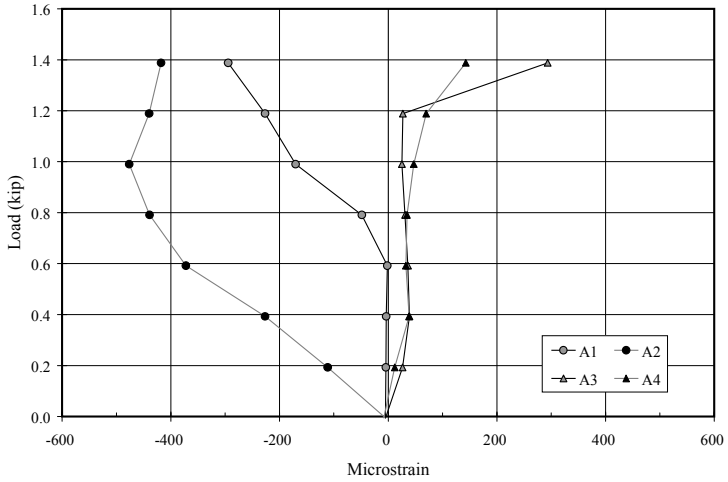

Figure E.4 Measured Strains near North Anchor Head – Test S 1 – Specimen 1

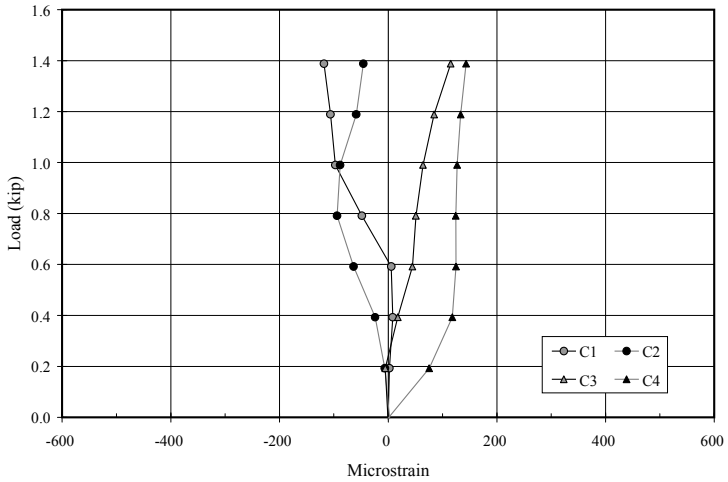

Figure E.5 Measured Strains near South Anchor Head – Test S 1 – Specimen 1

E.1.3 Natural Frequencies

Natural frequencies were measured five times for Specimen 1 (Table E.3). Three wire breaks were reported between NF 0 and NF 3, and the measured frequencies for the second through the sixth modes of vibration decreased slightly. Significant changes in all six natural frequencies were observed in NF 4.

Table E.3 Measured Natural Frequencies for Specimen 1 (Hz)

Mode of Vibration	NF 0	NF 1	NF 2	NF 3	NF 4
	7/14/05	9/16/05	10/05/05	10/24/05	10/27/05
1	4.6	4.6	4.6	4.6	4.2
2	9.4	9.3	9.2	9.1	8.6
3	14.5	14.3	14.2	14.0	13.2
4	20.0	19.7	19.5	19.4	18.3
5	25.6	25.1	24.9	24.5	23.6
6	32.2	31.7	31.2	30.7	29.7
Wire breaks reported	0	0	2	3	8

E.1.4 Observed Wire Breaks

The fatigue test was terminated after all fourteen wires fractured at the north end of the specimen and the specimen collapsed (Figure E.6). All wires in the top strand failed within 2-in. of the inside face of the anchor head and all wires in the bottom strand failed inside the anchor head (Figure E.7). Sixteen wire breaks were identified during the autopsy. In addition to the fourteen wire breaks near the north anchor head, two adjacent wires fractured near midspan (Figure E.7).

Grout at the north end of the specimen was severely cracked. Grout also cracked vertically at many sections. The crack developed from the top and bottom of the sections and continued through both of strands (Figure E.9).

(a) Overall Collapse

(b) Separated Section

(c) Looking South

(d) Looking North

Figure E.6 Collapse of Specimen 1

(a) Top Strand

(b) Bottom Strand

Figure E.7 Wire Breaks at North Anchor Head – Specimen 1

Figure E.8 Wire Breaks near Midspan – Specimen 1

Figure E.9 Typical Vertical Crack in Grout – Specimen 1

E.1.5 Acoustic Data

The acoustic sensors detected twelve wire breaks during the fatigue test for Specimen 1 (Table E.4). The first two wire breaks were detected at midspan and all subsequent breaks were detected at the north end of the specimen (Figure E.10). The fifth and sixth wire breaks were considered to occur simultaneously. The actual number of wire breaks at the north end was two greater than reported by the acoustic sensors.

Table E.4 Summary of Wire Breaks – Specimen 1

Method	**Number**	**North End**	**Midspan**	**South End**	**Total**
Observed during Autopsy	Total	14	2	—	16
	Unique Wires*	14	2	—	16
Acoustic Sensors	Total	12	2	—	14

* Multiple wire breaks in the same wire are not included in this category.

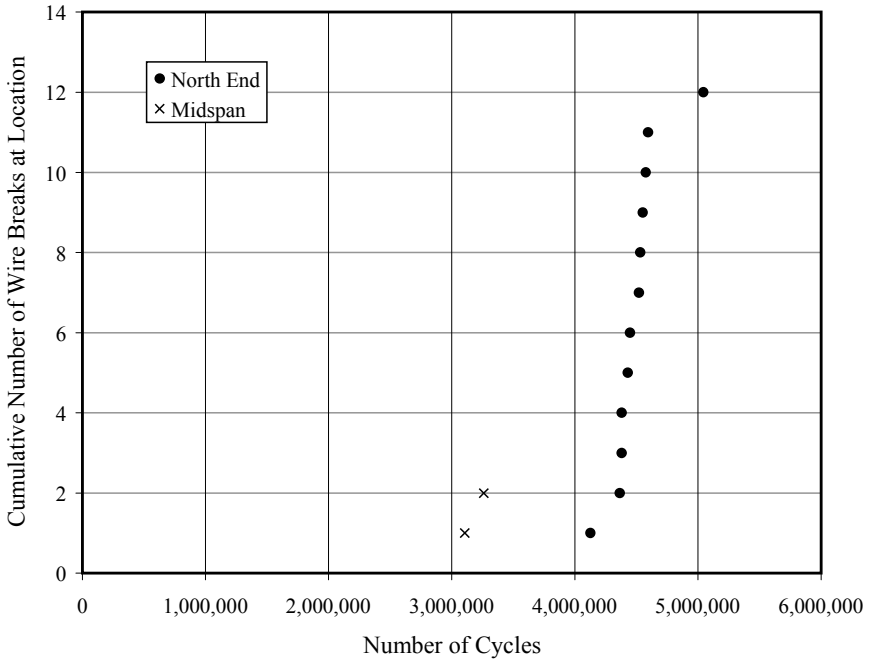

Figure E.10 Wire Breaks Detected from Acoustic Data – Specimen 1

The acoustic data indicated that the two wire breaks at midspan were 2 ft apart. As shown in Figure E.8, the wire breaks were adjacent. The acoustic data indicated that the wire breaks at the north end ranged from 2.5 to 14.5 in. from the inside face of the anchor head, with an average distance of 8.5 in. As shown in Figure E.7, all wire breaks were within 2 in. of the inside face of the anchor head.

E.2 SPECIMEN 2

Specimen 2 was subjected to 4.9 million loading cycles over a 37-day period. The fatigue test was terminated after the sixth wire break was detected by the acoustic sensors. The loads were applied 12.5 ft from the north end of the specimen and the fatigue test was conducted in displacement control.

The list of periodic measurements for Specimen 2 is given in Table E.5. The transverse stiffness was measured ten times during the fatigue test, strain response was measured seven times, and natural frequencies were measured nine times.

Table E.5 Overview of Periodic Tests – Specimen 2

Date and Time	Transverse Stiffness	Strains	Natural Frequency	Wire Breaks Reported	Cycles
2/21/06	TS 0	S 0	NF 0	0	0
2/24/06	TS 1	—	NF 1	0	—
2/28/06	TS 2	S 1	—	0	860,000
3/03/06	TS 3	—	NF 2	1	—
3/06/06	TS 4	—	NF 3	2	1,870,000
3/15/06	TS 5	S 2	NF 4	2	2,780,000
3/21/06	TS 6	S 3	NF 5	2	3,570,000
3/24/06	TS 7	S 4	NF 6	5	3,920,000
3/27/06	TS 8	S 5	NF 7	5	4,320,000
3/30/06	TS 9	S 6	NF 8	6	4,600,000

E.2.1 Transverse Stiffness

The transverse stiffness measurements for Specimen 2 are shown in Figure E.11 and summarized in Table E.6. The load-displacement relationships exhibited linear trends. The measured transverse stiffness decreased from 0.59 to 0.45 kip/in. from TS 0 to TS 9. The reduction between TS 0 and TS 5 was small, but increased after TS 6. In particular, the measured stiffness decreased from 0.51 to 0.45 kip/in. between TS 8 and TS 9.

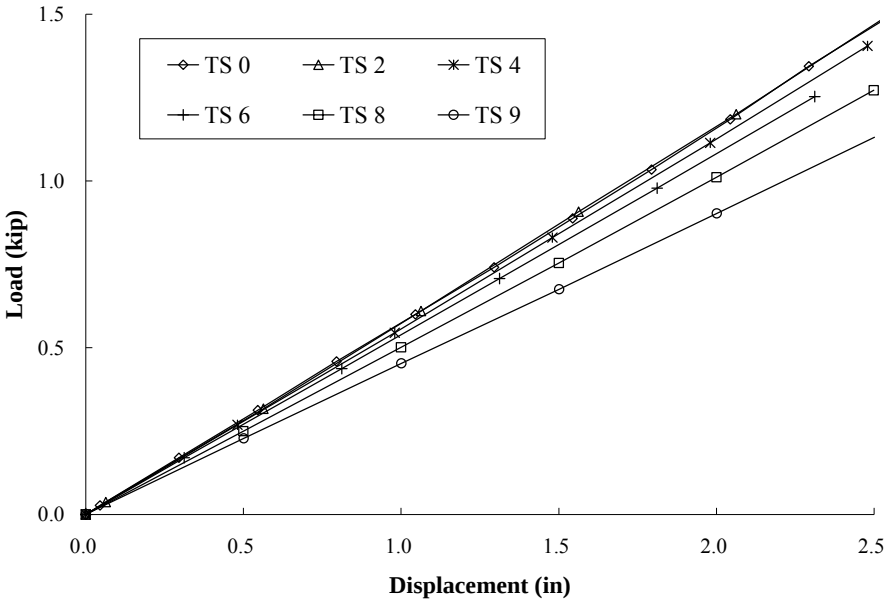

Figure E.11 Measured Transverse Stiffness of Specimen 2

Table E.6 Summary of Variation in Transverse Stiffness for Specimen 2

Measurement	Date	Stiffness (kip/in.)	Wire Breaks Reported
TS 0	2/21/06	0.59	0
TS 1	2/24/06	0.58	0
TS 2	2/28/06	0.59	0
TS 3	3/03/06	0.57	1
TS 4	3/06/06	0.57	2
TS 5	3/15/06	0.56	2
TS 6	3/21/06	0.54	2
TS 7	3/24/06	0.52	5
TS 8	3/27/06	0.51	5
TS 9	3/30/06	0.45	6

E.2.2 Distribution of Strains

Seven sets of strain measurements were collected for Specimen 2. Sixteen strain gages were positioned along the specimen, as summarized in Section C.6.3. The measured relationships between strain and applied load for the three sets of strain gages nearest the north anchor head are presented in Figure E.12 through Figure E.14. The strains exhibited extremely nonlinear trends with increasing load.

Strain gages closest to the north anchor head (Line A) malfunctioned after the initial test. A maximum strain variation of 1800 $\mu\varepsilon$ was recorded in gage A3 during this test, which corresponds to a stress of 56 ksi in the wire. The maximum strain variations in Lines B and C decreased as the number of fatigue cycles increased.

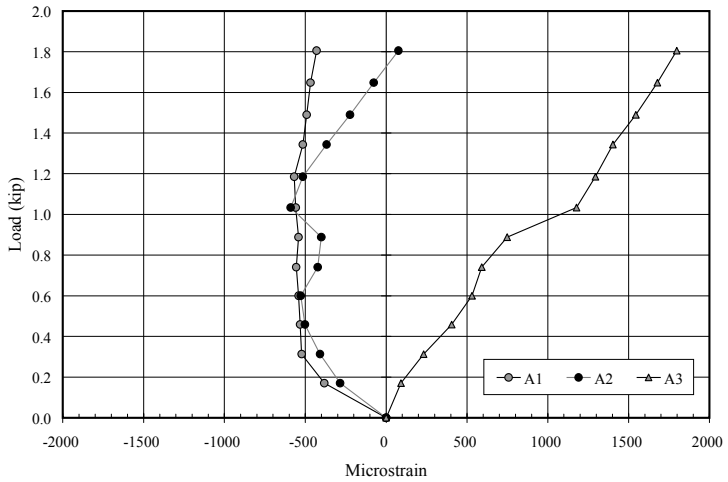

(a) Line A

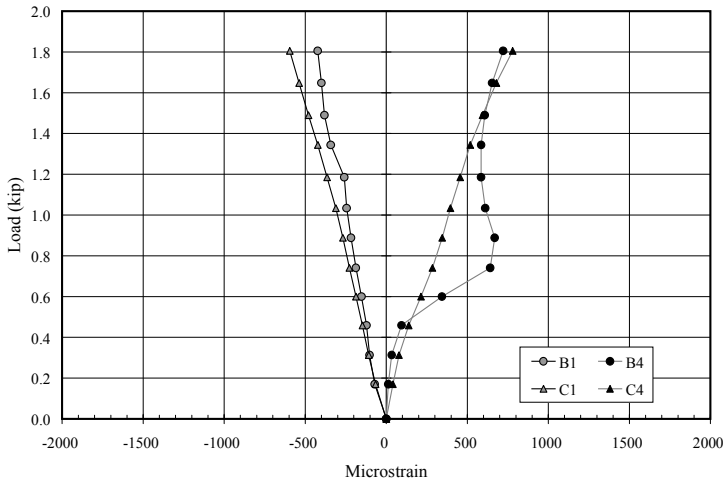

(b) Lines B and C

Figure E.12 Measured Strains – Test S 0 – Specimen 2

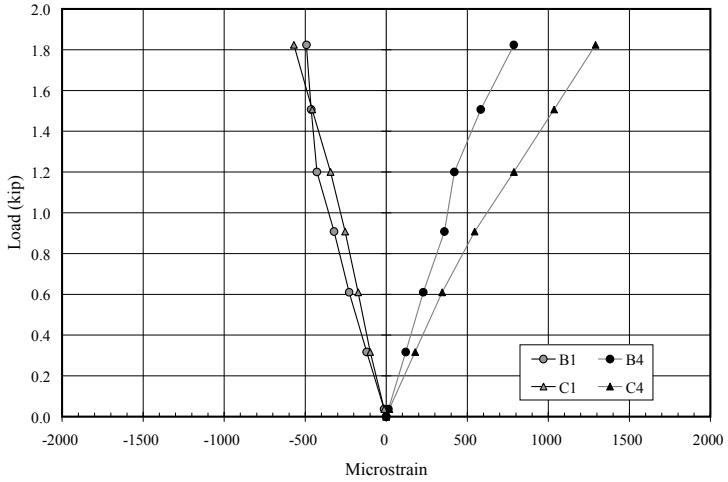

Figure E.13 Measured Strains – Test S 1 – Specimen 2

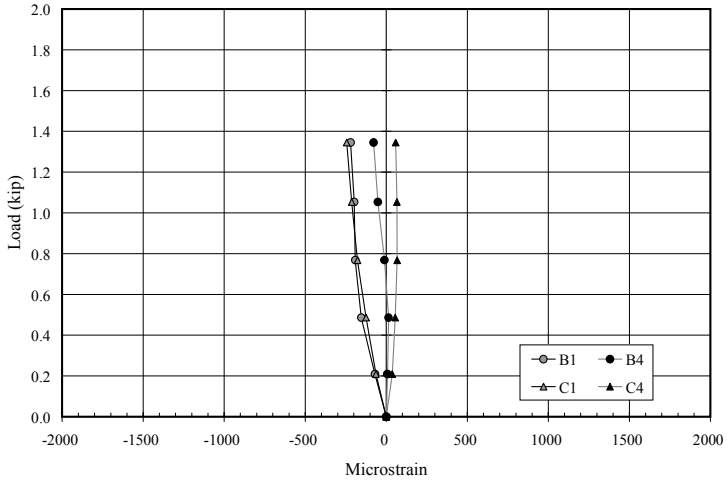

Figure E.14 Measured Strains –Test S 2 – Specimen 2

E.2.3 Natural Frequencies

Natural frequencies were measured nine times for Specimen 2. The test results are presented in Table E.7. The natural frequencies of all six modes decreased gradually from NF 0 to NF 8.

Table E.7 Measured Natural Frequencies for Specimen 2 (Hz)

Mode of Vibration	NF 0	NF 1	NF 2	NF 3	NF 4	NF 5	NF 6	NF 7	NF 8
	2/21/06	2/24/06	3/03/06	3/06/06	3/15/06	3/21/06	3/24/06	3/27/06	3/30/06
1	4.4	4.4	4.3	4.3	4.3	4.2	4.1	4.1	3.9
2	8.9	8.7	8.7	8.6	8.6	8.5	8.3	8.2	7.9
3	13.6	13.3	13.2	13.2	13.2	13.0	12.9	12.8	12.4
4	18.6	18.3	18.1	18.1	18.1	18.0	18.0	17.9	17.4
5	23.5	23.1	22.9	22.9	22.9	23.0	23.1	23.2	22.6
6	29.6	29.0	28.8	28.9	28.8	29.1	29.1	29.2	28.9
Wire breaks reported	0	0	1	2	2	2	5	5	6

E.2.4 Observed Wire Breaks

At the conclusion of the fatigue test, the specimen was disassembled to determine the extent of damage. Eight wire breaks were identified along the top strand. Six wires fractured within 8 in. of the inside face of the anchor head and two wires fractured inside the anchor head (Figure E.15). The center wire fractured twice. Corroded fretting product was observed on the surface of the top strand near the north anchor head. No wire breaks were observed along the bottom strand.

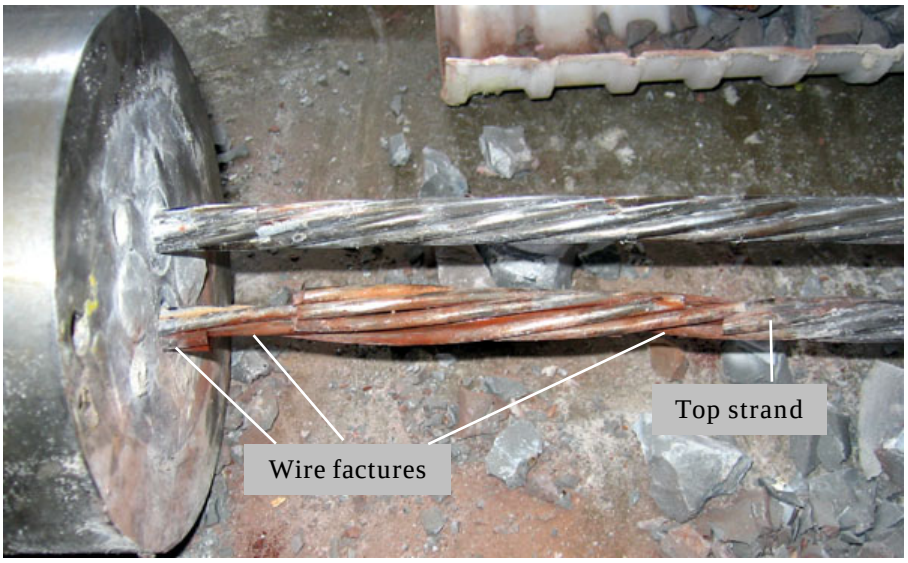

Figure E.15 Wire Fractures at North Anchor Head for Specimen 2

Grout near the north end was severely cracked. Vertical cracks were also identified along the entire length as shown in Figure E.16.

(a) North End (b) Typical Section

Figure E.16 Condition of Grout – Specimen 2

E.2.5 Acoustic Data

The acoustic sensors detected six wire breaks during the fatigue test for Specimen 2 (Table E.4). All wire breaks were detected near the north end of the specimen (Figure E.10), but the actual number of wire breaks was two greater than reported by the acoustic sensors.

Table E.8 Summary of Wire Breaks – Specimen 2

Method	**Number**	**North End**	**Midspan**	**South End**	**Total**
Observed during Autopsy	Total	8	—	—	8
	Unique Wires*	7	—	—	7
Acoustic Sensors	Total	6	—	—	6

* Multiple wire breaks in the same wire are not included in this category.

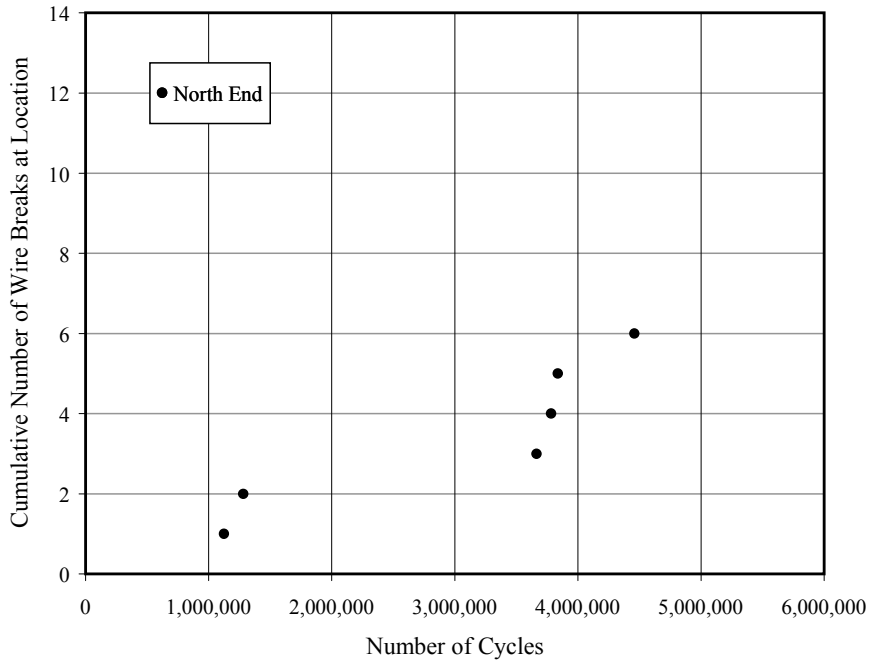

Figure E.17 Wire Breaks Detected from Acoustic Data – Specimen 2

The acoustic data indicated that the wire breaks at the north end ranged from 10 to 26 in. from the inside face of the anchor head, with an average distance of 18.5 in. As shown in Figure E.15, all wire breaks were within 8 in. of the inside face of the anchor head.

E.3 SPECIMEN 3

Specimen 3 was subjected to 1.6 million loading cycles over a 16-day period. The fatigue test was terminated after the eighth wire break was detected by the acoustic sensors. The loads were applied 12.5 ft from the north end of the specimen and the fatigue test was conducted in displacement control.

The list of periodic measurements for Specimen 3 is given in Table E.9. The transverse stiffness was measured six times during the fatigue test, strain response was measured six times, and natural frequencies were measured five times.

Table E.9 Overview of Periodic Tests – Specimen 3

Date	Transverse Stiffness	Strains	Natural Frequency	Wire Breaks Reported	Cycles
4/16/06	—	—	NF 0	0	0
4/25/06	TS 0	S 0	—	0	0
4/26/06	TS 1	S 1	—	0	134,000
4/28/06	TS 2	S 2	NF 1	0	365,000
5/01/06	TS 3	S 3	NF 2	4	749,000
5/04/06	TS 4	S 4	NF 3	6	1,027,000
5/11/06	TS 5	S 5	NF 4	8	1,651,000

E.3.1 Transverse Stiffness

The six transverse stiffness measurements for Specimen 3 are shown Figure E.18 and summarized in Table E.10. The load-displacement relationship exhibited a linear trend. From TS 0 to TS 5, the measured transverse stiffness decreased gradually from 0.59 to 0.48 kip/in. In this period, six wire breaks were reported by the acoustic sensors. A sharp reduction of stiffness was recorded between TS 4 and TS 5 (0.48 to 0.37 kip/in.).

Table E.10 Summary of Variation in Transverse Stiffness for Specimen 3

Measurement	Date	Stiffness (kip/in.)	Wire Breaks Reported
TS 0	4/25/06	0.59	0
TS 1	4/26/06	0.58	0
TS 2	4/28/06	0.58	0
TS 3	5/01/06	0.54	4
TS 4	5/04/06	0.48	6
TS 5	5/11/06	0.37	8

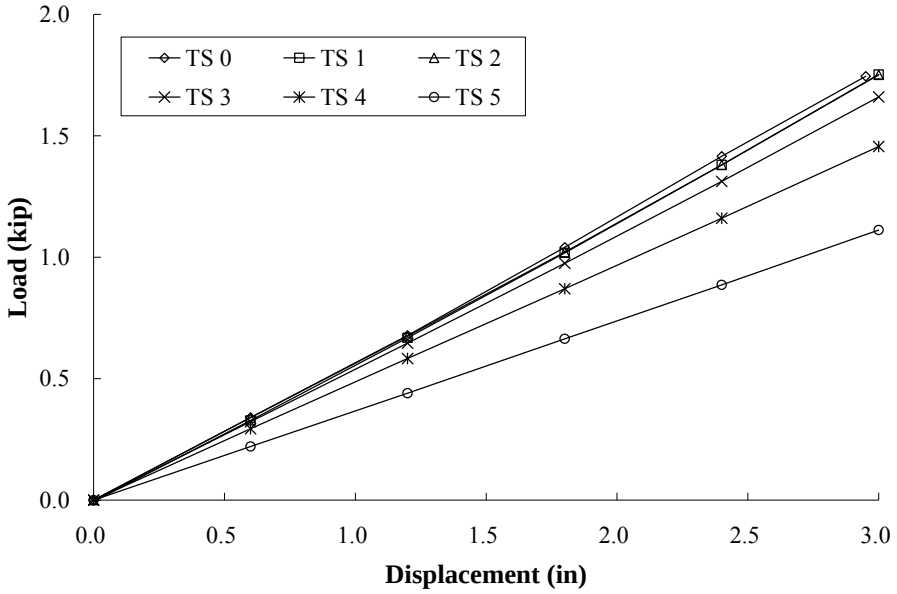

Figure E.18 Measured Transverse Stiffness for Specimen 3

E.3.2 Distribution of Strains

The distributions of strains along the two strands in Specimen 3 were investigated thoroughly. Thirty-two strain gages were used to monitor the response of the specimen (Section C.6.4) and strains were measured eight times during the first 150,000 fatigue cycles. The test schedule at the beginning of the fatigue test is summarized in Table E.11.

Table E.11 Initial Strain Measurements for Specimen 3

Measurement	Maximum Displacement (in.)
SM0-0	0.4
SM0-1	0.8
SM0-2	1.2
1,000 loading cycles	
SM0-3	1.2
SM0-4	2.0
1,000 loading cycles	
SM0-5	3.0
10,000 loading cycles	
SM0-6	3.0
134,500 loading cycles	
SM1	3.0

The strains measured at the beginning of the fatigue tests for Specimens 1 and 2 exhibited nonlinear trends with respect to the applied load (Figure E.2 and Figure E.12). While the strains were measured before the start of the fatigue tests, the grout in the specimens was likely cracked, because the research team loaded the specimens while checking the performance of the hydraulic system. In contrast, Specimen 3 was not preloaded before the first series of strain measurements were recorded, and the

amplitude of the applied displacements was intentionally selected to be low in the early tests to minimize the likelihood of cracking the grout.

The measured strains from the two lines of gages nearest the north anchor head (Lines A and B) are plotted in Figure E.19 for Test S 0-2, in Figure E.20 for Test S 0-4, and in Figure E.21 for Test S 0-6. The strain increased linearly with increasing load in Test S 0-2; however, the maximum strains recorded along Line B exceeded the maximum strains recorded along Line A.

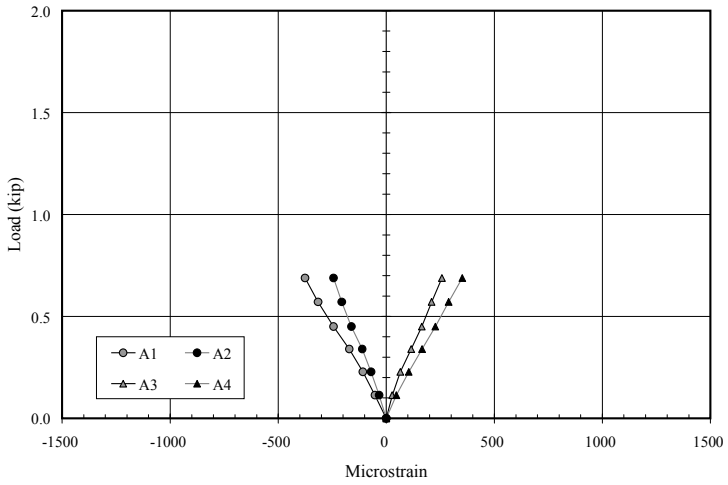

(a) Line A

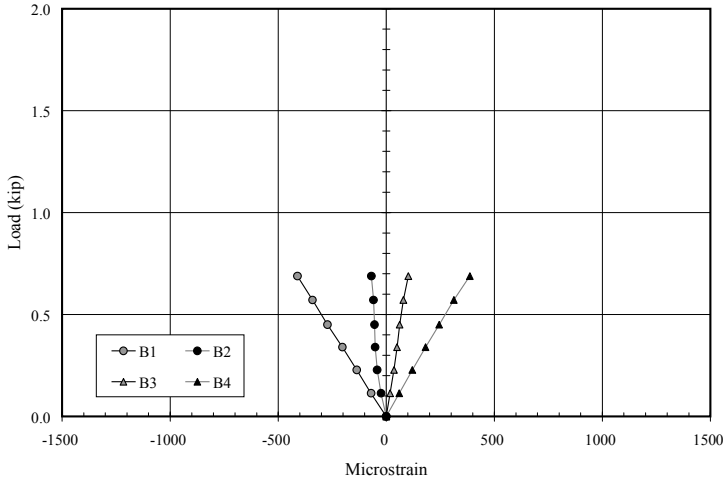

(b) Line B

Figure E.19 Measured Strains – Test S 0-2 – Specimen 3

Nonlinear response was observed along Line A during Test S 0-4 (Figure E.20). The strains along Line B increased linearly with increasing load. Again, the maximum strains recorded along Line B exceeded the maximum strains recorded along Line A.

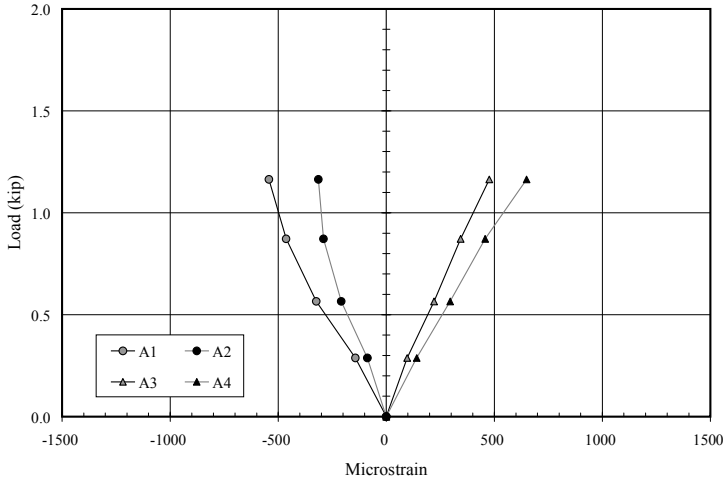

(a) Line A

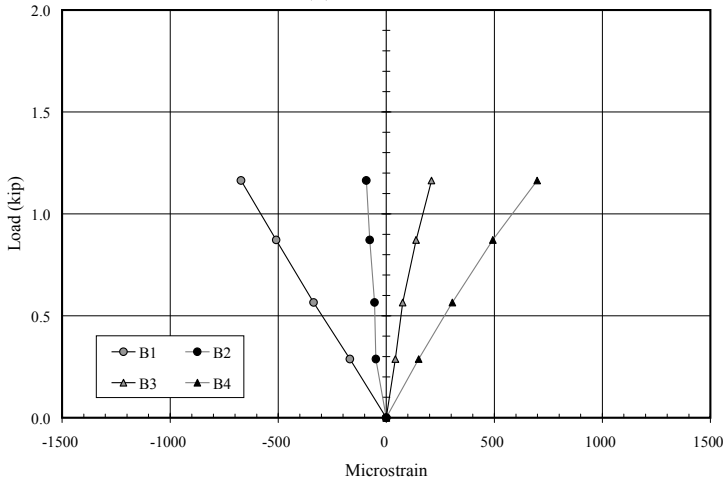

(b) Line B

Figure E.20 Measured Strains – Test S 0-4 – Specimen 3

By Test S 0-6 (Figure E.21), two of the strain gages along Line B had malfunctioned, and all working gages along Lines A and B exhibited nonlinear response. A maximum strain variation of 1280 $\mu\varepsilon$ was recorded in gage A4 during Test S 0-6, which corresponds to a stress of 40 ksi in the wire.

The strain data suggest that cracking of the grout, which would be expected to increase during the initial set of measurements, influences the strains in the strand. By Test S 1, five of the eight strain gages along Lines A and B had malfunctioned.

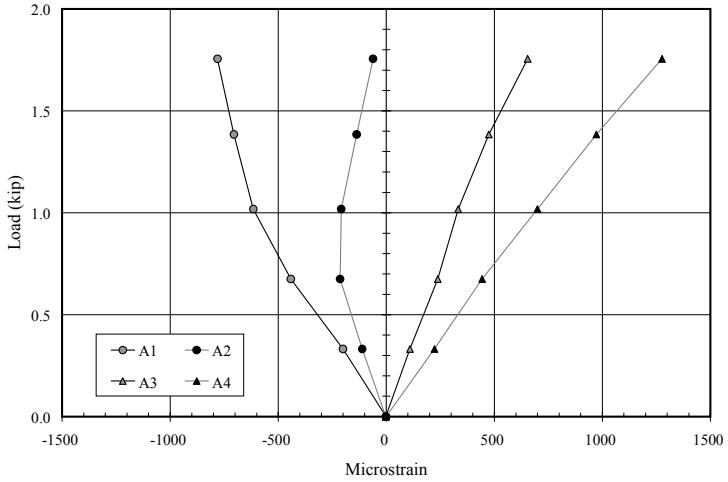

(a) Line A

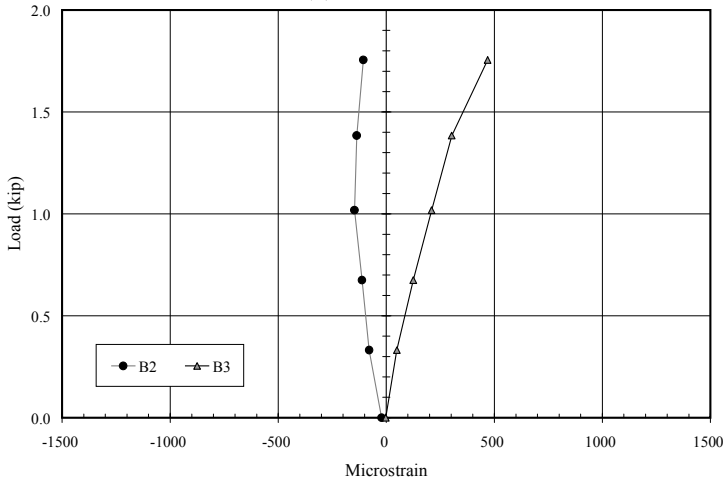

(b) Line B

Figure E.21 Measured Strains – Test S 0-6 – Specimen 3

E.3.3 Natural Frequencies

Natural frequencies were measured five times for Specimen 3 (Table E.12). The natural frequencies decreased gradually as the number of wire breaks increased. The variation of natural frequencies was observed first in NF 2.

Table E.12 Measured Natural Frequency for Specimen 3 (Hz)

Mode of Vibration	NF 0	NF 1	NF 2	NF 3	NF 4
	4/16/06	4/28/06	5/01/06	5/04/06	5/11/06
1	4.3	4.3	4.2	3.9	3.5
2	8.8	8.7	8.5	7.9	7.1
3	13.7	13.5	13.2	12.4	11.2
4	19.0	18.7	18.2	17.3	15.8
5	24.7	23.8	23.2	22.8	21.2
6	31.6	30.3	29.4	29.1	27.3
Wire breaks reported	0	0	4	6	8

E.3.4 Observed Wire Breaks

At the conclusion of the fatigue test, the specimen was disassembled to determine the extent of damage. Twelve wire breaks were identified at the north end of the specimen: nine wire breaks in the bottom strand and three wire breaks in the top strand (Figure E.22).

In the bottom strand, six wires fractured inside the anchor head. Three of the outer wires in the bottom strand fractured outside the anchor head. Two of these outer wires sustained two wire breaks – one inside the anchor head and one outside. In the top strand, all three wire breaks occurred within 1 in. of the inside face of the anchor head.

(a) Wire Breaks in Top Strand

(b) Wire Breaks in Bottom Strand outside Anchor Head

(c) Wire Breaks in Bottom Strand inside Anchor Head

(d) Four Wire Fractures in Bottom Strand at Wedges

Figure E.22 Observed Wire Fractures for Specimen 3

Grout was severely cracked near the north end of the specimen. A vertical crack extended the entire length of the specimen (Figure E.23).

(a) North End (Duct Partially Opened)

(b) North End (Duct Fully Opened)

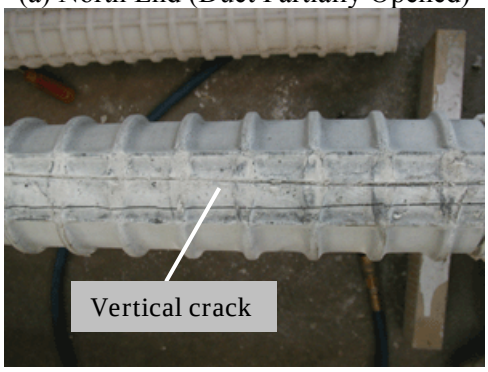

(c) South End

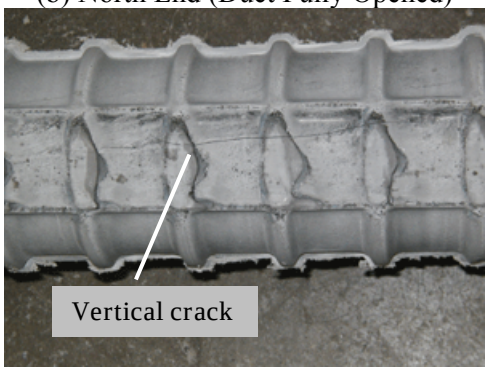

(d) Near Applied Load

Figure E.23 Observed Condition of Grout – Specimen 3

E.3.5 Acoustic Data

The acoustic sensors detected eight wire breaks during the fatigue test for Specimen 3 (Table E.13). All wire breaks were detected near the north end of the specimen (Figure E.24), but the actual number of wire breaks was four greater than reported by the acoustic sensors.

Table E.13 Summary of Wire Breaks – Specimen 3

Method	**Number**	**North End**	**Midspan**	**South End**	**Total**
Observed during Autopsy	Total	12	—	—	12
	Unique Wires*	10	—	—	10
Acoustic Sensors	Total	8	—	—	8

* Multiple wire breaks in the same wire are not included in this category.

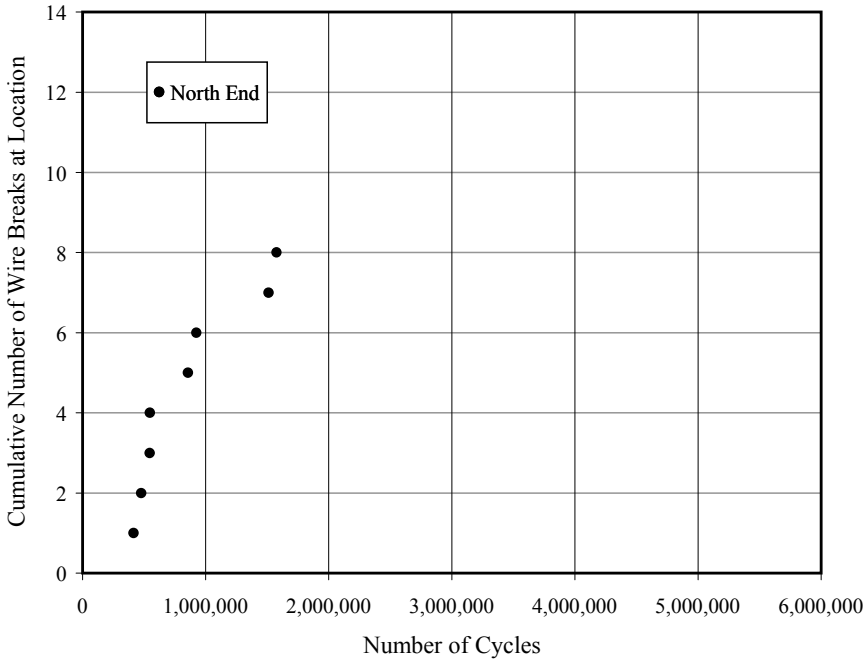

Figure E.24 Wire Breaks Detected from Acoustic Data – Specimen 3

The acoustic data indicated that the wire breaks at the north end ranged from 15 to 37 in. from the inside face of the anchor head, with an average distance of 17.5 in. As shown in Figure E.22, all wire breaks were within 1 in. of the inside face of the anchor head, and half of the breaks occurred within the anchor head.